

IntechOpen

# Carbon Dioxide Chemistry, Capture and Oil Recovery

*Edited by Iyad Karamé,  
Janah Shaya and Hassan Srouf*





---

# **CARBON DIOXIDE CHEMISTRY, CAPTURE AND OIL RECOVERY**

---

Edited by **Iyad Karamé, Janah Shaya**  
and **Hassan Srour**

## Carbon Dioxide Chemistry, Capture and Oil Recovery

<http://dx.doi.org/10.5772/intechopen.68466>

Edited by Iyad Karamé, Janah Shaya and Hassan Srour

### Contributors

Fernando Vega, Mercedes Cano, Sara Camino, Luz. M. Gallego Fernández, Esmeralda Portillo, Benito Navarrete, Hitoshi Ishida, Akira Nishimura, Wei Chieh Chung, Moo-Been Chang, Raul Nunes Carvalho Jr, Vânia Maria Borges Cunha, Marcilene Paiva Da Silva, Wanessa Almeida Da Costa, Mozaniel Santana De Oliveira, Fernanda Wariss Figueiredo Bezerra, Anselmo Castro De Melo, Rafael Henrique Holanda Pinto, Nelio Teixeira Machado, Marilena Emmi Araújo, Xia Shao, Lingyun Yang, Peter Scott, Subhra Jana, Arindam Modak, Tien Trung Nguyen, Ngoc Khanh Pham Ngoc Khanh, Abdelmalek Atia, Kamal Mohammedi, Wathsala Jinadasa, Maths Halstensen, Klaus-Joachim Jens, Syed Zaidi, Sajeda Alsaydeh, Iyad Karamé

### © The Editor(s) and the Author(s) 2018

The rights of the editor(s) and the author(s) have been asserted in accordance with the Copyright, Designs and Patents Act 1988. All rights to the book as a whole are reserved by INTECHOPEN LIMITED. The book as a whole (compilation) cannot be reproduced, distributed or used for commercial or non-commercial purposes without INTECHOPEN LIMITED's written permission. Enquiries concerning the use of the book should be directed to INTECHOPEN LIMITED rights and permissions department ([permissions@intechopen.com](mailto:permissions@intechopen.com)).

Violations are liable to prosecution under the governing Copyright Law.



Individual chapters of this publication are distributed under the terms of the Creative Commons Attribution 3.0 Unported License which permits commercial use, distribution and reproduction of the individual chapters, provided the original author(s) and source publication are appropriately acknowledged. If so indicated, certain images may not be included under the Creative Commons license. In such cases users will need to obtain permission from the license holder to reproduce the material. More details and guidelines concerning content reuse and adaptation can be found at <http://www.intechopen.com/copyright-policy.html>.

### Notice

Statements and opinions expressed in the chapters are those of the individual contributors and not necessarily those of the editors or publisher. No responsibility is accepted for the accuracy of information contained in the published chapters. The publisher assumes no responsibility for any damage or injury to persons or property arising out of the use of any materials, instructions, methods or ideas contained in the book.

First published in London, United Kingdom, 2018 by IntechOpen

eBook (PDF) Published by IntechOpen, 2019

IntechOpen is the global imprint of INTECHOPEN LIMITED, registered in England and Wales, registration number:

11086078, The Shard, 25th floor, 32 London Bridge Street

London, SE19SG – United Kingdom

Printed in Croatia

British Library Cataloguing-in-Publication Data

A catalogue record for this book is available from the British Library

Additional hard and PDF copies can be obtained from [orders@intechopen.com](mailto:orders@intechopen.com)

Carbon Dioxide Chemistry, Capture and Oil Recovery

Edited by Iyad Karamé, Janah Shaya and Hassan Srour

p. cm.

Print ISBN 978-1-78923-574-6

Online ISBN 978-1-78923-575-3

eBook (PDF) ISBN 978-1-83881-322-2

# We are IntechOpen, the world's leading publisher of Open Access books Built by scientists, for scientists

**3,650+**

Open access books available

**114,000+**

International authors and editors

**118M+**

Downloads

**151**

Countries delivered to

Our authors are among the  
**Top 1%**

most cited scientists

**12.2%**

Contributors from top 500 universities



**WEB OF SCIENCE™**

Selection of our books indexed in the Book Citation Index  
in Web of Science™ Core Collection (BKCI)

Interested in publishing with us?  
Contact [book.department@intechopen.com](mailto:book.department@intechopen.com)

Numbers displayed above are based on latest data collected.  
For more information visit [www.intechopen.com](http://www.intechopen.com)





# Meet the editors



Iyad Karamé, PhD, is a professor at the Faculty of Sciences, Lebanese University and the director of the LCOM. He attained his PhD degree from the Lyon 1 University in January 2004. He was an assistant professor and a researcher (ATER) at the Ecole normale supérieure de Lyon during 2004–2005, a researcher at the Leibniz Institut für Katalyse in Rostock (Germany) (2005–2006), and a researcher at the LCOMS, CPE-Lyon, until 2008. His principal axes of research are green organometallic catalysis, CO<sub>2</sub> chemistry, materials for solar energy, and synthesis of chelating macrocycles for the complexation of metals. He is an editor of three books: *Hydrogenation*, *Recent Advances in Organocatalysis*, and *Green Chemical Processing and Synthesis*, published by IntechOpen.



Janah Shaya, PhD, is a researcher and an instructor at the Institut de physique et chimie des matériaux de Strasbourg (IPCMS), University of Strasbourg in collaboration with Kyushu University, Japan. He joined the IPCMS in 2016. He attained his PhD degree from the University of Nice, Sophia Antipolis, in France in September 2016. His principal axes of research are organic synthesis, catalysis, material sciences, biosensors, photophysics electrochemistry, and applications (energy storage systems and CO<sub>2</sub> valorization). He is currently the co-editor of “Carbon Dioxide Chemistry” book with IntechOpen.



Hassan Srour, PhD, is an instructor at the Faculty of Sciences, Lebanese University. He was a research and development engineer at the École supérieure de chimie physique électronique de Lyon (C2P2-CPE de Lyon). He attained his PhD degree from the University of Claude Bernard Lyon 1 in France in October 2013. He was a postdoctoral fellow at the Ecole normale supérieure de Lyon (ENS), France (November 2013–March 2016). His principal axes of research are organic synthesis, polymer electrolytes, electrochemistry, and catalysis for different applications (energy storage systems and CO<sub>2</sub> valorization). He is an editor of *Recent Advances in Organocatalysis* and *Green Chemical Processing and Synthesis*, published by IntechOpen.





---

# Contents

---

## **Preface XI**

### **Section 1 Introduction 1**

- Chapter 1 **Introductory Chapter: An Outline of Carbon Dioxide Chemistry, Uses and Technology 3**  
Janah Shaya, Hassan Srour and Iyad Karamé

### **Section 2 Catalytic Transformations of CO<sub>2</sub>: Reduction and Reforming 15**

- Chapter 2 **Electrochemical/Photochemical CO<sub>2</sub> Reduction Catalyzed by Transition Metal Complexes 17**  
Hitoshi Ishida

- Chapter 3 **Carbon Dioxide Conversion to Methanol: Opportunities and Fundamental Challenges 41**  
Sajeda A. Al-Saydeh and Syed Javaid Zaidi

- Chapter 4 **Effect of Overlapping Fe/TiO<sub>2</sub> Coated on Netlike Glass Disc and Cu Disc on CO<sub>2</sub> Reduction 63**  
Akira Nishimura

- Chapter 5 **CO<sub>2</sub> Reforming with CH<sub>4</sub> via Plasma Catalysis System 85**  
Wei Chieh Chung and Moo Been Chang

### **Section 3 Theoretical Approach and Labeling of CO<sub>2</sub> 103**

- Chapter 6 **Understanding Interaction Capacity of CO<sub>2</sub> with Organic Compounds at Molecular Level: A Theoretical Approach 105**  
Pham Ngoc Khanh and Nguyen Tien Trung

- Chapter 7 **[11C]Carbon Dioxide: Starting Point for Labeling PET Radiopharmaceuticals 123**  
Lingyun Yang, Peter J. H. Scott and Xia Shao
- Section 4 Carbon Dioxide Capture and Oil Extraction 139**
- Chapter 8 **Solvents for Carbon Dioxide Capture 141**  
Fernando Vega, Mercedes Cano, Sara Camino, Luz M. Gallego Fernández, Esmeralda Portillo and Benito Navarrete
- Chapter 9 **Advances in Porous Adsorbents for CO<sub>2</sub> Capture and Storage 165**  
Arindam Modak and Subhra Jana
- Chapter 10 **Process Analytical Technology for CO<sub>2</sub> Capture 185**  
M.H. Wathsala N. Jinadasa, Klaus-J. Jens and Maths Halstensen
- Chapter 11 **Carbon Dioxide Use in High-Pressure Extraction Processes 211**  
Vânia Maria Borges Cunha, Marcilene Paiva da Silva, Wanessa Almeida da Costa, Mozaniel Santana de Oliveira, Fernanda Wariss Figueiredo Bezerra, Anselmo Castro de Melo, Rafael Henrique Holanda Pinto, Nelio Teixeira Machado, Marilena Emmi Araujo and Raul Nunes de Carvalho Junior
- Chapter 12 **A Review on the Application of Enhanced Oil/Gas Recovery through CO<sub>2</sub> Sequestration 241**  
Abdelmalek Atia and Kamal Mohammedi

---

## Preface

---

Carbon dioxide (CO<sub>2</sub>) is an ancient molecule that is constantly inducing next generations of urgent yet innovative research. CO<sub>2</sub> is a stable and relatively inert triatomic molecule that exists as a gas at ambient temperature and pressure. It is generated naturally from various sources such as forest fires, volcanic eruptions, and respiration of living organisms. The photosynthesis of plants and other autotrophs play an indispensable role in balancing the carbon/oxygen cycle and, consequently, in maintaining the life on earth. The global concentration of CO<sub>2</sub> in the atmosphere was approximately 270 ppm by volume prior to the industrial revolution. Nowadays, the carbon dioxide level has reached up to 405 ppm, approximately a 50% increase. This steady increase in CO<sub>2</sub> emissions stems from the large consumption of fossil fuels and anthropogenic activity in addition to the wide deforestation for land usage.

Pollution is regarded as the issue of our era, since dominant industries deem its control as an expense that overwhelms the domains that are beneficial to the advances of science. Finding alternatives to indispensable fields such as providing energy, food, drugs, and dyes for medicinal probes, among others, seems to conflict with the innovative progress reported every day in academia and industry. The greenhouse effect is one of the utmost contemporary issues in this regard. Carbon dioxide is currently the most abundant greenhouse gas (GHG). CO<sub>2</sub> plays a detrimental role in preventing the heat loss and protecting the life on earth during nighttime. However, the increased concentrations of GHGs, particularly CO<sub>2</sub>, are believed to cause drastic changes such as global warming and ocean acidification.

Several international conventions and governmental protocols have been formulated to reduce the CO<sub>2</sub> emissions, such as the *Kyoto Protocol*, the *UN Framework Convention on Climate Change*, and the *Intergovernmental Panel on Climate Change*. To date, there is no universal agreement on these laws, and many countries and industries do not abide by these conventions. Therefore, immediate actions and solutions are demanded to circumvent the potential influence of the yet high CO<sub>2</sub> emissions on the climate. In general, the total CO<sub>2</sub> emissions can be controlled by reducing the energy intensity, limiting the carbon intensity, or by improving the CO<sub>2</sub> sequestration. In the short term, carbon-based fossil fuels will persist to be the main source of energy. Thus, there is an urgent need to develop economically feasible and efficient processes for capturing, separating, storing, sequestering, and utilizing the continuous CO<sub>2</sub> emissions. The future trends, however, should be directed to reduce energy consumption and dependence on fossil fuels and to develop large-scale renewable and less carbon-intensive sources of energy, such as nuclear energy (e.g., H<sub>2</sub>), biofuels, geothermal, and tidal energy.

This book "Carbon Dioxide Chemistry, Capture, and Oil Recovery" combines peer-reviewed scientific contributions that indicate the state of the art of different carbon dioxide processes and describe the novel work and theoretical studies in these domains. The introductory chapter is meant to be a general review on the chemistry of carbon dioxide and its uses with an emphasis on CO<sub>2</sub> technologies, particularly the carbon capture and storage (CCS) and carbon capture and utilization (CCU) projects.

The *first section* of the book discusses the catalytic transformations of CO<sub>2</sub> (reduction and reforming) in four chapters. *Chapter 2* focuses on the electrochemical/photochemical reduction of CO<sub>2</sub> via transition metal complexes as the molecular catalysts with a particular emphasis on *cis*-[Ru(bpy)<sub>2</sub>(CO)<sub>2</sub>]<sup>2+</sup> (bpy: 2,2'-bipyridine) and *trans*(Cl)-[Ru(bpy)(CO)<sub>2</sub>Cl<sub>2</sub>] as representative examples. *Chapter 3* reviews the novel technologies and current barriers for the conversion of CO<sub>2</sub> into methanol through heterogeneous and homogeneous catalysis and electrochemical, photochemical, and photoelectrochemical conversions. It elaborates the role of pyridinium and the rate-determining step of pyridinium-catalyzed CO<sub>2</sub> reduction. *Chapter 4* reports a novel work related to overlapping Fe/TiO<sub>2</sub> coated on netlike glass disc and Cu disc by sol-gel and dip-coating processes. The chapter studies the effect of the designed photocatalysts on the CO<sub>2</sub> reduction. Lastly, *Chapter 5* discusses the cutting-edge development in the application of catalytic, nonthermal plasma, and hybrid plasma catalysis for the dry reforming of methane with CO<sub>2</sub>, describing the fundamentals, reaction mechanisms, opportunities, and barriers, as well as the features of various reactors.

*Section II* describes some theoretical approaches and labeling of CO<sub>2</sub> in two separate chapters. *Chapter 6* is dedicated to assess the interactions of CO<sub>2</sub> with naked, substituted, and functionalized hydrocarbons at the molecular level using theoretical approaches and computational techniques. This detailed study serves to obtain insights into the design of CO<sub>2</sub>-philic materials, and hence, it is a cornerstone in the search and comprehension of new materials that adsorb CO<sub>2</sub>. *Chapter 7* is an interesting and important general overview on the rapidly growing field of carbon-11 radiochemistry and the introduction of carbon-11 by various methods. Carbon-11 is one of the most important radioisotopes in nuclear medicine and is an important starting point for labeling the positron emission tomography (PET) radiopharmaceuticals.

*Section III* targets the carbon dioxide capture and oil extraction in five distinct chapters. *Chapter 8* explores the classical and new generations of solvents for this purpose. Precisely, it elaborates the chemical and physical absorptions, their mechanisms and kinetics, as well as a critical analysis of their advantages and disadvantages. Within the same guidelines, *Chapter 9* describes the highly efficient adsorbents such as metal organic frameworks (MOFs), porous organic polymers (POPs), porous clays, N-doped carbon, and others as the next generation of CO<sub>2</sub> capture through nanospace chemistry. *Chapter 10* is concerned with process analytical technology (PAT), which can replace traditional chemical analyses and can be embedded in carbon capture technologies. This investigation elaborates an example of the implementation of a process analyzer to CO<sub>2</sub> capture by the alkanolamine absorption process using chemometrics modeling and real-time Raman spectroscopy to quantify the CO<sub>2</sub> concentration. *Chapter 11* intends to show the recent application scenarios of carbon dioxide use at high pressures as the solvent in extraction processes of natural extracts enriched with bioactive compounds. The chapter comprises a case study of experimental strategy used for the supercritical carbon dioxide extraction of bioactive compounds from açai berry pulp and

calculations of the CO<sub>2</sub> processes using equations of state. Lastly, *Chapter 12* aims to give an extensive literature survey and examines research papers that focus on EOR-CO<sub>2</sub> processes and projects that have been tested in the field. To recall, these processes are concerned with the injection of CO<sub>2</sub> into oil field geological formations aiming to combine CO<sub>2</sub> sequestration and enhanced oil recovery.

We would like to express our appreciation to all the renowned authors who strongly contributed to this project and to their cutting-edge research. We would also like to thank Ms. Kristina Kardum, the coordinator of this project. We hope that the readers find this book as enjoyable and illuminating as our previous projects *Hydrogenation*, *Recent Advances in Organocatalysis*, and *Green Chemical Processing and Synthesis*, and any comments are warmly welcome.

**Iyad Karamé**

Faculty of Sciences I, Lebanese University  
Beirut, Lebanon

**Janah Shaya**

IPCMS, University of Strasbourg  
Strasbourg, France

**Hassan Srour**

Faculty of Sciences V, Lebanese University  
Nabatieh, Lebanon



---

# Introduction

---





---

# Introductory Chapter: An Outline of Carbon Dioxide Chemistry, Uses and Technology

---

Janah Shaya, Hassan Srour and lyad Karamé

Additional information is available at the end of the chapter

<http://dx.doi.org/10.5772/intechopen.79461>

---

## 1. Introduction

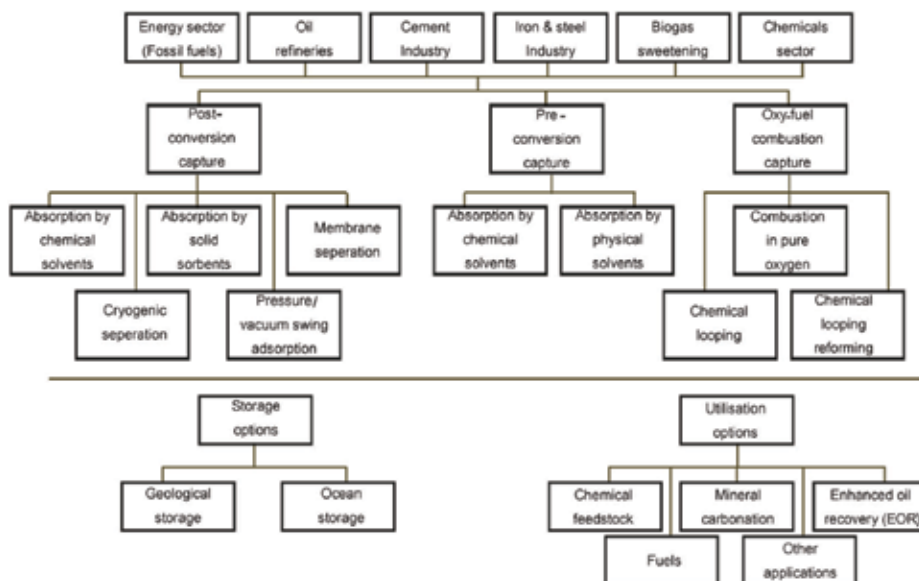
Carbon dioxide (CO<sub>2</sub>) is a stable and relatively inert triatomic molecule that exists as a gas at ambient temperature and pressure. A CO<sub>2</sub> molecule exhibits a linear structure in which the carbon is bonded to each oxygen atom *via* a sigma and pi bond forming two C=O bonds. Each C=O bond has a length of 116.3 pm and 750 kJ.mol<sup>-1</sup> bonding energy, considerably higher than the bonding energy of C=C, C–O, and C–H bonds [1]. Carbon dioxide is generated naturally from various sources such as forest fires, volcanic eruptions, and respiration of living organisms. The photosyntheses of plants and other autotrophs play an indispensable role in balancing the carbon/oxygen cycle and consequently in maintaining the earth life. The global concentration of CO<sub>2</sub> in the atmosphere was approximately 270 ppm by volume prior to industrial revolution. Nowadays, the carbon dioxide level has reached up to 405 ppm, approximately a 50% increase. This steady increase in CO<sub>2</sub> emissions stems from the large consumption of fossil fuels and anthropogenic activity (power plants, oil refineries, cement, iron, and steel industries, biogas sweetening, and chemical industry and processing) in addition to the wide deforestation for land usage [2].

Pollution is regarded as the issue of our era, since dominant industries deem its control as an expense that overwhelms the domains that are beneficial to the advances of science. Finding alternatives to indispensable fields such as providing energy, food, drugs, and dyes for medicinal probes, among others, seems to conflict the innovative progress reported every day in academia and industry. The greenhouse effect is one of the utmost contemporary issues in this regard. Carbon dioxide is currently the most abundant greenhouse gas (GHG). Greenhouse gases such as ozone, nitrous oxide, methane, chlorofluorocarbons (CFCs), and CO<sub>2</sub> has a detrimental role in preventing the heat loss and protecting

the life on earth during nighttime. However, the increased concentrations of GHGs, particularly  $\text{CO}_2$ , are believed to cause drastic changes such as global warming and ocean acidification [3].

Global warming refers to the increase in the average global temperatures, mostly noticeable in the melting of ice caps in polar regions and the rising of sea levels. Specifically, the greenhouse effect of  $\text{CO}_2$  relies on its asymmetric stretching and bending vibrational modes, which allow this gas to absorb and emit infrared radiation at wavelengths of 4.26 and 14.99  $\mu\text{m}$ , respectively [1, 4]. On the other hand, ocean acidification refers to the ongoing decrease in the pH of water in seas and oceans. About 30–40% of the anthropogenic  $\text{CO}_2$  are dissolved in oceans and seas forming carbonic acids to achieve chemical equilibrium. Consequently, the formed  $\text{H}^+$  ions are leading to decrease the pH of earth water from slightly basic conditions toward neutrality or even acidity in the long term, hence affecting the life cycles of marine organisms and the subsequent food chains [5].

Several international conventions and governmental protocols have been formulated to reduce the  $\text{CO}_2$  emissions such as *The Kyoto Protocol*, *the UN Framework Convention on Climate Change*, and *the Intergovernmental Panel on Climate Change*. To date, there is no universal agreement on these laws, and many countries and industries do not abide by these conventions. Therefore, immediate actions and solutions are demanded to circumvent the potential influence of the yet high  $\text{CO}_2$  emissions on the climate. In general, the total  $\text{CO}_2$  emission can be controlled by reducing the energy intensity, limiting the carbon intensity, or by improving the  $\text{CO}_2$  sequestration. In the short term, carbon-based fossil fuels will persist to be the main source of energy. Thus, there is an urgent need to develop economically feasible and efficient processes for capturing, separating, storing, sequestering, and utilizing the continuous  $\text{CO}_2$



**Figure 1.** Major sources of  $\text{CO}_2$  emissions and technologies used in CCS and CCU.

emissions. The future trends, however, should be directed to reduce energy consumption and dependence on fossil fuels and to develop and employ renewable and less carbon-intensive sources of energy on large scale, such as nuclear energy (e.g.,  $H_2$ ), biofuels, geothermal, and tidal energy [4, 6, 7].

This introductory chapter discusses the *basic properties* and the *major technologies of carbon dioxide*. **Figure 1** outlines the main sources of  $CO_2$  emissions and the various methods used or envisioned for  $CO_2$  capture, storage (CCS), and utilization (CCU). The most important technologies will be introduced in the next sections of this preview and will be further detailed in the separate chapters of this “Book project.”

## 2. Carbon dioxide capture

Carbon dioxide capture technologies involve the processes of producing relatively high purity stream of  $CO_2$  for transport and storage, since most  $CO_2$  emissions from electricity generation and industries are released as flue gas (4–14% by volume  $CO_2$ ). Storage of flue gas is possible in principle by compression to a pressure typically higher than 10 MPa, thus requiring a huge amount of energy aside from the large volumes produced that can rapidly fill the storage reservoirs. Therefore, carbon capture and storage (CCS) technologies represent an economic solution for storage of flue gases [4, 8].

Three methods are known for capturing  $CO_2$  in combustion systems of fossil fuels, namely *postconversion capture*, *preconversion capture*, and *oxy-fuel combustion* (**Figure 1**).

### 2.1. Postconversion capture

The separation of  $CO_2$  from waste gas streams after the conversion (mainly combustion) of the carbon source is known as postconversion process. Different technologies are developed for this capture process such as adsorption by solid sorbents, vacuum swing adsorption, absorption by solvents, and cryogenic separation. These methods are still considered energy demanding. Solvent absorption is elaborated here as an example of the capture. In particular, physical absorption of  $CO_2$  relies on its solubility based on Henry’s Law without inducing a chemical reaction. Thus, low temperatures and elevated  $CO_2$  partial pressures are needed for this application. In contrast, chemical absorption depends on the chemical reaction between  $CO_2$  (at low partial pressure) and the used solvent forming weak bonds. The latter is more adjusted to capture  $CO_2$  emissions in industrial processes given the flue gas conditions of ambient pressure and large volumes with varied concentrations of  $CO_2$ , which might be low in some processes.

### 2.2. Preconversion capture

It involves the capture of  $CO_2$  produced by an intermediate step in some conversions such as in ammonia synthesis. It is commonly achieved using absorption by solvents or adsorption processes. This capture also suffers from the high energy demands.

### 2.3. Oxy-fuel combustion capture

This technology is employed only in combustion conversions that generate flue gas rich in  $\text{CO}_2$  but free from  $\text{N}_2$  and  $\text{NO}_x$  products. The energy demands are lower in this capture process, but the expenses majorly stem from the need of using pure oxygen in the combustion process to avoid generating the coproducts and their separation afterward.

## 3. Carbon dioxide storage

Once captured,  $\text{CO}_2$  can be compressed and transported by shipment or *via* pipelines to storage destinations in the ground (geological sequestration), oceans (still in probation phase), or as mineral carbonates (considered as both utilization and storage process) [4] (**Figure 1**).

In *geological storage*,  $\text{CO}_2$  is injected under high pressure into stable rocks rich in pores that trap natural fluids at a depth between 0.8 and 1 km. Different trapping mechanisms, temperatures, and pressures can be employed allowing the storage of  $\text{CO}_2$  as liquid, compressed gas, or in its supercritical condition, subject to the characteristics of the reservoir. Geological formations include unmineable coal seams, depleted oil, and gas reservoirs.

In contrast, *mineral carbonation* or metal carbonate formation involves the direct or indirect reaction between  $\text{CO}_2$  and a metal oxide such as Ca and Mg, naturally found as silicate minerals. Aside from the availability of minerals, the advantage of this technology is the production of stable carbonates that are suitable for long period of storage that can last for centuries without leakage. The other benefit is the direct use of  $\text{CO}_2$  from flue gas without the costly need of establishing a pure stream, since other gas impurities such as  $\text{NO}_x$  do not influence the carbonation reaction. The large-scale applications of this method are not fully developed yet and still encountering a high overall cost [4, 9].

## 4. Carbon capture and utilization

Carbon capture and storage (CCS) technologies suffer till now from economic and technical limitations for large-scale employment such as the huge capital investment, shortage of geological storage sites, and high leakage rates of  $\text{CO}_2$ . Carbon capture and utilization (CCU) strategy, however, has emerged as a prospective alternative to CCS aiming to turn the  $\text{CO}_2$  emissions into relevant products such as fuels and chemicals. Both of the technologies target capturing anthropogenic  $\text{CO}_2$  emissions before being released to the environment, but they differ in the final destination where CCS aims at long-term storage, while CCU at conversions into useful products. CCU presents a set of advantages over CCS, namely the reduction of costs by synthesis of valuable products and the investment of  $\text{CO}_2$  as an available, nontoxic, and “renewable” resource being constantly emitted. Nonetheless, CCU can be only a short-lived solution, which delays the release of  $\text{CO}_2$  to later stages. Another important aspect that raises strong concerns in the large-scale application of both CCU and CCS is to ensure that the mitigation of the climate change is not achieved at the expense of other environmental issues [10, 11].

Carbon dioxide is indeed an extremely valuable molecule that can be utilized in diverse beneficial ways, as illustrated in **Figure 1** and detailed herein.

#### 4.1. Direct utilization of CO<sub>2</sub>

Carbon dioxide is commonly used in fire extinguishers and photosynthesis as well as a carbonating agent and preservative in food and drink industries.

In addition, *supercritical carbon dioxide* (scCO<sub>2</sub>) has found indispensable applications in supercritical fluid technology. scCO<sub>2</sub> is a fluid state of CO<sub>2</sub> where it is held at or above its critical temperature (304.25 K) and pressure (7.39 MPa). In processes at high pressure (at or above the critical parameters), the density drastically increases, so scCO<sub>2</sub> can fill the volume as a gas but with a density like a liquid. scCO<sub>2</sub> is used in sustainable extractions of bioactive compounds and as a greener alternative for multiphase catalytic reactions, where it is employed as a promoter or modifier of liquid-phase organic reactions although not as a reactor. The dissolved CO<sub>2</sub> in the organic phase acts as a “promoter” by altering the physical properties of the solvent from pure organic phase into high-density CO<sub>2</sub> state that can dissolve gaseous reactants such as O<sub>2</sub>, CO, H<sub>2</sub>, thereby accelerating the involved reactions such as oxidation, hydroformylation, and hydrogenation, respectively. In contrast, the impact of scCO<sub>2</sub> on the chemical properties is modulated by its interactions with the functional groups of substrates and/or intermediates (whether gases or not), as proved by the *in situ* high-pressure Fourier transform infrared spectroscopy. Hence, it acts here as a “modifier” to the reactivity of these groups and, thereby, to the selectivity of the reaction (e.g., Heck reactions). It is worth noting that most of the abovementioned uses are limited to CO<sub>2</sub> emission streams of high purity (from ammonia production, for instance) [10, 12].

#### 4.2. Enhanced oil (EOR) and coal-bed methane recovery (ECBM)

The injection of CO<sub>2</sub> in the extraction processes of crude oil (EOR or tertiary recovery) and natural gas (ECBM), respectively, from oil fields and coal deposits represent an attractive option to obtain the otherwise unrecoverable fossil fuels. These methods have been tested successfully and are being extensively researched to reduce the costs, optimize the CCS and CCU conditions, and thus to avoid the reemission of CO<sub>2</sub> to the environment. In EOR, the injection of CO<sub>2</sub> under supercritical conditions allows an efficient mixing with oil, decreasing the viscosity and consequently increasing the extraction yields by 5–15%. The ECBM employs a similar technique in which the injected CO<sub>2</sub> occupies the porous spaces of the coal bed and adsorbs onto the carbon at twice the rate of methane, leading to its faster displacement and enhanced recovery. It is worth noting that surfactants and other gases as well as varied methods like thermal energy processes are also applied in EOR and ECBM processes.

#### 4.3. Conversion of CO<sub>2</sub> into chemicals and fuels

CO<sub>2</sub> represents an abundant and a safe resource of C and O, which can be employed in the synthesis of variety of useful products conforming to the principles of Green Chemistry. For instance, employing CO<sub>2</sub> as an alternative to toxic reactants such as phosgene and CO is attracting huge attention. The types of transformations of carbon dioxides along with

examples of the main products are illustrated in **Table 1**. They will be further discussed in this section with the exception of the biological process that will follow in the section of biofuels and the inorganic carbonate formation that was already discussed as a storage option [13].

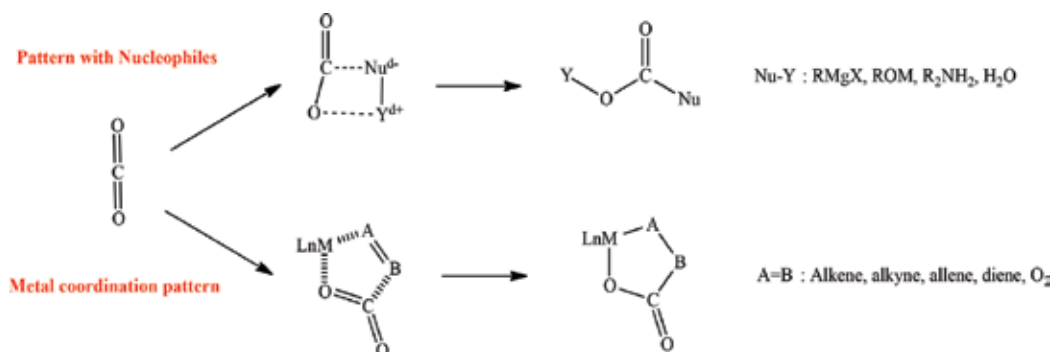
The chemistry of CO<sub>2</sub> can be classified into two general categories (**Scheme 1**):

- a. The “basic CO<sub>2</sub> transformations” depend on the polarization of C=O bonds where the higher electronegative oxygen atoms carry a partial negative charge of -0.296 and the carbon center has a partial positive charge of +0.592. This polarization ensures the reaction of nucleophiles (amines, Grignard reagents, phenolates, etc.) at the carbon center.
- b. The “more advanced chemical interactions of CO<sub>2</sub>” rely on the coordination of the triatomic molecules to metals, inducing major changes in its chemical reactivity by altering both its molecular geometry (e.g., linear to more activated bent) and its electronic distribution (e.g., less electron-deficient carbon upon coordination). Various catalysts have so far been investigated to achieve this goal and activate the stable and relatively nonreactive CO<sub>2</sub>. This area is still considered a hot topic in organometallic and theoretical research due to the various coordination modes between CO<sub>2</sub> and different metals [1].

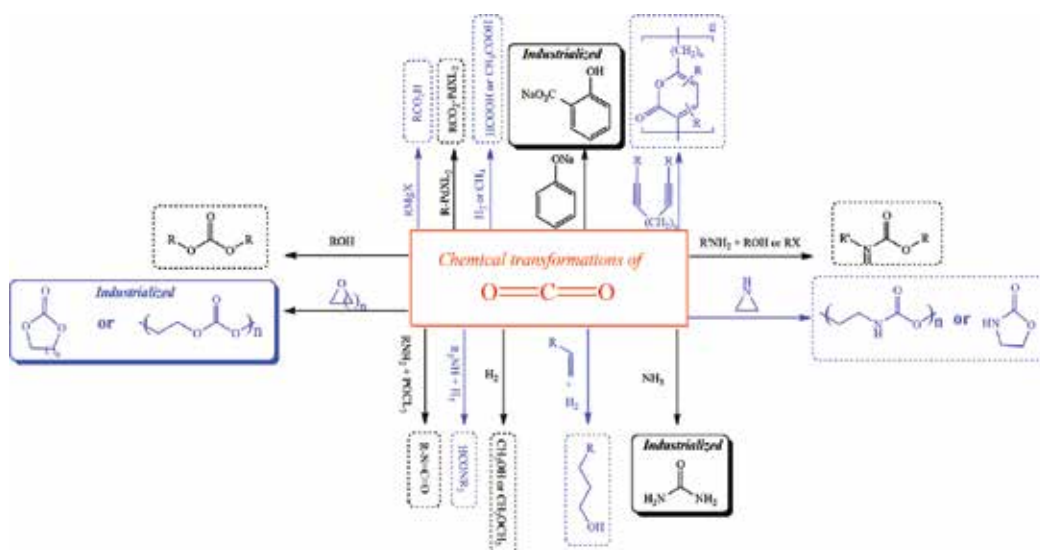
Based on these two chemistry modes, numerous transformations of CO<sub>2</sub> have been reported achieving a range of useful chemical products. The majority of these transformations are summarized in the pattern shown in **Scheme 2** and have been reviewed by Sakakura et al. The transformations involve either (i) using the CO<sub>2</sub> molecule as a precursor for organic compounds such as carbonates, carbamates, polymers, and acrylates *via* carboxylation reactions or (ii) reduction of the C=O bonds resulting in chemicals such as methanol, dimethyl ether, methane, urea (important fertilizer), syngas, and even formic acid and CO. Formic acid is a safe storage material of H<sub>2</sub>, and CO can be transformed into liquid hydrocarbons by Fischer-Tropsch process. Some CO<sub>2</sub> conversions have been industrialized (**Scheme 2**) and currently play important roles in recovering the anthropogenic emissions of CO<sub>2</sub>. The main drawbacks of these technologies are the short term of storage, intensive demand of energy, and requirement of highly selective catalysis processes due to the low chemical activity and high thermodynamic stability of CO<sub>2</sub> in addition to the short term of storage [13].

Transformation	Main products
Chemical (nonhydrogenative)	Carbamates, carbonates, urea, carboxylates
Chemical (hydrogenative)	HCOOH, hydrocarbons, MeOH, EtOH
Photochemical or electrochemical	CO, CH <sub>4</sub> , MeOH, HCOOH
Reforming	CO + H <sub>2</sub>
Biological	Sugar, EtOH, CH <sub>3</sub> COOH
Inorganic	M <sub>2</sub> CO <sub>3</sub>

**Table 1.** Types of chemical transformations of carbon dioxide.



**Scheme 1.** General patterns of the chemical transformations of CO<sub>2</sub>.



**Scheme 2.** The major chemical transformations of CO<sub>2</sub>.

The recent advances in all fields of catalysis (organocatalysis, photocatalysis, palladium catalysis, etc.) [14–18] were paralleled by important progress in the transformations of CO<sub>2</sub>, particularly in *electrochemical* and *photochemical reductions* and *reforming* in both its catalytic and nonthermal plasma techniques. The design of new efficient electro- and photocatalysts consequently reflects on ameliorating the selectivity and decreasing the inherent energy requirement by using renewable sources such as solar energy.

The electrochemical and photochemical reductions of CO<sub>2</sub> involve varied experimental approaches, but they have essentially similar nature. They both rely on external energy stimulus to activate the chemically inert CO<sub>2</sub> and effectuate a thermodynamically uphill reaction. Furthermore, the surface charge transfer step in the photocatalytic reduction of CO<sub>2</sub> is indeed an electrochemical process and is generally promoted by adding a cocatalyst (electrocatalyst).

Both processes can proceed *via* transfer of 2, 4, 6, 8, 12, or more electrons depending on the nature of the employed catalyst and the experimental conditions, and they hence yield various products as mentioned before.

#### 4.3.1. Electrochemical reduction of $\text{CO}_2$

The kinetics of the electrochemical reduction is sluggish due to the reorganization of the linear  $\text{CO}_2$  molecule into more active bent form, which creates overpotential to the first electron transfer after the adsorption of the molecule onto the working electrode. This step is mostly identified as the rate-determining step initiating at  $-1.9$  V, and it forms  $\text{CO}_2^{\bullet-}$  anion radical that is further protonated into  $\text{HCOO}^{\bullet}$  or  $\text{HOOC}^{\bullet}$  and reduced into  $\text{HCOO}^-$  (formate) or  $\text{CO}$ , respectively. The majority of electrochemical reductions of  $\text{CO}_2$  produce  $\text{HCOOH}$  or  $\text{CO}$  as primary products. Very few electrocatalysts (e.g., Cu) ensure the further reduction of  $\text{CO}$  into hydrocarbons, but without an elucidated mechanism till now. Various electrolytic materials have been investigated in the  $\text{CO}_2$  reduction processes including metals (Sn, Pd, Cu, Pt, etc.), layered transition metal dichalcogenides (e.g.,  $\text{WS}_2$ ,  $\text{MoSe}_2$ , and  $\text{MoS}_2$ ), and heteroatom-functionalized carbonaceous catalysts such as N-doped carbon nanofibers and graphene quantum dots [19].

#### 4.3.2. Photochemical reduction of $\text{CO}_2$

The photocatalytic reduction of  $\text{CO}_2$  has been widely studied using different semiconductors of the following types: metal oxides, sulfides, or nitrides, layered metal materials like layered double hydroxide, metal-organic frameworks, and metal-free carbonaceous materials such as graphitic carbon nitride. The photocatalytic reduction can be summarized into five steps:

- Absorption of photons by the semiconductor photocatalyst generating the hole and electron pairs.
- Charge separation of the generated electrons and holes.
- $\text{CO}_2$  adsorption and transfer of electrons to the  $\text{CO}_2$  molecules.
- Surface redox reaction involving the reduction of the  $\text{CO}_2$  and the oxidation of the common reductants such as  $\text{H}_2\text{O}$  and  $\text{H}_2$ .
- Desorption of the products [19, 20].

#### 4.3.3. $\text{CO}_2$ reforming with methane

Lastly, reforming of  $\text{CO}_2$  and  $\text{CH}_4$  into syngas (mixture of  $\text{H}_2/\text{CO}$ ) can be performed by catalytic and nonthermal plasma methods or by the novel hybrid technique combining both. Catalytic methods still suffer from high thermal energy consumption, catalyst deactivation by coke deposition, and high costs. Selected examples of catalysts for reforming process are Pt, Pd, Ir, Rh, Ru, Co, and Ni. The general mechanism of the dry methane reforming (DRM) involves the adsorption of  $\text{CO}_2$  and  $\text{CH}_4$  onto the catalyst followed by dissociation of the



molecules into CO, and O, C, and H atoms. The atoms recombine forming additional CO molecule and H<sub>2</sub> gas, followed by desorption of the gases where the CO desorption constitutes the rate-determining step in the process.

Nonthermal plasma relies on electronic energy. Electrons are accelerated by an external electric field to collide with CO<sub>2</sub> and CH<sub>4</sub> transferring their energy to induce the dissociation of the molecules when the energy exceeds 4.5 and 8.8 eV, respectively. The dissociation generates radicals and more active species, which reform the CO and H<sub>2</sub> products. The main characteristic of this method is the low selectivity since the radicals can reform into side products such as hydrocarbons [4].

#### 4.4. Biofuels from microalgae

The photosynthetic microorganisms (e.g., microalgae) constitute future alternative energy sources to fossil fuels and can serve to fix CO<sub>2</sub> directly from waste streams, decreasing the high existing levels. Microalgae can transform solar energy into chemical forms *via* photosynthesis and possess faster growth rate than plants. They can be cultivated in diverse environments as open or closed ponds and photobioreactors with minimum requirement of nutrients. After cultivation, the biomass content is harvested, dried, and converted into fuels by thermochemical (e.g., pyrolysis) or biochemical (e.g., fermentation) processes. The limited cultivation areas and the costs of the harvesting stage are still burdening the large-scale routes of this prospective CO<sub>2</sub> utilization [21].

### 5. Maturity of carbon dioxide technologies

The carbon dioxide technologies that have been described in this perspective can be recapitulated based on their maturity for industrial employment as follows.

- “*Mature market*,” such as gas separation and transport, EOR, and industrial transformations to chemicals like urea.
- “*Economically feasible*,” such as pre- and postconversion capture.
- “*Demonstration phase*,” such as oxy-fuel combustion and ECBM.
- “*Research phase*,” such as mineral carbonation and ocean storage.

### 6. Conclusion

This chapter introduced the basic properties of carbon dioxide that are used to develop the technologies for its utilization or storage in order to help in mitigating its global warming effects. The major sources of CO<sub>2</sub> emissions were outlined and the carbon capture storage and utilization (CCS and CCU) technologies were discussed. The chemical transformations of CO<sub>2</sub>

were given particular emphasis as tools to reduce the high CO<sub>2</sub> levels and to understand the chemistry of CO<sub>2</sub>. Within that aspect, the electrochemical and photochemical reductions and the reforming of CO<sub>2</sub> with methane were especially described. The chapter was concluded by the classification of the storage and utilization technologies according to their maturity in the market.

## Author details

Janah Shaya<sup>1</sup>, Hassan Srour<sup>2,3</sup> and Iyad Karamé<sup>2\*</sup>

\*Address all correspondence to: iyad.karameh@ul.edu.lb

1 Institut de Physique et Chimie des Matériaux (IPCMS), UMR 7504, CNRS-Université de Strasbourg, Strasbourg, France

2 Laboratory of Catalysis Organometallic and Materials (LCOM), Faculty of Sciences I, Lebanese University, Beirut, Lebanon

3 Department of Chemistry, Faculty of Sciences V, Lebanese University, Nabatieh, Lebanon

## References

- [1] North M. Chapter 1—What is CO<sub>2</sub>? Thermodynamics, basic reactions and physical chemistry. Harvard & Vancouver: Elsevier B.V.; 2015. pp. 3-17. DOI: 10.1016/B978-0-444-62746-9.00001-3
- [2] Yun Y. Recent Advances in Carbon Capture and Storage. Rijeka: Intech Open; 2017. DOI: 10.5772/62966
- [3] Llamas B. Greenhouse Gases. Rijeka: Intech Open; 2016. ISBN: 978-953-51-2273-9
- [4] Cuéllar-Franca RM, Azapagic A. Carbon capture, storage and utilisation technologies: A critical analysis and comparison of their life cycle environmental impacts. *Biochemical Pharmacology*. 2015;**9**:82-102. DOI: 10.1016/j.jcou.2014.12.001
- [5] Mostofa KMG, Liu C-Q, Zhai W, et al. Reviews and syntheses: Ocean acidification and its potential impacts on marine ecosystems. *Biogeosciences*. 2016;**13**(6):1767-1786. DOI: 10.5194/bg-13-1767-2016
- [6] Karamé I. Hydrogenation. Rijeka: Intech Open; 2012. DOI: 10.5772/3208
- [7] Karamé I. Green Chemical Processing and Synthesis. Rijeka: Intech Open; 2012. DOI: 10.5772/65562
- [8] Koornneef J, Van T, Van A, Ramirez A. Carbon Dioxide Capture and Air Quality. Rijeka: InTech; 2011. DOI: 10.5772/18075

- [9] Romanov V, Soong Y, Carney C, Rush GE, Nielsen B, O'Connor W. Mineralization of carbon dioxide: A literature review. *ChemBioEng Reviews*. 2015;**2**(4):231-256. DOI: 10.1002/cben.201500002
- [10] Bhanage BM, Arai M. Transformation and Utilization of Carbon Dioxide. Berlin: Springer Science & Business Media; 2014. ISBN: 978-3-642-44988-8
- [11] Styring P, Quadrelli E-S, Armstrong K. Carbon Dioxide Utilisation: Closing the Carbon Cycle. 1st ed. Elsevier; 2014. ISBN: 9780444627483
- [12] Centi G, Perathoner S. Green Carbon Dioxide: Advances in CO<sub>2</sub> Utilization. Hoboken, New Jersey: John Wiley & Sons Inc.; 2014. ISBN: 978-1-118-59088-1
- [13] Sakakura T, Choi J-C, Yasuda H. Transformation of carbon dioxide. *Chemical Reviews*. 2007;**107**(6):2365-2387. DOI: 10.1021/cr068357u
- [14] Karamé I. Recent Advances in Organocatalysis. Rijeka: Intech Open; 2016. DOI: 10.5772/61548
- [15] Chen C-C, Shaya J, Fan H-J, Chang Y-K, Chi H-T, Lu C-S. Silver vanadium oxide materials: Controlled synthesis by hydrothermal method and efficient photocatalytic degradation of atrazine and CV dye. *Separation and Purification Technology*. 2018;**206**:1-16. DOI: 10.1016/j.seppur.2018.06.011
- [16] Huang S, Chen C, Tsai H, Shaya J, Lu C. Photocatalytic degradation of thiobencarb by a visible light-driven MoS<sub>2</sub> photocatalyst. *Separation and Purification Technology*. 2018;**197**:147-155. DOI: 10.1016/j.seppur.2018.01.009
- [17] Shaya J, Deschamps M-A, Michel BY, Burger A. Air-stable Pd catalytic systems for sequential one-pot synthesis of challenging unsymmetrical aminoaromatics. *The Journal of Organic Chemistry*. 2016;**81**(17):7566-7573. DOI: 10.1021/acs.joc.6b01248
- [18] Shaya J, Fontaine-Vive F, Michel BY, Burger A. Rational design of push-pull fluorene dyes: Synthesis and structure-photophysics relationship. *Chemistry - A European Journal*. 2016;**22**(30):10627-10637. DOI: 10.1002/chem.201600581
- [19] Wu J, Huang Y, Ye W, Li Y. CO<sub>2</sub> reduction: From the electrochemical to photochemical approach. *Advancement of Science*. 2017;**4**(11):1700194-1700129. DOI: 10.1002/adv.201700194
- [20] Karamian E, Sharifnia S. On the general mechanism of photocatalytic reduction of CO<sub>2</sub>. *Biochemical Pharmacology*. 2016;**16**:194-203. DOI: 10.1016/j.jcou.2016.07.004
- [21] Milano J, Ong HC, Masjuki HH, et al. Microalgae biofuels as an alternative to fossil fuel for power generation. *Renewable and Sustainable Energy Reviews*. 2016;**58**(C):180-197. DOI: 10.1016/j.rser.2015.12.150



# Catalytic Transformations of CO<sub>2</sub>: Reduction and Reforming

---



---

# Electrochemical/Photochemical CO<sub>2</sub> Reduction Catalyzed by Transition Metal Complexes

---

Hitoshi Ishida

Additional information is available at the end of the chapter

<http://dx.doi.org/10.5772/intechopen.75199>

---

## Abstract

Conversion of CO<sub>2</sub> into useful chemicals is attractive as a solution of the fossil fuel shortage and the global warming problems. Reduction of CO<sub>2</sub> into carbon monoxide (CO) and formic acid (HCOOH) is also important for obtaining the materials in organic syntheses. There are a lot of studies on the catalysts for electrochemical/photochemical CO<sub>2</sub> reduction. Especially, transition metal complexes have actively researched as the molecular catalysts for CO<sub>2</sub> reduction. In this chapter, the electrochemical/photochemical CO<sub>2</sub> reduction catalyzed by *cis*-[Ru(bpy)<sub>2</sub>(CO)<sub>2</sub>]<sup>2+</sup> (bpy: 2,2'-bipyridine) and *trans*(Cl)-[Ru(bpy)<sub>2</sub>(CO)<sub>2</sub>Cl<sub>2</sub>] is described as a representative example.

**Keywords:** CO<sub>2</sub> reduction, artificial photosynthesis, electrochemistry, photochemistry, ruthenium

---

## 1. Introduction

Utilization of CO<sub>2</sub> becomes more and more important with increasing CO<sub>2</sub> emission which causes the global warming and the ocean acidification problems [1, 2]. The huge CO<sub>2</sub> emission also relates on depletion of fossil fuels. The conversion of CO<sub>2</sub> into useful fuels and chemicals is very urgent to solve the abovementioned problems. The use of biomass instead of fossil fuels is actively researched and partly undertaken [3]. In many chemical laboratories, fixation of CO<sub>2</sub> into organic compounds by organometallic catalysts is vigorously studied [4].

Reduction of CO<sub>2</sub> with electrons is an attractive chemical conversion to obtain the useful products for fuels and chemical materials. It is so simple that it can be applied to photocatalyses which supply electrons from electron donors such as water. The equilibrium potentials (E<sup>0</sup> V vs. SHE

---

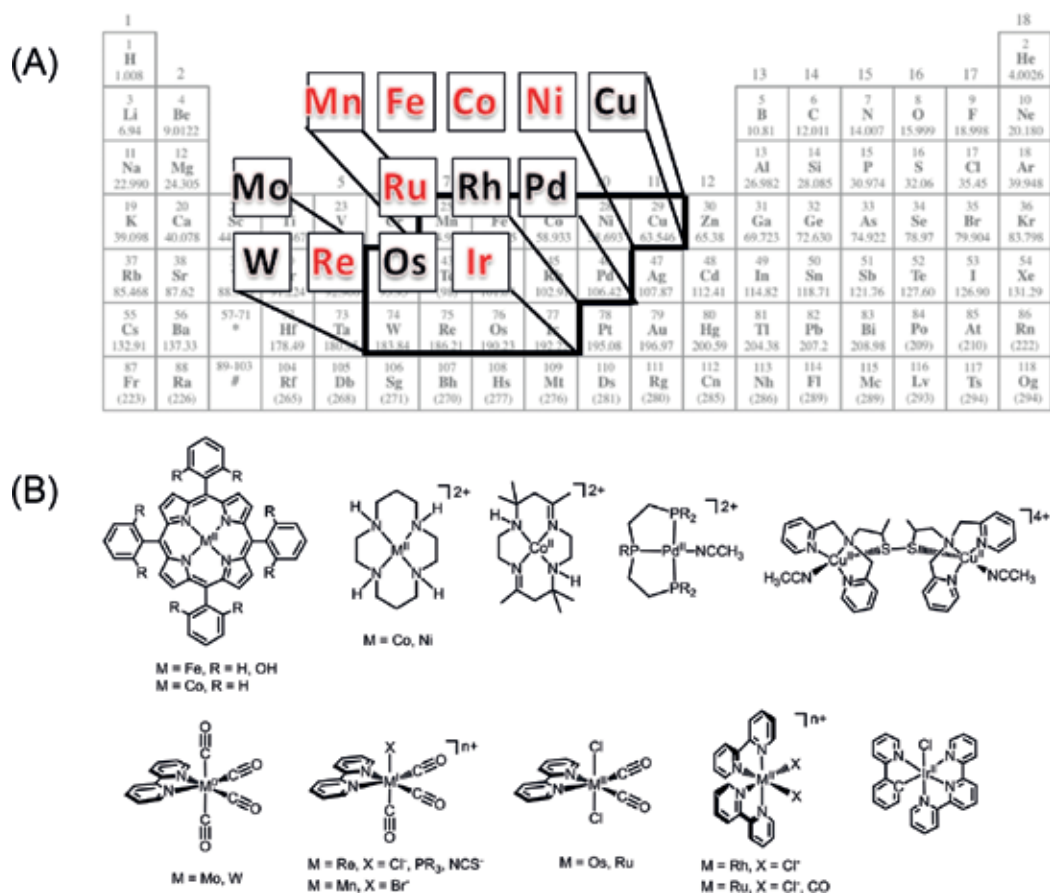
at pH 7) for CO<sub>2</sub> reduction are listed in **Figure 1** [5, 6]; they are thermodynamic values and tend to positively shift with increasing the numbers of electrons participated. One-electron reduction of CO<sub>2</sub> requires very high energy. Furthermore, the product, CO<sub>2</sub> anion radical (CO<sub>2</sub><sup>•-</sup>), is difficult to give useful organic chemicals because it is a very strong reducing reagent to reduce other molecules and recover CO<sub>2</sub>. Thus, the CO<sub>2</sub> reductions with multielectrons are desired; however, their reactions are generally difficult even in the electrochemical reduction. A reason is that the intermediates would release from the surface of the electrode as the products before accepting further electrons. To achieve CO<sub>2</sub> reduction with more than two electrons, the catalysts which allow to lower the activation energies are required. In other words, the catalysts can undergo the CO<sub>2</sub> reduction at the potentials closed to the equilibrium ones. The two-electron reduction of CO<sub>2</sub> produces carbon monoxide (CO) and formic acid (HCOOH). The equilibrium potentials are more negative than the proton reduction to afford H<sub>2</sub>. Therefore, the catalysts which can selectively reduce CO<sub>2</sub> rather than H<sup>+</sup> are also desired. Both CO and HCOOH are useful chemicals: CO can be converted into liquid hydrocarbons by using the Fischer-Tropsch reaction [7], and HCOOH which can be readily converted to H<sub>2</sub> is a safe storage material for H<sub>2</sub> [8].

A lot of metal complexes have been researched for the CO<sub>2</sub> reduction catalyses [9–16]. Until now, the metal complexes of Mn [17–19], Fe [20, 21], Co [22–24], Ni [24–28], Cu [29], Mo [30], Ru [31–64], Rh [65, 66], Pd [67, 68], W [30], Re [69–76], Os [77, 78], Ir [65, 66, 79, 80] have been reported as the catalysts for CO<sub>2</sub> reduction. **Figure 2A** shows the elements of the metal complexes acting as the electrochemical CO<sub>2</sub> reduction catalysts. The metal complexes indicated in red include the catalysts for photochemical reduction. **Figure 2B** shows the examples of the metal complexes as the CO<sub>2</sub> reduction catalysts. These catalysts based on metal complexes are sometimes called as “molecular catalysts” because they can be designed on the molecular levels by selecting the metal elements and the ligands. The representative and efficient catalysts for CO<sub>2</sub> reduction are nickel(II) cyclam (cyclam: 1,4,8,11-tetraazacyclotetradecane),

				<i>E</i> <sup>0'</sup>
CO <sub>2</sub>	+	e <sup>-</sup>	→	CO <sub>2</sub> <sup>•-</sup> -1.90 V
CO <sub>2</sub>	+	2 H <sup>+</sup>	+	2 e <sup>-</sup> →     HCOOH     -0.61 V
CO <sub>2</sub>	+	2 H <sup>+</sup>	+	2 e <sup>-</sup> →     CO + H <sub>2</sub> O     -0.52 V
CO <sub>2</sub>	+	4 H <sup>+</sup>	+	4 e <sup>-</sup> →     HCHO + H <sub>2</sub> O     -0.48 V
CO <sub>2</sub>	+	6 H <sup>+</sup>	+	6 e <sup>-</sup> →     CH <sub>3</sub> OH + H <sub>2</sub> O     -0.38 V
CO <sub>2</sub>	+	8 H <sup>+</sup>	+	8 e <sup>-</sup> →     CH <sub>4</sub> + 2H <sub>2</sub> O     -0.24 V
2 H <sup>+</sup>	+	2 e <sup>-</sup>	→	H <sub>2</sub> -0.41 V

**Figure 1.** Equilibrium potentials for CO<sub>2</sub> reduction (*E*<sup>0'</sup> V vs. SHE (pH 7)).





**Figure 2.** Metal complexes reported as CO<sub>2</sub> reduction catalysts: (A) the metal elements in the complexes (the elements in the metal complexes for photocatalyses are indicated in red) and (B) the molecular structures.

ruthenium(II) polypyridyl carbonyl complexes and rhenium(I) bipyridyl tricarbonyl complexes. Recently, the complexes with nonprecious metals such as manganese(II) and iron(II) attract much attention. They are abundant and readily available, while they are less durable and efficient as the disadvantageous points.

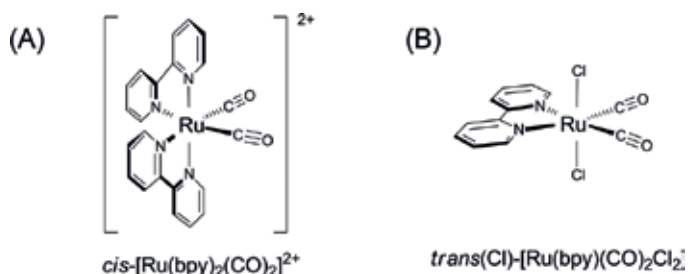
In this chapter, the electrochemical CO<sub>2</sub> reduction catalyzed by the ruthenium complexes as the examples is described. The reduction products are CO and formic acid, while the nickel and rhenium complexes selectively yield CO. Discussion for the catalytic mechanisms is introduced particularly for the factors determining the product selectivity. In the next section, the photocatalytic CO<sub>2</sub> reduction assisting by the photosensitizers is described. The reaction procedures, the principles for selecting the photosensitizers and the electron donors, and the photocatalytic mechanisms are summarized. Furthermore, application of the homogeneous catalytic systems to heterogeneous catalyses, which is practically advantageous in the viewpoints of separation of the catalysts from the reactants and the products, is described. In the final section, the artificial photosynthetic systems, which would be realized by utilizing the molecular catalysts, are prospected.

## 2. Electrochemical CO<sub>2</sub> reduction

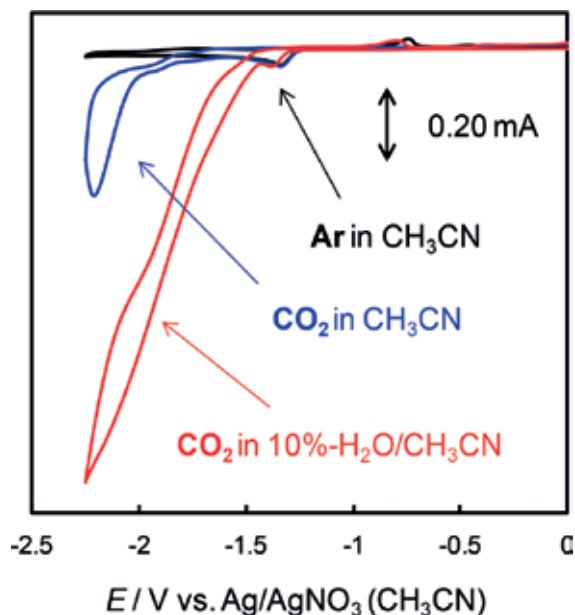
The representative molecular catalysts based on ruthenium complexes are *cis*-[Ru(bpy)<sub>2</sub>(CO)<sub>2</sub>]<sup>2+</sup> (bpy: 2,2'-bipyridine), *trans*(Cl)-[Ru(bpy)(CO)<sub>2</sub>Cl<sub>2</sub>] and the derivatives (**Figure 3**). They have the bipyridyl ligand which would act as an electron reservoir. The efficient catalysts have the carbonyl ligand, which would draw electrons. It tends to lower the reduction potentials of the metal complexes as well as to lower the overpotentials for the CO<sub>2</sub> reduction.

### 2.1. Electrochemical analysis

Electrochemical analyses (e.g., cyclic voltammetric measurements) are recommended to know the electrochemical properties of the molecular catalysts. The analyses do not only teach us the reduction potentials of the metal complexes but also show whether the complexes can react with CO<sub>2</sub> or not. **Figure 4** shows the cyclic voltammograms (CVs) of *cis*-[Ru(bpy)<sub>2</sub>(CO)<sub>2</sub>]<sup>2+</sup> in CH<sub>3</sub>CN or CH<sub>3</sub>CN/H<sub>2</sub>O (9:1). The Ag-Ag<sup>+</sup> (CH<sub>3</sub>CN) reference electrode (0.10 M Tetrabutylammonium perchlorate (TBAP) /0.01 M AgNO<sub>3</sub> in CH<sub>3</sub>CN) is used; the potential (0.00 V vs. Ag/AgNO<sub>3</sub> (CH<sub>3</sub>CN)) corresponds to -0.09 V vs. Fc/Fc<sup>+</sup> in CH<sub>3</sub>CN. The CV of *cis*-[Ru(bpy)<sub>2</sub>(CO)<sub>2</sub>]<sup>2+</sup> in CH<sub>3</sub>CN under Ar shows an irreversible reduction wave at -1.3 V vs. Ag-Ag<sup>+</sup> (CH<sub>3</sub>CN) as shown in **Figure 4** (black line). The irreversible reduction suggests that the one-electron reduction accompanies with a chemical reaction followed by further one-electron reduction. Such a reaction mechanism is called as electrochemical-chemical-electrochemical (ECE) one. The CV under CO<sub>2</sub> is a little different from that under Ar, suggesting that the reduced species react with CO<sub>2</sub> (**Figure 4**, blue line). In CH<sub>3</sub>CN/H<sub>2</sub>O (9:1), the CV exhibits a strong cathodic current under CO<sub>2</sub> (**Figure 4**, red line), which corresponds to the catalytic reduction of CO<sub>2</sub> in the presence of a proton source such as water. The catalytic reduction currents can be analyzed to estimate the efficiency of the catalyst [20, 81]; however, it should be noted that the cathodic currents do not always exhibit the catalytic CO<sub>2</sub> reduction [82]. The electrolyses of the metal complexes under CO<sub>2</sub> should be carried out to confirm the catalytic efficiency.



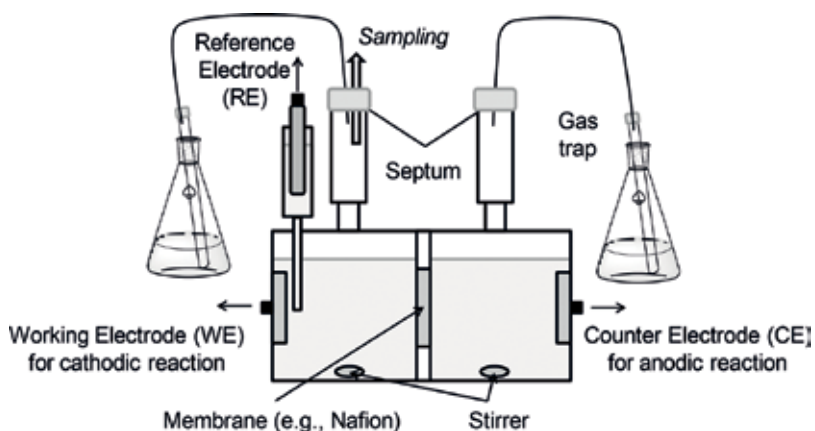
**Figure 3.** Ruthenium-bipyridyl complexes as electrochemical CO<sub>2</sub> reduction catalysts: (A) *cis*-[Ru(bpy)<sub>2</sub>(CO)<sub>2</sub>]<sup>2+</sup> and (B) *trans*(Cl)-[Ru(bpy)(CO)<sub>2</sub>Cl<sub>2</sub>].



**Figure 4.** Cyclic voltammograms of *cis*-[Ru(bpy)<sub>2</sub>(CO)<sub>2</sub>](PF<sub>6</sub>)<sub>2</sub>: In Ar (black) or CO<sub>2</sub>-saturated CH<sub>3</sub>CN (blue) or in CO<sub>2</sub>-saturated CH<sub>3</sub>CN/H<sub>2</sub>O (9:1) (red) containing NBu<sub>4</sub>ClO<sub>4</sub> (0.10 M).

## 2.2. Electrolysis

A typical electrolysis cell is shown in **Figure 5**. The cell for reduction (the side of the working electrode) is separated from the cell for oxidation (the counter electrode) with a membrane such as Nafion. A glassy carbon or a Pt plate is used for the electrodes. The metal complex is dissolved in the reaction solution and acts as the homogenous catalyst. CO<sub>2</sub> is bubbled

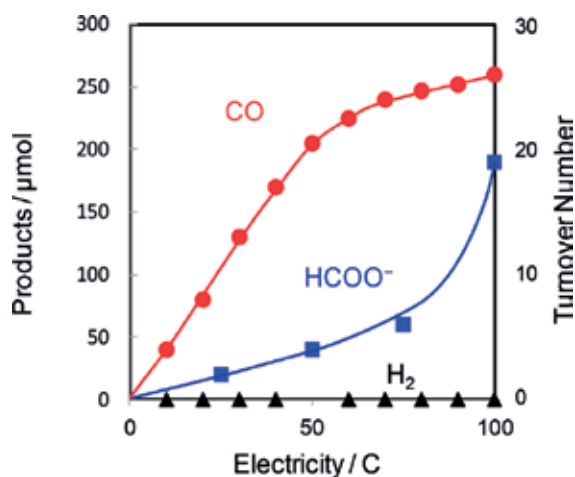


**Figure 5.** Electrolysis cell for electrochemical CO<sub>2</sub> reduction.

with a needle through the septum before electrolysis. Electrochemical  $\text{CO}_2$  is carried out in batch mode. Reduction of  $\text{CO}_2$  occurs on the working electrode at the electrochemical cell. Sampling of the gaseous and liquid phases is performed by a syringe through the septum. The gaseous products ( $\text{CO}$  and  $\text{H}_2$ ) are analyzed by gas chromatography. The liquid product,  $\text{HCOOH}$ , is analyzed by electrophoresis, ion chromatography or gas chromatography. The electrolysis is carried out by the controlled potential method, where the potential is determined from the electrochemical analysis (e.g., CVs). The chronopotentiometry, in which the current is constant during the electrolysis, is important for the industrial use. However, the results in the constant potential lead to elucidate the catalyses because the electrolysis potential relates on the catalytic species. Thus, almost all the scientific researches adopt the controlled potential electrolyses.

### 2.3. Electrocatalytic $\text{CO}_2$ reduction by $\text{cis-}[\text{Ru}(\text{bpy})_2(\text{CO})_2]^{2+}$

The ruthenium complexes are used as the homogeneous catalysts by dissolving in the reaction solution. The electrolysis of the  $\text{CO}_2$ -saturated  $\text{H}_2\text{O}/\text{DMF}$  (1:1) solution of  $\text{cis-}[\text{Ru}(\text{bpy})_2(\text{CO})_2]^{2+}$  was carried out at  $-1.50$  V vs. SCE with an Hg pool as the working electrode (Figure 6) [62]. The catalyst could selectively reduce  $\text{CO}_2$  to afford  $\text{CO}$  and  $\text{HCOOH}$ , while  $\text{H}_2$ , the reduction product of water, scarcely evolved. As the reaction proceeded, the speed for  $\text{CO}$  production got slow, but  $\text{HCOOH}$  production became fast. It was interpreted as the result of the decreasing the proton concentration ( $[\text{H}^+]$ ) in the reaction solution by consumption of the proton during the reduction. Actually, the reactions in the buffered solution with  $\text{H}_3\text{PO}_4\text{-NaOH}$  exhibited that the production speeds of the  $\text{CO}_2$  reduction were unchanged during the reactions. It was the decisive result that  $\text{HCOOH}$  selectively produced when phenol with the high pKa (ca. 9.95) was used as the proton source. These results suggest that there is an acid-base equilibrium between two intermediates in which one is for  $\text{CO}$  production and another for  $\text{HCOOH}$ .



**Figure 6.** Plots of the amounts of products vs. the electricity in the electrolysis ( $-1.50$  V vs. SCE) of  $\text{CO}_2$ -saturated  $\text{H}_2\text{O}/\text{DMF}$  (1:1 v/v) solution containing  $\text{cis-}[\text{Ru}(\text{bpy})_2(\text{CO})_2](\text{PF}_6)_2$  ( $5.0 \times 10^{-4}$  M) and  $\text{LiCl}$  (0.10 M) as the supporting electrolyte at room temperature.

Thus, the mechanism involving the equilibrium among the carbonyl complex  $[\text{Ru}(\text{bpy})_2(\text{CO})_2]^{2+}$ , the carboxylic acid complex  $[\text{Ru}(\text{bpy})_2(\text{CO})(\text{C}(\text{O})\text{OH})]^+$  and the CO<sub>2</sub> adduct complex  $[\text{Ru}(\text{bpy})_2(\text{CO})(\text{CO}_2)]$  was proposed for the catalytic CO<sub>2</sub> reduction (Figure 7, left cycle) [58, 62]. All the complexes were isolated, and the crystal structures were characterized [83]. In the mechanism,  $[\text{Ru}(\text{bpy})_2(\text{CO})_2]^{2+}$  is reduced to yield the coordinated unsaturated species  $[\text{Ru}(\text{bpy})_2(\text{CO})]$  with evolving CO. The five coordinated complex reacts with CO<sub>2</sub> to afford the  $\eta^1\text{-CO}_2$  adduct complex,  $[\text{Ru}(\text{bpy})_2(\text{CO})(\text{CO}_2)]$ , in which CO<sub>2</sub> coordinates to the metal center at the carbon atom. The electronic structure of the CO<sub>2</sub> bound complex still remains unknown. In the original report [62], it is drawn as  $[\text{Ru}(\text{bpy})_2(\text{CO})(\text{COO}^-)]^+$  in which as electron localizes on the CO<sub>2</sub> ligand. In Figure 7, it is drawn as  $[\text{Ru}(\text{bpy})_2(\text{CO})(\text{CO}_2)]^0$  which is the resonance structure of  $[\text{Ru}(\text{bpy})_2(\text{CO})(\text{COO}^-)]^+$ . The CO<sub>2</sub> adduct complex is protonated to give the carboxylic acid complex  $[\text{Ru}(\text{bpy})_2(\text{CO})(\text{C}(\text{O})\text{OH})]^+$  and further protonated to recover the carbonyl complex  $[\text{Ru}(\text{bpy})_2(\text{CO})_2]^{2+}$ . The carboxylic acid complex could be reduced to yield HCOOH, and the carbonyl complex to produce CO. The proposed idea reasonably elucidates the experimental results that the catalytic CO<sub>2</sub> reduction gives CO and HCOOH under protic and less protic conditions, respectively. This idea is also supported by the result that the ruthenium complex derivatives give the CO/HCOO<sup>-</sup> selectivity depending on the different equilibrium constants [58]. The carbonyl complex reacts with dimethylamine to afford the carbamoyl complex  $[\text{Ru}(\text{bpy})_2(\text{CO})(\text{C}(\text{O})\text{N}(\text{CH}_3)_2)]^+$ , and the electrochemical CO<sub>2</sub> reduction in the presence of dimethylamine produces *N,N*-dimethylformamide (DMF) [84]. It is also an evidence which the carbonyl complex would exist in the catalysis.

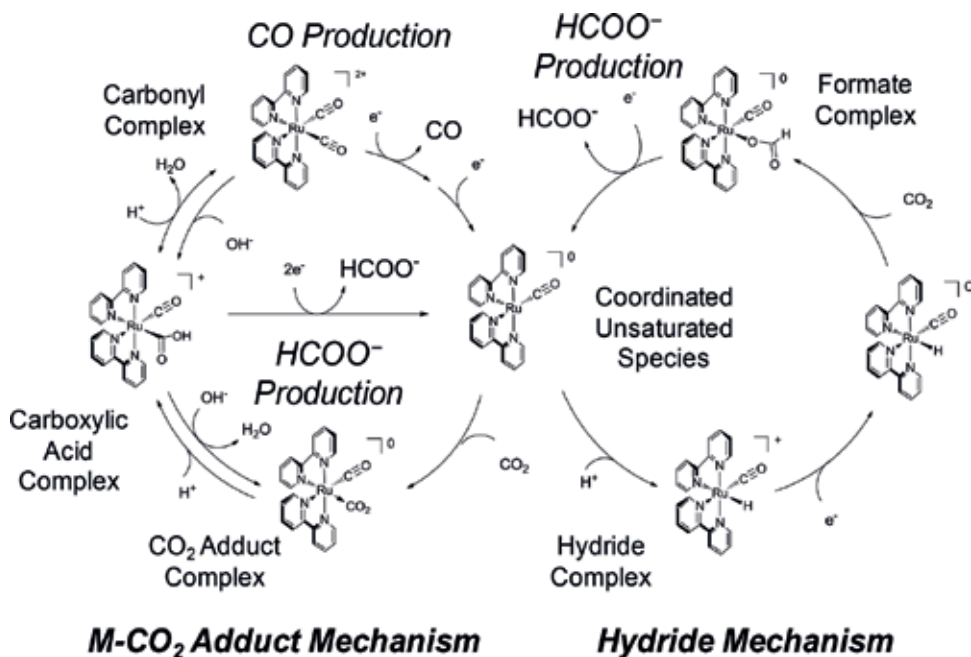


Figure 7. Two proposed mechanisms for CO<sub>2</sub> reduction catalyzed by *cis*-[Ru(bpy)<sub>2</sub>(CO)X]<sup>n+</sup> (X = CO (n = 2); H (n = 1)); Metal-CO<sub>2</sub> adduct mechanism and hydride mechanism.

On the other hand, the ruthenium hydride complex  $[\text{Ru}(\text{bpy})_2(\text{CO})\text{H}]^+$  is known to react with  $\text{CO}_2$  to yield the formate complex  $[\text{Ru}(\text{bpy})_2(\text{CO})(\text{OC}(\text{O})\text{H})]^+$  [85]. In the conversion,  $\text{CO}_2$  is inserted into the Ru-H bond. The formate complex can release formate ion ( $\text{HCOO}^-$ ) and is considered to be an intermediate for  $\text{HCOO}^-$  production. Based on the results, the hydride mechanism is proposed (Figure 7, right cycle). In the mechanism, the coordinated unsaturated species  $[\text{Ru}(\text{bpy})_2(\text{CO})]$  does not react with  $\text{CO}_2$  but a proton to yield the hydride complex. The hydride mechanism reasonably explains the  $\text{CO}_2$  reduction to produce  $\text{HCOO}^-$ . However, it has a couple of problems [16]. One is that the mechanism is difficult to elucidate the CO production. Production of  $\text{HCOO}^-$  may occur through the hydride mechanism, while CO may produce through the M- $\text{CO}_2$  adduct mechanism. In this case, the product selectivity ( $\text{CO}/\text{HCOO}^-$ ) should be controlled by the reactivity difference between CO and  $\text{H}^+$  with the coordinated unsaturated complex. Under the protic conditions, the selectivity of  $\text{HCOO}^-$  production should be enhanced; however, the selectivity of the catalyses gives the opposite tendency. Thus, the pH in the solution or the pKa value of the proton source dependence on the electrochemical  $\text{CO}_2$  reduction cannot be explained. Another is that the ruthenium catalyst does not evolve  $\text{H}_2$  so much in the  $\text{CO}_2$  reduction. It suggests that the catalyst intermediate strongly binds with  $\text{CO}_2$  rather than  $\text{H}^+$ .

Nevertheless, the hydride mechanism is supported by many researchers. It is because there are many research works on the  $\text{CO}_2$  insertion into Metal-H bonds to afford the corresponding metal formate complexes. On the other hand, the research works on the carboxylic acid complex are fewer, and no mechanical pathways of  $\text{HCOO}^-$  production from the carboxylic acid complex are not understood on the molecular levels.

#### 2.4. Electrocatalytic $\text{CO}_2$ reduction by *trans*(Cl)- $[\text{Ru}(\text{bpy})(\text{CO})_2\text{Cl}_2]$

*Trans*(Cl)- $[\text{Ru}(\text{bpy})(\text{CO})_2\text{Cl}_2]$  is known to be an efficient catalyst for electrochemical  $\text{CO}_2$  reduction [58]. The catalytic activity and the product selectivity are similar as these of *cis*- $[\text{Ru}(\text{bpy})_2(\text{CO})_2]^{2+}$ . Reduction of *trans*(Cl)- $[\text{Ru}(\text{bpy})(\text{CO})_2\text{Cl}_2]$  induces to release  $\text{Cl}^-$  ion to afford the coordinated unsaturated complex. This complex is considered to an intermediate which can bind with  $\text{CO}_2$ ; however, it induces polymerization in the absence of  $\text{CO}_2$  as shown in Figure 8 [86, 87]. The polymer with Ru(0)-Ru(0) bonds is also an efficient electrocatalyst for  $\text{CO}_2$  reduction [50, 54]. The complex is electrochemically reduced to polymerize on the cathode electrode. The electrode modified with the polymer is moved to another electric cell, and it works in the presence of  $\text{CO}_2$  as the active electrode for electrochemical  $\text{CO}_2$  reduction. Researches to make

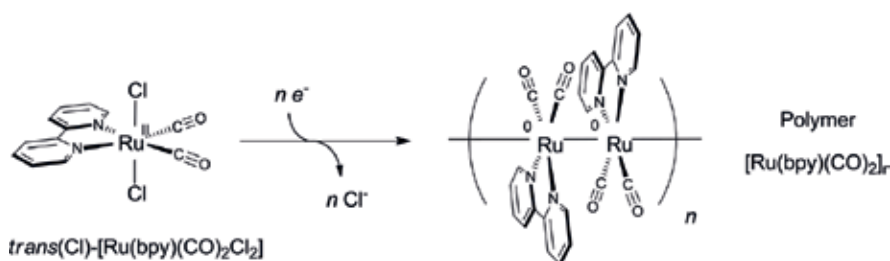
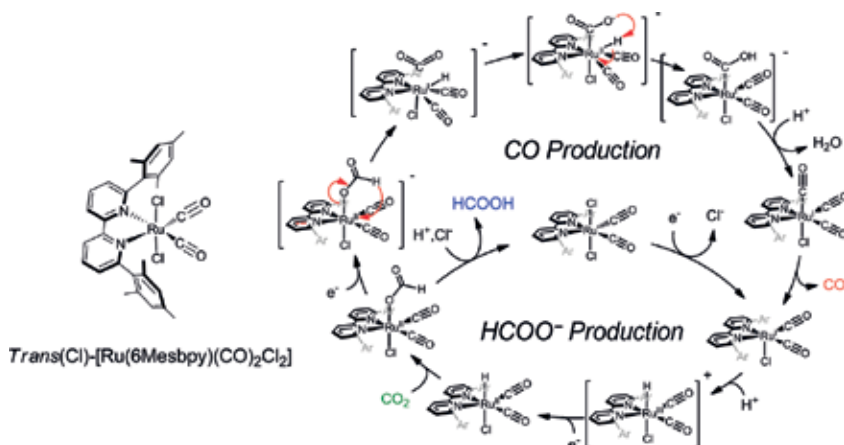


Figure 8. Electroreductive polymerization of *trans*(Cl)- $[\text{Ru}(\text{bpy})(\text{CO})_2\text{Cl}_2]$ .



**Figure 9.** A proposed mechanism of electrochemical CO<sub>2</sub> reduction catalyzed by *trans*(Cl)-[Ru(6Mesbpy)(CO)<sub>2</sub>Cl<sub>2</sub>].

the modified electrode stable have been actively done: introduction of pyrrole groups to the bipyridyl ligand also yields pyrrole polymers to stabilize the ruthenium polymer.

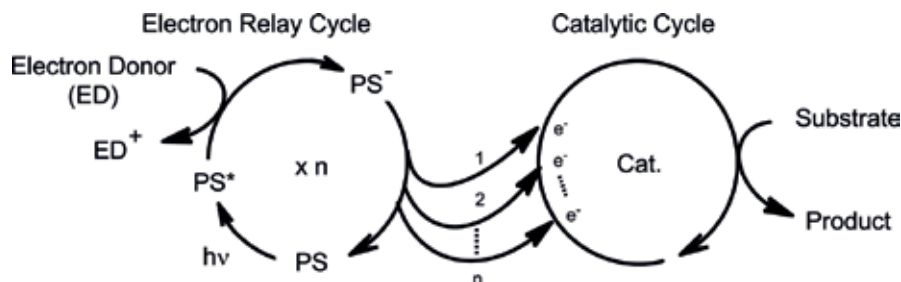
The catalytic reaction mechanisms are also unknown but are considered similar as these of *cis*-[Ru(bpy)<sub>2</sub>(CO)<sub>2</sub>]<sup>2+</sup>. Machan et al. reported the electrochemical CO<sub>2</sub> reduction catalyzed by *trans*(Cl)-[Ru(6Mesbpy)(CO)<sub>2</sub>Cl<sub>2</sub>], which has two bulky groups at 6,6'-positions in 2,2'-bipyridine [35]. The complex does not polymerize because of the steric hindrance. They discussed the reaction mechanisms based on the hydride mechanism (**Figure 9**). The precursor complex is at the center of the scheme. It is reduced with releasing Cl<sup>-</sup> ion to yield the coordinated unsaturated species, which does not bind with CO<sub>2</sub> but H<sup>+</sup> to afford the hydride complex. The hydride complex reacts with CO<sub>2</sub> to yield the formate complex, which is reduced to produce HCOO<sup>-</sup> with recovering the original complex. However, the catalyst mainly produces CO not HCOO<sup>-</sup>. In the mechanism, the formate complex converts to the carboxylic acid complex and then the carbonyl complex by dehydration. The conversion of the formate complex to the carbonyl complex via the carboxylic acid complex is not known, and therefore further researches are expected.

Homogeneous catalysts are advantageous from the viewpoints of elucidating the catalytic reaction mechanisms compared to heterogeneous ones because the homogenous catalysts can be examined by using many spectroscopic techniques. Nevertheless, the mechanisms of the electrochemical CO<sub>2</sub> reduction catalyzed by the ruthenium complexes still remain unknown. There may be potentially many intermediates and pathways in the catalyses, and they depend on the reaction conditions and the subtle difference among the catalyst structures [16, 37].

### 3. Photochemical CO<sub>2</sub> reduction

In the preceding section, the electrocatalytic activities of the ruthenium complexes are introduced. The electrocatalyst can be utilized in photocatalytic systems by combining with a photosensitizer (PS). **Figure 10** shows a schematic drawing of the photocatalytic system, in which the excited PS (PS\*) receives an electron from an electron donor to afford the one-electron



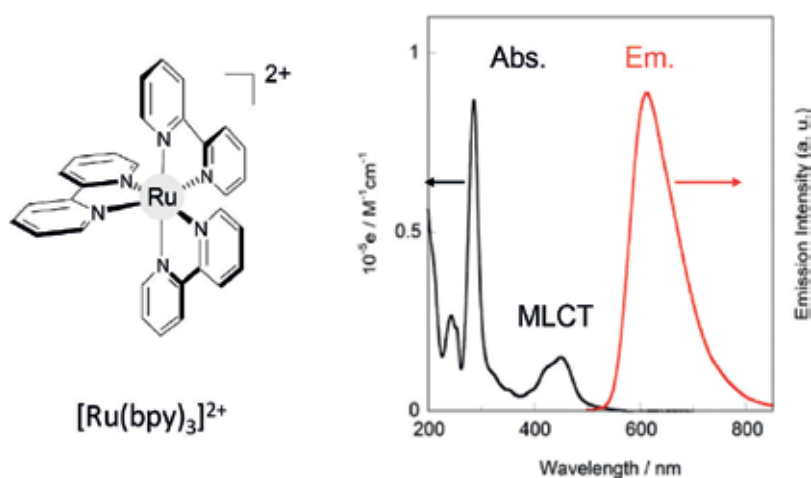


**Figure 10.** A schematic drawing of photocatalytic reduction by combining a photosensitizer (PS) with an electrocatalyst (Cat.).

reduced PS ( $PS^-$ ). The  $PS^-$  is the more powerful reagent than  $PS^*$ , and it can inject an electron to the electrocatalyst. The catalyst can work similarly as the electroreduction occurs. In this section, the photocatalytic  $CO_2$  reduction by the ruthenium complexes is expounded.

### 3.1. Photosensitizer and sacrificial electron donors

The most common photosensitizer used in photocatalytic  $CO_2$  reduction is  $[Ru(bpy)_3]^{2+}$  and the derivatives. **Figure 11** shows the absorption and emission spectra of  $[Ru(bpy)_3]^{2+}$  in acetonitrile. The complex exhibits an absorption band at 400–500 nm, which is assignable to metal-to-ligand charge transfer (MLCT). When excited at the band, the emission at the longer wavelengths is observed. The emission is not fluorescence but room-temperature phosphorescence, which is sensitive to  $O_2$ . Therefore, the emission spectrum should be carefully measured under deaerated conditions [88]. The lifetime of the excited state of  $[Ru(bpy)_3]^{2+}$  is 1.10  $\mu s$  in acetonitrile [89, 90]. The quantum yield has been recently reevaluated as 0.095 in acetonitrile [91]. The oxidation potential (corresponding to the reducing ability) of the excited state ( $PS^*$ ) is  $-0.81$  V vs. SCE ( $CH_3CN$ ), while this of the one-electron reduced species ( $PS^-$ ) is  $-1.33$  V. As the electrochemical



**Figure 11.** Absorption and emission (phosphorescence) spectra of  $[Ru(bpy)_3]^{2+}$  in deaerated  $CH_3CN$  at room temperature.



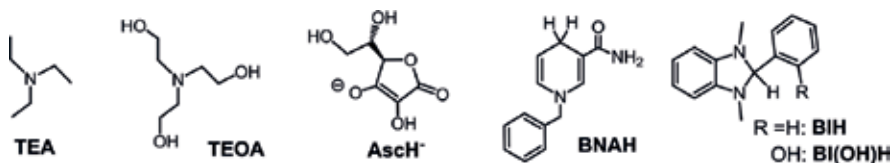
CO<sub>2</sub> reduction catalyzed by the ruthenium complexes proceeds under electrolysis at -1.30 V vs. SCE, it requires the reducing ability of PS<sup>-</sup>. In general, the CO<sub>2</sub> reduction requires higher energy than H<sub>2</sub> production by reduction of H<sub>2</sub>O, and therefore, the photocatalytic CO<sub>2</sub> reduction does not utilize the excited state but the one-electron reduced species.

To generate the one-electron reduced species PS<sup>-</sup>, the electron donors can reductively quench the excited state of the photosensitizer. As the reduction potential of the excited state of [Ru(bpy)<sub>3</sub>]<sup>2+</sup> is +0.77 V vs. SCE (CH<sub>3</sub>CN), the electron donors which can be oxidized at less positive potentials than +0.77 V. **Figure 12** shows the examples of the electron donors which are actually used in photocatalytic CO<sub>2</sub> reduction [16, 92]. Ascorbate ion (AscH<sup>-</sup>) can be used in aqueous solution, but amines (triethylamine (TEA) and triethanolamine (TEOA)) cannot work in the presence of water because they are protonated to afford the ammonium ions which cannot give an electron. 1-Benzyl-1,4-dihydronicotineamide (BNAH) is a model compound of NADH in nature. NADH is a two-electron donor and is oxidized to yield NAD<sup>+</sup>. However, the model compound BNAH cannot give two electrons in the oxidation by the excited state of [Ru(bpy)<sub>3</sub>]<sup>2+</sup> but provides one electron to afford the dimer BNA<sub>2</sub>. 1,3-Dimethyl-2-phenyl-2,3-dihydro-1*H*-benzo[d]imidazole (BIH) and the derivatives (e.g., BI(OH)H), which have much stronger reducing power than BNAH, have been recently utilized in photocatalytic CO<sub>2</sub> reduction. BIH provides two electrons to yield the oxidation product BI<sup>+</sup>.

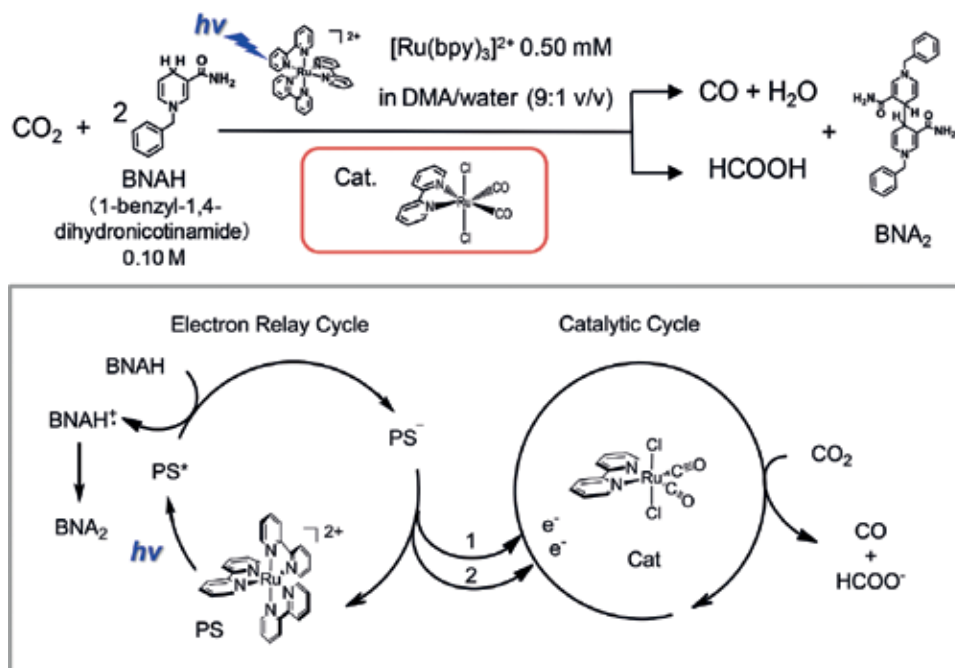
These electron donors are called the sacrificial reagents because the one-electron oxidized species occur chemical changes or decompose so as to prevent back electron transfer. They are useful in order to investigate the reductive half reaction. However, from the viewpoint of the energy balance, the reduction-oxidation (redox) systems in which water is oxidized and CO<sub>2</sub> is reduced are desired.

### 3.2. Photocatalytic CO<sub>2</sub> reduction

Our group have investigated the photochemical CO<sub>2</sub> reduction by the system consisting of *trans*-(Cl)-[Ru(bpy)(CO)<sub>2</sub>Cl<sub>2</sub>], [Ru(bpy)<sub>3</sub>]<sup>2+</sup> and BNAH as the catalyst, the photosensitizer, and the electron donor, respectively (**Figure 13**). The catalysis had been carried out in *N,N*-dimethylformamide (DMF)/water [57, 59]. However, it was indicated that hydration of DMF affording formate became a serious problem in quantifying formate [93]. We proposed the use of *N,N*-dimethylacetamide (DMA), of which the dehydration does not produce formate but acetate, instead of DMF [39]. Although the photocatalysis strongly depends on the solvent system, the reaction proceeds in DMA/water similarly as in DMF/water.

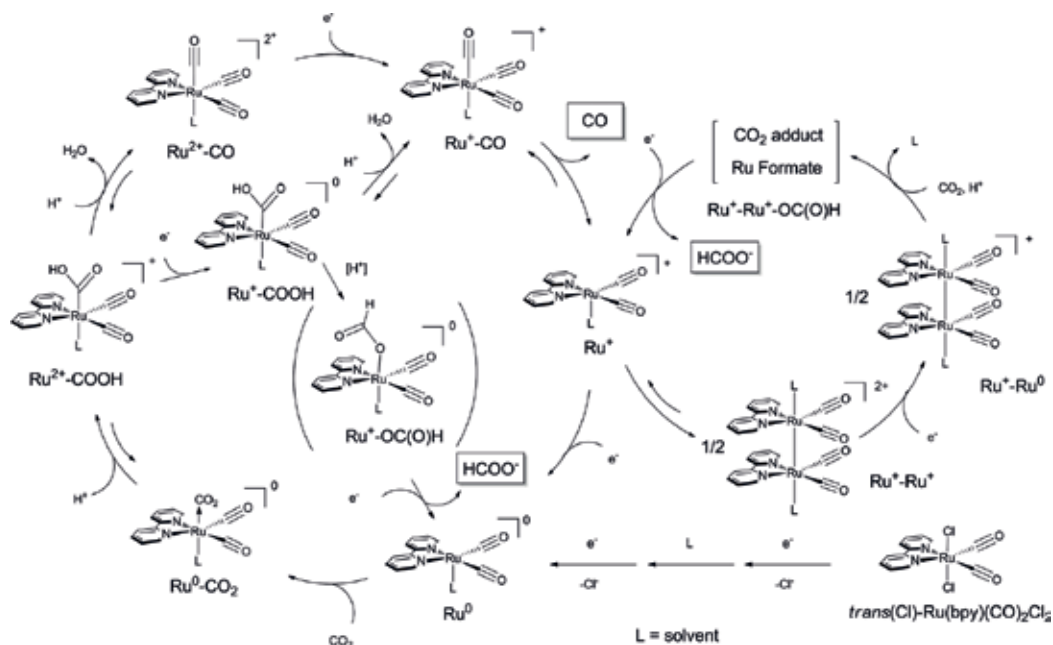


**Figure 12.** Examples of the electron donors (D) used in photochemical CO<sub>2</sub> reduction.



**Figure 13.** Photochemical CO<sub>2</sub> reduction catalyzed by *trans*-(Cl)-[Ru(bpy)(CO)<sub>2</sub>Cl<sub>2</sub>] with [Ru(bpy)<sub>3</sub>]<sup>2+</sup> (a photosensitizer (PS)) and BNAH (an electron donor).

The catalytic reaction proceeds by receiving electrons from the photochemically driven electron relay system. For two-electron reduction of CO<sub>2</sub> to CO or HCOOH, the electron relay cycle has to go round two times when the catalytic cycle turns one time. The electron source is not an electrode, but the reaction had been supposed to proceed according to the same mechanism as in electrochemical reduction. However, it has been recently indicated that in some cases, the reaction mechanisms of the photochemical CO<sub>2</sub> reduction are likely different from the electrochemical one [16]. For example, unusual catalyst concentration dependence on the product selectivity (CO/HCOO<sup>-</sup>) in the photocatalysis has been observed: at high catalyst concentration the selectivity of HCOO<sup>-</sup> increases [37]. To elucidate the peculiar catalyst concentration effect, the mechanisms as shown in the right cycle in **Figure 14** are proposed. At the high concentration of the catalyst, the reduced catalyst forms a dimer, which is proposed to selectively afford HCOO<sup>-</sup>. The dimer of the complex is similar as the intermediate of polymerization, but it is not detected in the photocatalytic system because the absorption spectrum cannot be conformed due to the overlapped absorption of [Ru(bpy)<sub>3</sub>]<sup>2+</sup>. Alternatively, the photocatalytic CO<sub>2</sub> reduction by *trans*-(Cl)-[Ru(6Mesbpy)(CO)<sub>2</sub>Cl<sub>2</sub>] which does not dimerize because of the steric hindrance of the ligand has been examined. The ruthenium complex selectively produces CO in the photochemical CO<sub>2</sub> reduction, and it demonstrates that the dimerization of the catalyst relates on the HCOO<sup>-</sup> production. It is suggested that the catalyst concentration dependence is not observed in a DMA/ethanol solution. It indicates that HCOO<sup>-</sup> also produces in the cycle consisting of mono-nuclear ruthenium complexes as proposed for the electrocatalytic CO<sub>2</sub> reduction (**Figure 14**, left cycle) [31].



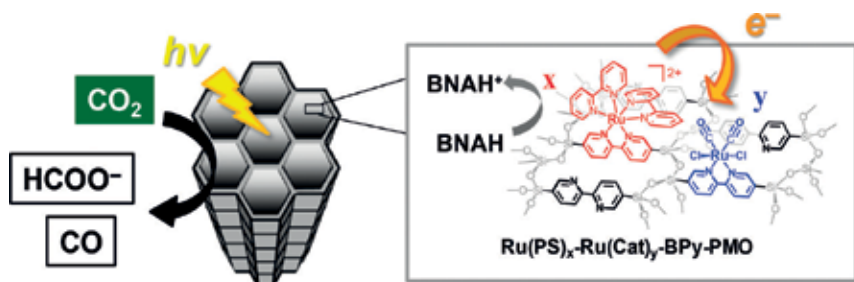
**Figure 14.** A proposed reaction mechanism for photocatalytic CO<sub>2</sub> reduction by *trans*(Cl)-[Ru(bpy)(CO)<sub>2</sub>Cl<sub>2</sub>].

The photochemical CO<sub>2</sub> reduction catalyzed by *trans*(Cl)-[Ru(2,2'-bipyridine)(CO)<sub>2</sub>Cl<sub>2</sub>] bearing two methyl groups at 4,4'- or 5,5'-positions in the ligand has been recently reported [64]. As the catalytic activities of these complexes at low catalyst concentrations are almost the same, the intrinsic activities are considered to be identical. However, the catalytic activities of these complexes are different at high catalyst concentration, where the rate-determining step is not in the catalytic cycle but in the electron relay cycle: the ruthenium complex with dimethyl groups at 5,5'-positions in the 2,2'-bipyridyl ligand is higher than that at 4,4'-positions. The efficiency of the back-electron transfer from the reduced catalyst to the photosensitizer is lower, or the cage escape yield for the sensitizer-catalyst complex is higher in the 5,5'-dimethyl complex than in the 4,4'-complex.

These phenomena have not been observed in electrochemical CO<sub>2</sub> reduction. It is probably because that the homogenous photocatalytic CO<sub>2</sub> reduction contains the diffusion process of the electron relay between the photosensitizer and the catalyst. The speed of the electron supply also sometimes affects the reaction mechanisms [16, 37].

### 3.3. Application to heterogeneous catalysts

Heterogeneous catalysts are industrially important because they are useful for separating the starting materials and the products from the catalyst and can be recovered and reused. The molecular catalysts can be utilized to develop the heterogeneous catalysts. For photocatalysts of CO<sub>2</sub> reduction, combining the molecular catalysts with semiconductor [32, 94, 95], metal-organic frameworks (MOFs) [96, 97] or periodic mesoporous organosilicas (PMOs) [98–101]

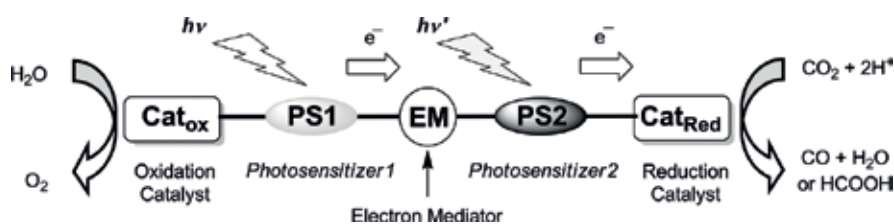


**Figure 15.** Photocatalytic  $\text{CO}_2$  reduction by periodic mesoporous organosilica (PMO) containing two different ruthenium complexes as photosensitizing and catalytic sites.

are actively researched. We have also developed a novel PMO consisting of 2,2'-bipyridyl framework by introducing two different ruthenium complexes as a photosensitizing site ( $\text{Ru}(\text{PS})$ ) and a catalytic site ( $\text{Ru}(\text{Cat})$ ) as shown in **Figure 15** [99]. Photochemical  $\text{CO}_2$  reduction by the PMO catalyst has catalytically produced CO and formate. The product selectivity (CO/formate) becomes large with increasing the ratio of  $\text{Ru}(\text{PS})$  to  $\text{Ru}(\text{Cat})$  ( $x/y$ ). The photocatalysts can be recycled at least three times without losing the catalytic activity, demonstrating that the  $\text{Ru}(\text{PS})$  and  $\text{Ru}(\text{Cat})$  units are strongly immobilized on the BPy-PMO framework.

#### 4. Future prospects

The molecular catalysts are applicable to various photocatalytic systems. Ultimately, our goal is to construct an artificial photosynthetic system. An example is shown in **Figure 16**. In the system, the electrons are not supplied from the sacrificial electron donor but from water which is the same as in natural photosynthetic system. As the  $\text{CO}_2$  reduction requires a high potential, two photosensitizing systems would be combined as the Z-scheme mechanism in the natural photosynthesis. In order to realize the artificial photosynthesis, we have to overcome some problems. One is to perform these reactions (water oxidation, photo-induced electron transfer and  $\text{CO}_2$  reduction, etc.) under the similar conditions or in the separated circumstances. Another is to match the velocities among the reactions; even if the efficient catalyst for  $\text{CO}_2$  reduction was obtained, the speeds for the water oxidation and the electron supply have to match with that of  $\text{CO}_2$  reduction.



**Figure 16.** A schematic drawing for an artificial photosynthetic system.

There would be many other problems to construct the artificial photosynthesis. However, the real system which can efficiently work has already existed in nature. We will realize it with a lot of ideas to overcome many problems one by one.

## Acknowledgements

This work was supported by a Grant-in-Aid for Scientific Research (C) from the Ministry of Education, Culture, Sports, Science and Technology (17K05815). This work was also supported by the PRESTO Program of JST, and a Grant-in-Aid for Scientific Research on Innovative Areas, "Artificial Photosynthesis (AnApple)" (No. 15H00882), from the Japan Society for the Promotion of Science (JSPS).

## Author details

Hitoshi Ishida

Address all correspondence to: [ishida@sci.kitasato-u.ac.jp](mailto:ishida@sci.kitasato-u.ac.jp)

Department of Chemistry, Graduate School of Science, Kitasato University, Japan

## References

- [1] Olah GA, Prakash GKS, Goepfert A. Anthropogenic chemical carbon cycle for a sustainable future. *Journal of the American Chemical Society*. 2011;**133**:12881-12898. DOI: 10.1021/ja202642y
- [2] Arakawa H, Aresta M, Armor JN, Barteau MA, Beckman EJ, Bell AT, Bercaw JE, Creutz C, Dinjus E, Dixon DA, Domen K, DuBois DL, Eckert J, Fujita E, Gibson DH, Goddard WA, Goodman DW, Keller J, Kubas GJ, Kung HH, Lyons JE, Manzer LE, Marks TJ, Morokuma K, Nicholas KM, Periana R, Que L, Rostrup-Nielson J, Sachtler WMH, Schmidt LD, Sen A, Somorjai GA, Stair PC, Stults BR, Tumas W. Catalysis research of relevance to carbon management: Progress, challenges, and opportunities. *Chemical Reviews*. 2001;**101**:953-996. DOI: 10.1021/cr000018s
- [3] Mikkelsen M, Jorgensen M, Krebs FC. The teraton challenge. A review of fixation and transformation of carbon dioxide. *Energy & Environmental Science*. 2010;**3**:43-81. DOI: 10.1039/b912904a
- [4] Sakakura T, Choi J-C, Yasuda H. Transformation of carbon dioxide. *Chemical Reviews*. 2007;**107**:2365-2387. DOI: 10.1021/cr068357u
- [5] Schwarz HA, Dodson RW. Reduction potentials of CO<sub>2</sub><sup>-</sup> and the alcohol radicals. *The Journal of Physical Chemistry*. 1989;**93**:409-414. DOI: 10.1021/j100338a079

- [6] Yamazaki Y, Takeda H, Ishitani O. Photocatalytic reduction of CO<sub>2</sub> using metal complexes. *Journal of Photochemistry and Photobiology C Photochemistry Reviews*. 2015;**25**:106-137. DOI: <https://doi.org/10.1016/j.jphotochemrev.2015.09.001>
- [7] Hildebrandt D, Glasser D, Hausberger B, Patel B, Glasser BJ. Producing transportation fuels with less work. *Science*. 2009;**323**:1680-1681. DOI: 10.1126/science.1168455
- [8] Singh AK, Singh S, Kumar A. Hydrogen energy future with formic acid: A renewable chemical hydrogen storage system. *Catalysis Science & Technology*. 2016;**6**:12-40. DOI: 10.1039/c5cy01276g
- [9] DuBois DL. Development of molecular electrocatalysts for energy storage. *Inorganic Chemistry*. 2014;**53**:3935-3960. DOI: 10.1021/ic4026969
- [10] Appel AM, Bercaw JE, Bocarsly AB, Dobbek H, DuBois DL, Dupuis M, Ferry JG, Fujita E, Hille R, Kenis PJA, Kerfeld CA, Morris RH, Peden CHF, Portis AR, Ragsdale SW, Rauchfuss TB, Reek JNH, Seefeldt LC, Thauer RK, Waldrop GL. Frontiers, opportunities, and challenges in biochemical and chemical catalysis of CO<sub>2</sub> fixation. *Chemical Reviews*. 2013;**113**:6621-6658. DOI: 10.1021/cr300463y
- [11] Schneider J, Jia H, Muckerman JT, Fujita E. Thermodynamics and kinetics of CO<sub>2</sub>, CO, and H<sup>+</sup> binding to the metal centre of CO<sub>2</sub> reduction catalysts. *Chemical Society Reviews*. 2012;**41**:2036-2051. DOI: 10.1039/c1cs15278e
- [12] Windle CD, Perutz RN. Advances in molecular photocatalytic and electrocatalytic CO<sub>2</sub> reduction. *Coordination Chemistry Reviews*. 2012;**256**:2562-2570. DOI: 10.1016/j.ccr.2012.03.010
- [13] Yui T, Tamaki Y, Sekizawa K, Ishitani O. Photocatalytic reduction of CO<sub>2</sub>: From molecules to semiconductors. *Topics in Current Chemistry*. 2011;**303**:151-184. DOI: 10.1007/128\_2011\_139
- [14] Takeda H, Ishitani O. Development of efficient photocatalytic systems for CO<sub>2</sub> reduction using mononuclear and multinuclear metal complexes based on mechanistic studies. *Coordination Chemistry Reviews*. 2010;**254**:346-354. DOI: 10.1016/j.ccr.2009.09.030
- [15] Savéant J-M. Molecular catalysis of electrochemical reactions. Mechanistic aspects. *Chemical Reviews*. 2008;**108**:2348-2378. DOI: 10.1021/cr068079z
- [16] Kuramochi Y, Ishitani O, Ishida H. Reaction mechanisms of catalytic photochemical CO<sub>2</sub> reduction using Re(I) and Ru(II) complexes. *Coordination Chemistry Reviews*. 2018. DOI: 10.1016/j.ccr.2017.11.023
- [17] Sampson MD, Nguyen AD, Grice KA, Moore CE, Rheingold AL, Kubiak CP. Manganese catalysts with bulky bipyridine ligands for the electrocatalytic reduction of carbon dioxide: Eliminating dimerization and altering catalysis. *Journal of the American Chemical Society*. 2014;**136**:5460-5471. DOI: 10.1021/ja501252f
- [18] Takeda H, Koizumi H, Okamoto K, Ishitani O. Photocatalytic CO<sub>2</sub> reduction using a Mn complex as a catalyst. *Chemical Communications*. 2014;**50**:1491-1493. DOI: 10.1039/c3cc48122k

- [19] Bourrez M, Molton F, Chardon-Noblat S, Deronzier A. [Mn(bipyridyl)(CO)<sub>3</sub>Br]: An abundant metal carbonyl complex as efficient electrocatalyst for CO<sub>2</sub> reduction. *Angewandte Chemie, International Edition*. 2011;**50**:9903-9906. DOI: 10.1002/anie.201103616
- [20] Costentin C, Drouet S, Robert M, Savéant J-M. A local proton source enhances CO<sub>2</sub> electroreduction to CO by a molecular Fe catalyst. *Science*. 2012;**338**:90-94. DOI: 10.1126/science.1224581
- [21] Hammouche M, Lexa D, Momenteau M, Saveant JM. Chemical catalysis of electrochemical reactions. Homogeneous catalysis of the electrochemical reduction of carbon dioxide by iron(0) porphyrins. Role of the addition of magnesium cations. *Journal of the American Chemical Society*. 1991;**113**:8455-8466. DOI: 10.1021/ja00022a038
- [22] Matsuoka S, Yamamoto K, Ogata T, Kusaba M, Nakashima N, Fujita E, Yanagida S. Efficient and selective electron mediation of cobalt complexes with cyclam and related macrocycles in the p-terphenyl-catalyzed photoreduction of carbon dioxide. *Journal of the American Chemical Society*. 1993;**115**:601-609. DOI: 10.1021/ja00055a032
- [23] Ziesel R, Hawecker J, Lehn J-M. Photogeneration of carbon monoxide and of hydrogen via simultaneous photochemical reduction of carbon dioxide and water by visible-light irradiation of organic solutions containing Tris(2,2'-bipyridine)ruthenium(II) and cobalt(II) species as homogeneous catalysts. *Helvetica Chimica Acta*. 1986;**69**:1065-1084. DOI: 10.1002/hlca.19860690514
- [24] Tinnemans AHA, Koster TPM, Thewissen DHMW, Mackor A. Tetraaza-macrocyclic cobalt(II) and nickel(II) complexes as electron-transfer agents in the photo(electro)chemical and electrochemical reduction of carbon dioxide. *Recueil des Travaux Chimiques des Pays-Bas*. 1984;**103**:288-295. DOI: 10.1002/recl.19841031004
- [25] Rudolph M, Dautz S, Jäger E-G. Macrocyclic [N<sub>4</sub><sup>2-</sup>] coordinated nickel complexes as catalysts for the formation of oxalate by electrochemical reduction of carbon dioxide. *Journal of the American Chemical Society*. 2000;**122**:10821-10830. DOI: 10.1021/ja001254n
- [26] Grant JL, Goswami K, Spreer LO, Otvos JW, Calvin M. Photochemical reduction of carbon dioxide to carbon monoxide in water using a nickel(II) tetra-azamacrocycle complex as catalyst. *Journal of the Chemical Society, Dalton Transactions*. 1987:2105-2109. DOI: 10.1039/dt9870002105
- [27] Beley M, Collin JP, Ruppert R, Sauvage JP. Electrocatalytic reduction of carbon dioxide by nickel cyclam<sup>2+</sup> in water: Study of the factors affecting the efficiency and the selectivity of the process. *Journal of the American Chemical Society*. 1986;**108**:7461-7467. DOI: 10.1021/ja00284a003
- [28] Beley M, Collin J-P, Ruppert R, Sauvage J-P. Nickel(II)-cyclam: An extremely selective electrocatalyst for reduction of CO<sub>2</sub> in water. *Journal of the Chemical Society, Chemical Communications*. 1984:1315-1316. DOI: 10.1039/c39840001315
- [29] Angamuthu R, Byers P, Lutz M, Spek AL, Bouwman E. Electrocatalytic CO<sub>2</sub> conversion to oxalate by a copper complex. *Science*. 2010;**327**:313-315. DOI: 10.1126/science.1177981

- [30] Clark ML, Grice KA, Moore CE, Rheingold AL, Kubiak CP. Electrocatalytic CO<sub>2</sub> reduction by M(bpy-R)(CO)<sub>4</sub> (M = Mo, W; R = H, tBu) complexes. Electrochemical, spectroscopic, and computational studies and comparison with group 7 catalysts. *Chemical Science*. 2014;**5**:1894-1900. DOI: 10.1039/c3sc53470g
- [31] Ishida H, Sakaba A. Temperature dependence of photocatalytic CO<sub>2</sub> reduction by trans(Cl)-Ru(bpy)(CO)<sub>2</sub>Cl<sub>2</sub>: Activation energy difference between CO and formate production. *Faraday Discussions*. 2017;**198**:263-277. DOI: 10.1039/c6fd00242k
- [32] Kuriki R, Matsunaga H, Nakashima T, Wada K, Yamakata A, Ishitani O, Maeda K. Nature-inspired, highly durable CO<sub>2</sub> reduction system consisting of a binuclear ruthenium(II) complex and an organic semiconductor using visible light. *Journal of the American Chemical Society*. 2016;**138**:5159-5170. DOI: 10.1021/jacs.6b01997
- [33] Kuriki R, Ishitani O, Maeda K. Unique solvent effects on visible-light CO<sub>2</sub> reduction over ruthenium(II)-complex/carbon nitride hybrid photocatalysts. *ACS Applied Materials & Interfaces*. 2016;**8**:6011-6018. DOI: 10.1021/acsami.5b11836
- [34] Yoshitomi F, Sekizawa K, Maeda K, Ishitani O. Selective formic acid production via CO<sub>2</sub> reduction with visible light using a hybrid of a perovskite tantalum oxynitride and a binuclear ruthenium(II) complex. *ACS Applied Materials & Interfaces*. 2015;**7**:13092-13097. DOI: 10.1021/acsami.5b03509
- [35] Machan CW, Sampson MD, Kubiak CP. A molecular ruthenium electrocatalyst for the reduction of carbon dioxide to CO and Formate. *Journal of the American Chemical Society*. 2015;**137**:8564-8571. DOI: 10.1021/jacs.5b03913
- [36] Kuriki R, Sekizawa K, Ishitani O, Maeda K. Visible-light-driven CO<sub>2</sub> reduction with carbon nitride: Enhancing the activity of ruthenium catalysts. *Angewandte Chemie, International Edition*. 2015;**54**:2406-2409. DOI: 10.1002/anie.201411170
- [37] Kuramochi Y, Itabashi J, Fukaya K, Enomoto A, Yoshida M, Ishida H. Unexpected effect of catalyst concentration on photochemical CO<sub>2</sub> reduction by trans(Cl)-Ru(bpy)(CO)<sub>2</sub>Cl<sub>2</sub>: New mechanistic insight into the CO/HCOO<sup>-</sup> selectivity. *Chemical Science*. 2015;**6**:3063-3074. DOI: 10.1039/c5sc00199d
- [38] Kuramochi Y, Fukaya K, Yoshida M, Ishida H. Trans(Cl)-[Ru(5,5'-diamide-2,2'-bipyridine)(CO)<sub>2</sub>Cl<sub>2</sub>]: Synthesis, structure, and photocatalytic CO<sub>2</sub> reduction activity. *Chemistry – A European Journal*. 2015;**21**:10049-10060. DOI: 10.1002/chem.201500782
- [39] Kuramochi Y, Kamiya M, Ishida H. Photocatalytic CO<sub>2</sub> reduction in N,N-dimethylacetamide/water as an alternative solvent system. *Inorganic Chemistry*. 2014;**53**:3326-3332. DOI: 10.1021/ic500050q
- [40] Maeda K, Kuriki R, Zhang M, Wang X, Ishitani O. The effect of the pore-wall structure of carbon nitride on photocatalytic CO<sub>2</sub> reduction under visible light. *Journal of Materials Chemistry A*. 2014;**2**:15146-15151. DOI: 10.1039/c4ta03128h
- [41] Maeda K, Sekizawa K, Ishitani O. A polymeric-semiconductor-metal-complex hybrid photocatalyst for visible-light CO<sub>2</sub> reduction. *Chemical Communications*. 2013;**49**:10127-10129. DOI: 10.1039/c3cc45532g



- [42] Tamaki Y, Morimoto T, Koike K, Ishitani O. Photocatalytic CO<sub>2</sub> reduction with high turnover frequency and selectivity of formic acid formation using Ru(II) multinuclear complexes. *Proceedings of the National Academy of Sciences of the United States of America*. 2012;**109**:15673-15678. DOI: 10.1073/pnas.1118336109
- [43] Yamanaka K-I, Sato S, Iwaki M, Kajino T, Morikawa T. Photoinduced electron transfer from nitrogen-doped tantalum oxide to adsorbed ruthenium complex. *Journal of Physical Chemistry C*. 2011;**115**:18348-18353. DOI: 10.1021/jp205223k
- [44] Suzuki TM, Tanaka H, Morikawa T, Iwaki M, Sato S, Saeki S, Inoue M, Kajino T, Motohiro T. Direct assembly synthesis of metal complex-semiconductor hybrid photocatalysts anchored by phosphonate for highly efficient CO<sub>2</sub> reduction. *Chemical Communications*. 2011;**47**:8673-8675. DOI: 10.1039/c1cc12491a
- [45] Sato S, Arai T, Morikawa T, Uemura K, Suzuki TM, Tanaka H, Kajino T. Selective CO<sub>2</sub> conversion to Formate conjugated with H<sub>2</sub>O oxidation utilizing semiconductor/complex hybrid photocatalysts. *Journal of the American Chemical Society*. 2011;**133**:15240-15243. DOI: 10.1021/ja204881d
- [46] Arai T, Tajima S, Sato S, Uemura K, Morikawa T, Kajino T. Selective CO<sub>2</sub> conversion to formate in water using a CZTS photocathode modified with a ruthenium complex polymer. *Chemical Communications*. 2011;**47**:12664-12666. DOI: 10.1039/c1cc16160a
- [47] Sato S, Morikawa T, Saeki S, Kajino T, Motohiro T. Visible-light-induced selective CO<sub>2</sub> reduction utilizing a ruthenium complex electrocatalyst linked to a p-type nitrogen-doped Ta<sub>2</sub>O<sub>5</sub> semiconductor. *Angewandte Chemie International Edition in English*. 2010;**49**:5101-5105. S5101/5101-S5101/5111. DOI: 10.1002/anie.201000613
- [48] Arai T, Sato S, Uemura K, Morikawa T, Kajino T, Motohiro T. Photoelectrochemical reduction of CO<sub>2</sub> in water under visible-light irradiation by a p-type InP photocathode modified with an electropolymerized ruthenium complex. *Chemical Communications*. 2010;**46**:6944-6946. DOI: 10.1039/c0cc02061c
- [49] Creutz C, Chou MH. Rapid transfer of hydride ion from a ruthenium complex to C1 species in water. *Journal of the American Chemical Society*. 2007;**129**:10108-10109. DOI: 10.1021/ja074158w
- [50] Chardon-Noblat S, Deronzier A, Ziessel R, Zsoldos D. Electroreduction of CO<sub>2</sub> catalyzed by polymeric [Ru(bpy)(CO)<sub>2</sub>]<sub>n</sub> films in aqueous media: Parameters influencing the reaction selectivity. *Journal of Electroanalytical Chemistry*. 1998;**444**:253-260. DOI: 10.1016/S0022-0728(97)00584-6
- [51] Chardon-Noblat S, Deronzier A, Ziessel R, Zsoldos D. Selective synthesis and electrochemical behavior of trans(Cl)- and cis(Cl)-[Ru(bpy)(CO)<sub>2</sub>Cl<sub>2</sub>] complexes (bpy = 2,2'-Bipyridine). Comparative studies of their electrocatalytic activity toward the reduction of carbon dioxide. *Inorganic Chemistry*. 1997;**36**:5384-5389. DOI: 10.1021/ic9701975
- [52] Nagao H, Mizukawa T, Tanaka K. Carbon-carbon bond formation in the electrochemical reduction of carbon dioxide catalyzed by a ruthenium complex. *Inorganic Chemistry*. 1994;**33**:3415-3420. DOI: 10.1021/ic00093a033

- [53] Collomb-Dunand-Sauthier M-N, Deronzier A, Ziessel R. Electrocatalytic reduction of carbon dioxide with mono(bipyridine)carbonylruthenium complexes in solution or as polymeric thin films. *Inorganic Chemistry*. 1994;**33**:2961-2967. DOI: 10.1021/ic00091a040
- [54] Collomb-Dunand-Sauthier MN, Deronzier A, Ziessel R. Electrocatalytic reduction of CO<sub>2</sub> in water on a polymeric [ $\text{Ru}^0(\text{bpy})(\text{CO})_2$ ]<sub>n</sub> (bpy = 2,2'-bipyridine) complex immobilized on carbon electrodes. *Journal of the Chemical Society, Chemical Communications*. 1994:189-191. DOI: 10.1039/c39940000189
- [55] Chardon-Noblat S, Collomb-Dunand-Sauthier MN, Deronzier A, Ziessel R, Zsoldos D. Formation of polymeric [ $\text{Ru}^0(\text{bpy})(\text{CO})_2$ ]<sub>n</sub> films by electrochemical reduction of  $[\text{Ru}(\text{bpy})_2(\text{CO})_2](\text{PF}_6)_2$ : Its implication in CO<sub>2</sub> electrocatalytic reduction. *Inorganic Chemistry*. 1994;**33**:4410-4412. DOI: 10.1021/ic00097a034
- [56] Lehn JM, Ziessel R. Photochemical reduction of carbon dioxide to formate catalyzed by (2,2'-bipyridine)- or (1,10-phenanthroline)ruthenium(II) complexes. *Journal of Organometallic Chemistry*. 1990;**382**:157-173. DOI: 10.1016/0022-328x(90)85224-m
- [57] Ishida H, Terada T, Tanaka K, Tanaka T. Photochemical carbon dioxide reduction catalyzed by bis(2,2'-bipyridine)dicarbonylruthenium(2+) using triethanolamine and 1-benzyl-1,4-dihydronicotinamide as an electron donor. *Inorganic Chemistry*. 1990;**29**:905-911. DOI: 10.1021/ic00330a004
- [58] Ishida H, Fujiki K, Ohba T, Ohkubo K, Tanaka K, Terada T, Tanaka T. Ligand effects of ruthenium 2,2'-bipyridine and 1,10-phenanthroline complexes on the electrochemical reduction of carbon dioxide. *Journal of the Chemical Society, Dalton Transactions*. 1990:2155-2160. DOI: 10.1039/DT9900002155
- [59] Ishida H, Tanaka K, Tanaka T. Photochemical carbon dioxide reduction by an NADH model compound in the presence of ruthenium complexes  $[\text{Ru}(\text{bpy})_3]^{2+}$  and  $[\text{Ru}(\text{bpy})_2(\text{CO})_2]^{2+}$  (bpy = 2,2'-bipyridine) in water/DMF. *Chemistry Letters*. 1988;**17**:339-342. DOI: 10.1246/cl.1988.339
- [60] Ishida H, Tanaka K, Tanaka T. Photoreduction of carbon dioxide in the  $[\text{Ru}(\text{bpy})_2(\text{CO})_2]^{2+}$  (bpy = 2,2'-bipyridine)/ $[\text{Ru}(\text{bpy})_3]^{2+}$  or  $[\text{Ru}(\text{phen})_3]^{2+}$  (phen = phenanthroline)/triethanolamine/N,N-dimethylformamide system. *Chemistry Letters*. 1987;**16**:1035-1038. DOI: 10.1246/cl.1987.1035
- [61] Ishida H, Tanaka H, Tanaka K, Tanaka T. Selective formation of formate in the electrochemical carbon dioxide reduction catalyzed by  $[\text{Ru}(\text{bpy})_2(\text{CO})_2]^{2+}$  (bpy = 2,2'-bipyridine). *Journal of the Chemical Society, Chemical Communications*. 1987:131-132. DOI: 10.1039/c39870000131
- [62] Ishida H, Tanaka K, Tanaka T. Electrochemical CO<sub>2</sub> reduction catalyzed by ruthenium complexes  $[\text{Ru}(\text{bpy})_2(\text{CO})_2]^{2+}$  and  $[\text{Ru}(\text{bpy})_2(\text{CO})\text{Cl}]^+$ . Effect of pH on the formation of CO and HCOO. *Organometallics*. 1987;**6**:181-186. DOI: 10.1021/om00144a033
- [63] Ishida H, Tanaka K, Tanaka T. The electrochemical reduction of carbon dioxide catalyzed by ruthenium carbonyl complexes. *Chemistry Letters*. 1985;**14**:405-406. DOI: 10.1246/cl.1985.405

- [64] Kuramochi Y, Itabashi J, Toyama M, Ishida H. Photochemical CO<sub>2</sub> reduction catalyzed by trans(Cl)-Ru(2,2'-bipyridine)(CO)<sub>2</sub>Cl<sub>2</sub> bearing two methyl groups at 4,4'-, 5,5'- or 6,6'-positions in the ligand. *ChemPhotoChem*. 2018;**2**:314-322. DOI: 10.1002/cptc.201700201
- [65] Rasmussen SC, Richter MM, Yi E, Place H, Brewer KJ. Synthesis and characterization of a series of novel rhodium and iridium complexes containing polypyridyl bridging ligands: Potential uses in the development of multimetal catalysts for carbon dioxide reduction. *Inorganic Chemistry*. 1990;**29**:3926-3932. DOI: 10.1021/ic00345a005
- [66] Bolinger CM, Story N, Sullivan BP, Meyer TJ. Electrocatalytic reduction of carbon dioxide by 2,2'-bipyridine complexes of rhodium and iridium. *Inorganic Chemistry*. 1988;**27**:4582-4587. DOI: 10.1021/ic00298a016
- [67] Bernatis PR, Miedaner A, Haltiwanger RC, DuBois DL. Exclusion of six-coordinate intermediates in the electrochemical reduction of CO<sub>2</sub> catalyzed by [Pd(triphosphine)(CH<sub>3</sub>CN)](BF<sub>4</sub>)<sub>2</sub> complexes. *Organometallics*. 1994;**13**:4835-4843. DOI: 10.1021/om00024a029
- [68] DuBois DL, Miedaner A. Mediated electrochemical reduction of CO<sub>2</sub>. Preparation and comparison of an isoelectronic series of complexes. *Journal of the American Chemical Society*. 1987;**109**:113-117. DOI: 10.1021/ja00235a019
- [69] Riplinger C, Sampson MD, Ritzmann AM, Kubiak CP, Carter EA. Mechanistic contrasts between manganese and rhenium bipyridine electrocatalysts for the reduction of carbon dioxide. *Journal of the American Chemical Society*. 2014;**136**:16285-16298. DOI: 10.1021/ja508192y
- [70] Kou Y, Nabetani Y, Masui D, Shimada T, Takagi S, Tachibana H, Inoue H. Direct detection of key reaction intermediates in photochemical CO<sub>2</sub> reduction sensitized by a rhenium bipyridine complex. *Journal of the American Chemical Society*. 2014;**136**:6021-6030. DOI: 10.1021/ja500403e
- [71] Morimoto T, Nishiura C, Tanaka M, Rohacova J, Nakagawa Y, Funada Y, Koike K, Yamamoto Y, Shishido S, Kojima T, Saeki T, Ozeki T, Ishitani O. Ring-shaped Re(I) multinuclear complexes with unique photofunctional properties. *Journal of the American Chemical Society*. 2013;**135**:13266-13269. DOI: 10.1021/ja406144h
- [72] Tamaki Y, Koike K, Morimoto T, Yamazaki Y, Ishitani O. Red-light-driven Photocatalytic reduction of CO<sub>2</sub> using Os(II)-re(I) supramolecular complexes. *Inorganic Chemistry*. 2013;**52**:11902-11909. DOI: 10.1021/ic4015543
- [73] Agarwal J, Fujita E, Schaefer HF, Muckerman JT. Mechanisms for CO production from CO<sub>2</sub> using reduced rhenium tricarbonyl catalysts. *Journal of the American Chemical Society*. 2012;**134**:5180-5186. DOI: 10.1021/ja2105834
- [74] Takeda H, Koike K, Inoue H, Ishitani O. Development of an efficient photocatalytic system for CO<sub>2</sub> reduction using rhenium(I) complexes based on mechanistic studies. *Journal of the American Chemical Society*. 2008;**130**:2023-2031. DOI: 10.1021/ja077752e
- [75] Gholamkhash B, Mametsuka H, Koike K, Tanabe T, Furue M, Ishitani O. Architecture of supramolecular metal complexes for photocatalytic CO<sub>2</sub> reduction: Ruthenium-rhenium

- bi- and tetranuclear complexes. *Inorganic Chemistry*. 2005;**44**:2326-2336. DOI: 10.1021/ic048779r
- [76] Hawecker J, Lehn JM, Ziessel R. Photochemical and electrochemical reduction of carbon dioxide to carbon monoxide mediated by (2,2'-bipyridine)tricarbonylchlororhenium(I) and related complexes as homogeneous catalysts. *Helvetica Chimica Acta*. 1986;**69**:1990-2012. DOI: 10.1002/hlca.19860690824
- [77] Chauvin J, Lafalet F, Chardon-Noblat S, Deronzier A, Jakonen M, Haukka M. Towards new molecular photocatalysts for CO<sub>2</sub> reduction: Photo-induced electron transfer versus CO dissociation within [Os(NN)(CO)<sub>2</sub>Cl<sub>2</sub>] complexes. *Chemistry – A European Journal*. 2011;**17**:4313-4322. DOI: 10.1002/chem.201003098
- [78] Bruce MRM, Megehee E, Sullivan BP, Thorp HH, O'Toole TR, Downard A, Pugh JR, Meyer TJ. Electrocatalytic reduction of carbon dioxide based on 2,2'-bipyridyl complexes of osmium. *Inorganic Chemistry*. 1992;**31**:4864-4873. DOI: 10.1021/ic00049a027
- [79] Sato S, Morikawa T, Kajino T, Ishitani O. A highly efficient mononuclear iridium complex photocatalyst for CO<sub>2</sub> reduction under visible light. *Angewandte Chemie International Edition In English*. 2013;**52**:988-992. DOI: 10.1002/anie.201206137
- [80] Kang P, Cheng C, Chen Z, Schauer CK, Meyer TJ, Brookhart M. Selective electrocatalytic reduction of CO<sub>2</sub> to formate by water-stable iridium dihydride pincer complexes. *Journal of the American Chemical Society*. 2012;**134**:5500-5503. DOI: 10.1021/ja300543s
- [81] Costentin C, Passard G, Savéant J-M. Benchmarking of homogeneous electrocatalysts: Overpotential, turnover frequency, limiting turnover number. *Journal of the American Chemical Society*. 2015;**137**:5461-5467. DOI: 10.1021/jacs.5b00914
- [82] Mukhopadhyay TK, MacLean NL, Gan L, Ashley DC, Groy TL, Baik M-H, Jones AK, Trovitch RJ. Carbon dioxide promoted H<sup>+</sup> reduction using a bis(imino)pyridine manganese electrocatalyst. *Inorganic Chemistry*. 2015;**54**:4475-4482. DOI: 10.1021/acs.inorgchem.5b00315
- [83] Tanaka H, Tzeng BC, Nagao H, Peng SM, Tanaka K. Comparative study on crystal structures of ruthenium bipyridine carbonyl complexes [Ru(bpy)<sub>2</sub>(CO)<sub>2</sub>](PF<sub>6</sub>)<sub>2</sub>, [Ru(bpy)<sub>2</sub>(CO)(C(O)OCH<sub>3</sub>)]B(C<sub>6</sub>H<sub>5</sub>)<sub>4</sub>·CH<sub>3</sub>CN, and [Ru(bpy)<sub>2</sub>(CO)(η<sup>1</sup>-CO<sub>2</sub>)]·3H<sub>2</sub>O (bpy = 2,2'-bipyridyl). *Inorganic Chemistry*. 1993;**32**:1508-1512. DOI: 10.1021/ic00060a029
- [84] Hitoshi I, Hiroaki T, Koji T, Toshio T. Electrochemical reaction of CO<sub>2</sub> with Me<sub>2</sub>NH to afford N,N-dimethylformamide, catalyzed by [Ru(bpy)<sub>2</sub>(CO)<sub>2</sub>]<sup>2+</sup> (bpy = 2,2'-bipyridine). *Chemistry Letters*. 1987;**16**:597-600. DOI: 10.1246/cl.1987.597
- [85] Pugh JR, Bruce MRM, Sullivan BP, Meyer TJ. Formation of a metal-hydride bond and the insertion of carbon dioxide. Key steps in the electrocatalytic reduction of carbon dioxide to formate anion. *Inorganic Chemistry*. 1991;**30**:86-91. DOI: 10.1021/ic00001a016
- [86] Chardon-Noblat S, Deronzier A, Zsoldos D, Ziessel R, Haukka M, Pakkanen T, Venalainen T. Mode of formation of polymer {[Ru(bipy)(CO)<sub>2</sub>]<sub>n</sub>} (bipy = 2,2'-bipyridine) films. *Journal of the Chemical Society, Dalton Transactions*. 1996:2581-2583

- [87] Masciocchi N, Sironi A, Chardon-Noblat S, Deronzier A. X-ray powder diffraction study of organometallic polymers: [Ru(L)(CO)<sub>2</sub>]<sub>n</sub> (L = 2,2'-bipyridine or 1,10-phenanthroline). *Organometallics*. 2002;**21**:4009-4012. DOI: 10.1021/om020298x
- [88] Ishida H, Bünzli J-C, Beeby A. Guidelines for measurement of luminescence spectra and quantum yields of inorganic and organometallic compounds in solution and solid state (IUPAC technical report). *Pure and Applied Chemistry*. 2016;**88**:701. DOI: 10.1515/pac-2014-0706
- [89] Kalyanasundaram K. Photophysics, photochemistry and solar energy conversion with tris(bipyridyl)ruthenium(II) and its analogues. *Coordination Chemistry Reviews*. 1982;**46**:159-244. DOI: 10.1016/0010-8545(82)85003-0
- [90] Juris A, Balzani V, Barigelletti F, Campagna S, Belser P, von Zelewsky A. Ru(II) polypyridine complexes: Photophysics, photochemistry, electrochemistry, and chemiluminescence. *Coordination Chemistry Reviews*. 1988;**84**:85-277. DOI: 10.1016/0010-8545(88)80032-8
- [91] Suzuki K, Kobayashi A, Kaneko S, Takehira K, Yoshihara T, Ishida H, Shiina Y, Oishi S, Tobita S. Reevaluation of absolute luminescence quantum yields of standard solutions using a spectrometer with an integrating sphere and a back-thinned CCD detector. *Physical Chemistry Chemical Physics*. 2009;**11**:9850-9860. DOI: 10.1039/b912178a
- [92] Tamaki Y, Ishitani O. Supramolecular photocatalysts for the reduction of CO<sub>2</sub>. *ACS Catalysis*. 2017;**7**:3394-3409. DOI: 10.1021/acscatal.7b00440
- [93] Paul A, Connolly D, Schulz M, Pryce MT, Vos JG. Effect of water during the quantitation of formate in photocatalytic studies on CO<sub>2</sub> reduction in dimethylformamide. *Inorganic Chemistry*. 2012;**51**:1977-1979. DOI: 10.1021/ic202121s
- [94] Sekizawa K, Maeda K, Domen K, Koike K, Ishitani O. Artificial Z-scheme constructed with a supramolecular metal complex and semiconductor for the photocatalytic reduction of CO<sub>2</sub>. *Journal of the American Chemical Society*. 2013;**135**:4596-4599. DOI: 10.1021/ja311541a
- [95] Nakada A, Nakashima T, Sekizawa K, Maeda K, Ishitani O. Visible-light-driven CO<sub>2</sub> reduction on a hybrid photocatalyst consisting of a Ru(II) binuclear complex and a Ag-loaded TaON in aqueous solutions. *Chemical Science*. 2016;**7**:4364-4371. DOI: 10.1039/c6sc00586a
- [96] Kajiwarra T, Fujii M, Tsujimoto M, Kobayashi K, Higuchi M, Tanaka K, Kitagawa S. Photochemical reduction of low concentrations of CO<sub>2</sub> in a porous coordination polymer with a ruthenium(II)-CO complex. *Angewandte Chemie, International Edition*. 2016;**55**:2697-2700. DOI: 10.1002/anie.201508941
- [97] Sun D, Gao Y, Fu J, Zeng X, Chen Z, Li Z. Construction of a supported Ru complex on bifunctional MOF-253 for photocatalytic CO<sub>2</sub> reduction under visible light. *Chemical Communications*. 2015;**51**:2645-2648. DOI: 10.1039/c4cc09797a
- [98] Wang X, Thiel I, Fedorov A, Coperet C, Mougél V, Fontecave M. Site-isolated manganese carbonyl on bipyridine-functionalities of periodic mesoporous organosilicas: Efficient CO<sub>2</sub> photoreduction and detection of key reaction intermediates. *Chemical Science*. 2017;**8**:8204-8213. DOI: 10.1039/c7sc03512h

- [99] Kuramochi Y, Sekine M, Kitamura K, Maegawa Y, Goto Y, Shirai S, Inagaki S, Ishida H. Photocatalytic CO<sub>2</sub> reduction by periodic mesoporous organosilica (PMO) containing two different ruthenium complexes as photosensitizing and catalytic sites. *Chemistry—A European Journal*. 2017;**23**:10301-10309. DOI: 10.1002/chem.201701466
- [100] Ueda Y, Takeda H, Yui T, Koike K, Goto Y, Inagaki S, Ishitani O. A visible-light harvesting system for CO<sub>2</sub> reduction using a RuII-ReI photocatalyst adsorbed in mesoporous organosilica. *ChemSusChem*. 2015;**8**:439-442. DOI: 10.1002/cssc.201403194
- [101] Takeda H, Ohashi M, Tani T, Ishitani O, Inagaki S. Enhanced photocatalysis of rhenium(I) complex by light-harvesting periodic mesoporous organosilica. *Inorganic Chemistry*. 2010;**49**:4554-4559. DOI: 10.1021/ic1000914

---

# Carbon Dioxide Conversion to Methanol: Opportunities and Fundamental Challenges

---

Sajeda A. Al-Saydeh and Syed Javaid Zaidi

Additional information is available at the end of the chapter

<http://dx.doi.org/10.5772/intechopen.74779>

---

## Abstract

Greenhouse gases mitigation is one of most important challenges facing societies nowadays. Therefore, the way to reduce greenhouse gas emissions should be using carbon free sources that do not generate extra CO<sub>2</sub> to the atmosphere. However, there is a great potential in energy carriers and other materials from CO<sub>2</sub>, with many challenges to overcome. It has been suggested that the reduction of CO<sub>2</sub> and conversion to renewable fuels and valuable chemicals may be considered as a promising solution to reduce the greenhouse gas emissions. This chapter discusses the recent developments and remaining challenges of CO<sub>2</sub> utilization for the efficient production of methanol. This includes novel technologies, approaches, and current barriers for the conversion of CO<sub>2</sub> to methanol through heterogeneous catalysis, homogenous catalysis, electrochemical, photochemical, and photoelectrochemical conversion, which will contribute to the economic growth and mitigate the hazardous emissions for cleaner environment. A review of various state-of-the-art technologies for CO<sub>2</sub> conversion to methanol was carried out aiming to establish the advances in this area and present an overview of the recent research trend for future development of new ideas for CO<sub>2</sub> reduction into methanol in a large scale.

**Keywords:** CO<sub>2</sub> utilization, heterogeneous catalysis, homogeneous catalysis, electrochemical conversion, photochemical conversion, photoelectrochemical conversion

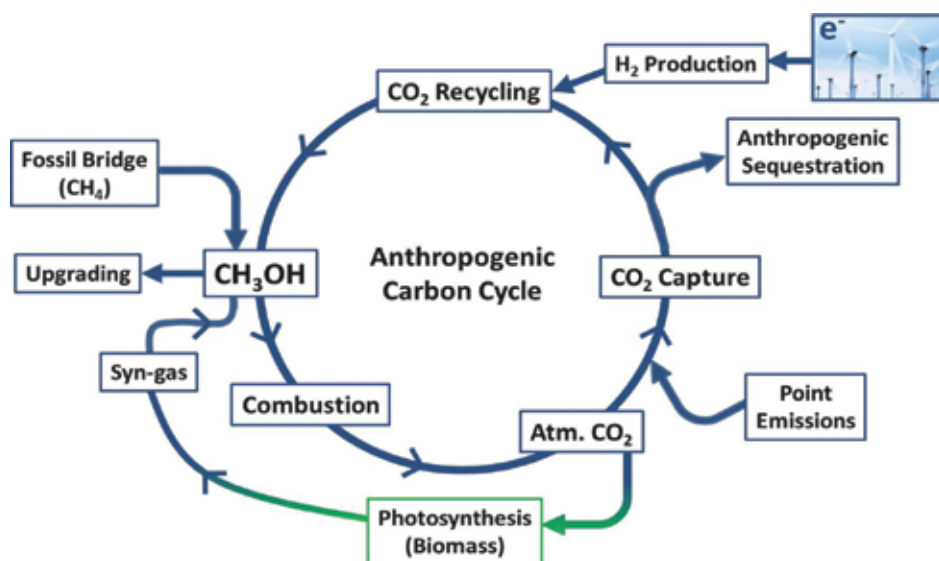
---

## 1. Introduction

Nowadays, the demand for energy is rapidly increasing because of the economic growth worldwide. In order to meet this growing demand, an abundant amount of fossil fuel (oil, coal, and natural gas) is needed [1]. Fossil fuel combustion is often considered as one of the main threats to the environment because of the CO<sub>2</sub> release in the atmosphere. CO<sub>2</sub>, which is

---

considered as a primary greenhouse-gas (GHG), is periodically exchanged within land surface, ocean, and atmosphere where a variety of creatures, including animals, plants, and microorganisms absorb and produce it daily. However, the process of releasing and consuming  $\text{CO}_2$  trends has to be balanced by nature. Since 1750, when the industrial revolution began, so did climate change following the activities related to industries. In order to reduce the greenhouse gas emissions,  $\text{CO}_2$  sequestration and storage (CSS) processes gained a widespread attention. However, it will increase the amount of available captured  $\text{CO}_2$  as feedstock of zero cost. Therefore, utilizing  $\text{CO}_2$  and converting it into fuels and chemicals, which is called carbon capture and recycling (CCR) process, is an active option used worldwide to convert usable products into valuable products, and it is used to mitigate  $\text{CO}_2$  emissions which is more preferable compared to CSS option [2–5]. During the last years, conversion of  $\text{CO}_2$  into value-added chemicals (i.e., ethanol, methanol, and formic acid) using different ways has received a great attention from the researchers as it can be seen as a solution to reduce the global warming [6–8], energy crisis (i.e., fossil fuels depletion) [9–11], and the storage of energy [12] problems. Methanol is a renewable energy source that can be produced from any raw material containing carbon (mainly  $\text{CO}_2$ ), as well as it is a clean source of energy that can be used as transportation fuel. In general, for a fuel to satisfy the market demand, it must be sustainable material, clean, and able to be synthesized from available resources. Nowadays, as a matter of fact, most of the production companies around the world use methanol as a raw material to produce different products. Methanol is used in producing solvents like the acetic acid, which represents 10% of the global demand [13]. Methanol can also be used in direct methanol fuel cells (DMFC), which is used for the conversion of chemical energy in methanol directly to electrical power under ambient conditions [14]. Methanol is considered to be one of the most important organic feedstocks that can be used in the industries with an annual production of 65 million tons worldwide [15]. However, “Methanol Economy” term includes an anthropogenic carbon cycle for methanol production as shown in **Figure 1**, which can be used as a renewable fuel or to



**Figure 1.** Anthropogenic carbon cycle for methanol production [20].



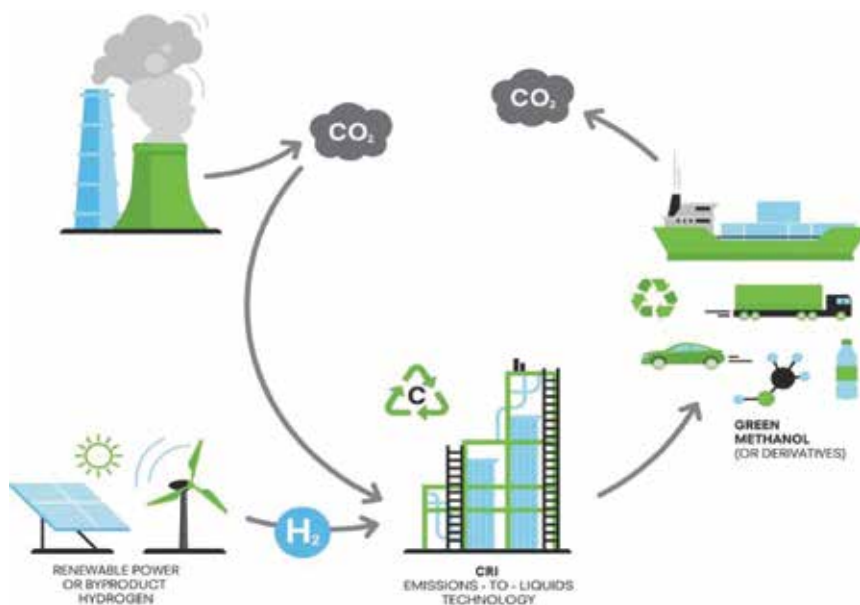


Figure 2. Green methanol production by Carbon Recycling International [18].

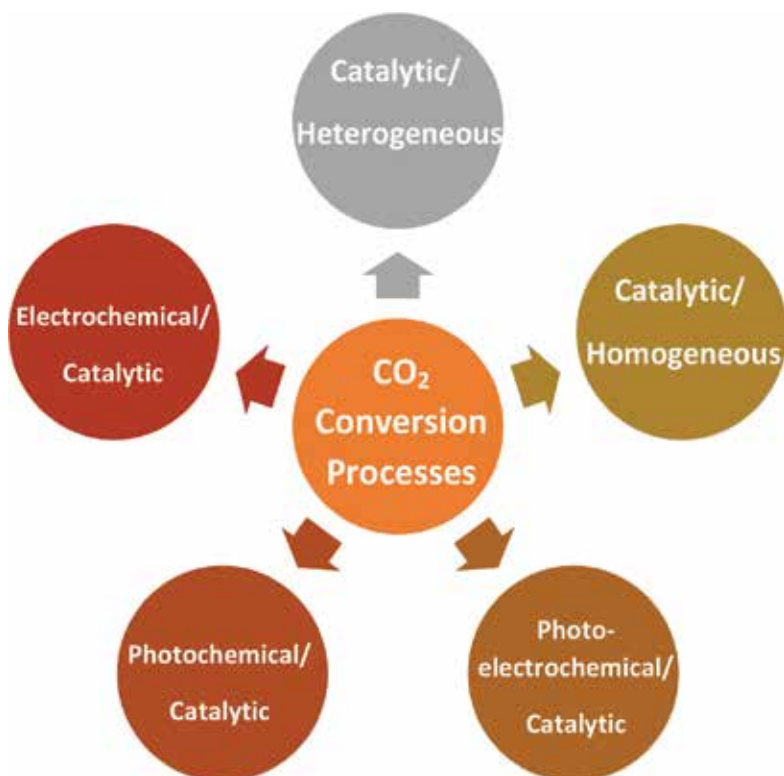


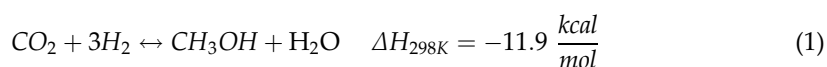
Figure 3. Outline of chemical conversion processes of CO<sub>2</sub>.

produce nearly all products that are derived from fossil fuels [16, 17]. Carbon Recycling International (CRI)'s George Olah plant is considered to be the world's largest CO<sub>2</sub> methanol plant. In 2015, Carbon Recycling International (CRI) scaled up the plant from a capacity of 1.3 million liters of methanol per year to more than 5 million liters a year. The plant now recycles 5.5 thousand tons of CO<sub>2</sub> a year. All energy used in the plant comes from the Icelandic grid that is generated from geothermal and hydro energy [18]. As shown in **Figure 2**, the plant uses electricity to make H<sub>2</sub> which reacts with CO<sub>2</sub> in a catalytic reaction for methanol production. The various pathways and processes for CO<sub>2</sub> conversion to methanol are described schematically in **Figure 3**. There are different CO<sub>2</sub> conversion routes such as the catalytic method which comes in the form of conventional, electrocatalytic, photocatalytic, and photoelectrocatalytic conversion [19].

## 2. Methods to convert CO<sub>2</sub> into methanol

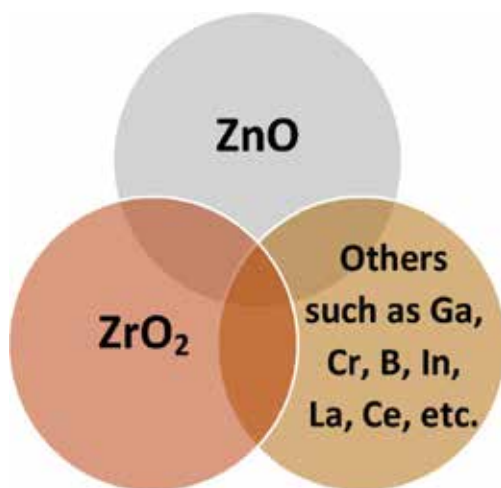
### 2.1. Chemical conversion

The catalytic hydrogenation of CO<sub>2</sub> with H<sub>2</sub> is considered to be the most straightforward way for methanol and DME production from CO<sub>2</sub>, as shown in Eq. (1). During the 1920s and 1930s, the earliest methanol production plants were operated in the USA, which were using CO<sub>2</sub> and H<sub>2</sub> to produce methanol. Both heterogeneous and homogeneous catalysts systems have been studied by many researchers for CO<sub>2</sub> hydrogenation process. However, heterogeneous catalysts have many advantages in terms of separation, stability, handling, cost, and recycling of the catalyst. Heterogeneous and homogeneous catalysts systems are discussed in the following sections [21–23].



#### 2.1.1. Heterogeneous catalytic conversion

Although homogeneous catalysis is also used for methanol production from CO<sub>2</sub>, heterogeneous catalysis is the preferred choice for chemical reaction engineers due to the advantages of heterogeneous catalysis. This includes easy separation of fluid from solid catalyst, convenient handling in different types of reactors (i.e., fixed-, fluidized- or moving-bed), and the used catalyst can be regenerated. Recently, a large number of experiments have been conducted for the development of stable and efficient heterogeneous catalysts for the reduction of CO<sub>2</sub> to produce methanol. However, many studies proved that the Cu based catalysts with different additives such as ZrO<sub>2</sub> and ZrO play an important role to improve the stability and activity of the heterogeneous catalyst (**Figure 4**). Therefore, some of the catalysts, that are shown in **Figure 4**, are already exist and used in demonstration and pilot plants. Some of the metals (i.e., Cu and Zn) and their oxides have been developed to be used as an efficient heterogeneous catalyst for the conversion of CO<sub>2</sub> to methanol [24, 25]. This type of catalyst is similar to Cu/ZnO/Al<sub>2</sub>O<sub>3</sub> based catalysts that are used to produce methanol in the industry. However, it



**Figure 4.** Supports and additives used for Cu-based catalysts.

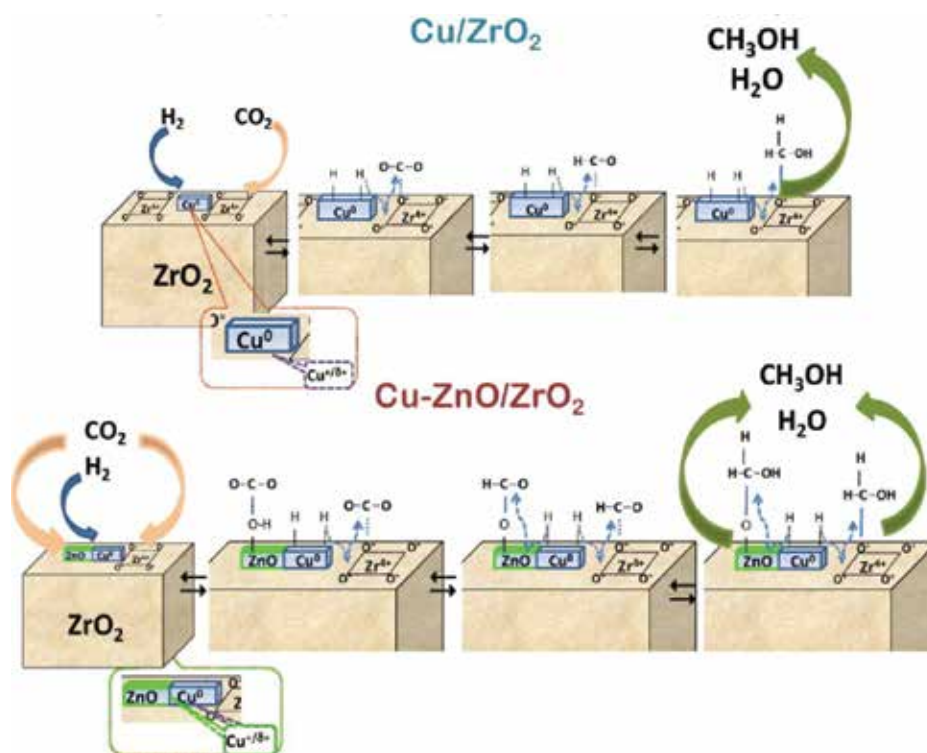
has been proved that the commercial methanol catalyst such as the heterogeneous mixture of zinc oxide, alumina, and copper (30, 10, and 60%, respectively) produces very little amount of methanol [26]. Various reviews discussed the different factors that may affect the methanol production from syngas such as catalyst preparation, catalyst design, reaction kinetics, reactor design, and catalyst deactivation [22, 27–30]. Therefore, the future research works should be focused on the methanol production from CO<sub>2</sub> and H<sub>2</sub> in which the amount of produced methanol by this way is higher compared to the syngas. In order to sustain high plant output, the catalyst should remain active to be used for several years. Moreover, improving the activity and stability of catalyst over time is very important in the economics of any methanol plant [31]. Recently, Lurgi, which is the leader in methanol synthesis process technology, has been collaborated with Süd-Chemie using a high activity catalyst (C79-05-GL, based on Cu/ZnO) to convert CO<sub>2</sub> and H<sub>2</sub> into methanol [24, 32]. The Lurgi methanol reactor is a tube-based converter which contains the catalysts in fixed tubes and uses a steam pressure control to achieve the controlled temperature reaction. This type of reactor is able to achieve low recycle ratios and high yield. Therefore, Lurgi has been developed to two-stage converter system which uses two combined Lurgi reactors for high methanol capacities. However, the space velocities and temperatures in the first converter will be higher than the single-stage converter in which it needs to achieve only partial conversion of synthesis gas to methanol. This makes the converter to be smaller and produces high-pressure steam due to the high temperatures which will help in saving the energy costs. The exit gas, from the first converter, contains methanol, and it will be directly sent to the second reaction stage that operates at a lower reaction rate [31]. Even if the operating temperature of the Lurgi system is around 260°C which is higher than that used for conventional catalysts to produce methanol, but the methanol selectivity of this system is excellent. However, the activity of this catalyst is decreased with the same rate as commercial catalyst's activity, which is currently used in the industries to produce methanol. There are different companies commercializing high stable catalysts for methanol production such as Mitsubishi Gas Chemical, Sinetix, and Haldor Topsøe. Arena et al. [33]

studied the solid-state interactions, functionality, and adsorption sites of Cu–ZnO/ZrO<sub>2</sub> catalysts and its ability for the conversion of CO<sub>2</sub> to methanol. Characterization data indicated that the strong Cu–ZnO interaction effectively promotes the dispersion and reactivity of metal copper to oxygen. The metal/oxide interface in Cu–ZnO/ZrO<sub>2</sub> catalysts plays an important role in hydrogenation of CO<sub>2</sub> to methanol. As shown in **Figure 5**, the dual-site nature of the reaction path explains the formal structure-insensitive character of CO<sub>2</sub> conversion over Cu–ZnO/ZrO<sub>2</sub> catalysts.

## 2.1.2. Homogenous catalytic conversion

### 2.1.2.1. Homogeneous catalysts for CO<sub>2</sub> Hydrogenation to produce methanol

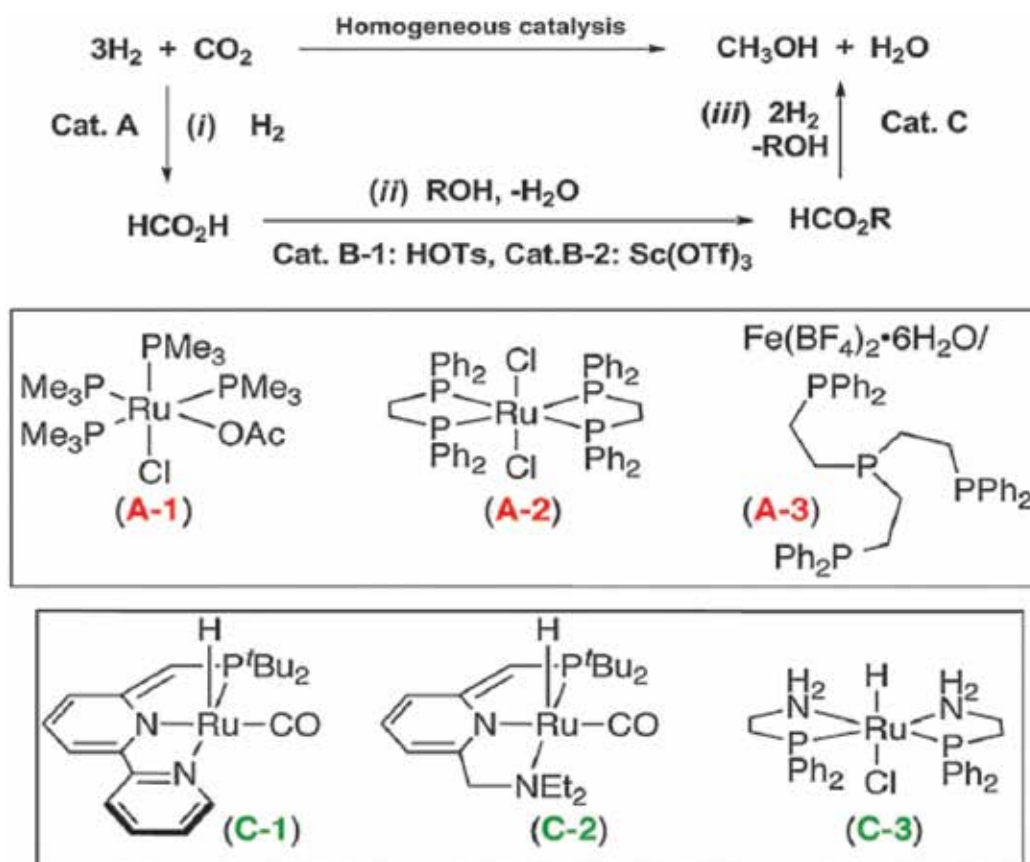
Although different heterogeneous catalysts were tested for the direct CO<sub>2</sub> conversion to methanol, yet very limited homogeneous catalysts have been mentioned in the literature. Tominaga et al. [34] reported an example of direct CO<sub>2</sub> conversion to methanol using homogeneous catalysts. They studied the ability of Ru<sub>3</sub>(CO)<sub>12</sub> catalyst precursor in the presence of KI additive for the CO<sub>2</sub> hydrogenation to form methane, methanol, and CO. Also, it was proved by the same authors that the performance of Ru<sub>3</sub>(CO)<sub>12</sub>–KI for CO<sub>2</sub> conversion is much better than the other transition metal carbonyl catalysts such as W(CO)<sub>6</sub>, Fe<sub>2</sub>(CO)<sub>9</sub>, Ir<sub>4</sub>(CO)<sub>12</sub>, Mo(CO)<sub>6</sub>, Co<sub>2</sub>(CO)<sub>8</sub>, and Rh<sub>4</sub>(CO)<sub>12</sub> [35]. Recently, cascade process has been used to reduce CO<sub>2</sub> to



**Figure 5.** Heterogeneous catalytic process for conversion of CO<sub>2</sub> to methanol using Cu/ZrO<sub>2</sub> and Cu-ZnO/ZrO<sub>2</sub> [33].

methanol instead of six electrons process [36]. Cascade process using homogeneous catalysts can be divided into three steps, which are hydrogenation of CO<sub>2</sub> to formic acid; then, the formic acid will be esterified to generate formate esters; and finally, the formate ester will be hydrogenated to produce methanol (**Figure 6**) as mentioned by Huff and Sanford [36].

Different catalysts will be used in each step of this approach under specific reaction conditions which are high temperature (135°C) and pressure (40 bars). Wesselbaum et al. [37] reported the hydrogenation of CO<sub>2</sub> with 60 bars of H<sub>2</sub> and 20 bars of CO<sub>2</sub> at 140°C in the presence of [(triphos)Ru-(TMM)] (TMM = trimethylenemethane, Triphos = 1,1,1-tris(diphenylphosphinomethyl) ethane) giving a maximum turnover number of 221. Therefore, it has been proved by the same authors that this catalyst can be used in the hydrogenation process to convert formate esters to methanol. In addition to the direct CO<sub>2</sub> conversion to methanol, the conversion of CO<sub>2</sub> derivatives by hydrogenation, such as polycarbonates, carbonates, formates, and carbamates, has gained a huge attention due to the small barriers of these reactions (**Figure 7**) [38, 39].



**Figure 6.** CO<sub>2</sub> hydrogenation to produce methanol via cascade system [36].

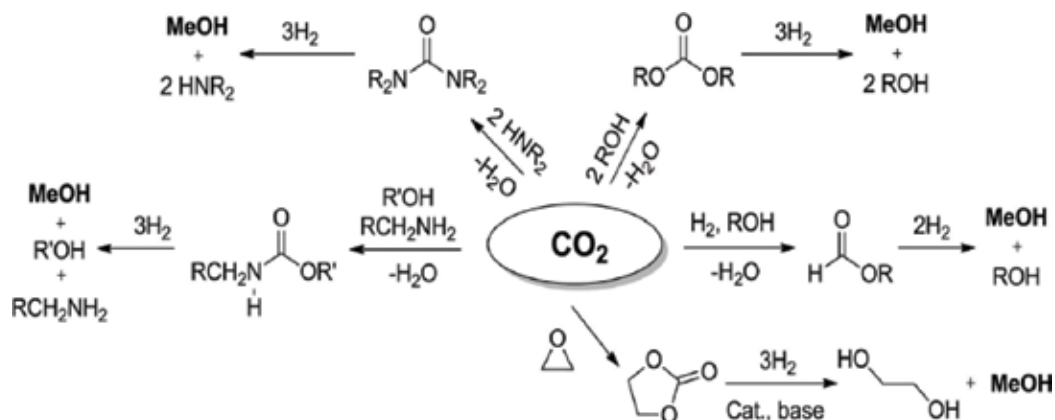


Figure 7. Indirect hydrogenation of  $\text{CO}_2$  for methanol production [39].

### 2.1.2.2. Homogeneous chemical conversion of $\text{CO}_2$ to methanol

Silanes and hydrides are the main reducing agents to be used in the homogeneous chemical reduction of  $\text{CO}_2$  to methanol in the presence of organocatalysts such as N-heterocyclic carbenes (NHC). Although the cost of the silanes is high, it was proved that the NHC-catalyst has the ability to reduce  $\text{CO}_2$  to methoxides under ambient conditions as mentioned by Zhang et al. [40]. As shown in **Figure 8**, the derivatives of silanol and methanol will be produced by the hydrolysis of methoxysilanes.

The application of frustrated Lewis pairs to reduce  $\text{CO}_2$  to methanol is considered to be another example of the metal-free catalysis (**Figure 9**) [41]. In the first step, the formatoborate derivative is produced via the reaction between  $\text{CO}_2$  and  $[\text{TMPH}] + [\text{HB}(\text{C}_6\text{F}_5)_3]^-$ . The coordinatively unsaturated  $\text{B}(\text{C}_6\text{F}_5)_3$  attacks the nucleophile and formato-bridged intermediate forms.

After that, the latter will react with  $[\text{TMPH}] + [\text{HB}(\text{C}_6\text{F}_5)_3]^-$  to produce the formaldehyde acetal derivative. Schwartz's reagent ( $(\text{Cp})_2\text{Zr}(\text{H})(\text{Cl})$ ) was used as a hydride source for the two-step

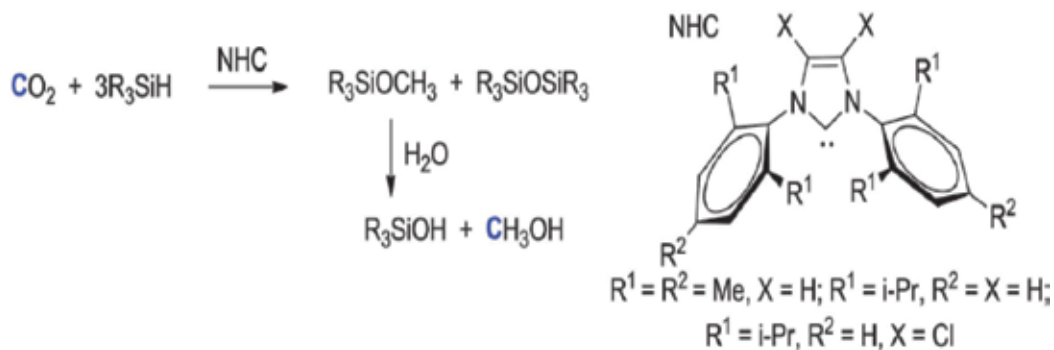


Figure 8. NHC-catalyzed  $\text{CO}_2$  conversion and the subsequent methanol hydrolytic [40].

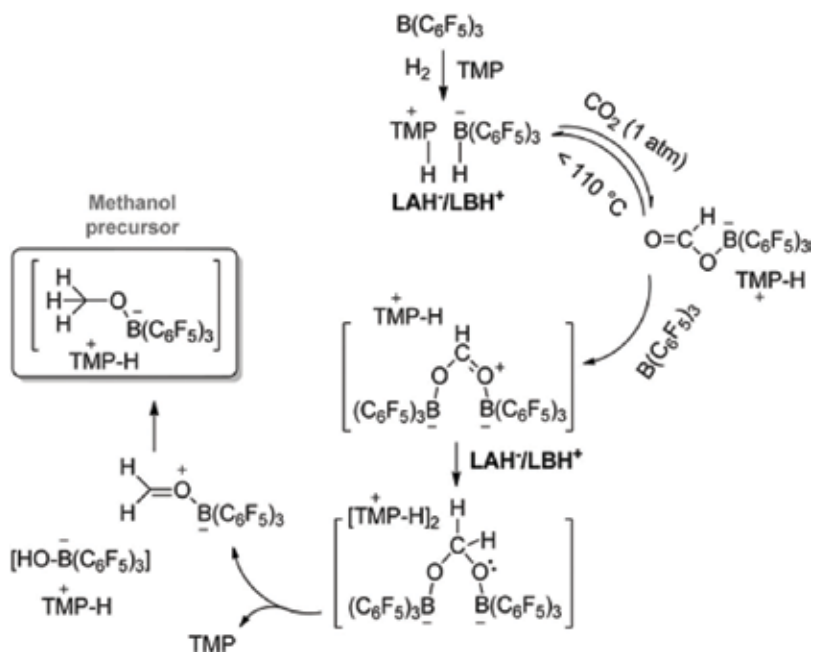


Figure 9. Lewis acid/Lewis base-catalyzed CO<sub>2</sub> hydrogenation [44].

reduction of CO<sub>2</sub> to formaldehyde and methanol, respectively as shown in (Figure 10) [42, 43]. In the first step, the conversion of CO<sub>2</sub> to formaldehyde produces some of the m-oxo complexes. Then, the deeper reduction of formaldehyde can be achieved by adding more Schwarz's reagent which leads to form zirconium methoxide in the second step.

## 2.2. Electrochemical reduction of CO<sub>2</sub> to methanol

During the last decades, electrochemical CO<sub>2</sub> conversion has been widely used on a laboratory scale, but it has not yet been successfully used in the industrial processes (large scale). The electrochemical reduction method is used for CO<sub>2</sub> conversion to valuable chemicals and fuels

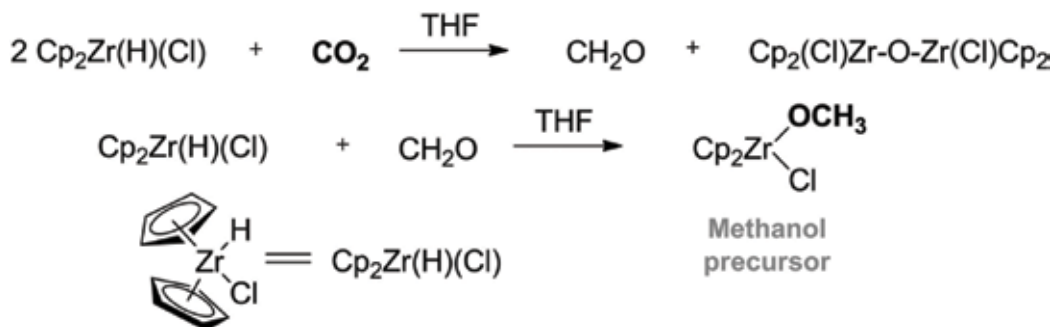


Figure 10. Two-step CO<sub>2</sub> reduction to methanol with Schwarz's reagent [44].



Half-cell reaction	E° vs. SHE
$CO_2 + 8H^+ + 8e^- \rightarrow CH_4 + 2H_2O$	+0.17
$CO_2 + 6H^+ + 6e^- \rightarrow CH_3OH + H_2O$	+0.031
$CO_2 + 4H^+ + 4e^- \rightarrow CH_2O + H_2O$	-0.028
$CO_2 + 2H^+ + 2e^- \rightarrow CO + H_2O$	-0.10
$CO_2 + 2H^+ + 2e^- \rightarrow HCOOH$	-0.11

**Table 1.** Standard potentials for CO<sub>2</sub> reduction [49].

such as methanol using electricity as the main source of energy [45–47]. Many experiments with different conditions and electrocatalysts have been conducted for CO<sub>2</sub> reduction on metal electrodes [48]. Different reduced products can be formed electrochemically from CO<sub>2</sub>, and some of these products are presented in **Table 1**. The selection of catalyst and reaction conditions plays a significant role as compared to the potential in controlling between various reduced products. However, all the listed standard potentials in **Table 1** are relatively close to the hydrogen evolution standard potential [49]. The hydrogen evolution reaction (HER) is very important during CO<sub>2</sub> electrocatalyst reduction in which H<sub>2</sub>O is typically present as an electrolyte (and proton source). For this reason, the reported metals that can be used as an electrocatalyst for CO<sub>2</sub> reduction have relatively high HER overpotentials. A huge effort must be conducted in order to find the optimum electrode for CO<sub>2</sub> electrochemical reduction which will reduce the selectivity of CO<sub>2</sub> at low overpotentials and high rates without reducing water simultaneously [44].

There is a distinct advantage of directly converting the captured CO<sub>2</sub> into methanol of producing a useful product that can be used in many energy-consuming devices. This process allows for recycling captured CO<sub>2</sub> and produce methanol that could be used as a renewable energy instead of fossil fuel in energy-consuming devices. In other words, by electroreduction process, CO<sub>2</sub> could be reduced directly in the electrolysis cell back to methanol in one step. Different electrodes can be used to achieve methanol directly from CO<sub>2</sub> [44], as shown in **Table 2**. In 1983, Canfield and Frese [50] proved that some semiconductors such as *n*-GaAs, *p*-InP, and *p*-GaAs have the ability to produce methanol directly from CO<sub>2</sub> although at extremely low current densities and faradaic efficiencies (FEs). Many other researchers did some efforts to increase both the current density as well as faradaic efficiency of the process. Seshadri et al. [51] found that the pyridinium ion is a novel homogeneous electrocatalyst for CO<sub>2</sub> reduction to methanol at low overpotential. Recently, Pyridine has been widely explored in which it is used to act as co-catalyst to form the active pyridinium species in situ [52–56]. Generally, the one-electron reduction products of CO<sub>2</sub> show lower current density than the two-electron reduction products such as CO. The direct electrochemical reduction of CO<sub>2</sub> to methanol is a promising process to reduce the amount of captured CO<sub>2</sub>.

Popić et al. [57] proved that the Ru and Ru modified by Cd and Cu adatoms can be used as an electrode for CO<sub>2</sub> reduction at relatively small overpotentials. The obtained results showed that on the surface of pure Ru, Ru modified by Cu and Cd adatoms, and RuOx+IrOx modified



Electrode	Type of electrode	E vs. NHE (V)	Current density (mA cm <sup>-2</sup> )	Faradaic efficiency (%)	Electrolyte	Reference
<i>p</i> -InP	Semiconductor	-1.06	0.06	0.8	Sat. Na <sub>2</sub> SO <sub>4</sub>	[50]
<i>n</i> -GaAs			0.16	1.0		
<i>p</i> -GaAs			0.08	0.52		
CuO	Metal oxide	-1.3	6.9	28	0.5 M KHCO <sub>3</sub>	[59]
RuO <sub>2</sub> /TiO <sub>2</sub> Nanotubes		-0.6	1	60	0.5 M NaHCO <sub>3</sub>	[58]
Pt-Ru/C	Alloy	-0.06	0.4	7.5	Flow cell	[60]
<i>n</i> -GaP	Homogeneous catalyst	-0.06	0.27	90	10 mM pyridine at pH = 5.2	[61]
Pd		-0.51	0.04	30	0.5 M NaClO <sub>4</sub> with pyridine	[51]

**Table 2.** CO<sub>2</sub> electrochemical reduction to methanol.

by Cu and Cd adatoms, the reduction of CO<sub>2</sub> was achieved to produce methanol during 8 h of holding the potential at -0.8 V. Therefore, in case of CO<sub>2</sub> reduction on Ru modified by Cu and Cd adatoms, the production of methanol was depended on the presence of adatoms at the surface of ruthenium. RuO<sub>2</sub> is a promising material to be used as an electrode for CO<sub>2</sub> reduction to methanol due to its high electrochemical stability and electrical conductivity. For that reason, Qu et al. [58] prepared RuO<sub>2</sub>/TiO<sub>2</sub> nanoparticles (NPs) and nanotubes (NTs) composite electrodes by loading of RuO<sub>2</sub> on TiO<sub>2</sub> nanoparticles and nanotubes, respectively. The obtained results showed that the current efficiency of producing methanol from CO<sub>2</sub> was up to 60.5% on the RuO<sub>2</sub>/TiO<sub>2</sub> NTs modified Pt electrode. Therefore, RuO<sub>2</sub> and RuO<sub>2</sub>/TiO<sub>2</sub> NPs composite electrodes showed lower electrocatalytic activity than RuO<sub>2</sub>/TiO<sub>2</sub> NTs composite modified Pt electrode for the electrochemical reduction of CO<sub>2</sub> to methanol. In order to increase the selectivity and efficiency of CO<sub>2</sub> electrochemical reduction process, nanotubes structure is suggested to be used as an electrode as the studies proved.

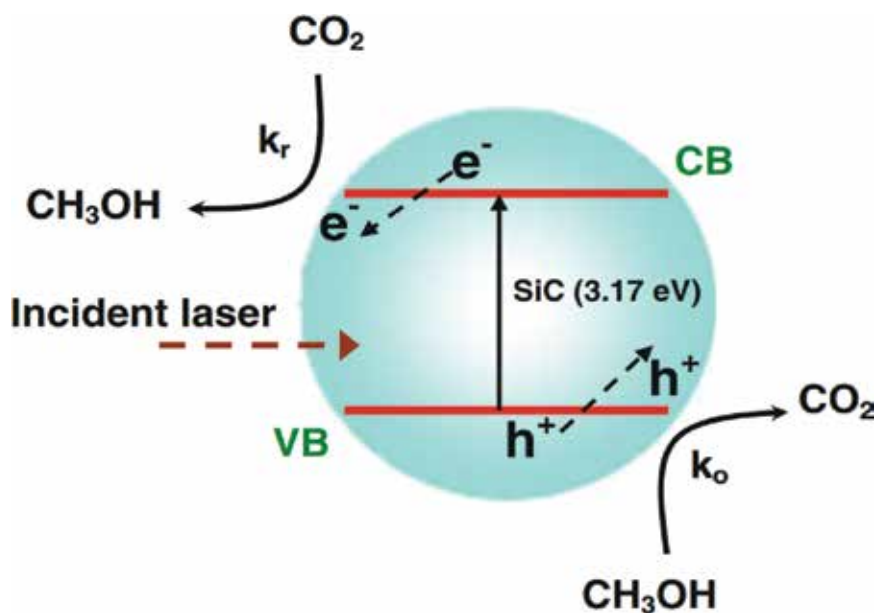
### 2.3. Photochemical reduction of CO<sub>2</sub> to methanol

Typically, the photochemical (or photocatalytic) CO<sub>2</sub> conversion method is used to convert captured CO<sub>2</sub> to methanol and other valuable products by using solar energy such as light or laser [62, 63]. Even if the selectivity for methanol is relatively low, the direct conversion of CO<sub>2</sub> to methanol using photocatalytic method has been studied [64]. However, recently, this method has received a great attention, and it is considered to be as the most attractive method for CO<sub>2</sub> utilization. The photocatalytic CO<sub>2</sub> conversion process is a complex combination of photophysical and photochemical processes together [62]. Therefore, this method has some similarities with electrocatalytic CO<sub>2</sub> reduction in which the molecular catalysts are used in both cases. Sacrificial hydride source is considered to be the major limitation to reduce CO<sub>2</sub> by photocatalytic method. Ascorbic acid, amine, and 1-benzyl-1,4-dihydronicotinamide are examples of sacrificial hydride source, which must be added to the solution to substitute for the

anode, that would be used in electrocatalytic CO<sub>2</sub> reduction process [65]. Several experiments have been conducted to test the ability of some semiconductors and metal oxides for CO<sub>2</sub> conversion to methanol. This include silicon carbide [66], TiO<sub>2</sub> [67–70], WO<sub>3</sub> [71], NiO [70], ZnO [70], and InTaO<sub>4</sub> [72] either by themselves or they can be combined with different heterogeneous catalysts to achieve the same goal. The main challenge in methanol production on semiconductors by using solar energy is that the formation reaction is reversible. Thus, in order to mitigate the methanol oxidation, it is very essential to find new strategies to achieve a practical industrial process [66, 70].

Gondal et al. [66] proved that the granular silicon carbide is a promising photocatalyst for CO<sub>2</sub> reduction to methanol. The granular silicon carbide ( $\alpha$ 6H-SiC) has been tested as a photocatalyst to reduce CO<sub>2</sub> and convert it into methanol using a 355-nm laser. The reaction cell was filled with  $\alpha$ 6H-SiC granules, pressurized with CO<sub>2</sub> gas at 50 psi and distilled water. Therefore, they mentioned that a pair of competitive reactions which are photo-oxidation and photo-reduction are existed in the photochemical process, as shown in **Figure 11**. When the reaction starts, the photooxidation rates ( $K_o$ ) will be slower than the photoreduction rates ( $K_r$ ) because of the low concentration of produced methanol. The obtained results showed that the maximum molar concentration of methanol and photonic efficiencies of CO<sub>2</sub> conversion into methanol achieved was around 1.25 mmol/l and 1.95%, respectively.

CdS/TiO<sub>2</sub> and Bi<sub>2</sub>S<sub>3</sub>/TiO<sub>2</sub> nanotube photocatalysts were tested by Li et al. [67], and their photocatalytic activities that reduce CO<sub>2</sub> to methanol under visible light irradiation have been studied. The obtained results proved that the synthetical TNTs are almost a good material to be act as photoreduction to convert CO<sub>2</sub> into methanol. The largest methanol production on



**Figure 11.** Schematic illustration of the photoreduction and photooxidation reactions in the photochemical process [67].

TNTs–CdS and TNTs–Bi<sub>2</sub>S<sub>3</sub> photocatalysts by using visible light irradiation for 5 h were 159.5 and 224.6 μmol/L, respectively. Luo et al. [68] studied the ability of Nd/TiO<sub>2</sub>, which is synthesized via the sol-gel method, to reduce CO<sub>2</sub> into methanol in an aqueous solution under UV irradiation. The experiment showed that the maximum methanol yield under UV irradiation for 8 h was 184.8 μmol/g, proving that the Nd/TiO<sub>2</sub> can increase the efficiency of CO<sub>2</sub> photocatalytic reduction compared to pure titanium oxide.

## 2.4. Photoelectrochemical reduction of CO<sub>2</sub> to methanol

The photoelectrocatalytic CO<sub>2</sub> reduction process is a combination of the photocatalytic and electrocatalytic methods together. Many research works were focused to find the best semiconductor material that can be used as a photoelectrode to convert CO<sub>2</sub> into methanol using any solar energy in PEC cell; however, no tested semiconductor met the desired stability and efficiency [73]. In fact, the photoelectrochemically reduction of CO<sub>2</sub> need around 1.5 eV of thermodynamic energy input. Therefore, the PEC cell needs greater energy input to make up the losses that causes by band bending (which is needed for charge separation at the surface of semiconductor), overvoltage potentials, and resistance losses [61, 74–81]. The first important step for the reduction of CO<sub>2</sub> to methanol by the photoelectrochemical (PEC) method is the hydrogen ions and electrons generation by the solar irradiance of semiconductor which is used as photocathode. The semiconductor (e.g., GaP, SiC) is illuminated by light as the source of energy that is higher than the semiconductor’s band gap. In that case, the electrons in semiconductor will be excited and transferred to conduction band from the valance band, and it will reach the cathode counter electrode through an external electrical wire. Furthermore, in order to produce the electrochemical reduction and oxidation reactions, the produced electron-hole pairs at or near the interface will be separated by the semiconductor and will be injected into the electrolyte [82–84]. A major problem in using the photoelectrochemical cells is the ability of n-type semiconductor materials to generate holes on the surface that can oxidize the

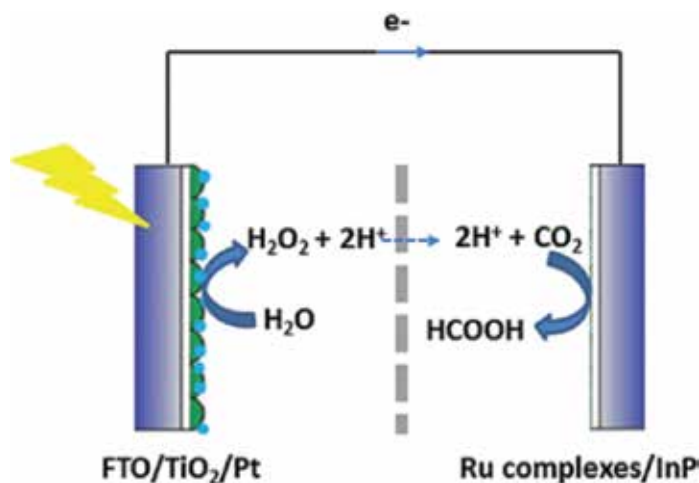
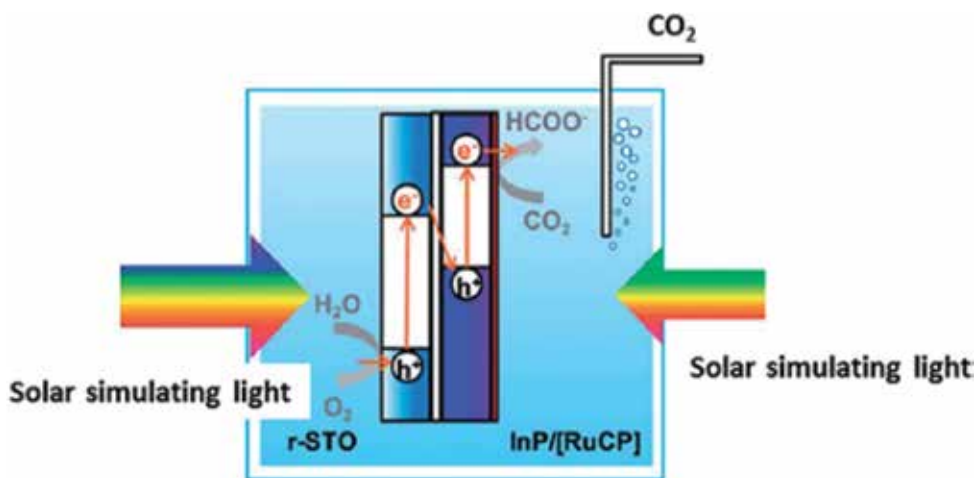


Figure 12. The two-compartment photoelectrochemical cell for CO<sub>2</sub> reduction [87].



**Figure 13.** The one-compartment photoelectrochemical cell for CO<sub>2</sub> reduction [87].

semiconductor itself [85]. Recently, the hybrid system which consists of a semiconductor light harvester and a complex of metal co-catalyst has received a huge attention. In this system, the water is considered the main source of electron donors and protons for the reduction of CO<sub>2</sub> at the surface of cathode. An example of hybrid system has been discussed by Zhao et al. [86]. They studied the full cell of photocathode with InP/Ru-complexes that was coupled with a TiO<sub>2</sub>/Pt based photoanode, as shown in **Figure 12**. In this full cell, in order to avoid the formate re-oxidation at the surface of photoanode, the proton exchange membrane was used as a separator. However, Arai et al. constructed a wireless full cell for photoelectrochemical CO<sub>2</sub> reduction in which the system consists of the InP/Ru-complex as a hybrid photocathode and a photoanode of SrTiO<sub>3</sub> (**Figure 13**). In this system, the redox reactions of CO<sub>2</sub> and H<sub>2</sub>O will occur via sunlight irradiation without applying any bias. The obtained results showed that the conversion efficiency from solar to chemical energy in these two full cells was 0.03% and 0.14% for TiO<sub>2</sub>-InP/[RuCP] and SrTiO<sub>3</sub>-InP/[RuCP], respectively. Barton et al. [61] successfully reduced CO<sub>2</sub> to methanol by using catalyzed p-GaP-based photoelectrochemical (PEC) cell in a process called chemical carbon mitigation. Chemical carbon mitigation term describes the photoinduced CO<sub>2</sub> conversion to methanol without the use of additional CO<sub>2</sub> generating power source. The obtained results showed that the methanol selectivity and CO<sub>2</sub> conversion were found to be 100 and 95%, respectively.

### 3. Future prospective and conclusions

Carbon dioxide conversion is presenting both an opportunity and a challenge worldwide for the sustainability of environment and energy. The main strategies of CO<sub>2</sub> reduction should focus on the utilization of CO<sub>2</sub>, the CO<sub>2</sub> recycling combined with the renewable energy to save carbon sources, and the useful chemicals production from CO<sub>2</sub>. Therefore, the conversion of CO<sub>2</sub> into energy product such as methanol will consume large amount of captured CO<sub>2</sub> in which the market scale of methanol is potentially extensive. Furthermore, the generated

methanol can be used instead of the fossil fuel, thus reducing the dependence on fossil fuel and contribute in the market growth of CO<sub>2</sub> utilization. Herein, a complete literature of different methods for CO<sub>2</sub> conversion into methanol is reported in this section. This include homogeneous/heterogeneous catalytic, electrochemical, photochemical, and photoelectrochemical reduction. However, the high performance in CO<sub>2</sub> conversion process can be achieved by using an effective catalyst. In general, the development of required catalyst can be used as a solution if the catalyst is already used, but it is required high cost to be scaled up or it does not exist and await discovery thus the challenges in catalytic processes are huge indeed. The poor product selectivity and the low/high reaction temperatures are considered to be the main barriers in the heterogeneous CO<sub>2</sub> reduction process. However, the above discussion shows that among various methods proposed for CO<sub>2</sub> conversion to methanol or to any valuable chemical, the electrochemical cells are the preferable over other methods. Nevertheless, many barriers still exist in the CO<sub>2</sub> electrochemical reduction in which the electrocatalyst is needed to be used at higher selectivity as well as lower over potentials. Various heterogeneous electrocatalysts are selective, fast and energy-efficient, but they are considered to be unstable catalysts. Therefore, in the future, the electricity needed for electrochemical CO<sub>2</sub> reduction process on a large scale can come from different renewable energy sources such as hydro, wind, wave, geothermal, tides, and so on. In this sense, many research works should be focused on new electrocatalytic materials that can be used to allow working at higher current densities without loss of Faradaic efficiency. On the other hand, photochemical processes offer an attractive approach to reduce CO<sub>2</sub> to methanol using solar energy. However, this method is not widely used due to its critical conditions to absorb the required amount of solar energy. Otherwise, the prospects to develop the successful technologies for the efficient CO<sub>2</sub> conversion using solar energy are certainly long term (>5 years out). Nonetheless, photoelectrochemical reduction processes are discovered to be attractive approaches for the reduction of CO<sub>2</sub> to methanol. At present, the applications of solar photoelectrochemical devices are very limited due to its high cost and several reasons, as discussed above. However, it is very important for research efforts to continue in these areas because this technology will be extremely needed for efficient reduction of CO<sub>2</sub> in the coming years.

## Acknowledgements

The authors would like to acknowledge the support of Center for Advanced Materials, Qatar University (QU) for this work. Ms. Sajeda Alsaydeh also acknowledges QU for Graduate Assistantship awarded to her.

## Author details

Sajeda A. Al-Saydeh and Syed Javaid Zaidi\*

\*Address all correspondence to: [szaidi@qu.edu.qa](mailto:szaidi@qu.edu.qa)

Center for Advanced Materials (CAM), Qatar University, Doha, Qatar

## References

- [1] Leung DY, Caramanna G, Maroto-Valer MM. An overview of current status of carbon dioxide capture and storage technologies. *Renewable and Sustainable Energy Reviews*. 2014;**39**:426-443
- [2] Peters M, Mueller T, Leitner W. CO<sub>2</sub>: From waste to value. *Chemical Engineer*. 2009;(813): 46-47
- [3] Aresta M. *Carbon Dioxide as Chemical Feedstock*. John Wiley & Sons; 2010
- [4] Aresta M, Dibenedetto A. Utilisation of CO<sub>2</sub> as a chemical feedstock: Opportunities and challenges. *Dalton Transactions*. 2007;(28):2975-2992
- [5] Centi G, Perathoner S. Opportunities and prospects in the chemical recycling of carbon dioxide to fuels. *Catalysis Today*. 2009;**148**(3-4):191-205
- [6] Hicks JC, Drese JH, Fauth DJ, Gray ML, Qi G, Jones CW. Designing adsorbents for CO<sub>2</sub> capture from flue gas-hyperbranched aminosilicas capable of capturing CO<sub>2</sub> reversibly. *Journal of the American Chemical Society*. 2008;**130**(10):2902-2903
- [7] Ritter SK. What can we do with CO? *Chemical & Engineering News Archive*. 2007;**85**(18): 11-17
- [8] Robinson AB, Robinson NE, Soon W. Environmental Effects of increased atmospheric carbon dioxide. *Journal of American Physicians and Surgeons*. 2007;**12**:79-90
- [9] Dinger A et al. Batteries for electric cars: Challenges, opportunities, and the outlook to 2020. The Boston Consulting Group. 2010;7:2017
- [10] Moniz EJ. *Nanotechnology for the Energy Challenge*. John Wiley & Sons; 2010
- [11] Budzianowski WM. Negative carbon intensity of renewable energy technologies involving biomass or carbon dioxide as inputs. *Renewable and Sustainable Energy Reviews*. 2012;**16**(9):6507-6521
- [12] Centi G, Perathoner S. CO<sub>2</sub>-based energy vectors for the storage of solar energy. *Greenhouse Gases: Science and Technology*. 2011;**1**(1):21-35
- [13] Global Demand of Methanol By Products, NGI, Natural Gas Inte. 2015. Available from: <http://www.naturalgasintel.com/articles/5062-valero-looks-to-build-mega-methanol-plant-fueled-by-shale>. At 26th of Oct. 2015
- [14] McGrath KM, Prakash GKS, Olah GA. Direct methanol fuel cells. *Journal of Industrial and Engineering Chemistry*. 2004;**10**(7):1063-1080
- [15] MI. Methanol Institute. 2013. Available from: The Methanol Industry, <http://www.methanol.org/Methanol-Basics.aspx>
- [16] Olah GA, Goepfert A, Prakash GKS. *Beyond Oil and Gas: The Methanol Economy*. John Wiley & Sons; 2011

- [17] Olah GA, Prakash GKS, Goepfert A. Anthropogenic chemical carbon cycle for a sustainable future. *Journal of the American Chemical Society*. 2011;**133**(33):12881-12898
- [18] Carbon Recycling International (CRI), World's Largest CO<sub>2</sub> Methanol Plant. 2016. Available from: <http://carbonrecycling.is/george-olah/2016/2/14/worlds-largest-co2-methanol-plant>
- [19] Kondratenko EV, Mul G, Baltrusaitis J, Larrazábal GO, Pérez-Ramírez J. Status and perspectives of CO<sub>2</sub> conversion into fuels and chemicals by catalytic, photocatalytic and electrocatalytic processes. *Energy & Environmental Science*. 2013;**6**(11):3112-3135
- [20] Letcher T, Scott J, Patterson DA. Chemical processes for a sustainable future. Royal Society of Chemistry. 2014
- [21] Chorkendorff I, Niemantsverdriet JW. Concepts of Modern Catalysis and Kinetics. John Wiley & Sons; 2017
- [22] Cheng W-H. Methanol Production and Use. CRC Press; 1994
- [23] Paul JK editor. Methanol technology and Application in Motor Fuels. Park Ridge, NJ: Noyes Data Corporation; 1978. (Energy technology review; no. 31, Accessed from <https://nla.gov.au/nla.cat-vn1028256>)
- [24] Goehna H, Koenig P. Producing methanol from CO<sub>2</sub>. 1994
- [25] Saito M. R&D activities in Japan on methanol synthesis from CO<sub>2</sub> and H<sub>2</sub>. *Catalysis Surveys from Asia*. 1998;**2**(2):175-184
- [26] Chinchin GC, Denny PJ, Parker DG, Spencer MS, Whan DA. Mechanism of methanol synthesis from CO<sub>2</sub>/CO/H<sub>2</sub> mixtures over copper/zinc oxide/alumina catalysts: Use of 14 C-labelled reactants. *Applied Catalysis*. 1987;**30**(2):333-338
- [27] Bart JCJ, Sneed RPA. Copper-zinc oxide-alumina methanol catalysts revisited. *Catalysis Today*. 1987;**2**(1):1-124
- [28] Waugh KC. Methanol synthesis. *Catalysis Today*. 1992;**15**(1):51-75
- [29] Chinchin GC, Denny PJ, Jennings JR, Spencer MS, Waugh KC. Synthesis of methanol: Part 1. Catalysts and kinetics. *Applied Catalysis*. 1988;**36**:1-65
- [30] Klier K. Methanol synthesis. *Advances in Catalysis*. 1982;**31**:243-313
- [31] Tijm PJA, Waller FJ, Brown DM. Methanol technology developments for the new millennium. *Applied Catalysis A: General*. 2001;**221**(1):275-282
- [32] Inui T, Anpo M, Izui K, Yanagida S, Yamaguchi T. *Advances in Chemical Conversions for Mitigating Carbon Dioxide*. Elsevier; 1998
- [33] Arena F et al. Solid-state interactions, adsorption sites and functionality of Cu-ZnO/ZrO<sub>2</sub> catalysts in the CO<sub>2</sub> hydrogenation to CH<sub>3</sub>OH. *Applied Catalysis A: General*. 2008;**350**(1): 16-23

- [34] Tominaga K-i, Sasaki Y, Kawai M, Watanabe T, Saito M. Ruthenium complex catalysed hydrogenation of carbon dioxide to carbon monoxide, methanol and methane. *Journal of the Chemical Society, Chemical Communications*. 1993;(7):629-631
- [35] Tominaga K-i, Sasaki Y, Watanabe T, Saito M. Ethylene oxide-mediated reduction of CO<sub>2</sub> to CO and ethylene glycol catalysed by ruthenium complexes. *Journal of the Chemical Society, Chemical Communications*. 1995;(15):1489-1490
- [36] Huff CA, Sanford MS. Cascade catalysis for the homogeneous hydrogenation of CO<sub>2</sub> to methanol. *Journal of the American Chemical Society*. 2011;**133**(45):18122-18125
- [37] Wesselbaum S, vom Stein T, Klankermayer J, Leitner W. Hydrogenation of carbon dioxide to methanol by using a homogeneous ruthenium–phosphine catalyst. *Angewandte Chemie*. 2012;**124**(30):7617-7620
- [38] Balaraman E, Gunanathan C, Zhang J, Shimon LJW, Milstein D. Efficient hydrogenation of organic carbonates, carbamates and formates indicates alternative routes to methanol based on CO<sub>2</sub> and CO. *Nature Chemistry*. 2011;**3**(8):609-614
- [39] Choudhury J. New strategies for CO<sub>2</sub>-to-methanol conversion. *ChemCatChem*. 2012;**4**(5):609-611
- [40] Riduan SN, Zhang Y, Ying JY. Conversion of carbon dioxide into methanol with silanes over N-heterocyclic carbene catalysts. *Angewandte Chemie*. 2009;**121**(18):3372-3375
- [41] Ashley AE, Thompson AL, O'Hare D. Non-metal-mediated homogeneous hydrogenation of CO<sub>2</sub> to CH<sub>3</sub>OH. *Angewandte Chemie International Edition*. 2009;**48**(52):9839-9843
- [42] Gambarotta S, Strologo S, Floriani C, Chiesi-Villa A, Guastini C. Stepwise reduction of carbon dioxide to formaldehyde and methanol: Reactions of carbon dioxide and carbon dioxide like molecules with hydridochlorobis (cyclopentadienyl) zirconium (IV). *Journal of the American Chemical Society*. 1985;**107**(22):6278-6282
- [43] Fachinetti G, Floriani C, Pucci S. Stoichiometric reduction of CO and CO<sub>2</sub> to methanol: Evidence for carbon monoxide insertion into zirconium–hydrogen bond. *Journal of the Chemical Society, Chemical Communications*. 1978;(6):269-270
- [44] Goepfert A, Czaun M, Jones J-P, Prakash GKS, Olah GA. Recycling of carbon dioxide to methanol and derived products–closing the loop. *Chemical Society Reviews*. 2014;**43**(23):7995-8048
- [45] Jovanov ZP et al. Opportunities and challenges in the electrocatalysis of CO<sub>2</sub> and CO reduction using bifunctional surfaces: A theoretical and experimental study of Au–Cd alloys. *Journal of Catalysis*. 2016
- [46] Kuhl KP, Hatsukade T, Cave ER, Abram DN, Kibsgaard J, Jaramillo TF. Electrocatalytic conversion of carbon dioxide to methane and methanol on transition metal surfaces. *Journal of American Chemical Society*. 2014;**136**(40):14107-14113



- [47] Ganesh I. Conversion of carbon dioxide into methanol – A potential liquid fuel: Fundamental challenges and opportunities (a review). *Renewable and Sustainable Energy Reviews*. 2014;**31**(Supplement C):221-257
- [48] White RE, Vayenas CG, Gamboa-Aldeco ME. *Modern Aspects of Electrochemistry* No. 54. Springer; 2009
- [49] Pradier JP, Pradier C-M. *Carbon Dioxide Chemistry: Environmental Issues*. Elsevier; 2014
- [50] Canfield D, Frese KW Jr. Reduction of carbon dioxide to methanol on n- and p-GaAs and p-InP. Effect of crystal face, electrolyte and current density. *Journal of the Electrochemical Society*. 1983;**130**(8):1772-1773
- [51] Seshadri G, Lin C, Bocarsly AB. A new homogeneous electrocatalyst for the reduction of carbon dioxide to methanol at low overpotential. *Journal of Electroanalytical Chemistry*. 1994;**372**(1-2):145-150
- [52] Morris AJ, McGibbon RT, Bocarsly AB. Electrocatalytic carbon dioxide activation: The rate-determining step of Pyridinium-catalyzed CO<sub>2</sub> reduction. *ChemSusChem*. 2011;**4**(2): 191-196
- [53] Barton Cole E, Lakkaraju PS, Rampulla DM, Morris AJ, Abelev E, Bocarsly AB. Using a one-electron shuttle for the multielectron reduction of CO<sub>2</sub> to methanol: Kinetic, mechanistic, and structural insights. *Journal of the American Chemical Society*. 2010;**132**(33):11539-11551
- [54] Lim C-H, Holder AM, Musgrave CB. Mechanism of homogeneous reduction of CO<sub>2</sub> by pyridine: Proton relay in aqueous solvent and aromatic stabilization. *Journal of the American Chemical Society*. 2012;**135**(1):142-154
- [55] Keith JA, Carter EA. Theoretical insights into pyridinium-based photoelectrocatalytic reduction of CO<sub>2</sub>. *Journal of the American Chemical Society*. 2012;**134**(18):7580-7583
- [56] Ertem MZ, Konezny SJ, Araujo CM, Batista VS. Functional role of pyridinium during aqueous electrochemical reduction of CO<sub>2</sub> on Pt (111). *The Journal of Physical Chemistry Letters*. 2013;**4**(5):745-748
- [57] Popić JP, Avramov-Ivić ML, Vuković NB. Reduction of carbon dioxide on ruthenium oxide and modified ruthenium oxide electrodes in 0.5 M NaHCO<sub>3</sub>. *Journal of Electroanalytical Chemistry*. 1997;**421**(1):105-110
- [58] Qu J, Zhang X, Wang Y, Xie C. Electrochemical reduction of CO<sub>2</sub> on RuO<sub>2</sub>/TiO<sub>2</sub> nanotubes composite modified Pt electrode. *Electrochimica Acta*. 2005;**50**(16):3576-3580
- [59] Le M, Ren M, Zhang Z, Sprunger PT, Kurtz RL, Flake JC. Electrochemical reduction of CO<sub>2</sub> to CH<sub>3</sub>OH at copper oxide surfaces. *Journal of the Electrochemical Society*. 2011; **158**(5):E45-E49
- [60] Shironita S, Karasuda K, Sato K, Umeda M. Methanol generation by CO<sub>2</sub> reduction at a Pt-Ru/C electrocatalyst using a membrane electrode assembly. *Journal of Power Sources*. 2013;**240**:404-410

- [61] Barton EE, Rampulla DM, Bocarsly AB. Selective solar-driven reduction of CO<sub>2</sub> to methanol using a catalyzed p-GaP based photoelectrochemical cell. *Journal of the American Chemical Society*. 2008;**130**(20):6342-6344
- [62] Fan W, Zhang Q, Wang Y. Semiconductor-based nanocomposites for photocatalytic H<sub>2</sub> production and CO<sub>2</sub> conversion. *Physical Chemistry Chemical Physics*. 2013;**15**(8):2632-2649
- [63] Hossain MA, Ngo HH, Guo WS, Nguyen TV. Removal of copper from water by adsorption onto banana peel as bioadsorbent. *International Journal of Geomate*. 2012;**2**(2):227-234
- [64] Doherty MD, Grills DC, Muckerman JT, Polyansky DE, Fujita E. Toward more efficient photochemical CO<sub>2</sub> reduction: Use of scCO<sub>2</sub> or photogenerated hydrides. *Coordination Chemistry Reviews*. 2010;**254**(21):2472-2482
- [65] Dibenedetto A et al. Hybrid technologies for an enhanced carbon recycling based on the enzymatic reduction of CO<sub>2</sub> to methanol in water: Chemical and photochemical NADH regeneration. *ChemSusChem*. 2012;**5**(2):373-378
- [66] Gondal MA, Ali MA, Dastageer MA, Chang X. CO<sub>2</sub> conversion into methanol using granular silicon carbide ( $\alpha$ 6H-SiC): A comparative evaluation of 355 nm laser and xenon mercury broad band radiation sources. *Catalysis Letters*. 2013;**143**(1):108-117
- [67] Li X et al. Adsorption of CO<sub>2</sub> on heterostructure CdS (Bi<sub>2</sub>S<sub>3</sub>)/TiO<sub>2</sub> nanotube photocatalysts and their photocatalytic activities in the reduction of CO<sub>2</sub> to methanol under visible light irradiation. *Chemical Engineering Journal*. 2012;**180**:151-158
- [68] Luo D, Chen C, Zhang N, Hong S, Wu H, Liu Z. Characterization and DFT research of Nd/TiO<sub>2</sub>: Photocatalyst for synthesis of methanol from CO<sub>2</sub> and H<sub>2</sub>O. *Zeitschrift für Physikalische Chemie*. 2009;**223**(12):1465-1476
- [69] Wu JCS, Lin H-M, Lai C-L. Photo reduction of CO<sub>2</sub> to methanol using optical-fiber photoreactor. *Applied Catalysis A: General*. 2005;**296**(2):194-200
- [70] Yahaya AH, Gondal MA, Hameed A. Selective laser enhanced photocatalytic conversion of CO<sub>2</sub> into methanol. *Chemical Physics Letters*. 2004;**400**(1):206-212
- [71] Chen X, Zhou Y, Liu Q, Li Z, Liu J, Zou Z. Ultrathin, single-crystal WO<sub>3</sub> nanosheets by two-dimensional oriented attachment toward enhanced photocatalytic reduction of CO<sub>2</sub> into hydrocarbon fuels under visible light. *Applied Materials & Interfaces*. 2012;**4**:3372-3377
- [72] Tsai C-W, Chen HM, Liu R-S, Asakura K, Chan T-S. Ni@ NiO core-shell structure-modified nitrogen-doped InTaO<sub>4</sub> for solar-driven highly efficient CO<sub>2</sub> reduction to methanol. *The Journal of Physical Chemistry C*. 2011;**115**(20):10180-10186
- [73] Hennig H. Semiconductor Photocatalysis: Principles and Applications. In: Horst K, editor. Wiley Online Library; 2015
- [74] Spataru N, Tokuhiko K, Terashima C, Rao TN, Fujishima A. Electrochemical reduction of carbon dioxide at ruthenium dioxide deposited on boron-doped diamond. *Journal of Applied Electrochemistry*. 2003;**33**(12):1205-1210

- [75] Ryu J, Andersen TN, Eyring H. Electrode reduction kinetics of carbon dioxide in aqueous solution. *The Journal of Physical Chemistry*. 1972;**76**:3278-3286
- [76] Ogura K, Salazar-Villalpando MD. CO<sub>2</sub> electrochemical reduction via adsorbed halide anions. *JOM—Journal of the Minerals, Metals and Materials Society*. 2011;**63**(1):35-38
- [77] Bhardwaj R, Pan RL, Gross EL. Solar energy conversion by chloroplast photoelectrochemical cells. *Nature*. 1981;**289**(5796):396-398
- [78] Licht S. A description of energy conversion in photoelectrochemical solar cells. *Nature*. 1987;**330**(6144):148-151
- [79] Grätzel M. Photoelectrochemical cells. *Nature*. 2001;**414**(6861):338-344
- [80] Grätzel M, Kalyanasundaram K. Artificial photosynthesis: Efficient dye-sensitized photoelectrochemical cells for direct conversion of visible light to electricity. *Current Science*. 1994:706-714
- [81] Yae S et al. Solar to chemical conversion using metal nanoparticle modified microcrystalline silicon thin film photoelectrode. *Solar Energy Materials and Solar Cells*. 2007;**91**(4): 224-229
- [82] Fujishima A, Honda K. Electrochemical photolysis of water at a semiconductor electrode. *Nature*. 1972;**238**(5358):37-38
- [83] Fujishima A, Kohayakawa K, Honda K. Formation of hydrogen gas with an electrochemical photo-cell. *Bulletin of the Chemical Society of Japan*. 1975;**48**(3):1041-1042
- [84] Watanabe T, Fujishima A, Honda K. Photoelectrochemical Hydrogen Production. 1979. pp. 137-169
- [85] Ganesh I. Conversion of carbon dioxide to methanol using solar energy—A brief review. *Materials Sciences and Applications*. 2011;**2**(10):1407
- [86] Zhao J, Wang X, Xu Z, Loo JSC. Hybrid catalysts for photoelectrochemical reduction of carbon dioxide: A prospective review on semiconductor/metal complex co-catalyst systems. *Journal of Materials Chemistry A*. 2014;**2**(37):15228-15233



---

# Effect of Overlapping Fe/TiO<sub>2</sub> Coated on Netlike Glass Disc and Cu Disc on CO<sub>2</sub> Reduction

---

Akira Nishimura

Additional information is available at the end of the chapter

<http://dx.doi.org/10.5772/intechopen.70389>

---

## Abstract

Fe-doped TiO<sub>2</sub> (Fe/TiO<sub>2</sub>) film photocatalyst was prepared by sol-gel and dip-coating process to respond to the visible spectrum. Netlike glass fiber and Cu disc that are base materials used for coating Fe/TiO<sub>2</sub> were investigated to promote the CO<sub>2</sub> reduction performance of the photocatalyst. The prepared Fe/TiO<sub>2</sub> film coated on netlike glass fiber and Cu disc was characterized by scanning electron microscope (SEM) and electron probe micro analyzer (EPMA). Additionally, the CO<sub>2</sub> reduction experiment using Fe/TiO<sub>2</sub> film coated on netlike glass disc, Cu disc, and their overlap was carried out by illuminating an Xe lamp or without ultraviolet (UV) light, respectively. As a result, the concentration of produced CO increases by Fe doping irrespective of base material used under the illumination condition with UV light as well as without UV light. The peak concentration of CO for the Fe/TiO<sub>2</sub> double overlapping is approximately 1.5 times as large as the Fe/TiO<sub>2</sub> single overlapping under the illumination condition with UV light due to the promotion of electron transfer between the two overlapped photocatalysts. However, the promotion ratio is approximately 1.1 times under the illumination condition without UV light.

**Keywords:** photocatalyst, Fe-doped TiO<sub>2</sub>, CO<sub>2</sub> reduction, base material, overlapping effect

---

## 1. Introduction

After the industrial revolution, the averaged concentration of CO<sub>2</sub>, which causes the global warming in the world, has been increased from 278 to 400 ppmV by 2015 [1]. Therefore, it requested a new CO<sub>2</sub> reduction or utilization technology in order to recycle CO<sub>2</sub>.

According to the review of CO<sub>2</sub> conversion technologies [2], there are six vital CO<sub>2</sub> conversions: chemical conversions, electrochemical reductions, biological conversions, reforming,

inorganic conversions, and photochemical reductions [3]. Recently, artificial photosynthesis or the photochemical reduction of CO<sub>2</sub> to fuel has become an attractive route due to its economically and environmentally friendly behavior [2].

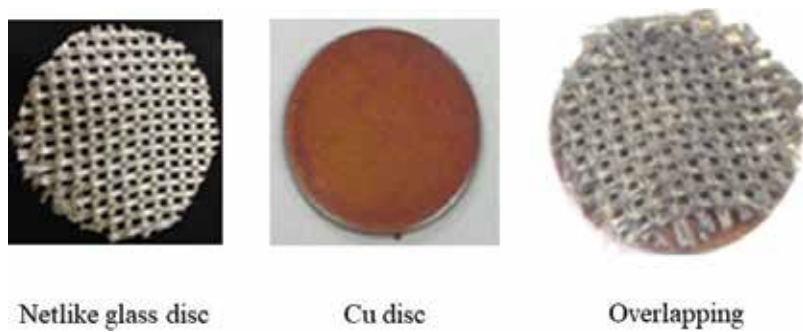
TiO<sub>2</sub> is the principal catalyst for almost all types of photocatalytic reaction. It is well known that CO<sub>2</sub> can be reduced into fuels such as CO, CH<sub>4</sub>, CH<sub>3</sub>OH and H<sub>2</sub>, and so forth by using TiO<sub>2</sub> as the photocatalyst under ultraviolet (UV) light illumination [4–9]. After practical application of this technology, a carbon circulation system would then be established: CO<sub>2</sub> from the combustion of fuel produced by TiO<sub>2</sub> is reformed to fuels again using solar energy, and true zero emission can be achieved. However, the CO<sub>2</sub> reduction performance of TiO<sub>2</sub> is still low. One of the barriers to realize a carbon circulation system utilizing solar energy is that TiO<sub>2</sub> is only photoactive at the wavelength below 400 nm due to its relatively large band gap energy (~3.2 eV) [10].

Recently, studies on CO<sub>2</sub> photochemical reduction by TiO<sub>2</sub> have been carried out from the viewpoint of performance promotion by extending absorption range toward visible region [11–15]. Noble metal doping such as Pt, Pd, Rh, Au and Ag [11], nanocomposite CdS/TiO<sub>2</sub> combining two different band gap photocatalysts [12], N<sub>2</sub>-modified TiO<sub>2</sub> [13], light harvesting complex of green plant-assisted Rh-doped TiO<sub>2</sub> [14] and dye-sensitized TiO<sub>2</sub> [15] have been developed for this process. However, the concentration in the products achieved is still low, ranging from 10 to 1000 ppmV [4, 6–9] or from 1 to 100 μmol/g-cat [11–15]. Therefore, the big breakthrough for increasing the concentration level of products is necessary to advance the CO<sub>2</sub> reduction technology in order to make the technology practically useful.

In the present paper, TiO<sub>2</sub> sol-gel and dip-coating process with doping is adopted in order to extend its photoresponsivity to the visible spectrum to promote the CO<sub>2</sub> reduction performance. This process can incorporate dopants into TiO<sub>2</sub> lattice, resulting in better optical and catalytic properties [16]. In addition, the integration of dopants into the sol during the gelation process facilitates direct interaction between TiO<sub>2</sub> and dopants during the sol-gel process [17].

It was reported that doping transition metal was a useful technique for extending the absorbance of TiO<sub>2</sub> into the visible region [18]. For doping, various metal ions have been used, but among them, Fe<sup>3+</sup> is considered as a strong candidate as it has a similar radius to Ti<sup>4+</sup> (Fe<sup>3+</sup> = 78.5 pm, Ti<sup>4+</sup> = 74.5 pm) [19] and can easily fit into the crystal lattice of TiO<sub>2</sub> [18, 20, 21]. Moreover, the redox potential (energy differential) of Fe<sup>2+</sup>/Fe<sup>3+</sup> is close to that of Ti<sup>3+</sup>/Ti<sup>4+</sup>, resulting in shifting its optical absorption into the visible region [18, 20, 21]. Due to easy availability as well as the above-described characteristics, Fe is selected as the dopant in the present study.

In the present study, a net glass fiber (SILIGLASS U, produced by Nihonmuki Co.) and Cu disc are used as base materials for coating TiO<sub>2</sub> film by sol-gel and dip-coating process. **Figure 1** shows the netlike glass disc, Cu disc, and two overlapped base materials. The netlike glass fiber is a net composed of glass fiber whose diameter is about 10 μm. The fine glass fibers are knitted, resulting in the diameter of aggregate fiber about 1 mm. According to the manufacture specifications of netlike glass fiber, the porous diameter of glass fiber is about 1 nm and the specific surface is about 400 m<sup>2</sup>/g. The netlike glass fiber consists of SiO<sub>2</sub> whose purity is over 96 wt%. The aperture of net is about 2 × 2 mm. Since the netlike glass fiber has a porous characteristic, it is believed



**Figure 1.** The base materials used for coating TiO<sub>2</sub> film.

that TiO<sub>2</sub> film and doped metal are captured by netlike glass fiber easily during sol-gel and dip-coating process. In addition, it can be expected that a CO<sub>2</sub> absorption performance of prepared photocatalyst is promoted due to the porous structure of netlike glass fiber. On the other hand, Cu disc is also adopted since the recombination of electron and hole produced by photochemical reaction can be prevented by a free electron emitted from Cu disc. The coupling effect of prepared photocatalysts coated on overlapped netlike glass fiber and Cu disc on CO<sub>2</sub> reduction performance is investigated. The illumination light is able to penetrate through the netlike glass fiber and reach on Cu disc. If the synergy effect between the photocatalyst coated on netlike glass fiber and that on Cu disc was obtained due to an active electron transfer between them, the promotion of CO<sub>2</sub> reduction performance would be achieved. There is no previous study on the coupling effect on CO<sub>2</sub> reduction performance of metal-doped TiO<sub>2</sub> or nondoped TiO<sub>2</sub>.

In the present study, TiO<sub>2</sub> film doped with Fe (Fe/TiO<sub>2</sub>) was prepared and characterized by scanning electron microscope (SEM) and electron probe micro analyzer (EPMA) analysis. The CO<sub>2</sub> reduction characteristics of Fe/TiO<sub>2</sub> coated on netlike glass fiber and/or Cu disc under the condition of illuminating Xe lamp with or without UV light were investigated.

## 2. Experimental

### 2.1. Procedure to prepare Fe/TiO<sub>2</sub> film

Sol-gel and dip-coating process, which is a general procedure, was selected to prepare Fe/TiO<sub>2</sub> film. TiO<sub>2</sub> sol solution consists of [(CH<sub>3</sub>)<sub>2</sub>CHO<sub>4</sub>] Ti (purity of 95 wt%, produced by Nacalai Tesque Co.) of 0.3 mol, anhydrous C<sub>2</sub>H<sub>5</sub>OH (purity of 99.5 wt%, produced by Nacalai Tesque Co.) of 2.4 mol, distilled water of 0.3 mol and HCl (purity of 35 wt%, produced by Nacalai Tesque Co.) of 0.07 mol. Fe particles (produced by Merck KGaA, particle size below 10 μm) were added to TiO<sub>2</sub> sol solution. Netlike glass fiber was cut to disc, and its diameter and thickness were 50 and 1 mm, respectively. The Cu disc used has diameter and thickness of 50 and 1 mm, respectively. The base material was dipped into Fe/TiO<sub>2</sub> sol solution at the speed of 1.5 mm/s and pulled up at the fixed speed of 0.22 mm/s. Then, it was dried out and fired under the controlled firing temperature (FT) and firing duration time (FD), with Fe/TiO<sub>2</sub> film

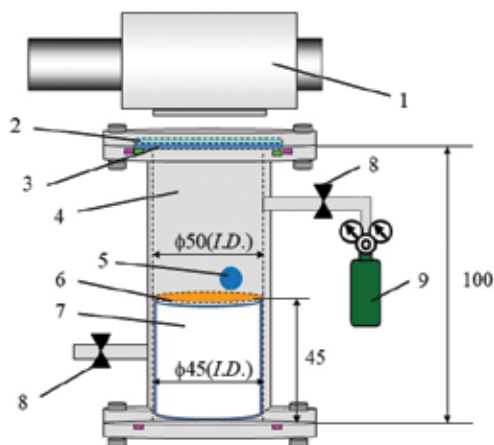
fastened on the base material. FT and FD were set at 623 K and 180 s, respectively. The ratio of amount of added Fe to amount of TiO<sub>2</sub> sol solution (R) was set at 10 wt%.

## 2.2. Characterization of Fe/TiO<sub>2</sub> film

The surface structure and crystallization characteristics of Fe/TiO<sub>2</sub> film were evaluated by SEM (JXA-8530F, produced by JEOL Ltd.) and EPMA (JXA-8530F, produced by JEOL Ltd.). Since these two measuring instruments use electron for analysis, the sample should be an electron conductor. Though Cu disc is a good electron conductor, netlike glass disc is not an electron conductor. In this study, the carbon vapor deposition was conducted by the dedicated device (JEE-420, produced by JEOL Lt.) for Fe/TiO<sub>2</sub> coated on netlike glass disc before analysis by SEM and EPMA. The thickness of carbon deposited on sample was approximately 20–30 nm. The electron probe emits the electron to the sample under an acceleration voltage of 15 kV and a current of  $3.0 \times 10^{-8}$  A; the surface structure of sample is analyzed by SEM. The characteristics of X-ray are detected by EPMA at the same time, resulting in the concentration of chemical element analyzed according to the relationship between the characteristics of X-ray energy and the atomic number. The spatial resolution of SEM and EPMA is 10  $\mu$ m. The EPMA analysis helps not only to understand the coating state of prepared photocatalyst but also to measure the amount of doped metal within TiO<sub>2</sub> film on the base material.

## 2.3. CO<sub>2</sub> reduction experiment

**Figure 2** shows that experimental setup of the reactor consisting of stainless pipe (100 mm (H)  $\times$  50 mm (ID)), a netlike glass or Cu that is disc shaped (50 mm (D)  $\times$  1 mm (t)) with Fe/TiO<sub>2</sub> film placed on the Teflon cylinder (50 mm (H)  $\times$  50 mm (D)), a quartz glass disc (84 mm



1. Xe lamp, 2. Sharp cut filter, 3. Quartz glass disc, 4. Stainless pipe, 5. Gas sampling tap, 6. Photocatalyst, 7. Teflon cylinder, 8. Valve, 9. CO<sub>2</sub> gas cylinder (99.995 vol%)

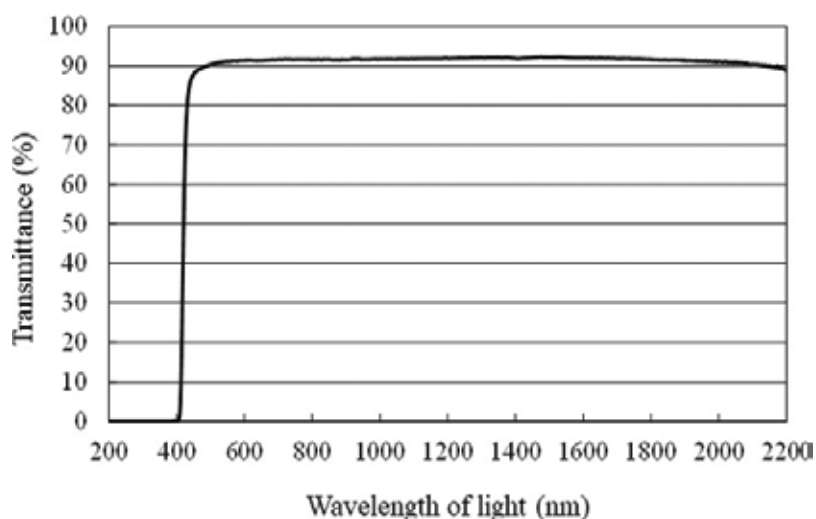
**Figure 2.** Schematic drawing of CO<sub>2</sub> reduction experimental setup.



(D) × 10 mm (t)), a sharp cut filter cutting off the light whose wavelength is below 400 nm (SCF-49.5C-42 L, produced by SIGMA KOKI Co. Ltd.), Xe lamp (L2175, produced by Hamamatsu Photonics K. K.) and CO<sub>2</sub> gas cylinder (purity of 99.995 vol%).

The size of reactor for charging CO<sub>2</sub> is  $1.25 \times 10^{-4}$  m<sup>3</sup>. The Xe lamp illuminates the netlike glass disc or Cu disc coated with Fe/TiO<sub>2</sub> film, which is located inside the stainless pipe, through the sharp cut filter and the quartz glass disc that are at the top of the stainless pipe. The Xe lamp illuminates the light whose wavelength ranged from 185 to 2000 nm. A sharp cut filter can remove UV components of the light, resulting in the wavelength of light from Xe lamp ranging from 401 to 2000 nm. **Figure 3** indicates that the sharp cut filter can remove the light whose wavelength ranged below 400 nm. During the experiment, the light intensity of Xe lamp illuminating the photocatalyst without and with setting the sharp cut filter is estimated at 81.9 and 60.7 mW/cm<sup>2</sup>, respectively.

To start CO<sub>2</sub> reduction experiment in this study, CO<sub>2</sub> gas whose purity was 99.995 vol% was flowed through the reactor as a purged gas for approximately 15 min. The valves at the inlet and the outlet of reactor were closed after charging CO<sub>2</sub>. The gas pressure and gas temperature in the reactor were set at 0.1 MPa and 298 K, respectively, the distilled water of 100 μL was injected into the reactor through a gas pipe and Xe lamp was started to illuminate at the same time. The water injected vaporized completely in the reactor. Since Xe lamp emits the heat, the gas temperature in reactor was attained at 343 K within an hour and maintained at approximately 343 K during the experiment. The water of 5.56 mmol and CO<sub>2</sub> of 576 mmol were in the reactor. The gas in the reactor was sampled by a gas syringe every 24 h during the experiment, which was analyzed by FID gas chromatograph (GC353B, produced by GL Science) and methanizer (MT221, produced by GL Science). FID gas chromatograph and methanizer can detect a gas whose concentration is 1 ppmV order level.



**Figure 3.** Light transmittance data of sharp cut filter.

### 3. Results and discussion

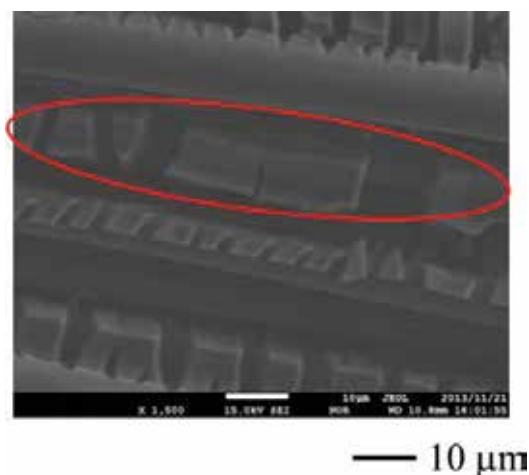
#### 3.1. Characterization of Fe/TiO<sub>2</sub> film by SEM and EPMA

**Figures 4 and 5** show SEM images of TiO<sub>2</sub> and Fe/TiO<sub>2</sub> film coated on netlike glass disc, respectively. The SEM images were taken at 1500 times magnification under the acceleration voltage of 15 kV and the current of  $3.0 \times 10^{-8}$  A.

**Figures 6 and 7** show EPMA images of TiO<sub>2</sub> and Fe/TiO<sub>2</sub> film coated on netlike glass disc, respectively. The EPMA analysis was carried out to obtain 1500 times magnified SEM images as shown in **Figures 4 and 5**. In EPMA image, the concentrations of each element in observation area are indicated by different colors. Dilute colors indicate that the amount of element is large, while dense colors indicate that the amount of element is small.

To identify the position of each element, the colored circles are added to these SEM and EPMA images. The red circles shown in SEM images of **Figures 4 and 5** indicate that the amount of Ti is large as pointed out in EPMA images of **Figures 6 and 7**. From these figures, it can be observed that TiO<sub>2</sub> film with teethlike shape is coated on netlike glass fiber. It is also seen that TiO<sub>2</sub> film builds a bridge among several glass fibers. It is believed that the temperature profile of TiO<sub>2</sub> solution adhered on the netlike glass disc is not uniform because the thermal conductivities of Ti and SiO<sub>2</sub> are different during firing process. The thermal conductivities of Ti and SiO<sub>2</sub> at 600 K are 19.4 and 1.82 W/(mK), respectively [22]. Since the thermal expansion and shrinkage around netlike glass fiber occur, thermal crack of TiO<sub>2</sub> film is caused. Therefore, TiO<sub>2</sub> film on netlike glass fiber is teethlike.

The yellow circle shown in SEM image of **Figure 5** indicates the existence of metal particles as pointed out in EPMA images of **Figure 7**. It is observed from **Figure 5** that Fe particles adhere on the netlike glass fiber directly. According to **Figure 5**, the size of doped metal is below



**Figure 4.** The SEM image of TiO<sub>2</sub> film coated on netlike glass disc.

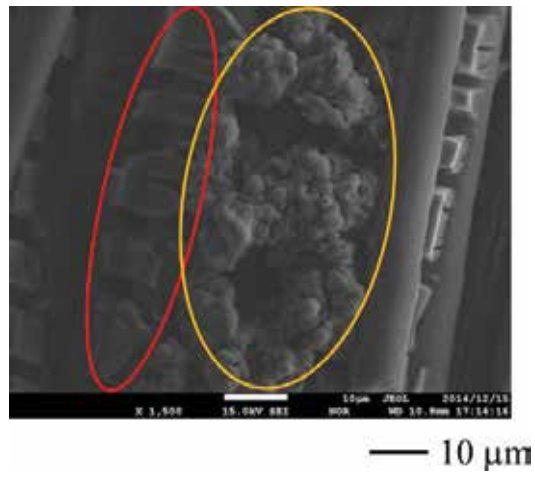


Figure 5. The SEM image of Fe/TiO<sub>2</sub> film coated on netlike glass disc.

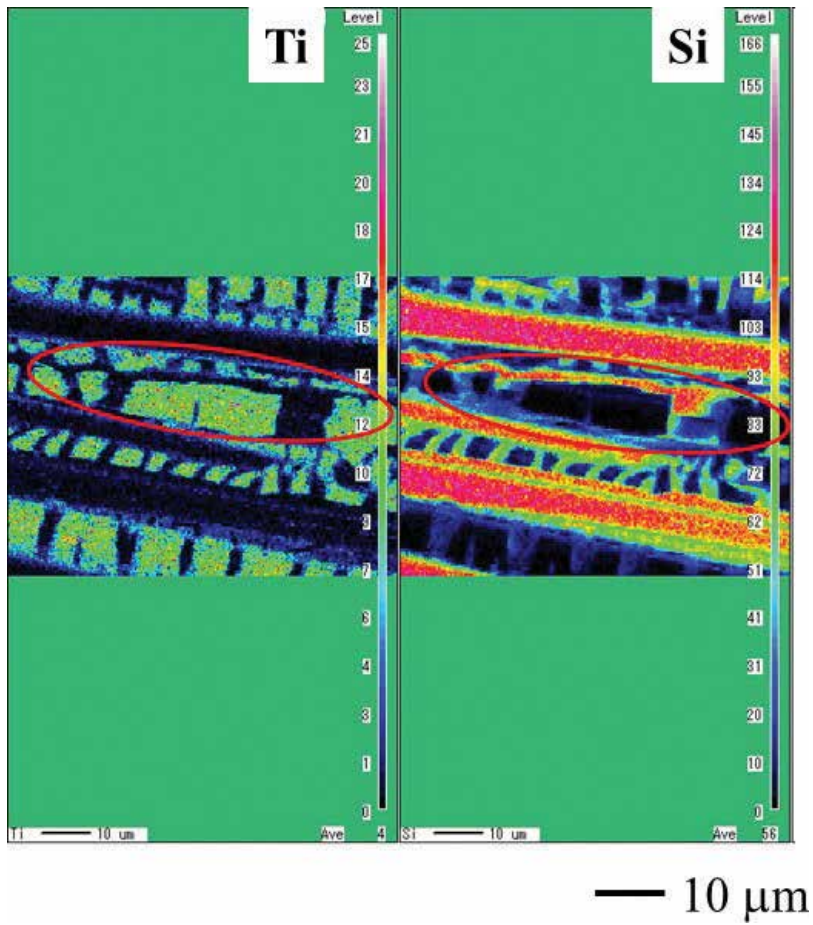
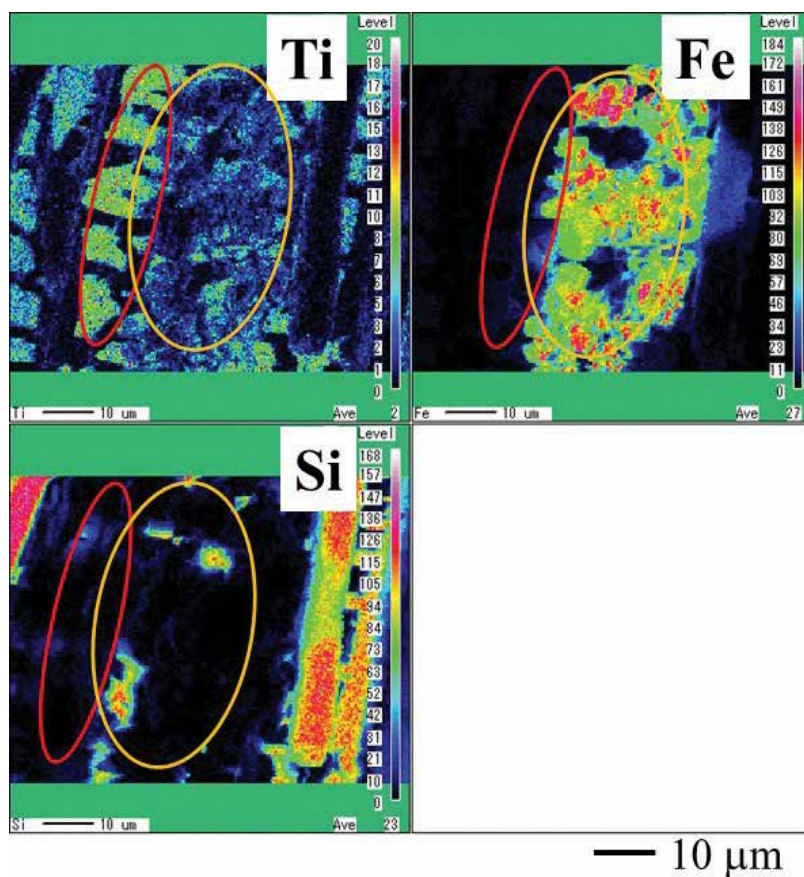


Figure 6. The EPMA image of TiO<sub>2</sub> film coated on netlike glass disc.



**Figure 7.** The EPMA image of Fe/TiO<sub>2</sub> film coated on netlike glass disc.

10 μm. Since the Fe particles used have diameters below 10 μm, it is confirmed that the Fe particles can be loaded without agglomeration by the sol-gel and dip-coating process.

**Figures 8 and 9** show SEM image of TiO<sub>2</sub> and Fe/TiO<sub>2</sub> film coated on Cu disc, respectively. The SEM images were taken at 1500 times magnification under an acceleration voltage of 15 kV and a current of  $3.0 \times 10^{-8}$  A.

**Figures 10 and 11** show EPMA images of TiO<sub>2</sub> and Fe/TiO<sub>2</sub> film coated on Cu disc, respectively. EPMA analysis was carried out to obtain 1500 times magnified SEM images as shown in **Figures 8 and 9**.

According to **Figures 9 and 11**, the TiO<sub>2</sub> film is contracted around Fe particles. The surface characteristics of TiO<sub>2</sub> or Fe/TiO<sub>2</sub> are explained as follows [23]:

- i. Before firing process, TiO<sub>2</sub> or Fe/TiO<sub>2</sub> sol solution is adhered on Cu disc uniformly.
- ii. The temperature profile of TiO<sub>2</sub> or Fe/TiO<sub>2</sub> sol solution adhered on Cu disc is not uniform during firing process since the thermal conductivities of Cu, Ti and Fe are different. Thermal conductivities of Cu, Ti and Fe at 600 K are 383, 19.4, and 54.7 W/(mK),

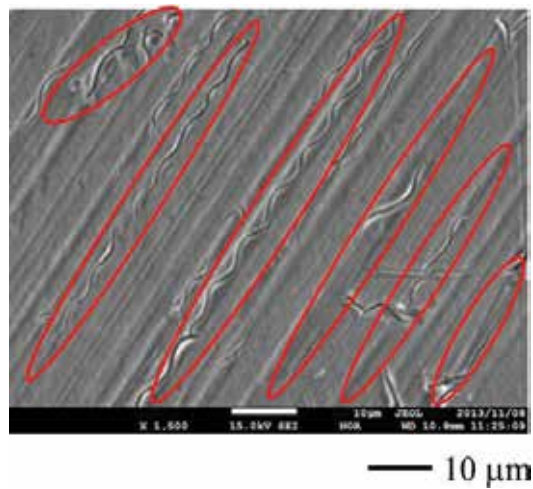


Figure 8. SEM image of TiO<sub>2</sub> film coated on Cu disc.

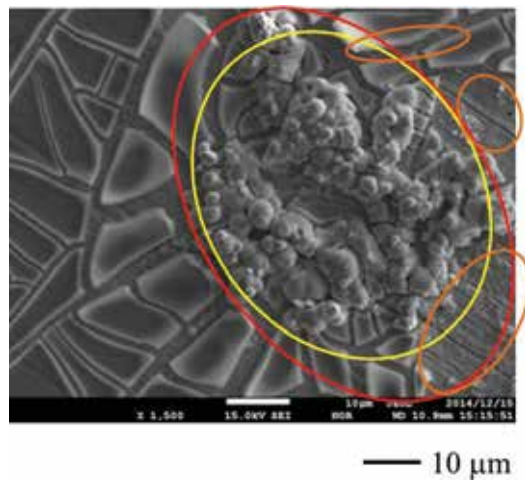
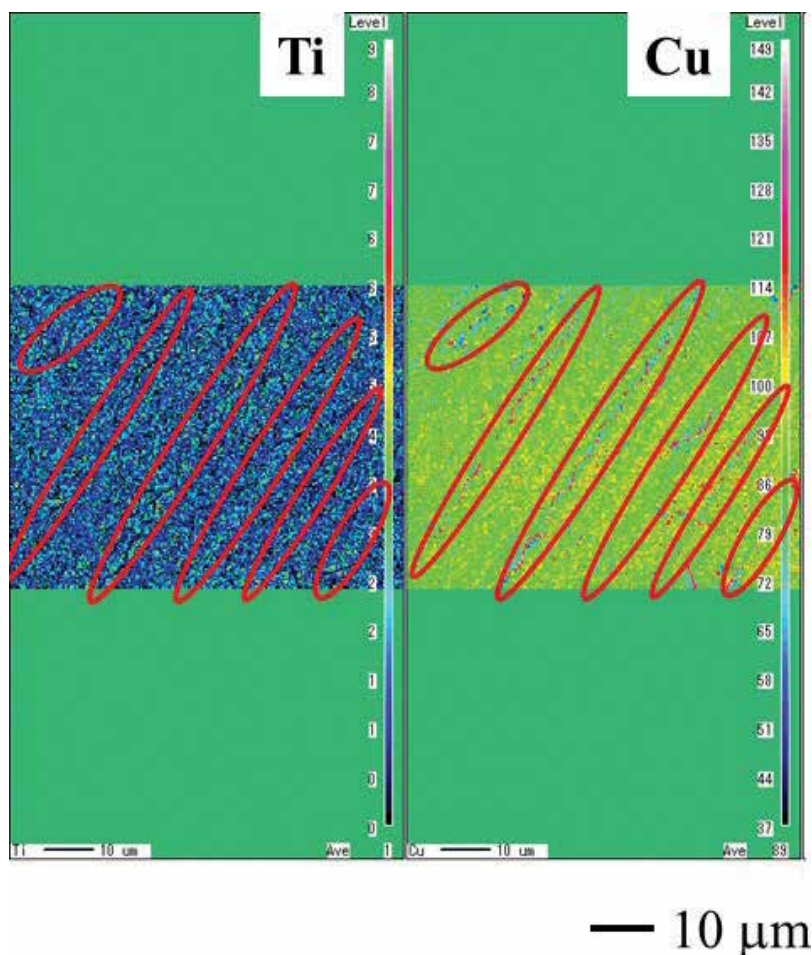


Figure 9. SEM image of Fe/TiO<sub>2</sub> film coated on Cu disc.

respectively [22]. Therefore, the thermal expansion around Fe particles and the thermal shrinkage around the other areas of TiO<sub>2</sub> sol occur for Fe/TiO<sub>2</sub>, while the thermal expansion and shrinkage between TiO<sub>2</sub> and Cu disc occur for nonmetal-doped TiO<sub>2</sub> film.

- iii. Because of thermal stress caused by the uneven distribution of temperature, the cracks around Fe and the shrinkage of TiO<sub>2</sub> film around the cracks occur after firing process. Therefore, a large amount of Cu pointed out by orange circles, which is an element of basis Cu disc, around Fe is observed in Figure 11. In addition, a large amount of Ti around Fe is also seen in the same figure.





**Figure 10.** EPMA image of  $\text{TiO}_2$  film coated on Cu disc.

The center of netlike glass disc or Cu disc whose diameter is  $300\ \mu\text{m}$  is analyzed by EPMA to evaluate the amount of doped Fe within  $\text{TiO}_2$  film quantitatively. The ratio of Fe to Ti is measured by averaging the data detected by EPMA.

**Table 1** lists weight percentages of elements Fe and Ti in the  $\text{Fe/TiO}_2$  film coated on netlike glass disc or Cu disc. From this table, it can be seen that more Fe is contained in the  $\text{Fe/TiO}_2$  film on netlike glass disc than that on Cu disc, under the doping condition, that is, R of 10 wt%. As expected, the netlike glass fiber can capture the dopant metal powder well during dip-coating process due to the porous structure. However, Cu disc hardly captures the dopant metal powder during dip-coating process since the surface of Cu disc is smooth. From these results, it is clear that the amount of dopants that could be doped is influenced by the base material when the sol-gel and dip-coating process is adopted for metal doping.

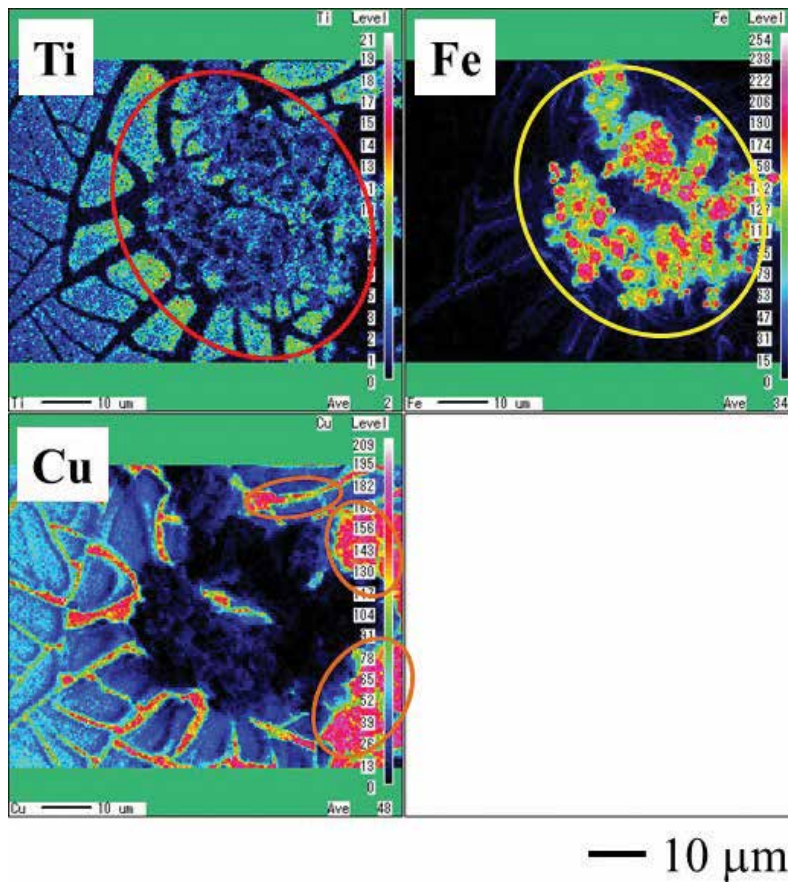


Figure 11. EPMA image of Fe/TiO<sub>2</sub> film coated on Cu disc.

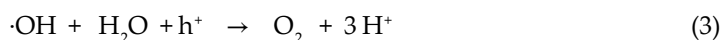
Photocatalyst type	Weight ratio		
	Ti (wt%)	Fe (wt%)	Total (wt%)
Fe/TiO coated on netlike glass disc	74.76	25.24	100
Fe/TiO coated on Cu disc	98.15	1.85	100

Table 1. Weight ratio of elements Fe and Ti within the prepared metal-doped TiO<sub>2</sub> film.

### 3.2. CO<sub>2</sub> reduction characteristics of Fe/TiO<sub>2</sub> coated on netlike glass disc or Cu disc

Figure 12 shows the concentration changes of CO produced in the reactor along the time under the Xe lamp with UV light on, for TiO<sub>2</sub> or Fe/TiO<sub>2</sub> film coated on netlike glass disc or Cu disc or their overlap. In this figure, a single overlapping means the photocatalyst coated on the upper surface of netlike glass disc is overlapped over the photocatalyst coated on Cu disc, while a double overlapping means that the photocatalyst coated on both the upper and lower surfaces of netlike glass disc is overlapped over the photocatalyst coated on Cu disc. In

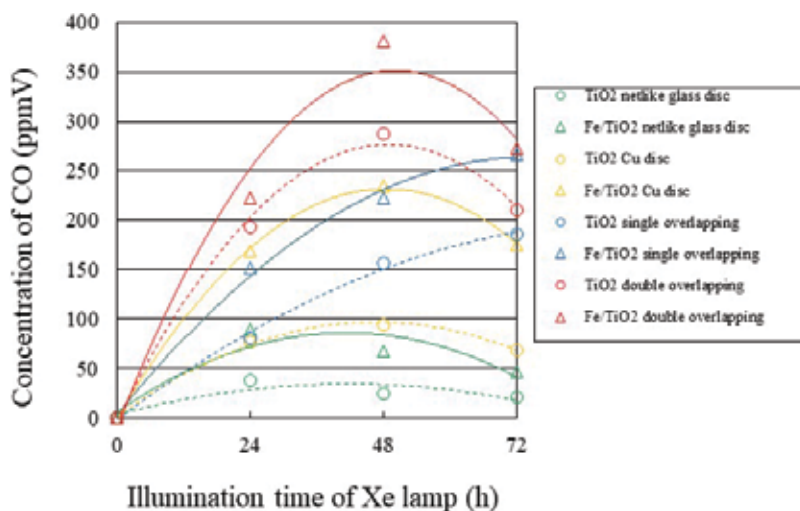
this experiment, CO is the only fuel produced from the reactions. The reaction scheme for CO production by the photochemical reaction with CO<sub>2</sub> and H<sub>2</sub>O is shown as follows [4, 7, 24–26]:



In the first step, hole  $h^+$  and electron  $e^-$  are generated by illuminating light on photocatalyst as shown in Eq. (1). The generated hole reacts with H<sub>2</sub>O in the oxidation reaction step, resulting in proton  $\text{H}^+$  produced as shown in Eqs. (2) and (3). The proton and electron react with CO<sub>2</sub> in the reduction reaction step, resulting that CO is produced as shown in Eq. (4).

Since the concentrations of CO in most experiments started to decrease after illumination of 48–72 hours for illumination conditions with UV light due to the reverse reaction by CO and O<sub>2</sub>, which is a by-product as shown in Eq. (3). **Figure 12** shows only the concentration up to 72 h. Before the experiments, a blank test, which was running the same experiment without illumination of Xe lamp, had been carried out to set up a reference case. No fuel was produced in the blank test as expected.

According to **Figure 12**, the concentration of CO increases due to Fe doping irrespective of base material. The improvement of photocatalytic performance by Fe doping under the illumination condition with UV light can be caused by the generation of shallow charge traps in



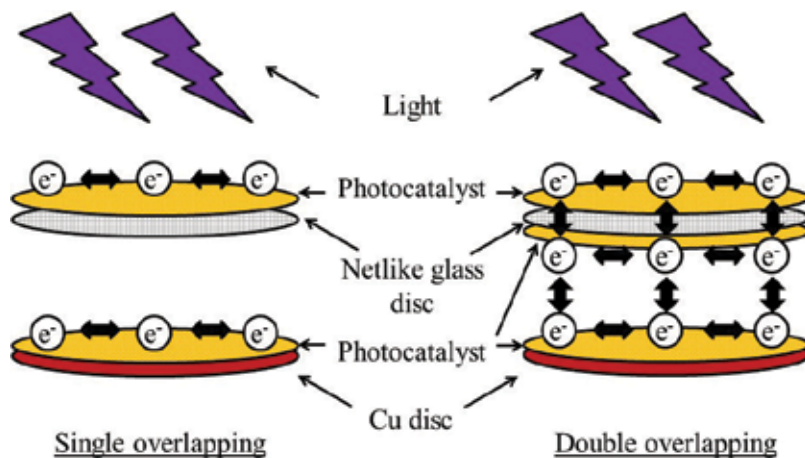
**Figure 12.** Comparison of concentrations of produced CO among photocatalysts coated on different base materials under the illumination condition with UV light.



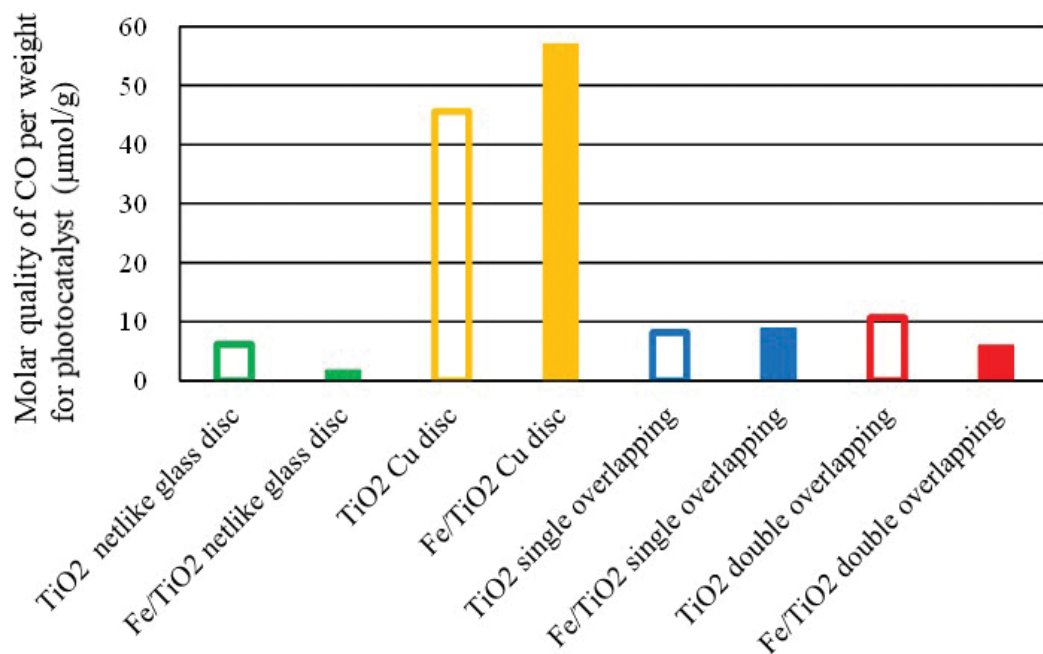
the crystal structure, which decreases the recombination rate of electron-hole pairs [20]. In addition, the concentration of CO produced by Fe/TiO<sub>2</sub> coated on Cu disc is higher than that on netlike glass disc. Though the weight ratio of Fe for Fe/TiO<sub>2</sub> coated on netlike glass disc is larger than that on Cu disc as shown in **Table 1**, the reaction surface area, which can receive the light, is small due to aperture of net. Therefore, the photocatalytic performance of Fe/TiO<sub>2</sub> coated on netlike glass disc is lower than that on Cu disc. Moreover, the Fe/TiO<sub>2</sub> single overlapping shows the small superiority over Fe/TiO<sub>2</sub> coated on netlike glass disc and Fe/TiO<sub>2</sub> coated on Cu disc. Although the present study expected the positive synergy effect of combination of two photocatalysts coated on different base materials, the positive effect observed was very small. Since the netlike glass fiber consists of SiO<sub>2</sub>, which is an electrical insulation material, the electron transfer between the two overlapped photocatalysts might not be realized well. However, in the experiment of Fe/TiO<sub>2</sub> double overlapping, the photocatalytic performance is promoted, resulting that the peak concentration of CO is approximately 1.5 times as large as the Fe/TiO<sub>2</sub> single overlapping. The reason is thought to be that the electron transfer between two overlapped photocatalysts is promoted, resulting that the synergy effect of combination of two photocatalysts coated on different base materials is obtained.

**Figure 13** illustrates the difference of electron transfer phenomenon between single and double overlapping. In this figure, the hole produced by photochemical reaction is not shown mainly to clarify the electron transfer phenomenon. It is believed that the path for electron transfer is constructed by double overlapping.

**Figure 14** shows the comparison of molar quantities of CO per weight of photocatalyst among the prepared photocatalysts. These values are estimated based on the maximum CO obtained under the illumination condition with UV light up to 72 h. According to this figure, the molar quantity of CO per weight of Fe/TiO<sub>2</sub> coated on Cu disc shows the highest performance since the weight of Fe/TiO<sub>2</sub> coated on Cu disc (= 0.02 g-cat) is smaller than that on netlike glass disc (= 0.25 g-cat). Though the netlike glass fiber captures the large amount of TiO<sub>2</sub> sol and Fe particle during dipping process well, some Fe/TiO<sub>2</sub> adhered in the pores of netlike glass fiber might not be activated well due to the lack of light illumination. Although it is believed that



**Figure 13.** Comparison of electron transfer phenomena between single and double overlapping.

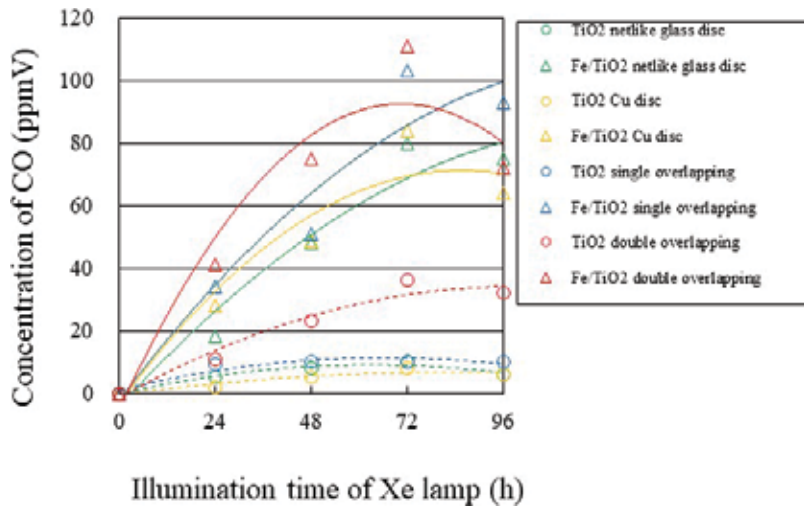


**Figure 14.** Comparison of CO<sub>2</sub> reduction performances per weight of photocatalyst under the illumination condition with UV light.

the Fe doping could assist CO<sub>2</sub> reduction if the light could illuminate inside the pore of netlike glass disc, the positive effect of Fe doping on CO<sub>2</sub> reduction performance per weight of photocatalyst base under the overlapping condition was not as significant as that in the case of Fe/TiO<sub>2</sub> coated on netlike glass disc. In addition, the mass transfer in the space between the two photocatalysts coated on netlike glass disc and Cu disc should be enhanced in order to meet the photoreaction rate under the overlapping condition. If the produced fuel remains in the space between two photocatalysts, the reactant of CO<sub>2</sub> and H<sub>2</sub>O could be blocked to reach the surface of photocatalyst, resulting that the photochemical reaction could not be carried out well even though the light is illuminated for the photocatalyst. Therefore, it is necessary to control the amount of doped Fe, which is coated on the surface and on the pore of the netlike glass fiber, as well as to optimize the aperture of netlike glass fiber.

**Figure 15** shows the concentration changes of CO produced in the reactor along the time under the Xe lamp illumination without UV light, for TiO<sub>2</sub> or Fe/TiO<sub>2</sub> film coated on netlike glass disc or Cu disc or their overlap. In this experiment, CO is the only fuel produced from the reactions. Since the concentration of CO almost started to decrease after illumination of 72–96 h for all cases due to the reverse reaction by CO and O<sub>2</sub>, which is the by-product as shown in Eq. (3), **Figure 15** shows the concentration only up to 96 h.

From **Figure 15**, it can be seen that the CO<sub>2</sub> reduction performance of TiO<sub>2</sub> is promoted by Fe doping due to extension of the photoresponsivity of TiO<sub>2</sub> to the visible spectrum as well as decrease in the recombination rate of electron-hole pairs by the generation of



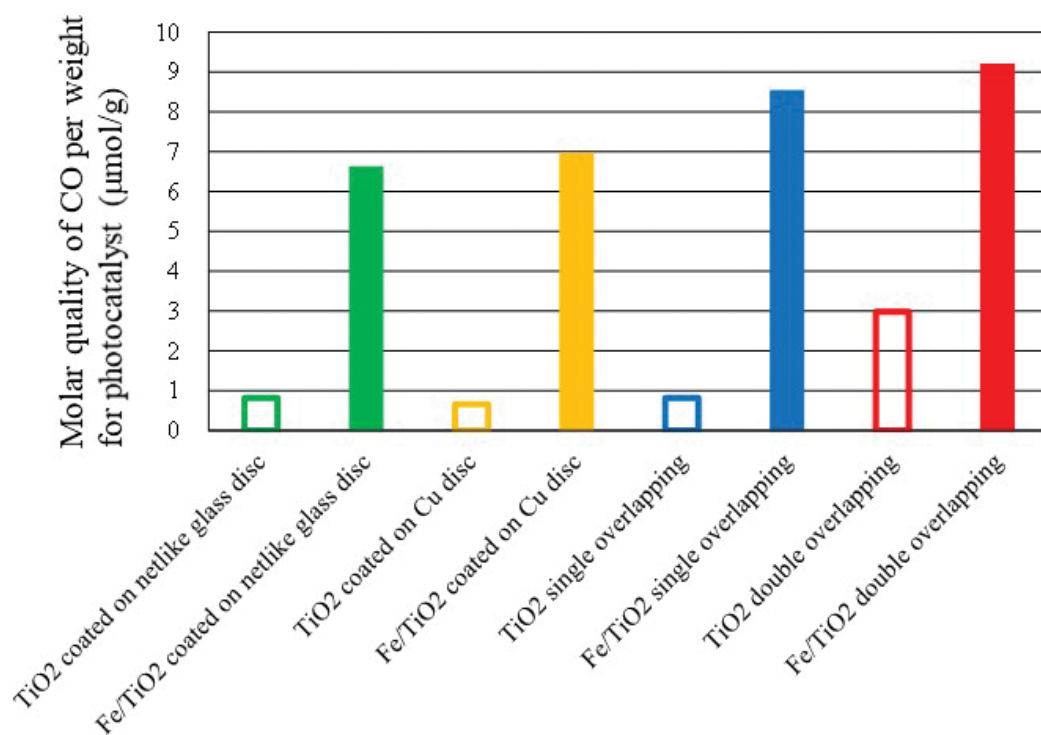
**Figure 15.** Comparison of concentrations of produced CO among the photocatalysts coated on different base materials under the illumination condition without UV light.

shallow charge traps in the crystal structure. In addition, the maximum concentration of CO obtained by Fe/TiO<sub>2</sub> coated on netlike glass disc is almost the same as that by Fe/TiO<sub>2</sub> coated on Cu disc, which has a different tendency from the results obtained under the UV illumination condition. Under the illumination condition without UV light, it is believed that the amount of doped Fe is important to absorb the visible light to perform the photocatalytic reaction. Since the amount of doped Fe for Fe/TiO<sub>2</sub> coated on netlike glass disc is much larger than that for Fe/TiO<sub>2</sub> coated on Cu disc as shown in **Table 1**, the CO<sub>2</sub> reduction performance of Fe/TiO<sub>2</sub> coated on netlike glass disc equals that on Cu disc, while that on netlike glass disc is lower than that on Cu disc under the illumination condition with UV light.

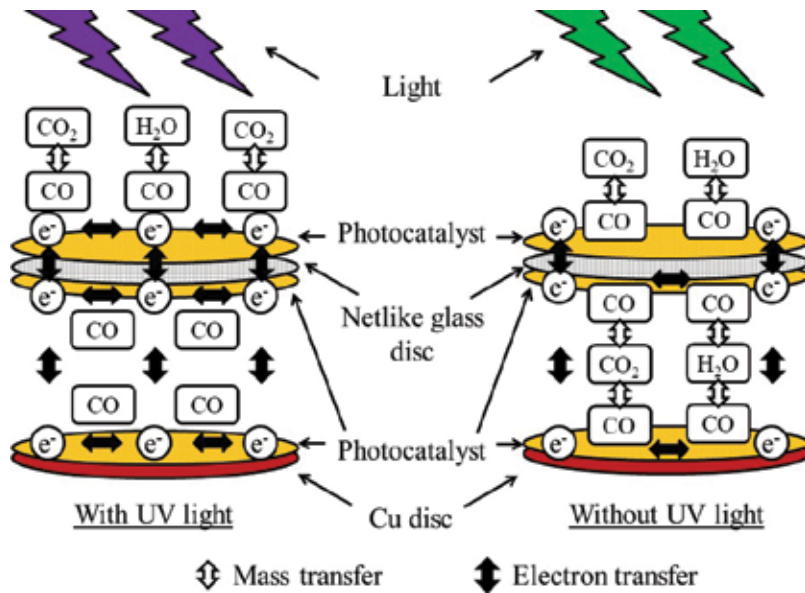
Furthermore, according to **Figure 15**, the positive effect of overlapping is obtained, especially under the double overlapping condition. As mentioned before, since the netlike glass fiber consists of SiO<sub>2</sub>, which is an electrical insulation material, the electron transfer between the two overlapped photocatalysts might not be realized well. However, the photocatalytic performance is promoted up to approximately 1.1 times by double overlapping when the maximum concentrations of CO are compared between the single and the double overlapping condition. The electron transfer between the two overlapped photocatalysts is promoted by double overlapping. However, compared to the previous cases with UV illumination, the improvement effect by double overlapping is small. Since the wavelength of illuminating light penetrating through netlike glass disc becomes longer due to losing energy, the electron produced by the Fe/TiO<sub>2</sub> coated on Cu disc, which is positioned under the netlike glass disc, decreases. The range of wavelength of light illuminating after penetrating through netlike glass disc is narrower than that in the UV illumination condition cases. Therefore, the effect of electron transfer promotion between the two overlapped photocatalysts is small compared with that in the UV illumination cases.

**Figure 16** shows the comparison of molar quantities of CO per weight of photocatalyst among the prepared photocatalysts. These values are estimated based on the maximum CO obtained under the no-UV illumination condition up to 96 h. It reveals that the molar quantity of CO per weight of Fe/TiO<sub>2</sub> under the double overlapping condition is the highest among all experimental conditions. In addition, it also reveals the positive effect of overlapping on CO<sub>2</sub> reduction performance in terms of molar quantity of CO per weight of photocatalyst is achieved in both single and double overlapping cases. It is believed that Fe/TiO<sub>2</sub> coated on Cu disc, which is positioned under the netlike glass disc, can utilize at least some of the light penetrating through the aperture of netlike glass disc for photochemical reactions, although the wavelength of the penetrating light becomes long.

The bigger synergy effect in terms of molar quantity of CO per weight of photocatalyst for two overlapped photocatalysts in no-UV cases is achieved when comparing with UV illumination cases. Since the photochemical reaction rate and the amount of produced fuel are small under the no-UV illumination condition compared to those under UV light, it would be beneficial to the mass transfer between produced fuel and reactant of CO<sub>2</sub> and H<sub>2</sub>O on the surface of photocatalyst in no-UV cases. As a result, the mass transfer and photochemical reaction are carried out effectively in no-UV cases. Therefore, the molar quantity of CO per weight of photocatalyst for overlapping cases is large in no-UV cases. According to previous reports [27, 28], the mass transfer is an inhibition factor to promote the CO<sub>2</sub> reduction performance of



**Figure 16.** Comparison of CO<sub>2</sub> reduction performances per weight of photocatalyst under the illumination condition without UV light.



**Figure 17.** Comparison of mass and electron transfer within two overlapped photocatalysts between the illumination condition with UV light and that without UV light.

photocatalyst and it is necessary to control the mass transfer rate to meet the photochemical reaction rate. **Figure 17** illustrates the comparison of mass and electron transfer within two overlapped photocatalysts in UV and no-UV illumination cases.

Compared to the previous researches [4, 6–9, 11–15], the CO<sub>2</sub> reduction performance of photocatalysts prepared in the present study is almost at the same level. However, the present study clarifies that the double overlapping arrangement is effective in improving the CO<sub>2</sub> reduction performance of Fe/TiO<sub>2</sub>. It, therefore, proposes that the netlike porous metal having an appropriate area of aperture can be a good base material for overlapping arrangement instead of netlike glass fiber since the former has a good electrical conductivity, light permeability, and gas diffusivity. In addition, the dopant like Cu, which can absorb the longer wavelength light than Fe [21], should be used in the layers at lower positioned photocatalysts in overlapping conditions. This proposal is similar to the concept of the hybrid photocatalyst using two photocatalysts having different band gaps [29–31].

#### 4. Conclusions

Based on the investigation into this study, the following conclusions can be drawn:

1. TiO<sub>2</sub> film with teethlike shape could be coated on netlike glass fiber, and Fe fine particles are loaded without agglomeration. However, TiO<sub>2</sub> film would contract around Fe particles when Fe/TiO<sub>2</sub> was coated on the Cu disc.

2. The amount of dopants that could be coated is influenced by the base material used.
3. Under the UV illumination condition, the concentration of produced CO increases due to Fe doping irrespective of the base material used. The photocatalytic performance of Fe/TiO<sub>2</sub> coated on the netlike glass disc is lower than that on the Cu disc. The peak concentration of CO for the Fe/TiO<sub>2</sub> double overlapping is approximately 1.5 times as large as the Fe/TiO<sub>2</sub> single overlapping.
4. Under the illumination condition without UV light, the CO<sub>2</sub> reduction performance of TiO<sub>2</sub> is also promoted by Fe doping due to extension of the photoresponsibility of TiO<sub>2</sub> to the visible spectrum as well as decrease in the recombination rate of electron–hole pairs by the generation of shallow charge traps in the crystal structure. The positive effect of overlapping is obtained especially under the double overlapping condition. From the viewpoint of the molar quantity of CO per weight of photocatalyst, the Fe/TiO<sub>2</sub> double overlapping shows the highest performance. It is believed that the mass transfer rates between produced fuel and reactants on the surface of photocatalyst are better matched with the photochemical reaction rates when Fe/TiO<sub>2</sub> is double overlapped.
5. The double overlapping arrangement is effective for improving the CO<sub>2</sub> reduction performance of Fe/TiO<sub>2</sub>.

## Acknowledgements

The author would like to gratefully thank JSPS KAKENHI for grant no. 25420921, Tanikawa Foundation, and Mazda Foundation for the financial support for this work.

## Author details

Akira Nishimura

Address all correspondence to: nisimura@mach.mie-u.ac.jp

Division of Mechanical Engineering, Graduate School of Engineering, Mie University, Tsu Mie, Japan

## References

- [1] The Japan Meteorological Agency. World Data Center for Greenhouse Gases [Internet]. 2001/07/02 [Updated: 2017/03/09]. Available from: <http://ds.data.jma.go.jp/gmd/wdcgg/wdcgg.html> [Accessed: 2017/06/08]
- [2] Das S, Daud WMAW. Photocatalytic CO<sub>2</sub> transformation into fuel: A review on advances in photocatalyst and photoreactor. *Renewable and Sustainable Energy Reviews*. 2014;**39**:765-805

- [3] Sakakura T, Choi J-C, Yasuda H. Transformation of carbon dioxide. *Chemical Reviews*. 2007;**107**:2365-2387
- [4] Adachi K, Ohta K, Mizuno T. Photocatalytic reduction of carbon dioxide to hydrocarbon using copper-loaded titanium dioxide. *Solar Energy*. 1994;**53**:187-190
- [5] Anpo M, Chiba K. Photocatalytic reduction of CO<sub>2</sub> on anchored titanium oxide catalysts. *Journal of Molecular Catalysis*. 1992;**74**:207-212
- [6] Dey GR, Belapurkar AD, Kishore K. Photo-catalytic reduction of carbon dioxide to methane using TiO<sub>2</sub> as suspension in water. *Journal of Photochemistry and Photobiology A: Chemistry*. 2004;**163**:503-508
- [7] Hirano K, Inoue K, Yatsu T. Photocatalysed reduction of CO<sub>2</sub> in aqueous TiO<sub>2</sub> suspension mixed with copper powder. *Journal of Photochemistry and Photobiology A: Chemistry*. 1992;**64**:255-258
- [8] Ishitani O, Inoue C, Suzuki Y, Ibusuki T. Photocatalytic reduction of carbon dioxide to methane and acetic acid by an aqueous suspension of metal-doped TiO<sub>2</sub>. *Journal of Photochemistry and Photobiology A: Chemistry*. 1993;**72**:269-271
- [9] Kaneco S, Kurimoto H, Shimizu Y, Ohta K, Mizuno T. Photocatalytic reduction of CO<sub>2</sub> using TiO<sub>2</sub> powders in supercritical fluid CO<sub>2</sub>. *Energy*. 1999;**24**:21-30
- [10] Gui MM, Chai S-P, Xu B-Q, Mohamed AR. Enhanced visible light responsive MWCNT/TiO<sub>2</sub> core-shell nanocomposites as the potential photocatalyst for reduction of CO<sub>2</sub> into methane. *Solar Energy Materials & Solar Cells*. 2014;**122**:183-189
- [11] Xie S, Wang Y, Zhang Q, Deng W, Wang Y. MgO and Pt-promoted TiO<sub>2</sub> as an efficient photocatalyst for the preferential reduction of carbon dioxide in the presence of water. *ACS Catalysis*. 2014;**4**:3644-3653
- [12] Beigi AA, Fatemi S, Salehi Z. Synthesis of nanocomposite CdS/TiO<sub>2</sub> and investigation of its photocatalytic activity for CO<sub>2</sub> reduction to CO and CH<sub>4</sub> under visible light irradiation. *Journal of CO<sub>2</sub> Utilization*. 2014;**7**:23-29
- [13] Michalkiewicz B, Majewska J, Kadziolka G, Bubacz K, Mozia S, Morawski AW. Reduction of CO<sub>2</sub> by adsorption and reaction on surface of TiO<sub>2</sub>-nitrogen modified photocatalyst. *Journal of CO<sub>2</sub> Utilization*. 2014;**5**:47-52
- [14] Lee C-W, Kourounioti RA, Wu JCS. Photocatalytic conversion of CO<sub>2</sub> to hydrocarbons by light-harvesting complex assisted Rh-doped TiO<sub>2</sub> photocatalyst. *Journal of CO<sub>2</sub> Utilization*. 2014;**5**:33-40
- [15] Ozcan O, Yukruk F, Akkaya EU, Uner D. Dye sensitized CO<sub>2</sub> reduction over pure and platinized TiO<sub>2</sub>. *Topics in Catalysis*. 2007;**44**:523-528
- [16] Subramanian M, Vijayalakshmi S, Venkataraj S, Jayavel R. Effect of cobalt doping on the structural and optical properties of TiO<sub>2</sub> film prepared by sol-gel process. *Thin Solid Films*. 2008;**516**:3776-3782

- [17] Zabova H, Cirkva V. Microwave photocatalysis III. Transition metal ion-doped TiO<sub>2</sub> thin films on mercury electrodeless discharge lamps: Preparation, characterization and their effect on the photocatalytic degradation of mono-chloroacetic acid and Rhodamine B. *Journal of Chemical Technology and Biotechnology*. 2009;**84**:1624-1630
- [18] Wang JA, Limas-Ballesteros R, Lopez T. Quantitative determination of titanium lattice defects and solid-state reaction mechanism in iron-doped TiO<sub>2</sub> photocatalysts. *Journal of Physical Chemistry B*. 2001;**105**:9692-9698
- [19] Laokiat L, Khemthong P, Grisdanurak N, Sreearunothai P, Pattanasiriwisawa W, Klysubun W. Photocatalytic degradation of benzene, toluene, ethylbenzene, and xylene (BTXE) using transition metal-doped titanium dioxide immobilized on fiberglass cloth. *Korean Journal of Chemical Engineering*. 2012;**29**:377-383
- [20] Ambrus Z, Balazs N, Alapi T. Synthesis, structure and photocatalytic properties of Fe(III)-doped TiO<sub>2</sub> prepared from TiCl<sub>3</sub>. *Applied Catalysis B: Environmental*. 2008;**81**:27-37
- [21] Nagaveni K, Hedge MS, Madras G. Structure and photocatalytic activity of Ti<sub>1-x</sub>M<sub>x</sub>O<sub>2δ</sub> (M=W, V, Ce, Zr, Fe, and Cu) synthesized by solution combustion method. *The Journal of Physical Chemistry B*. 2004;**108**:20204-20212
- [22] Japan Society of Mechanical Engineering. In: editors, editor. *Heat Transfer Hand Book*. 1st ed. Tokyo: Maruzen; 1993. p. 429
- [23] Nishimura A, Mitsui G, Nakamura K, Hirota M, Hu E. CO<sub>2</sub> reforming characteristics under visible light response of Cr- or Ag-doped TiO<sub>2</sub> prepared by sol-gel and dip-coating process. *International Journal of Photoenergy*. 2012;**2012**:184169
- [24] Goren Z, Willner I, Nelson AJ, Frank AJ. Selective photoreduction of CO<sub>2</sub>/HCO<sub>3</sub><sup>-</sup> to formate by aqueous suspensions and colloids of Pd-TiO<sub>2</sub>. *Journal of Physical Chemistry*. 1990;**94**:3784-3790
- [25] Tseng I-H, Chang W-C, Wu JCS. Photoreduction of CO<sub>2</sub> using sol-gel derived titania and titania-supported copper catalysts. *Applied Catalysis B: Environmental*. 2002;**37**:37-48
- [26] Nishimura A, Sugiura N, Fujita M, Kato S, Kato S. Influence of preparation conditions of coated TiO<sub>2</sub> film on CO<sub>2</sub> reforming performance. *Kagaku Kogaku Ronbunshu*. 2007;**33**:146-153
- [27] Nishimura A, Komatsu N, Mitsui G, Hirota M, Hu E. CO<sub>2</sub> reforming into fuel using TiO<sub>2</sub> photocatalyst and gas separation membrane. *Catalysis Today*. 2009;**148**:341-349
- [28] Nishimura A, Okano Y, Hirota M, Hu E. Effect of preparation condition of TiO<sub>2</sub> film and experimental condition on CO<sub>2</sub> reduction performance of TiO<sub>2</sub> photocatalyst membrane reactor. *International Journal of Photoenergy*. 2011;**2011**:305650
- [29] Marci G, Garcia-Lopez EI, Palmisano L. Photocatalytic CO<sub>2</sub> reduction in gas-solid regime in the presence of H<sub>2</sub>O by using GaP/TiO<sub>2</sub> composite as photocatalyst under simulated solar light. *Catalysis Communications*. 2014;**53**:38-41



- [30] Song G, Xin F, Yin X. Photocatalytic reduction of CO<sub>2</sub> in cyclohexanol on CdS-TiO<sub>2</sub> heterostructured photocatalyst. *Applied analysis A: General*. 2014;**473**:90-95
- [31] Song G, Xin F, Yin X. Photocatalytic reduction of carbon dioxide over ZnFe<sub>2</sub>O<sub>4</sub>/TiO<sub>2</sub> nanobelts heterostructure in cyclohexanol. *Journal of Colloid and Interface Science*. 2015;**442**:60-66



---

# CO<sub>2</sub> Reforming with CH<sub>4</sub> via Plasma Catalysis System

---

Wei Chieh Chung and Moo Been Chang

Additional information is available at the end of the chapter

<http://dx.doi.org/10.5772/intechopen.73579>

---

## Abstract

Reforming of CO<sub>2</sub> and CH<sub>4</sub> into syngas (mixture of H<sub>2</sub>/CO) can be an economical way to reduce anthropogenic emission of CO<sub>2</sub> and CH<sub>4</sub> and to generate alternative fuel. Up to date, catalysis and nonthermal plasma are two feasible techniques for CO<sub>2</sub>/CH<sub>4</sub> reforming. However, both techniques face some obstacles which limit their applications. For catalysis, high energy consumption and catalyst deactivation are the major disadvantages while nonthermal plasma has the drawbacks of low selectivity and unwanted byproduct formation. To overcome the above obstacles, combining catalyst and nonthermal plasma as a hybrid system can induce synergistic effects to enhance syngas production rate and stability of the operating system. For the purpose of enhancing CO<sub>2</sub> utilization efficiency, understanding the interactions between catalyst and nonthermal plasma is essential.

**Keywords:** reforming of CO<sub>2</sub>, syngas, plasma catalysis, synergistic effects

---

## 1. Introduction

Utilization of carbon dioxide is imperative and there is urgent demand for effective carbon dioxide reducing techniques. Reforming of carbon with methane, which is also called dry reforming of methane (DRM, the term “dry” is to distinguish from steam reforming which is to reform methane with water vapor) can be a feasible process to convert CO<sub>2</sub> and CH<sub>4</sub> into syngas (mixture of H<sub>2</sub>/CO). Currently, catalysis and nonthermal plasma are two essential techniques for DRM to generate syngas and to reduce the anthropogenic emissions of greenhouse gases (GHGs). Catalytic reforming of CH<sub>4</sub>/CO<sub>2</sub> is a high-selectivity, high production rate and well developed technique to generate syngas. Up to date, several types of catalysts have been investigated for their catalytic activity toward DRM, including noble metal catalysts [1], nickel-based catalysts [2], cobalt-based catalysts [3], spinels [4] and perovskites [5].

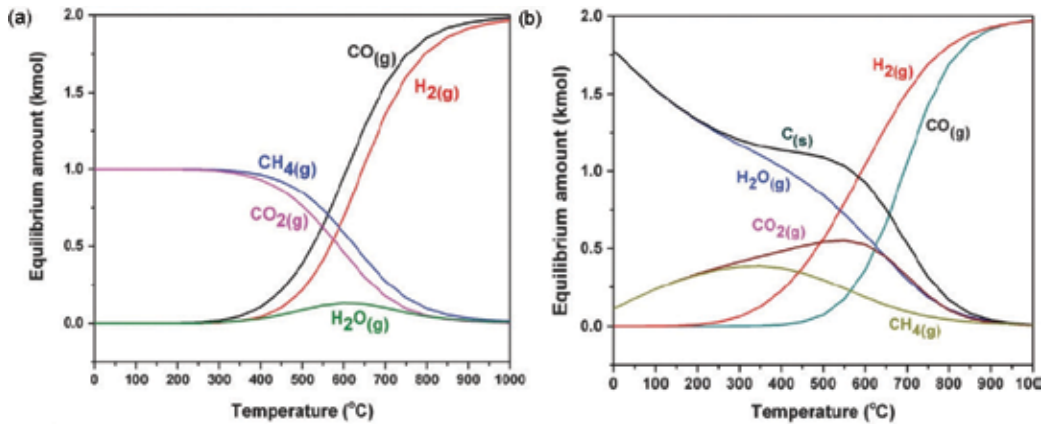
However, high operating temperature is required for effective conversion. Moreover, coke deposition leads to subsequent catalyst deactivation. Thus, how to effectively reduce operating temperature and coke deposition remains the big challenge for catalytic reforming [6, 7]. On the other hand, nonthermal plasma stands for an energy-saving reforming for GHGs reduction and many kinds of nonthermal plasma reactor have been designed and developed to enhance  $\text{CO}_2/\text{CH}_4$  conversion efficiency. Nonthermal plasma can generate syngas at a lower operating temperature since the driving force of nonthermal plasma is electric energy instead of thermal energy [8]. Even so, nonthermal plasma has some limitations including low GHGs conversions, low syngas selectivity and byproduct formation, e.g. carbon soot. The above disadvantages reduce the applicability of nonthermal plasma for DRM [9]. To overcome the shortcomings of catalytic reforming and nonthermal plasma reforming, combining catalyst and nonthermal plasma as a hybrid reactor can be a solution since various interactions can be induced between catalyst and nonthermal, including the change of physicochemical properties of catalyst, enhancement of electric field and activation of catalysis [10]. Based on the interactions between catalysis and nonthermal plasma, limitations of catalytic reforming and nonthermal plasma reforming including catalyst deactivation and byproduct formation can be resolved due to enhancement of reforming performance toward DRM [11–13].

In this chapter, application of three types of DRM system, i.e. catalysis, nonthermal plasma and hybrid plasma catalysis will be introduced and discussed for their fundamental concepts, including reaction mechanism, state-of-the-art development, opportunities and shortcomings. Some important features for various reactors will also be highlighted in this chapter as a reference.

## 2. Catalytic reforming

$\text{CO}_2$  and  $\text{CH}_4$  are stable molecules under atmospheric pressure, thus the temperature required for inducing spontaneous dissociation of  $\text{CO}_2$  and  $\text{CH}_4$  is comparatively high. **Figure 1** shows thermodynamic equilibrium for  $\text{CO}_2/\text{CH}_4$  reforming without catalyst achieved with Gibbs free energy minimization algorithm [14]. It indicates thermodynamic equilibrium of reactants ( $\text{CO}_2$  and  $\text{CH}_4$ ) and products ( $\text{CO}$ ,  $\text{H}_2$ ,  $\text{C}_{(s)}$  and  $\text{H}_2\text{O}_{(g)}$ ) with the assumption that carbon formation is inhibited. Assuming that carbon formation is inhibited, the temperature required for effective conversion of  $\text{CO}_2/\text{CH}_4$  is comparatively high ( $> 550^\circ\text{C}$ ) while water vapor can be generated simultaneously. Actually, carbon stands for the major byproduct during reforming and influences thermodynamics as well. At a lower operating temperature, water vapor and carbon are the major products and their formation can be inhibited when operating temperature is increased to over  $700^\circ\text{C}$ . Generally speaking, to generate syngas efficiently, operating temperature should be higher than  $700^\circ\text{C}$ , which is energy-consuming.

Catalyst is required to reduce the operating temperature of DRM since both  $\text{CO}_2$  and  $\text{CH}_4$  are stable and a great amount of thermal energy is needed to induce reforming. Noble metal-based catalysts including Pt, Pd, Ir, Rh and Ru have been investigated for their activities. They possess great activities toward DRM and good resistivities for coke deposition. The



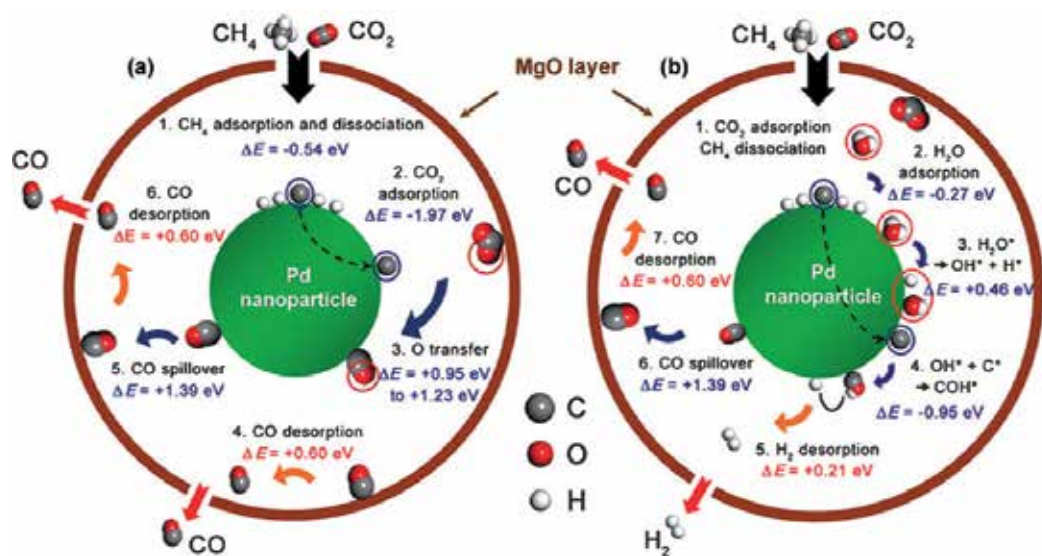
**Figure 1.** Thermodynamic equilibrium plots for DRM at 1 atm, from 0–1000°C and at inlet feed ratio of CO<sub>2</sub>/CH<sub>4</sub> =1 (a) Assuming no carbon formation occurs, (b) assuming carbon formation occurs. These plots were created by using Gibbs free energy minimization algorithm on HSC Chemistry 7.1 software [14].

activity order of the above metal catalysts also depends on support and preparation method. Generally, Rh and Ru catalysts are good candidates since they have better catalytic activities and durabilities than other noble metals [15, 16]. However, their costs are also high which limits their industrial applicability. Hence, transition metal-based catalysts such as nickel, cobalt-based catalysts are frequently developed and investigated. Ni-based catalysts are most applied for DRM since they have high adsorption capacities toward CO<sub>2</sub> and CH<sub>4</sub> and many researches have been conducted for the purpose of increasing selectivity of syngas and stability of catalyst in terms of resistivity of coke deposition [17,18].

Generally, pathways of catalytic reactions can be divided into three categories: Langmuir-Hinshelwood (L-H), Eley-Rideal (E-R) and Mars-van Krevelen (MVK), as described in **Table 1** [19]. Kinetic studies point out that DRM follows the reaction route of L-H mechanism. The reaction mechanism of DRM can be described as **Figure 2**, density functional theory (DFT) simulation results of DRM kinetics achieved with Pd/MgO catalyst indicate that CH<sub>4</sub> and CO<sub>2</sub> are firstly adsorbed on Pd and MgO surface and then dissociated into CO, O, C and H atoms [20]. It

Carbon structure	Designation	Temperature range (°C)
Surface carbide	C <sub>α</sub>	200–400
Amorphous carbon films	C <sub>β</sub>	250–500
Bulk Ni carbide	C <sub>γ</sub>	150–250
Vermicular filaments/whiskers	C <sub>ν</sub>	300–1000
Graphite platelet films	C <sub>ε</sub>	500–550

**Table 1.** Details of different carbon species formed on the catalyst surface [21].



**Figure 2.** Results from DFT studies on the multifunctional  $\text{CH}_4$  reforming mechanism under dry reforming conditions (a) and an  $\text{H}_2\text{O}$  atmosphere (b). The reaction proceeds in clockwise direction. Pd dissociates  $\text{CH}_4$  and MgO binds and activates  $\text{CO}_2$ . MgO opens a favorable CO production pathway.  $\text{H}_2\text{O}$  byproducts are attributed to  $\text{H}_2$  production. Pd dissociates  $\text{H}_2\text{O}$  into PdOH and PdH, PdOH and PdC were combined into PdCOH.  $\text{H}_2$  association from PdCOH and PdH is easier than direct  $\text{H}_2$  association from two PdH. These CO and  $\text{H}_2$  production pathways are accessible at low temperature and assure low-temperature activity of Pd-MgO/ $\text{SiO}_2$  (ME) [20].

is noted that CO desorption is an endothermic reaction, thus desorption of CO plays the role of rate-limiting reaction of DRM. Also, H atoms can further recombine to form  $\text{H}_2$  and desorb onto effluent gas stream. Moreover, if water vapor is added into the gas stream, water molecules participate in catalysis and more active species can be generated such as  $\text{OH}^*$ ,  $\text{H}^*$  and  $\text{COH}^*$  radicals, providing more formation routes of  $\text{H}_2$ , resulting in higher generation rate of  $\text{H}_2$ .

In terms of long-term operation of scaled-up catalytic reforming, coke deposition is the serious problem to shorten the duration of operation. Coke can be generated via several ways during reforming, as described in **Table 2**. Carbon formation can be classified into 5 categories, including the form of surface carbide, amorphous carbon films, metal carbide, whiskers and

Mechanism	Description
Langmuir-Hinshelwood	Both reactants are adsorbed on catalyst surface firstly. Next, adsorbed reactants can react with each other and form products. The final step is desorption of products and regeneration of active sites.
Eley-Rideal	One of reactants is firstly adsorbed on catalyst surface. Further reaction takes place between adsorbed specie and gas phase-specie.
Mars-van Krevelen	One of reactants is chemisorbed on catalyst, and then diffuses to lattice to react with the other adsorbed reactant.

**Table 2.** Categories of catalysis mechanisms.

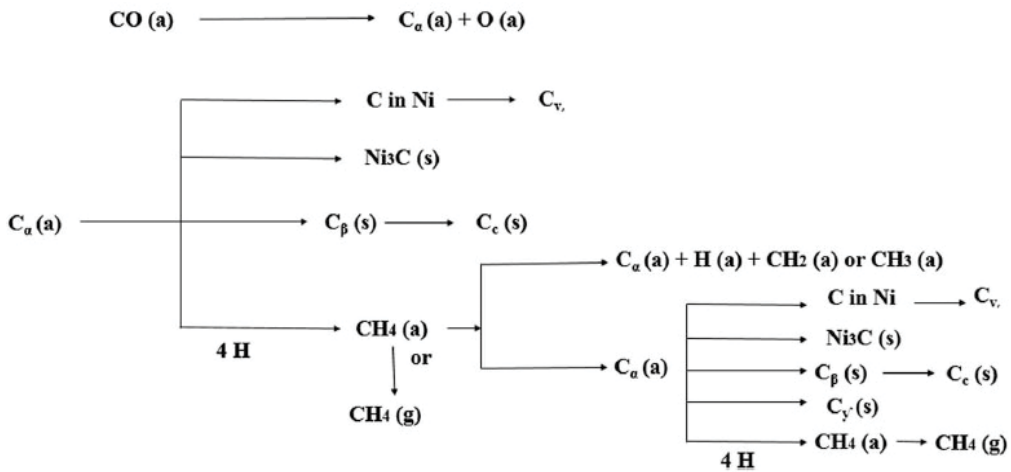
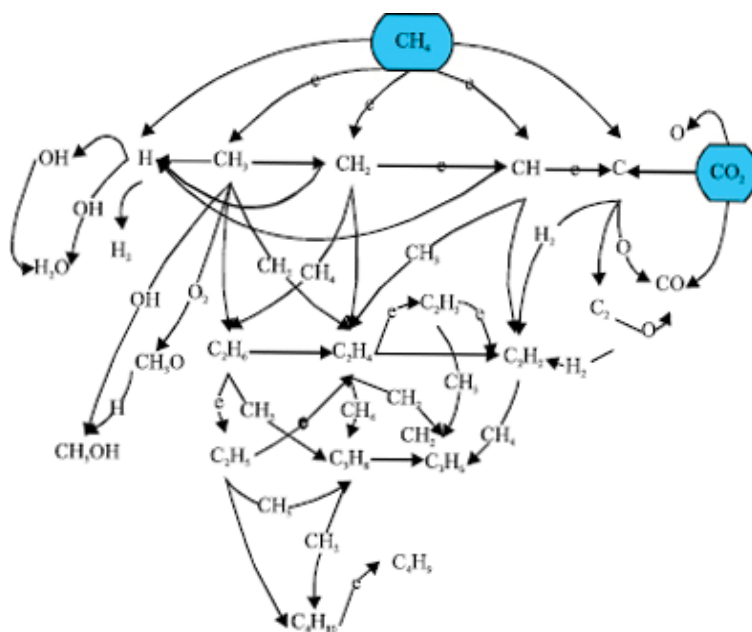


Figure 3. Mechanism of carbon formation at the catalyst surface [21].

platelet films, depending on the carbon source, temperature, structure and deposition site. Generally,  $C_\alpha$  is firstly formed via dissociation of  $\text{CO}_2$  and  $\text{CH}_4$  and this reaction is feasible at a lower temperature. Other carbon species including  $C_{\beta'}$ ,  $C_{\gamma'}$ ,  $C_v$  and  $C_c$  can be further synthesized via several ways as listed in Figure 3 [21]. It is noted that carbon can be transferred from one form to another. For example, amorphous carbon film can be transformed into graphite platelet films when the temperature is increased. Another example is that carbon whiskers can be easily formed from many types of carbon at a high temperature. To effectively reduce the formation of  $C_\alpha$ , operating temperature is suggested to be high. However, high operating temperature leads to formation of other carbon species. As a result, carbon deposition inevitably takes place since formation routes are various. Many works are conducted to reduce the problem of coke deposition, including catalyst modification via partial metal substitution, introduction of support and surface pre-treatment and reactor designing. Nevertheless, coke deposition still plays an important role in limiting performance and the increase of the cost of catalytic reforming.

### 3. Nonthermal plasma reforming

Nonthermal plasma stands for an alternative to treat GHGs since the driving force of nonthermal plasma is electronic energy instead of thermal energy. With the existence of external electric field, electrons can be accelerated and then collide with gas particles including  $\text{CO}_2$ ,  $\text{CH}_4$ , intermediates, radicals and ions. When energy is transferred from electron to the above species, chemical reactions take place such as electron impact excitation, dissociation and ionization, Penney ionization and electron attachment.  $\text{CH}_4$  and  $\text{CO}_2$  can be directly dissociated into smaller fractions when the transferred energy exceeds 8.8 and 4.5 eV, respectively [22, 23]. The dissociated products including methyl radical, methylene,



**Figure 4.** Possible reaction mechanisms in a nonthermal plasma reactor [24].

oxygen and hydrogen radical can further react with each other to form  $\text{H}_2$ ,  $\text{CO}$  and other byproducts, e.g. ethylene, water vapor and methanol. **Figure 4** depicts possible reaction routes for nonthermal plasma reforming [24].  $\text{CH}_4$  can be dissociated into various radicals, depending on how much energy is transferred from electron. On the other hand,  $\text{CO}_2$  can also be dissociated into  $\text{CO}$  and  $\text{O}$  simultaneously. The above reactive species including radicals,  $\text{H}$  and  $\text{O}$  atoms can further react to form hydrocarbon radicals and molecules. Radicals mentioned beforehand can react with  $\text{CH}_4$  and  $\text{CO}_2$  to enhance their dissociation rates. It is noted that electrons can react with those particles to dissociate them into smaller fragments and the more important point is that radicals are unstable to have high activity toward other particles.

Actually, direct dissociation of  $\text{CO}_2/\text{CH}_4$  is difficult to take place in nonthermal plasma due to high energy demand. In terms of  $\text{CO}_2$ , vibrational excited and electron excited  $\text{CO}_2$  are more easily generated and participate in DRM since the energy required for excitation is lower than  $\text{CO}_2$  dissociation. Those excited  $\text{CO}_2$  possess higher energy, thus, energy required to generate  $\text{CO}$ ,  $\text{O}$ ,  $\text{CO}_2^+$  and  $\text{O}_2^+$  can be reduced as illustrated in **Figure 5**. In terms of  $\text{CH}_4$ ,  $\text{CH}_x$  ( $x = 1-3$ ) radicals especially  $\text{CH}_3$  (methyl radical) and  $\text{CH}_2$  (methylene) are formed with different levels. These species are unstable and tend to react with other species [26]. When two or more radicals react with each other, higher hydrocarbons can be generated [25]. For example, when two  $\text{CH}_3^*$  radicals react with each other, ethane can be formed as illustrated in **Figure 6** [27]. From the perspective of DRM, hydrocarbons are byproducts since the purpose of DRM is to generate syngas. However, this process can be useful for generating hydrocarbons, such as plasma polymerization [28].

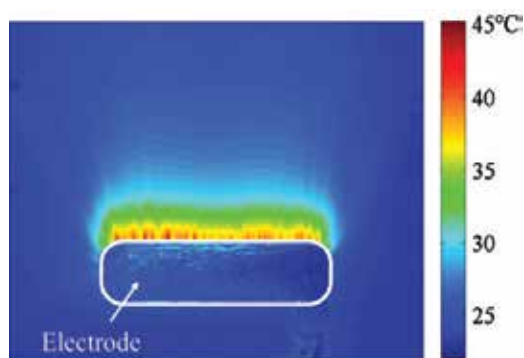




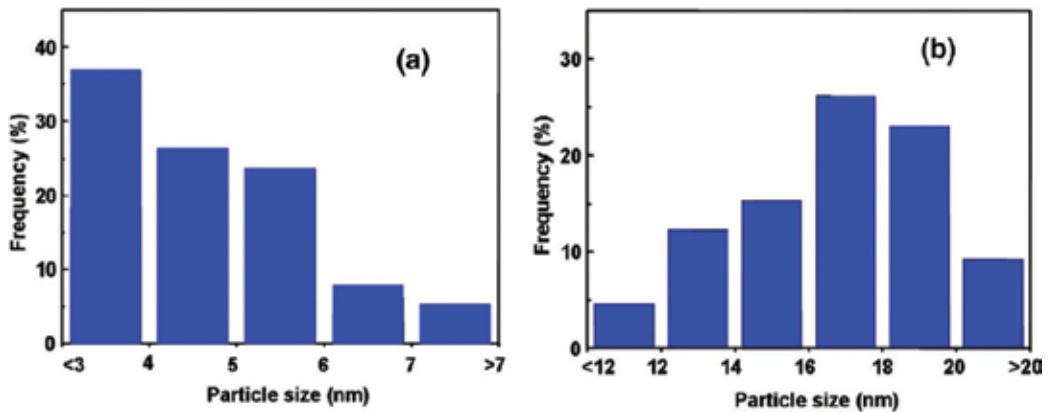


**Figure 7.** Schematic representation of the catalyst-packed dielectric barrier discharge reactor [29].

can be transferred onto catalyst surface. The most important part of transferred energy is thermal energy. Thermal energy can be transferred from electrons to particles on catalyst surface to heat up the particle, forming a hot spot, as shown in **Figure 8**. It is observed that with the packing of catalyst on the electrode, the surface temperature of electrode is increased since catalyst can absorb thermal energy transferred from particles [30]. As a result, catalytic reforming may take place on catalyst surface if local temperature (hot spot) exceeds the temperature required for catalysis. Next, local high temperature may induce restructuring of metal oxide clusters since their internal energy is increased. The result is that physicochemical properties of catalyst can be altered during reforming, such as particle size, pore structure, valence of metal, metal-support interactions, surface area, surface free energy, surface acidity/basicity and oxygen vacancy. In terms of catalysis, the above characteristics influence its catalytic activity well: firstly, particle size influences adsorption heat and thus adsorption and desorption rate are further changed. Electron bombardments can result in smaller average metal cluster size (**Figure 9**) and adsorption heat between  $\text{CO}_2/\text{CH}_4$  and catalyst and further enhance  $\text{CO}_2/\text{CH}_4$  adsorption and  $\text{H}_2/\text{CO}$  desorption rate [31]. Secondly, pore structure also affects  $\text{CO}_2/\text{CH}_4$  adsorption on surface and inside pores. Larger pore size may be feasible for reforming since the resistance of diffusion can be lower and leads to better desorption. However, the relationship between pore size and operating parameter of nonthermal plasma is still unclear, thus, how to control the pore size remains a challenging task [32]. Thirdly, larger surface area and density of oxygen

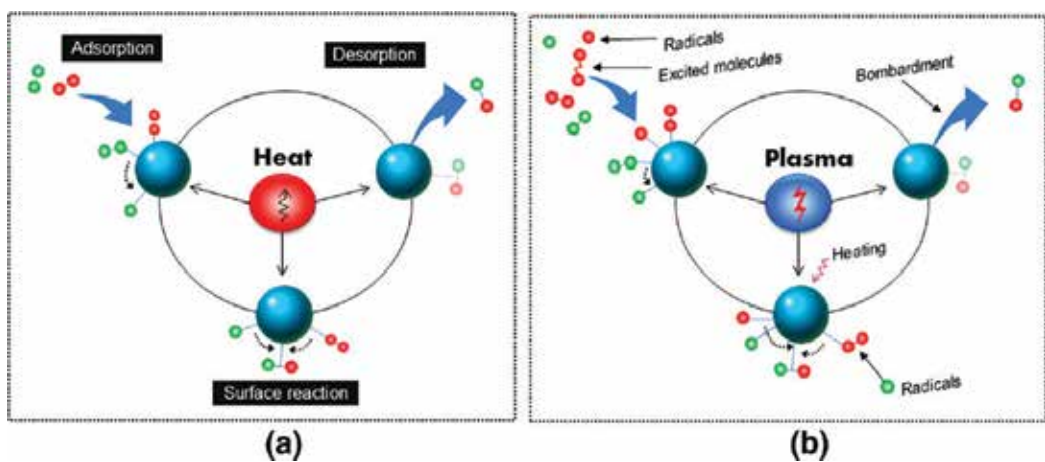


**Figure 8.** Absolute temperature distribution in a DBD, showing the occurrence of surface hot spots [30].



**Figure 9.** Particle size distribution achieved with TEM of (a) Plasma treated Ni/MgO and (b) conventional Ni/MgO catalysts [31].

vacancy are beneficial toward DRM since the former provides more adsorption sites and the latter provides more oxidizing agent [33]. Moreover, electron and ion bombardments can alter the chemical bonding between metal and oxygen, hence, density of oxygen in catalyst lattice can be increased. Fourthly, nonthermal plasma can affect the surface acidity/basicity since acidic and basic active species can be generated and then collide with catalyst. For catalytic reforming, surface acidity plays an important role since adsorbed CO<sub>2</sub> is acidic. In other words, catalyst possesses surface basicity are favorable for CO<sub>2</sub> adsorption and further dissociation [34]. Lastly, nonthermal plasma generates various stable and active species. Those active species can react with other species or can be adsorbed on catalyst surface, as presented in **Figure 10**. In plasma catalysis system, alternate reaction routes are provided since various active species are generated. Active species such as ions, radicals and electrons can be adsorbed to react

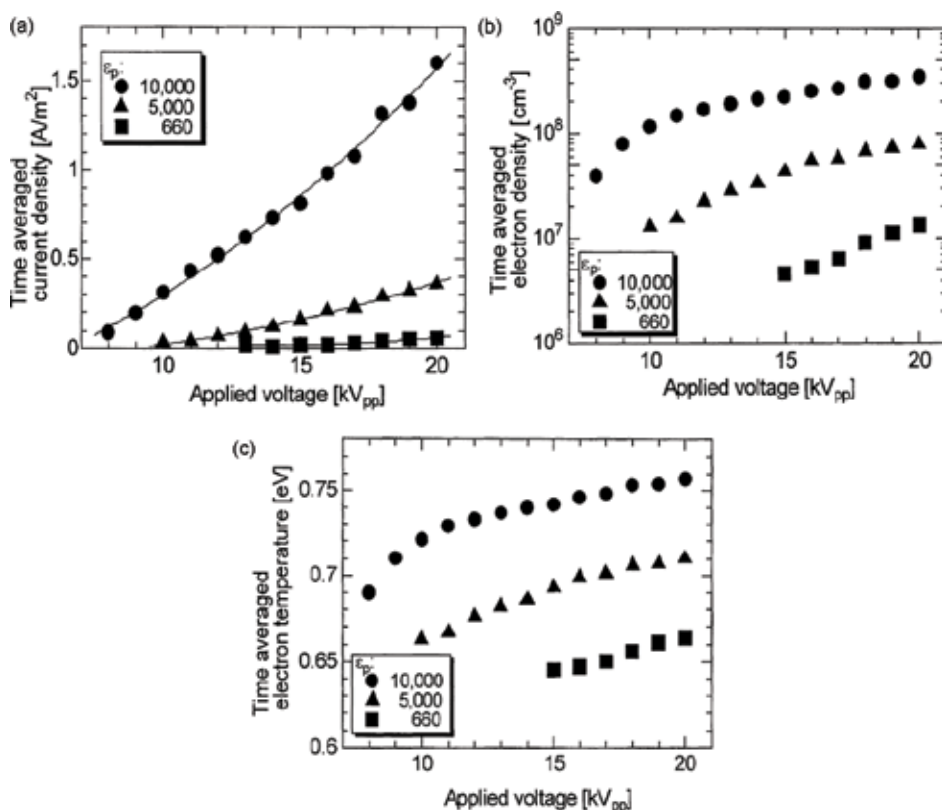


**Figure 10.** Three key steps in (a) thermal catalysis and (b) plasma-catalysis [10].

with other active species or can react with adsorbed species directly without prior adsorption. Hence, DRM does not necessarily follow L-H mechanism, which requires both two reactants are adsorbed on catalyst surface. In summary, nonthermal plasma can be applied for catalyst modification due to its capability to improve the physicochemical properties of catalyst. Also, nonthermal plasma can be combined with catalyst and the dissipated energy during discharge can possibly induce catalytic reforming. The most important advantage is that nonthermal plasma provides more reaction routes and more active species participating in DRM.

#### 4.2. Catalyst influencing plasma

Packing catalyst into discharge region can affect plasma properties including electric field, electron density and energy distribution. Most of catalysts are dielectrics, which can be polarized to form electric dipole, i.e. surface electric potential. Electric potential can further interact with external electric field, electron and other charged particles. Thus, discharge behavior of plasma is influenced by the existence of catalyst and its dielectric constant. **Figure 11** shows the dependence of deposited power, current density and electron temperature on the dielectric constant ( $\epsilon_p$ ) of packing catalyst [35]. Since the catalyst with a higher dielectric constant

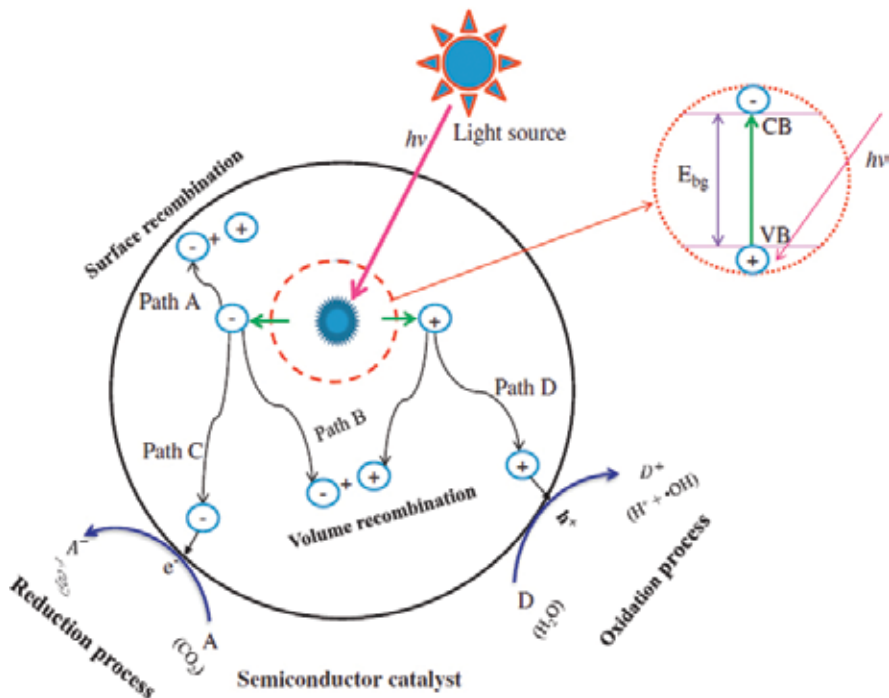


**Figure 11.** Simulation results of (a) time averaged input power, (b) time averaged discharge current and (c) time- and space-averaged electron temperature as a function of applied voltage for various pellet dielectric constant [35].

leads to higher polarization, plasma catalysis reactor with the catalyst possessing a higher dielectric constant has higher deposited energy, current density and electron temperature.

Catalysts generally possess various types of pores, e.g. micropore or macropore, the geometry and distribution of pores can also influence discharge properties. Local discharge may take place inside the pore if the size of pore is appropriate (larger than Debye's length), which is called microdischarge. Once discharge takes place inside the pore, species adsorbed inside the pore can be dissociated or excited into smaller fragments or active species to further provide alternative routes for CO<sub>2</sub>/CH<sub>4</sub> reforming.

During discharge, photons can be generated via excitation-relaxation. Photons may be absorbed by catalyst if the catalyst possesses a band structure similar to photocatalyst, i.e. a valence band (VB) and a conduction band (CB). The photons with kinetic energy higher or equal to the gap between VB and CV can transfer its energy to catalyst to activate electron near VB edge to CB and leave a hole in VB. Hence, electron-hole pair is formed at CB and VB, respectively. Electron at CB can induce reduction of CO<sub>2</sub> into CO, and electron hole at VB can oxidize CH<sub>4</sub> into CO and H<sub>2</sub> as indicated in **Figure 12** [36]. As a result, syngas generation can be enhanced if photocatalytic conversion of CO<sub>2</sub>/CH<sub>4</sub> can be activated. Unfortunately, photocatalysis has an important obstacle: recombination of electron-hole pair. Excited electron at CB is very stable and tends to return to VB, which is recombination of electron-hole pair. Recombination leads to lower energy utilization rate, as a result, how to reduce recombination rate is essential.



**Figure 12.** Mechanism and pathways for photocatalytic oxidation and reduction processes on the surface of heterogeneous photocatalyst [36].

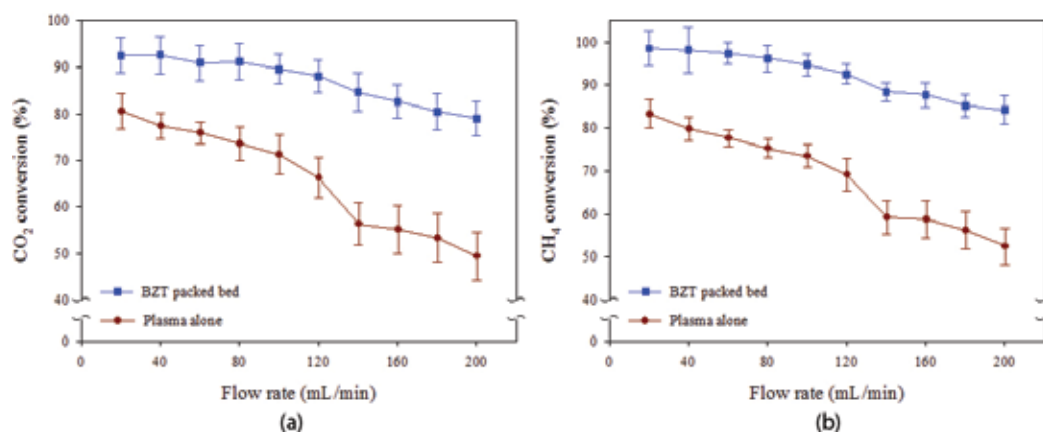


Figure 13. (a) CO<sub>2</sub> and (b) CH<sub>4</sub> conversions achieved with various reactors [37].

Chung and Chang (2016) combined BaZr<sub>0.05</sub>Ti<sub>0.05</sub>O<sub>3</sub> (BZT) catalyst (particle size ranging from 210 to 420 μm) and spark plasma reactor to form a hybrid system [37]. Results show that packing catalyst BZT into discharge region can increase electric field and current density, indicating that more kinetic electrons are generated in hybrid reactor. CO<sub>2</sub> and CH<sub>4</sub> conversions can be enhanced since the energy and amount of free electrons are increased, as shown in Figure 13 [37]. Next, the selectivities of H<sub>2</sub> and CO are also increased after packing BZT, and this can be attributed to the fact that catalyst provides formation site for H<sub>2</sub> and CO. Last, in terms of energy efficiency (moles of syngas generated per kilowatt-hour input), packing BZT into plasma reactor leads to higher energy consumption, thus, the energy efficiency achieved

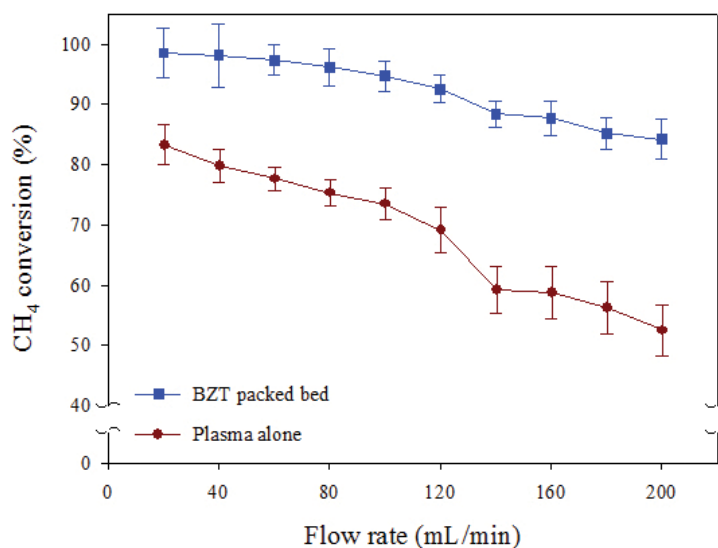


Figure 14. Energy efficiencies achieved with various reactors [37].

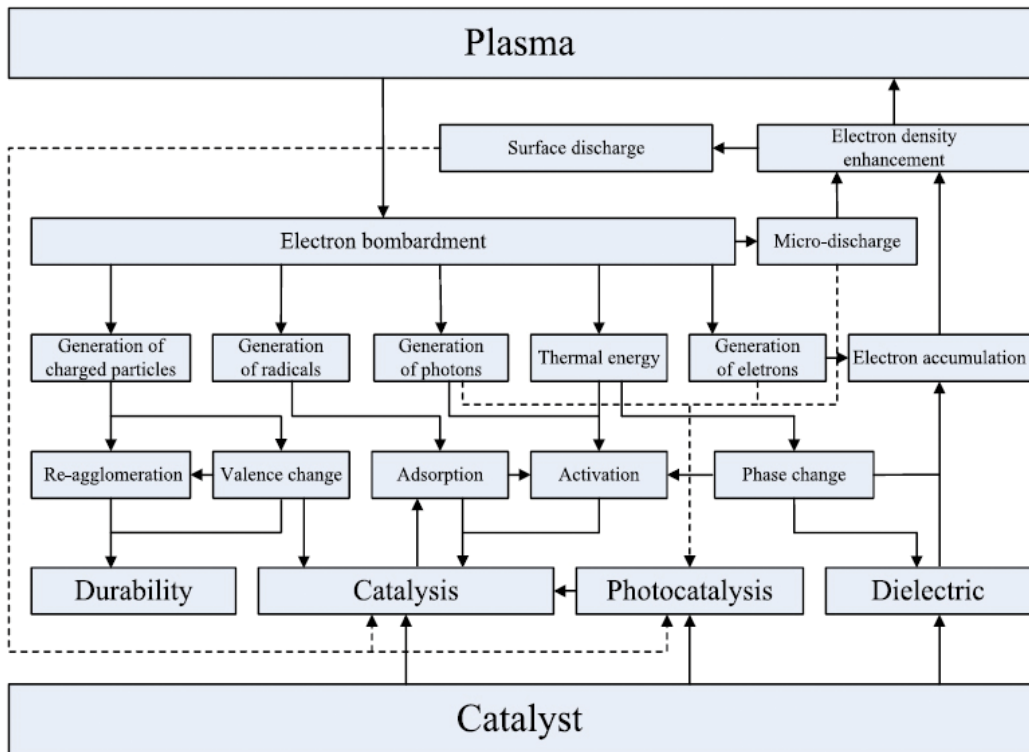


Figure 15. Interactions between nonthermal plasma and catalysis [33].

with the hybrid reactor is not necessarily higher than plasma reactor at a low reactant feeding rate. Increasing feeding rate can result in higher energy utilization rate to generate syngas and further enhance synergies between plasma and catalyst as shown in Figure 14 [37].

Overall, interactions between nonthermal plasma and catalysis are presented in Figure 15. Since electrons can be generated via nonthermal plasma to attain high kinetic energy. Energetic electrons can hit on catalyst surface to transfer energy and further influence the physicochemical properties of catalyst including particle size, surface area and pore structure. On the other hand, packing catalyst into plasma reactor can alter discharge behavior of plasma, depending on electrical and geometrical properties of catalyst. However, there remains unclear synergies and requires more works to discover and elucidate detailed interactions.

## 5. Conclusions

Catalysis and nonthermal plasma are two efficient approaches to generate syngas from CO<sub>2</sub> and CH<sub>4</sub>. Catalytic conversion of CO<sub>2</sub> and CH<sub>4</sub> follows the mechanism of L-H mechanism and CO desorption is the rate-determining step. Coke formation via multiple routes is the most important obstacle to limit the application of catalytic reforming. On the other

hand, nonthermal plasma provides an alternative reaction mechanism to convert  $\text{CO}_2$  and  $\text{CH}_4$ . During discharge, various active species can be generated to dissociate  $\text{CO}_2$  and  $\text{CH}_4$ , including free electron, radicals and vibrational excited species. However, the above phenomenon leads to byproducts formation that reduces syngas production rate. Combining catalyst and nonthermal plasma to form a hybrid system is a promising way to enhance converting efficiency of  $\text{CO}_2$  and  $\text{CH}_4$  into syngas, since various interactions can be induced in the hybrid system. The form and the degree of interactions depend on properties of catalyst, nonthermal plasma and the way of combination. Hence, properties of catalyst and nonthermal plasma should be taken into account when designing a hybrid system. For catalyst, surface structure, band structure, thermal stability, catalytic activity and dielectric constant are important. In other words, temperature, electron density and energy are key factors to be considered. Even though detailed synergistic effects are unknown, the development of plasma catalysis system is optimistic for the future application on DRM.

## Author details

Wei Chieh Chung and Moo Been Chang\*

\*Address all correspondence to: mbchang@ncuen.ncu.edu.tw

Graduate Institute of Environmental Engineering, National Central University,  
Taoyuan City, Taiwan

## References

- [1] Pakhare D, Spivey J. A review of dry ( $\text{CO}_2$ ) reforming of methane over noble metal catalysts. *Chemical Society Reviews*. 2014;**43**:7813-7837. DOI: 10.1039/c3cs60395d
- [2] Bian ZF, Das S, Wai MH, Hongmanorom P, Kawi S. A review on bimetallic Ni-based catalysts for  $\text{CO}_2$  reforming of methane. *ChemPhysChem*. 2017;**18**(22):3117-3134.
- [3] Budiman AH, Song SH, Chang TS, Shin CH, Choi MJ. Dry reforming of methane over cobalt catalysts: A literature review of catalyst development. *Catalysis Surveys from Asia*. 2012;**16**:183-197. DOI: 10.1007/s10563-012-9143-2
- [4] Nair MM, Kaliaguine S. Structured catalysts for dry reforming of methane. *New Journal of Chemistry*. 2016;**40**:40494060. DOI: 10.1039/c5nj03268g
- [5] Batiot-Dupeyrat C. Dry reforming of methane. In: Granger P, Parvulescu VI, Parvulescu VI, Prellier W, editors. *Perovskites and Related Mixed Oxides Concepts and Applications*. Weinheim, Germany: Wiley-VCH Verlag GmbH & Co; 2015. pp. 501-516. DOI: 10.1002/9783527686605.ch22



- [6] Wolfbeisser A, Sophiphun O, Bernardi J, Wittayakun J, Föttinger K, Rupprechter G. Methane dry reforming over ceria-zirconia supported Ni catalysts. *Catalysis Today*. 2016;**277**(2):234-245. DOI: 10.1016/j.cattod.2016.04.025Su
- [7] Su YJ, Pan KL, Chang MB. Modifying perovskite-type oxide catalyst LaNiO<sub>3</sub> with Ce for carbon dioxide reforming of methane. *International Journal of Hydrogen Energy*. 2014;**39**:4917-4925. DOI: 10.1016/j.ijhydene.2014.01.077
- [8] Mao SY, Tan ZX, Zhang LM, Huang QY. Plasma-assisted biogas reforming to syngas at room temperature condition. *Journal of the Energy Institute*. Forthcoming. DOI: 10.1016/j.joei.2017.01.003
- [9] Snoeckx R, Heijckers S, Wesenbeeck KV, Lenaerts S, Bogaerts A. CO<sub>2</sub> conversion in a dielectric barrier discharge plasma: N<sub>2</sub> in the mix as a helping hand or problematic impurity?. *Energy & Environmental Science*. 2016;**9**:999-1011. DOI: 10.1039/c5ee03304g
- [10] Kim HH, Teramoto Y, Negish N, Ogata A. A multidisciplinary approach to understand the interactions of nonthermal plasma and catalyst: A review. *Catalysis Today* 2015;**256**:13-22. DOI: 10.1016/j.cattod.2015.04.009
- [11] Chen HL, Lee HM, Chen SH, Chao Y, Chang MB. Review of plasma catalysis on hydrocarbon reforming for hydrogen production – Interaction, integration, and prospects. *Applied Catalysis B: Environmental*. 2008;**85**:1-9. DOI: 10.1016/j.apcatb.2008.06.021
- [12] Chen HL, Lee HM, Chen SH, Chang MB. Review of packed-bed plasma reactor for ozone generation and air pollution control. *Industrial and Engineering Chemistry Research*. 2008;**47**:2122-2130. DOI: 10.1021/ie071411s
- [13] Chen HL, Lee HM, Chen SH, Chang MB, Yu SJ, Li SN. Removal of volatile organic compounds by single-stage and two-stage plasma catalysis systems: A review of the performance enhancement mechanisms, current status, and suitable applications. *Environmental Science & Technology*. 2009;**43**:2216-2227. DOI: 10.1021/es802679b
- [14] Pakhare D, Shaw C, Haynes D, Shekhawat D, Spivey J. Effect of reaction temperature on activity of Pt- and Ru-substituted lanthanum zirconate pyrochlores (La<sub>2</sub>Zr<sub>2</sub>O<sub>7</sub>) for dry (CO<sub>2</sub>) reforming of methane (DRM). *Journal of CO<sub>2</sub> Utilization*. 2013;**1**:37-42. DOI: doi.org/10.1016/j.jcou.2013.04.001
- [15] Carrara C, Múnera J, Lombardo EA, Cornaglia LM. Kinetic and stability studies of Ru/La<sub>2</sub>O<sub>3</sub> used in the dry reforming of methane. *Topics in Catalysis*. 2008;**51**:98-106. DOI: 10.1007/s11244-008-9131-y
- [16] Jones G, Jakobsen JG, Shim SS, Kleis J, Andersson MP, Rossmeisl J, Abild-Pedersen F, Bligaard T, Helveg S, Hinnemann B, Rostrup-Nielsen JR, Chorkendorff I, Sehested J, Nørskov JK. First principles calculations and experimental insight into methane steam reforming over transition metal catalysts. *Journal of Catalysis*. 2008;**259**(1):147-160. DOI: 10.1016/j.jcat.2008.08.003

- [17] Cheng CK, Chan HJ. Potential of empty fruit bunch clinker as a support for nickel and cobalt catalysts in methane dry reforming: Waste to wealth approach. *Journal of the Taiwan Institute of Chemical Engineers*. 2016;**62**:76-83
- [18] Budiman AW, Song SH, Chang TS, Shin CH, Choi MJ. Dry reforming of methane over cobalt catalysts: A literature review of catalyst development. *Catalysis Surveys from Asia*. 2012;**16**:83-97. DOI: 10.1007/s10563-012-9143-2
- [19] Kamal MS, Hossain M, Razzak SA. Catalytic oxidation of volatile organic compounds (VOCs) – A review. *Atmospheric Environment*. 2016;**140**:117-134. DOI: 10.1016/j.atmosenv.2016.05.031
- [20] Kim HY, Park JN, Henkelman G, Kim JM. Design of a highly nanodispersed Pd-MgO/SiO<sub>2</sub> composite catalyst with multifunctional activity for CH<sub>4</sub> reforming. *ChemSusChem*. 2012;**5**:1474-1481. DOI: 10.1002/cssc.201100798
- [21] Arora S, Prasad R. An overview on dry reforming of methane: Strategies to reduce carbonaceous deactivation of catalysts. *RSC Advances*. 2016;**6**:108668. DOI: 10.1039/c6ra20450c
- [22] Bora B, Soto L. Influence of finite geometrical asymmetry of the electrodes in capacitively coupled radio frequency plasma. *Physics of Plasmas*. 2014;**21**(8):083509. DOI: 10.1063/1.4893148
- [23] Silva T, Britun N, Godfroid T, Snyders R. Optical characterization of a microwave pulsed discharge used for dissociation of CO<sub>2</sub>. *Plasma Sources Science and Technology*. 2014;**23**(2):025009. DOI: 10.1088/0963-0252/23/2/025009
- [24] Winanti WS, Bismo S, Purwanto WW. Carbon dioxide conversion to synthesis gas when combined with methane using a new designed of non-thermal plasma reactor. *Journal of Environmental Science and Technology* 2014;**7**:226-235. DOI: 10.3923/jest.2014.226.235
- [25] de la Fuente JF, Moreno SH, Stankiewicz AI, Stefanidis GD. A new methodology for the reduction of vibrational kinetics in non-equilibrium microwave plasma: Application to CO<sub>2</sub> dissociation. *Reaction Chemistry & Engineering* 2016;**1**:540-554. DOI: 10.1039/c6re00044dKim
- [26] Kim HH, Teramoto Y, Ogata A, Takagi H, Nanba T. Plasma catalysis for environmental treatment and energy applications. *Plasma Chemistry and Plasma Processing*. 2016;**36**:45-72. DOI: 10.1007/s11090-015-9652-7
- [27] Huang YC, Yu QS, Huang C. The study of creation of polymerizable species in radio frequency hydrocarbon plasma polymerization in a closed reactor system. *Thin Solid Films*. 2016;**618**(A):213-218. DOI: 10.1016/j.tsf.2016.02.038
- [28] Scarduelli G, Guella G, Ascenzi D, Tosi P. Synthesis of liquid organic compounds from CH<sub>4</sub> and CO<sub>2</sub> in a dielectric barrier discharge operating at atmospheric pressure. *Plasma Processes and Polymers*. 2011;**8**:2531. DOI: 10.1002/ppap.201000044

- [29] Mahammadunnisa S, Reddy PMK, Ramaraju B, Subrahmanyam C. Catalytic nonthermal plasma reactor for dry reforming of methane. *Energy & Fuels*. 2013;**27**:4441-4447. DOI: 10.1021/ef302193e
- [30] Tirumala R, Benard N, Moreau E, Fenot M, Lalizel G, Dorignac E. Temperature characterization of dielectric barrier discharge actuators: Influence of electrical and geometric parameters. *Journal of Physics D: Applied Physics* 2014;**47**(25):255203. DOI: 10.1088/0022-3727/47/25/255203
- [31] Hua W, Jin LJ, He XF, Liu JH, Hu HQ. Preparation of Ni/MgO catalyst for CO<sub>2</sub> reforming of methane by dielectric-barrier. *Catalysis Communications*. 2010;**11**:968-972. DOI: 10.1016/j.catcom.2010.04.007
- [32] Neyts EC, Ostrikov KK, Sunkara MK, Bogaerts A. Plasma catalysis: Synergistic effects at the nanoscale. *Chemical Reviews* 2015;**115**:13408-13446. DOI: 10.1021/acs.chemrev.5b00362
- [33] Chung WC, Chang MB. Review of catalysis and plasma performance on dry reforming of CH<sub>4</sub> and possible synergistic effects. *Renewable and Sustainable Energy Reviews*. 2016;**62**:13-31. DOI: 10.1016/j.rser.2016.04.007
- [34] Li Y, Chu W, Chen C, Hu JY. Preparation of the supported heteropolyacids catalyst by ultrasound-plasma treatment. *Journal of Wuhan University of Technology-Materials Science Edition*. 2008;**23**(2):234-238. DOI: 10.1007/s11595-006-2234-z
- [35] Takaki K, Chang JS. Atmospheric pressure of nitrogen plasmas in a ferroelectric packed bed barrier discharge reactor. *IEEE Transactions on Dielectrics and Electrical Insulation*. 2004;**11**(3):481-490. DOI: 10.1109/TDEI.2004.1306726
- [36] Tahir M, Amin NAS. Recycling of carbon dioxide to renewable fuels by photocatalysis: Prospects and challenges. *Renewable and Sustainable Energy Reviews*. 2013;**25**:560-579. DOI: 10.1016/j.rser.2013.05.027
- [37] Chung WC, Chang MB. Dry reforming of methane by combined spark discharge with a ferroelectric. *Energy Conversion and Management*. 2016;**124**:305-314. DOI: 10.1016/j.enconman.2016.07.023



---

## Theoretical Approach and Labeling of CO<sub>2</sub>

---



---

# Understanding Interaction Capacity of CO<sub>2</sub> with Organic Compounds at Molecular Level: A Theoretical Approach

---

Pham Ngoc Khanh and Nguyen Tien Trung

Additional information is available at the end of the chapter

<http://dx.doi.org/10.5772/intechopen.71878>

---

## Abstract

In this chapter, interactions of CO<sub>2</sub> with a number of organic compounds at molecular level are discussed in detail. The naked and substituted hydrocarbons along with compounds functionalized by hydroxyl, carbonyl, thiocarbonyl, carboxyl, sulfonyl, and amide groups have attracted much attention as CO<sub>2</sub>-philic agents. In general, interaction capacity between the functionalized organic compounds with CO<sub>2</sub> is stronger than the hydrocarbon and its derivatives. An addition of more CO<sub>2</sub> molecules into the interaction system formed by the functionalized organic compounds and CO<sub>2</sub> leads to an increase in the stability of the complexes. The obtained results indicate that  $\pi\cdots\pi$  linkages between CO<sub>2</sub> and aromatic rings can significantly contribute to the interactions between CO<sub>2</sub> and MOF/ZIF materials. Formic acid (HCOOH) is likely to be the most soluble compound as compared to the remaining host molecules (CH<sub>3</sub>OH, CH<sub>3</sub>NH<sub>2</sub>, HCHO, HCOOCH<sub>3</sub>, and CH<sub>3</sub>COCH<sub>3</sub>) when dissolved in CO<sub>2</sub>. The carbonyl (>C=O, >C=S) and sulfonyl (>S=O, >S=S) compounds have presented a higher stability, as compared to other functionalized groups, when they interact with CO<sub>2</sub>. Therefore, they can be valuable candidates in the design of CO<sub>2</sub>-philic materials and in the search of materials to adsorb CO<sub>2</sub>.

**Keywords:** supercritical carbon dioxide, Lewis acid-base, hydrogen bond, weak interaction

---

## 1. Introduction

Carbon dioxide (CO<sub>2</sub>) causes negative effect on global climate due to its “greenhouse effect” property multiplying by its high level in the atmosphere. Currently, its concentration is increasing due to the fossil fuels combustion process by human activities [1]. Nevertheless,

it is usually regarded as an environmentally benign solvent because of its less hazardous property. Furthermore, it is an attractive solvent owing to the ease of its removal capacity, abundance, inexpensive, and flexibility of the solvent parameters [2]. Consequently, supercritical CO<sub>2</sub> (sc-CO<sub>2</sub>) is well known as an efficient solvent over conventional organic ones in many chemical processes, and is expected to be useful in many applications of green chemistry such as extraction, separation, chemical reaction, and material processes [3–6]. Recently, sc-CO<sub>2</sub> has been employed in direct sol-gel reactions for the synthesis of oxide nanomaterials, oligomers, and polymers, etc. [7–10]. It is noteworthy that due to a lack of polarity, sc-CO<sub>2</sub> is a very feeble solvent for most polar solutes [11]. Nevertheless, due to the possession of a substantial quadrupole moment and a polar C=O bond, the majority of materials attached by carbonyl functional or fluoride groups are soluble in sc-CO<sub>2</sub>. In the context, continuing efforts have been reported for the purpose of enhancement in applicability of sc-CO<sub>2</sub> solvent through the use of “CO<sub>2</sub>-philes”, which makes insoluble or poorly soluble materials becoming more soluble in sc-CO<sub>2</sub> at an acceptable level of low temperature and pressure conditions [3, 12]. Experimental works have aimed at better understanding of behavior of the sc-CO<sub>2</sub> as solvent for organic compounds [13–18]. It might be assumed that CO<sub>2</sub> is a green yet feeble solvent because its full potential could not be realized without a thorough understanding of its solvent behavior at molecular level. Accordingly, numerous results on the CO<sub>2</sub>-philes have been reported during the 1990s [19, 20]. These CO<sub>2</sub>-philes are less favorable and effective both economically and environmentally because most of them are fluorinated polymers. Thus, in attempts to avoid expensive cost and environmental impacts of the fluorinated materials, during the last three decades, large-scale studies have focused on the design of nonfluorinated CO<sub>2</sub>-philes, specifically hydrocarbon-based and oxygenated hydrocarbon-based polymers [21, 22]. In 1996, Kazarian et al. discovered the formation of Lewis acid-base (LA-LB) type of interaction between CO<sub>2</sub> with the O atom of a number of carbonyl compounds (>C=O) for the first time [23]. Soon later, Beckman et al. successfully synthesized copolymer of nonfluorinated carbonate in sc-CO<sub>2</sub> at low pressure [21]. Interaction of CO<sub>2</sub> with delocalized  $\pi$  aromatic systems in the gas phase have been theoretically studied for the purpose of ranking in a database of a large variety of organic ligands, which would be valuable candidates for designing new metal-organic framework materials with enhanced affinity for CO<sub>2</sub> adsorption at low pressure. Accordingly, some extensive studies have been reported on the interactions of CO<sub>2</sub> with  $\pi$ -systems at level of theory and experiment [24–29]. In recent years, interactions of simple functionalized organic molecules, including CH<sub>3</sub>OH, CH<sub>3</sub>CH<sub>2</sub>OH [30–32], CH<sub>3</sub>OCH<sub>3</sub>, CH<sub>3</sub>OCH<sub>2</sub>CH<sub>2</sub>OCH<sub>3</sub> [33–35], HCHO, CH<sub>3</sub>CHO, CH<sub>3</sub>COOCH<sub>3</sub>, CH<sub>3</sub>COCH<sub>3</sub>, CH<sub>3</sub>COOH [36–41], and XCHZ (X = CH<sub>3</sub>, H, F, Cl, Br; Z = O, S) [42] CH<sub>3</sub>SZCH<sub>3</sub> (Z = O, S) [43] with CO<sub>2</sub> have been carried out using quantum chemical methods. Today, the interest in CO<sub>2</sub> computational chemistry is the interaction capacity of a solute molecule surrounded by a number of CO<sub>2</sub> molecules. Despite the fact that numerous studies have been performed, a full understanding of the CO<sub>2</sub> characteristics as a solvent remains a challenging task [1]. It is therefore clear that we need more systematic studies to gain a better understanding on the nature of the interactions involved, rather than considering the origin for a few disparate systems. Furthermore, there is also a great interest in deep understanding of the origin of the interactions between different types of organic compounds with CO<sub>2</sub> at molecular level for an effective use of CO<sub>2</sub> in different states.



This chapter focuses on evaluating interaction capacity of CO<sub>2</sub> with model organic compounds at level of molecule using theoretical approaches. Section 2 provides us with a brief summary of theoretical methods and computational techniques. Section 3 reviews the remarkable results of the investigation of interactions between CO<sub>2</sub> with organic compounds and is divided into two parts: (3.1) interactions of CO<sub>2</sub> with selected models of saturated and unsaturated hydrocarbons and their substituted derivatives, and modeled aromatic hydrocarbons; (3.2) interactions of CO<sub>2</sub> and modeled organic compounds with different functional groups and their substituted derivatives. Obtained results presented in Section 4 support for the enhancement of sc-CO<sub>2</sub> solvent used as a replacement for toxic classical organic solvents in industrial applications. In addition, the functional groups that present the more stable interaction with CO<sub>2</sub> at molecular level are revealed, which could be attached on the surface of materials to absorb and store CO<sub>2</sub> gas.

## 2. Computational details

Geometrical parameters of all the considered structures including monomers and complexes are optimized using suitable quantum-chemical methods such as the molecular orbital theory (MO) and density functional theory (DFT) and large basis sets, depending on investigated systems, such as 6-311++G(2d,2p), 6-311++G(3df,2pd), aug-cc-pVDZ, aug-cc-pVTZ, which have succeeded in investigating noncovalent interactions, especially hydrogen bonds [44, 45]. Harmonic vibrational frequencies are subsequently calculated at investigated level of theory to ensure that the optimized structures are local minima on the potential energy surfaces, and to estimate their zero-point energy (ZPE). The stabilization energy of each complex is calculated using the supermolecular method as the difference in total energies between that of each complex and the sum of the relevant monomers at the selected level of theory. The interaction energy is corrected by zero-point energy (ZPE) and basis set superposition errors (BSSE). The latter is computed using the function counterpoise procedure of Boys and Bernardi [46]. The “atoms-in-molecules” (AIM) [47] analyses are applied to identify critical points and to calculate their characteristics including electron density ( $\rho(r)$ ), Laplacian, electron potential and kinetic energy density, and total energy density. The GenNBO 5.G program [48] is used to perform NBO calculations, which is extensively applied to investigate chemical essences of hydrogen bonds and other weak interaction, and can provide information about natural hybrid orbitals, natural bond orbitals, natural population, occupancies in NBOs, hyperconjugation energies, rehybridization, and repolarization.

## 3. Interaction capacity of CO<sub>2</sub> with organic compounds

### 3.1. Interaction of CO<sub>2</sub> with model hydrocarbons

#### 3.1.1. Interaction of CO<sub>2</sub> with saturated hydrocarbons and their substituted derivatives

Saturated hydrocarbons are a primary energy source for our civilization. Fluorocarbons have been currently used as CO<sub>2</sub>-philic functionalities in many potential applications of chemistry utilizing liquid and supercritical CO<sub>2</sub> as a “green” alternative to conventional organic solvents

for chemical processes [20, 49–52]. The miscibility and dissolution of organic molecules in sc-CO<sub>2</sub> generally increase when the hydrogen atoms in molecules are substituted by fluorine atoms [49, 53]. It is crucial, therefore, to investigate interaction of CO<sub>2</sub> with saturated hydrocarbons and its substituted derivatives. A study [54] on density-dependent <sup>1</sup>H and <sup>19</sup>F NMR chemical shift of hydrocarbons and fluorocarbons in sc-CO<sub>2</sub> pointed out that there is a distinct difference in the chemical shift changes, as a function of density, for the two nuclei. In addition, the authors suggested a specific interaction of type “solute-solvent” in the system formed by the fluorocarbons and CO<sub>2</sub>, and a site specificity for the <sup>19</sup>F shifts due to the surface accessibility of the individual fluorine atoms. In 1996, interactions between CO<sub>2</sub> with ethane (C<sub>2</sub>H<sub>6</sub>) and hexafluoroethane (C<sub>2</sub>F<sub>6</sub>), in particular the (CO<sub>2</sub>)<sub>n</sub>⋯C<sub>2</sub>H<sub>6</sub> and (CO<sub>2</sub>)<sub>n</sub>⋯C<sub>2</sub>F<sub>6</sub> interactions, with n = 1–4, were examined using restricted Hartree-Fock method [55]. The interaction energy for the CO<sub>2</sub>⋯C<sub>2</sub>F<sub>6</sub> complex was calculated to be -3.35 kJ.mol<sup>-1</sup>, while it was -1.26 kJ.mol<sup>-1</sup> for the CO<sub>2</sub>⋯C<sub>2</sub>H<sub>6</sub> complex, indicating that the interaction of CO<sub>2</sub> with C<sub>2</sub>F<sub>6</sub> is stronger than that with C<sub>2</sub>H<sub>6</sub>. The obtained results showed key differences between the interaction of hydrocarbons and fluorocarbons with CO<sub>2</sub>. The interaction of the fluorocarbon with CO<sub>2</sub> is predominantly electrostatic in nature. Thus, the positively charged carbon atom in CO<sub>2</sub> has a strong attraction with the negatively charged fluorine atoms of the fluorocarbons, resulting in a favorable binding energy of 3.14–3.35 kJ.mol<sup>-1</sup> for each CO<sub>2</sub> molecule in the first solvent shell. The interaction of CO<sub>2</sub> with hydrocarbons is quite weak due to the noble nature of the hydrocarbons molecule. Nevertheless, Han and Jeong [56] pointed out that the results in Ref. [55] were incorrect because the calculations for interaction energy of the complexes were not corrected by the basis set superposition error.

In 1998, interactions of CO<sub>2</sub> with small hydrocarbons (CH<sub>4</sub> and C<sub>2</sub>H<sub>6</sub>) and fluorocarbons (CF<sub>4</sub> and C<sub>2</sub>F<sub>6</sub>) were reinvestigated using second-order many-body perturbation theory (MP2) methods by Diep et al. [57]. These authors surprisingly did not find any enhanced attraction between CO<sub>2</sub> and perfluorocarbons relative to the analogous hydrocarbons as in the publication of Cece et al. [55]. On the contrary, interaction energies of the obtained complexes range from -3.31 to -4.90 kJ.mol<sup>-1</sup>, in which the interaction energies are slightly more negative for the CO<sub>2</sub>-hydrocarbon complexes than for the corresponding CO<sub>2</sub>-perfluorocarbon ones, suggesting that the interaction capacity of CO<sub>2</sub> and hydrocarbons is stronger than that of fluorocarbons and CO<sub>2</sub>. Yonker and Palmer [58] studied the nuclear shielding of <sup>1</sup>H and <sup>19</sup>F nuclei in CH<sub>3</sub>F and CHF<sub>3</sub> by NMR and molecular dynamics simulations. Obtained results showed that there is no distinct or specific interaction between fluoromethane and CO<sub>2</sub>. A various work by Yee et al. [59] reported that the polarizability of CF<sub>4</sub> and C<sub>2</sub>F<sub>6</sub>, which is derived from dielectric constant measurement, is larger than that of CH<sub>4</sub> and C<sub>2</sub>H<sub>6</sub>, and noted that this reason should result in a proportional difference in the magnitude of the interaction between the induced dipoles. Consequently, they suggested that the repulsion of CO<sub>2</sub> is greater for CF<sub>4</sub> than for CH<sub>4</sub>. However, Diep et al. [57] argued that only the electronic component of the total polarizability cited by Yee et al. [59] is the adequate reason for the induced dipole-induced dipole interactions between the molecules. They showed that the electronic polarizability is comparable between the perfluorocarbons and the alike hydrocarbons. The CO<sub>2</sub>-philicity of fluorinated compounds with varying numbers of fluorine atoms in the system was investigated by Wallen et al. [60]. By using correlated ab-initio

calculations and studying effect of stepwise substitution of H atom of methane by fluorine, the authors explored origin of fluorocarbon and hydrocarbon interactions with CO<sub>2</sub>. The results suggested an optimum density of fluorine atoms that can be viewed as a maximum CO<sub>2</sub>-philicity, and CO<sub>2</sub> molecule plays both weak Lewis acid and base in these systems. In this work, the authors suggested the fundamentally different nature of interaction between CO<sub>2</sub>-fluorocarbon and CO<sub>2</sub>-hydrocarbon, in spite of comparable interaction energy. For complexes formed by fluorocarbons and CO<sub>2</sub>, their stability is contributed by interaction of carbon in CO<sub>2</sub> and fluorine in fluorocarbons, while the stability of complexes of hydrocarbons and CO<sub>2</sub> is thanks to two oxygen of CO<sub>2</sub>. It should be noteworthy that the stability of complex is also contributed by the C–H...O weak hydrogen. In summary, these molecular modeling computations have shed some light on the interaction of hydrocarbons and fluorocarbons with CO<sub>2</sub>, which may help to explain the difference in solubility of various saturated hydrocarbons and their substituted derivatives in sc-CO<sub>2</sub>.

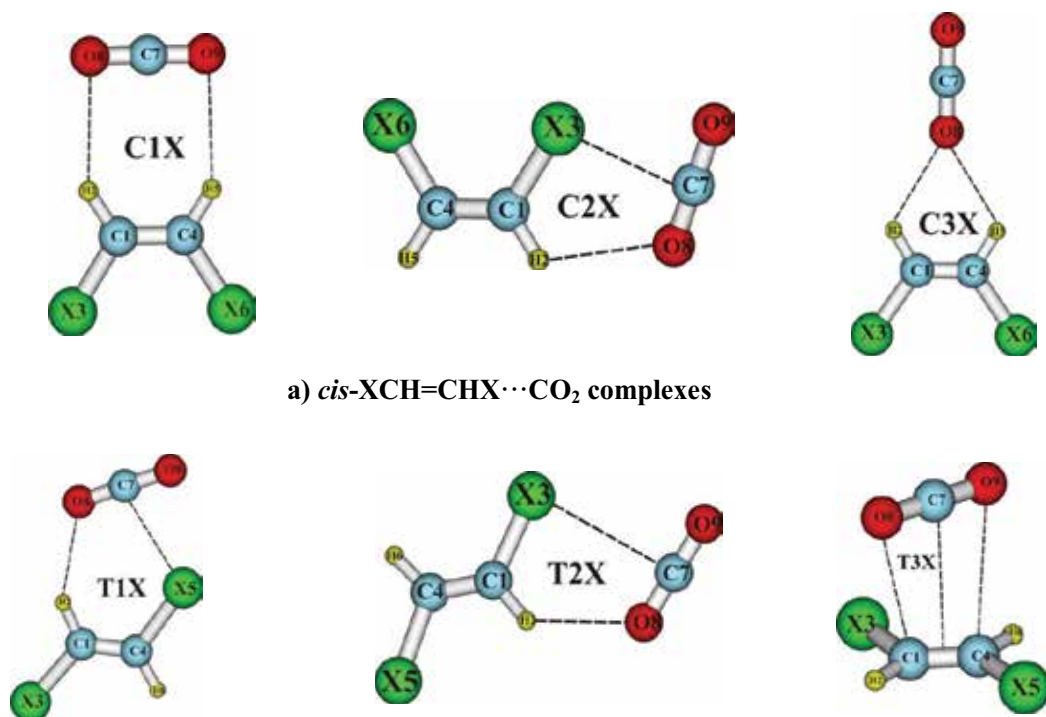
### 3.1.2. Interaction of CO<sub>2</sub> with unsaturated hydrocarbons and its substituted derivatives

Unsaturated hydrocarbons is one of the most important classes of materials for synthesizing polymers; and sc-CO<sub>2</sub> has been seen as a good solvent for this kind of synthesis. In 2009, interaction between C<sub>2</sub>H<sub>2</sub> with CO<sub>2</sub> was investigated by Alkorta et al. [61] and interaction energy was evaluated to be *ca.* -4.70 kJ.mol<sup>-1</sup> at M05-2x/6-311++G(d,p) and -5.99 kJ.mol<sup>-1</sup> at MP2/aug-cc-pVTZ, implying that the complex C<sub>2</sub>H<sub>2</sub>...CO<sub>2</sub> is stable on the potential energy surface. The stability of complex is determined by weak C...C interaction and is confirmed by AIM and NBO analyses. Indeed, AIM analysis shows the presence of this intermolecular contact owing to the values of electron density ( $\rho(r)$ ) and Laplacian ( $\nabla^2\rho(r)$ ) at its BCP to be 0.0067 and 0.0246 au. Furthermore, the NBO analysis also indicates that upon complexation the electron-rich carbon atom of CO<sub>2</sub> transfers electrons to the anti-bonding orbital of C<sub>2</sub>H<sub>2</sub> having electron-poor carbon atoms. In order to understand deeply origin of interaction of unsaturated hydrocarbons with CO<sub>2</sub>, the complexes of C<sub>2</sub>H<sub>4</sub> and CO<sub>2</sub> were investigated by our group in 2016 [1]. It is remarkable that the interaction energies corrected by both ZPE and BSSE for the C<sub>2</sub>H<sub>4</sub>...CO<sub>2</sub> complexes are in the range from -1.1 to -4.9 kJ.mol<sup>-1</sup>. The most stable structure of C<sub>2</sub>H<sub>4</sub>...CO<sub>2</sub> is in line with the report by Miller et al. that CO<sub>2</sub>'s main axis parallels the plane of C<sub>2</sub>H<sub>4</sub> but is not parallel to its C–C axis [62]. Obtained results showed that the p...π\* and π...π\* interactions play more important role than the C–H...O hydrogen bond in stabilizing the C<sub>2</sub>H<sub>4</sub>...CO<sub>2</sub> complexes. Remarkably, contribution of the π...π\* interaction to stabilization of the complex formed by CO<sub>2</sub>-philic compounds and CO<sub>2</sub> has been observed for the first time in this literature. The stability of complex C<sub>2</sub>H<sub>4</sub>...CO<sub>2</sub> (-4.9 kJ.mol<sup>-1</sup>) is more stable than the complexes of interaction between CO<sub>2</sub> with hydrocarbons and fluorinated hydrocarbons such as CH<sub>4</sub>, C<sub>2</sub>H<sub>6</sub>, CF<sub>4</sub>, C<sub>2</sub>F<sub>6</sub> (from -3.7 to -4.9 kJ.mol<sup>-1</sup> at the MP2/aug-cc-pVDZ) [56, 57, 61]. This review indicates that interaction capacity of CO<sub>2</sub> with unsaturated hydrocarbons is stronger than that of CO<sub>2</sub> with saturated hydrocarbons.

Our group [1] continued to investigate the interactions of the 1,2-dihalogenated derivatives of ethylene (XCH=CHX) with CO<sub>2</sub> in order to evaluate the substituent effects on the interactions. Six stable shapes of the optimized structures of XCH=CHX...CO<sub>2</sub> (X = F, Cl and Br) at the MP2/

aug-cc-pVDZ level are showed in **Figure 1**, which are denoted hereafter by **C1X**, **C2X** and **C3X** for *cis*-XCH=CHX $\cdots$ CO<sub>2</sub> pairs, and **T1X**, **T2X** and **T3X** for *trans*-XCH=CHX $\cdots$ CO<sub>2</sub> pairs.

The obtained results showed that stability of the complexes **C1X** and **C3X** is determined by the C–H $\cdots$ O hydrogen bonded interaction, whereas the presence of both the C–H $\cdots$ O hydrogen bond and C–X $\cdots$ C Lewis acid-base interaction leads to stabilization of the complexes **C2X**, **T1X** and **T2X**. For **T3X**, their stability is induced by a p $\cdots$  $\pi^*$  interaction from the lone pair n(O) to the  $\pi^*(C=C)$  orbital and a  $\pi\cdots\pi^*$  interaction from MO- $\pi(C=O)$  to MO- $\pi^*(C=C)$  orbital. The two H atoms in C<sub>2</sub>H<sub>4</sub> substituted by two alike halogen atoms X results in an additional presence of C–X $\cdots$ C Lewis acid-base interaction, thus contributing supplementary to the stabilization of the investigated complexes. In general, the *cis*-XCH=CHX $\cdots$ CO<sub>2</sub> complexes are more stable than the *trans* counterparts. In addition, CH<sub>2</sub>CH<sub>2</sub> $\cdots$ CO<sub>2</sub> is less stable than both *trans*-XCH=CHX $\cdots$ CO<sub>2</sub> and *cis*-XCH=CHX $\cdots$ CO<sub>2</sub>. Thus, the interaction energies with both ZPE and BSSE corrections are calculated to be from -1.7 to -7.5 kJ.mol<sup>-1</sup> for *cis*-XCH=CHX $\cdots$ CO<sub>2</sub> and from -4.4 to -6.8 kJ.mol<sup>-1</sup> for *trans*-XCH=CHX $\cdots$ CO<sub>2</sub>. Hence replacement of the two H atoms in CH<sub>2</sub>=CH<sub>2</sub> by the same halogen atoms actually increases the stability of complexes formed by interaction of XCH=CHX with CO<sub>2</sub> and causes a decrease of the role of the  $\pi\cdots\pi^*$  interaction in stabilization of the parent C<sub>2</sub>H<sub>4</sub> $\cdots$ CO<sub>2</sub> complex in comparison with the XCH=CHX $\cdots$ CO<sub>2</sub> ones.



**Figure 1.** The stable geometries of the complexes of CO<sub>2</sub> and XCH=CHX derivatives (X = F, Cl, and Br). (a) *cis*-XCH=CHX $\cdots$ CO<sub>2</sub> complexes, (b) *trans*-XCH=CHX $\cdots$ CO<sub>2</sub> complexes.

### 3.1.3. Interaction of CO<sub>2</sub> with some model aromatic hydrocarbons

Key aromatic hydrocarbons of commercial interests such as benzene, toluene, and xylene play a key role in the biochemistry of all living things. They are used to produce a range of important chemicals and polymers. In 2009, interactions between CO<sub>2</sub> and a large number of functionalized aromatic molecules were investigated by means of using density functional theory by Torrisi et al. [24] with the aim of ranking a large variety of organic ligands in a database, which could be suitable candidates for designing new metal organic framework materials with enhanced CO<sub>2</sub> adsorption capacity at ambient pressure. Two groups of substituted benzene derivatives including the electron-withdrawing halogen groups (tetrafluoro-, chloro-, bromo-, and dibromobenzene) and methyl electron donor (mono-, di-, and tetramethylbenzene) were considered since these substituents are very common components of aromatic ligands in MOF<sub>s</sub>. The results of interaction energy showed that halogen substitution causes relatively strong destabilization of complexes formed, which is increased with number of substituting groups, and thus reduces the magnitude of the aromatic ring adsorption toward CO<sub>2</sub>. Nevertheless, a decrease of electron density of the aromatic ring induces an increase in acidity for some of the aromatic hydrogen atoms, which helps weak hydrogen bond-like interactions of these hydrogen atoms with oxygen atom of CO<sub>2</sub> formed. On the other hand, substitution of hydrogen atom in aromatic ring by methyl group clearly strengthens its interaction capacity with CO<sub>2</sub>, which is usually very accessible on the internal surface of a MOF cavity, and hence it can be seen as a promising way to enhance the CO<sub>2</sub> affinity of the MOF, in which tetramethyl substitution manifests a maximum advantage of this particular class of ligand.

In 2013, Chen et al., by using high-level *ab initio* methods, suggested the  $\pi\cdots\pi$  interaction between CO<sub>2</sub> and three aromatic molecules, namely benzene (C<sub>6</sub>H<sub>6</sub>), pyridine (C<sub>5</sub>H<sub>5</sub>N), and pyrrole (C<sub>4</sub>H<sub>5</sub>N), which serve as common functional groups in metal-organic/zeoliticimidazolate framework materials [63]. The interaction energies for the complexes of CO<sub>2</sub> with aromatic hydrocarbons calculated at MP2/aug-cc-pVTZ are in the range from -11.9 to -15.4 kJ.mol<sup>-1</sup>, which are twice more negative than the most stable complex of the C<sub>2</sub>H<sub>4</sub>...CO<sub>2</sub> system (-4.9 kJ.mol<sup>-1</sup> at CCSD(T)/aug-cc-pVTZ//MP2/aug-cc-pVDZ level). This result implies that interaction capacity of CO<sub>2</sub> with aromatic hydrocarbons is stronger than that of CO<sub>2</sub> with unsaturated hydrocarbons. These authors also optimized the side-on structures of all possible complexes to compare the interaction strength of side-on configurations and  $\pi\cdots\pi$  top-on configurations. This work obtained the three most-stable side-on configurations, specifically S-C<sub>6</sub>H<sub>6</sub>...CO<sub>2</sub>, S-C<sub>5</sub>H<sub>5</sub>N...CO<sub>2</sub>, and S-C<sub>4</sub>H<sub>5</sub>N...CO<sub>2</sub>, as illustrated in **Figure 2**.

The side-on interaction is significantly weaker than the  $\pi\cdots\pi$  interaction in C<sub>6</sub>H<sub>6</sub>...CO<sub>2</sub> and C<sub>4</sub>H<sub>5</sub>N...CO<sub>2</sub> pairs. On the contrary, for the C<sub>5</sub>H<sub>5</sub>N...CO<sub>2</sub> pair the  $\pi\cdots\pi$  interaction [-11.6 kJ.mol<sup>-1</sup> for T-C<sub>5</sub>H<sub>5</sub>N...CO<sub>2</sub>(N) and -11.5 kJ.mol<sup>-1</sup> for TC<sub>5</sub>H<sub>5</sub>N...CO<sub>2</sub>(C)] is weaker than the side-on interaction (-18.0 kJ.mol<sup>-1</sup>). The obtained results showed that the EDA-type interactions are not available in real MOF/ZIF materials because the central cationic metal of MOF/ZIF materials is linked to the exposed aromatic N atom of the EDA-type interaction in S-C<sub>5</sub>H<sub>5</sub>N...CO<sub>2</sub>. In short, the results indicate that  $\pi\cdots\pi$  interaction between CO<sub>2</sub> and aromatic rings can significantly contribute to the interactions between CO<sub>2</sub> and MOFs/ZIFs.

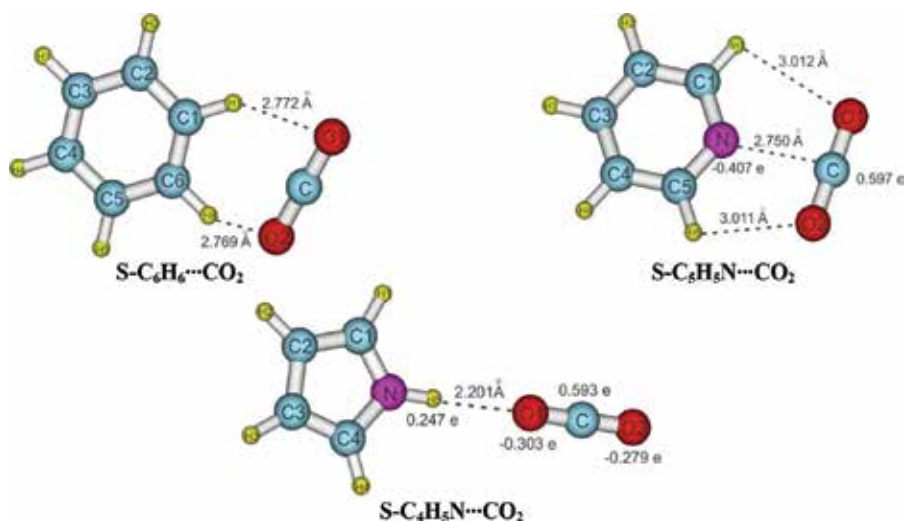


Figure 2. Optimized structures of  $S-C_6H_6 \cdots CO_2$ ,  $S-C_5H_5N \cdots CO_2$ , and  $S-C_4H_3N \cdots CO_2$ .

### 3.1.4. Concluding remarks on interaction of $CO_2$ with model hydrocarbons

Interactions of  $CO_2$  with model hydrocarbons including saturated, unsaturated, aromatic hydrocarbons and their substituted derivatives were investigated using high-level *ab initio* methods. In general, the strength of the complexes increases in going from the interaction of the saturated hydrocarbons with carbon dioxide to unsaturated hydrocarbons with carbon dioxide and finally to the parent aromatic hydrocarbons with carbon dioxide. The stability of the obtained complexes is determined by the  $C-H \cdots O$  hydrogen bonded interaction,  $C-X \cdots C$  Lewis acid-base interaction,  $\pi \cdots \pi$ ,  $p \cdots \pi^*$  and  $\pi \cdots \pi^*$  interactions. The contribution of the  $\pi \cdots \pi^*$  interaction to the formation of the complexes between  $CO_2$ -philic compounds and  $CO_2$  has been observed. The  $\pi \cdots \pi$  interactions were significantly stronger than the side-on hydrogen-bond interactions but weaker than EDA-type interaction. The  $\pi \cdots \pi$  interactions can significantly contribute to adsorption of  $CO_2$  in practical applications. Consequently, approach to the increase in the aromaticity of the linker should be an effective way with purpose of increasing the  $CO_2$  adsorption in MOF/ZIF materials.

## 3.2. Interaction of $CO_2$ with model functionalized organic compounds and their substituted derivatives

### 3.2.1. Interaction of $CO_2$ with model functionalized organic compounds

Up to now, a large number of complexes for interactions of  $CO_2$  with simple functionalized organic molecules have been studied using quantum chemical methods [33–43]. In more recent investigations, the Lewis acid-base interaction between  $CO_2$  and some carbonyl-functionalized compounds has been reported [34, 44, 64–67]. The existence of the  $C-H \cdots O$  hydrogen bond in complexes was confirmed clearly by Wallen et al. [38, 39, 60]. However, it is necessary to perform systematic studies to elucidate the nature of the

interactions formed in complexes, rather than considering the results obtained from few specific systems. We investigated complexes of CO<sub>2</sub> and some typically functionalized organic molecules such as methanol (CH<sub>3</sub>OH), methylamine (CH<sub>3</sub>NH<sub>2</sub>), formaldehyde (HCHO), formic acid (HCOOH), dimethylether (CH<sub>3</sub>OCH<sub>3</sub>), acetone (CH<sub>3</sub>COCH<sub>3</sub>) and methyl formate (HCOOCH<sub>3</sub>) [40]. Obtained results showed that the Lewis acid-base interaction such as C–N···C(CO<sub>2</sub>), C=O···C(CO<sub>2</sub>) plays a more dominant role compared to the C–H···O blue-shifting hydrogen bond in stabilizing most of the complexes. However, the stability of the HCOOH···CO<sub>2</sub> pair is mainly determined by O–H···O red-shifting hydrogen bond. All interaction energies are significantly negative, indicating that obtained complexes are quite stable. Particularly, the interaction energies with both ZPE and BSSE corrections are in the range from –3.3 to –14.2 kJ.mol<sup>-1</sup>, in which the HCOOH···CO<sub>2</sub> pair is the most stable, whereas the weakest one is the HCHO···CO<sub>2</sub> pair. As a consequence, solubility of HCOOH in sc-CO<sub>2</sub> is likely to be the largest in all the considered compounds. The interaction energies of some considered complexes are more negative than the values reported in the previous works [35, 64]. Thus, for the pair (CH<sub>3</sub>OH, CO<sub>2</sub>), its interaction energy of –13.3 kJ.mol<sup>-1</sup> with only ZPE correction, and –11.4 kJ.mol<sup>-1</sup> with both ZPE and BSSE corrections is more negative than that of –11.3 kJ.mol<sup>-1</sup> obtained with only BSSE correction at the MP2/aug-cc-pVTZ level [64]. Another example is that the BSSE corrected interaction energy of the CH<sub>3</sub>OCH<sub>3</sub>···CO<sub>2</sub> pair was computed to be –13.1 kJ.mol<sup>-1</sup> at the MP2/6-311++G(2d,2p)//MP2/6-311++G(d,p) level [35] while it is –13.7 kJ.mol<sup>-1</sup> with ZPE and BSSE corrections, and –16.3 kJ.mol<sup>-1</sup> with only ZPE correction in the present work.

In 2011, our group investigated the interactions of CO<sub>2</sub> with substituted derivatives of formaldehyde and thioformaldehyde [42]. The interaction energies (with ZPE and BSSE corrections) of –10.5 kJ.mol<sup>-1</sup> for CH<sub>3</sub>CHO···CO<sub>2</sub> and –9.1 kJ.mol<sup>-1</sup> for CH<sub>3</sub>CHS···CO<sub>2</sub> are more negative than for complexes of HCHO···CO<sub>2</sub> and HCHS···CO<sub>2</sub>, respectively. The obtained results supported that both O and S atoms act as Lewis bases and the >C=X (X = O, S) groups should be considered as potential candidates for the design of CO<sub>2</sub>-philic materials. The interactions between carbonyl compounds and CO<sub>2</sub> are stronger than those of fluorocarbons and fluorocarbonyl compounds. Obtained results suggested that the Lewis acid-base and hydrogen bonded interactions should be the key factors in governing the solubility of isolated monomers in sc-CO<sub>2</sub>, in which the crucial role of the former is suggested. The function of these interactions in the solvation of >C=O and >C=S compounds in sc-CO<sub>2</sub> may be important in terms of the specific solute-solvent.

In 2014, we investigated the interactions between some carbonyl compounds including acetone (CH<sub>3</sub>COCH<sub>3</sub>) with CO<sub>2</sub> [41]. Interaction energies of obtained complexes which are denoted by **H1**, **H2**, **H3**, and **H4** at the CCSD(T)/6-311++G(3df,2pd)//MP2/6-311++G(2d,2p) level are gathered in **Table 1**. The results indicate that the stability of studied complexes is contributed by both Lewis acid-base and hydrogen bonded interactions. As shown in **Table 1**, the interaction energy for **H1** (–10.3 kJ.mol<sup>-1</sup>) is less negative than that reported in Ref. [40] (–11.1 kJ.mol<sup>-1</sup>) at CCSD(T)/aug-cc-pVTZ but is more negative than that in Ref. [64] (–8.8 kJ.mol<sup>-1</sup>) at MP2/aug-cc-pVDZ. Notably, complex **H3** is less stable than **H1** in this work, which is different from the results reported by Ruiz-Lopez et al [68]. By using the levels of theory MP2/aug-cc-pVDZ and CCSD(T)/aug-cc-pVDZ, the authors suggested

	H1	H2	H3	H4
$\Delta E$	-12.7	-11.3	-12.7	-4.7
$\Delta E^*$	-10.3	-9.4	-9.2	-2.4

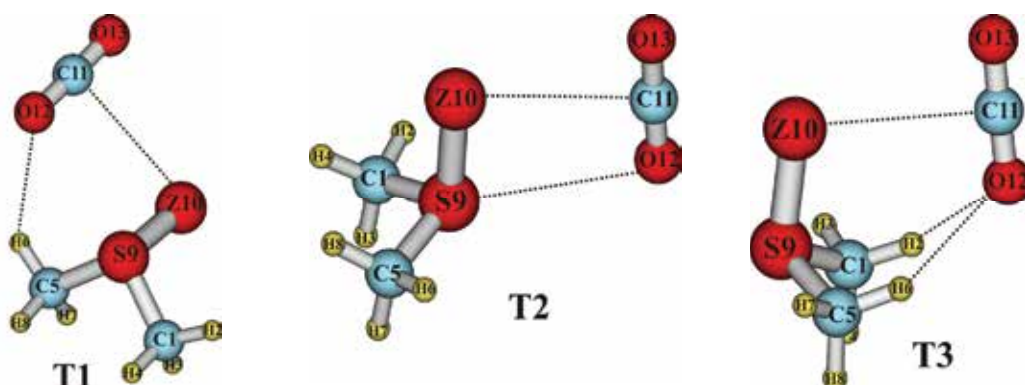
Source: Dai et al. [41].

**Table 1.** Interaction energies ( $\text{kJ}\cdot\text{mol}^{-1}$ ) corrected for only ZPE and for both ZPE and BSSE of the complexes.

that **H1** is *ca.*  $1.0 \text{ kJ}\cdot\text{mol}^{-1}$  higher in interaction energy than **H3**. These authors conclusively suggested that the  $>\text{C}=\text{O}$  group can be a valuable candidate in the design of  $\text{CO}_2$ -philic and adsorbent materials.

Further, interactions of  $\text{CO}_2$  with  $\text{CH}_3\text{SZCH}_3$  ( $Z = \text{O}, \text{S}$ ) were also investigated by our group [43]. Three stable shapes of the complexes at MP2/6-311++G(2d,2p) are presented in **Figure 3**, denoted hereafter by **T1**, **T2** and **T3**. Interaction energies of complexes at two different levels of theory are also given in the **Table 2**.

The  $\text{CH}_3\text{SZCH}_3\cdots\text{CO}_2$  ( $Z = \text{O}, \text{S}$ ) complexes are in general stabilized by the Lewis acid-base, chalcogen-chalcogen and hydrogen bonded interactions. However, the crucial role contributing to the overall stabilization energy should be the Lewis acid-base interaction. The obtained results pointed out a slight difference in the interaction energies between the two employed levels of theory. Thus, the interaction energies of the examined complexes range from  $-13.8$  to  $-17.2$  and  $-9.8$  to  $-14.4 \text{ kJ}\cdot\text{mol}^{-1}$  (at MP2/aug-cc-pVTZ//MP2/6-311++G(2d,2p)), and  $-13.6$  to  $-17.7$  and  $-9.6$  to  $-14.5 \text{ kJ}\cdot\text{mol}^{-1}$  (at CCSD(T)/6-311++G(3df,2pd)//MP2/6-311++G(2d,2p)) for only ZPE correction and for both ZPE and BSSE corrections, respectively (*cf.* **Table 2**). The results indicate that the formed complexes are significantly stable, and more stable than the complexes of the  $>\text{C}=\text{O}$  or  $>\text{C}=\text{S}$  functionalized compounds with  $\text{CO}_2$  reported in Refs. [38, 40, 42]. This implies a stronger interaction of  $\text{CO}_2$  with the  $>\text{S}=\text{O}$  and  $>\text{S}=\text{S}$  functionalized groups relative to the  $>\text{C}=\text{O}$  and  $>\text{C}=\text{S}$  counterparts. In addition, we



**Figure 3.** Stable shapes of complexes between  $\text{CH}_3\text{SZCH}_3$  ( $Z = \text{O}, \text{S}$ ) and  $\text{CO}_2$ .



Structures	Z = O			Z = S		
	T1	T2	T3	T1	T2	T3
ΔE <sup>a</sup>	-17.2	-14.3	-17.4	-17.1	-13.8	-16.9
ΔE <sup>b</sup>	-17.6	-14.8	-17.7	-16.8	-13.6	-16.4
ΔE <sup>*a</sup>	-14.4	-10.9	-13.7	-14.2	-9.8	-13.2
ΔE <sup>*b</sup>	-14.5	-11.3	-14.0	-13.5	-9.6	-12.0

<sup>a</sup>Taken from MP2/aug-cc-pVTZ//MP2/6-311++G(2d,2p).

<sup>b</sup>Taken from CCSD(T)/6-311++G(3df,2pd)//MP2/6-311++G(2d,2p).

Source: Phuong et al. [43].

**Table 2.** Interaction energies corrected for ZPE (ΔE<sup>0</sup>, in kJ.mol<sup>-1</sup>) and for ZPE and BSSE (ΔE\*, in kJ.mol<sup>-1</sup>) of obtained complexes.

also suggested a stronger interaction of CO<sub>2</sub> with the >S=O moiety compared to the >S=S one, and they both should be candidates for designing CO<sub>2</sub>-philic materials, CO<sub>2</sub> adsorption and storage materials in the future.

For the CH<sub>3</sub>SOCH<sub>3</sub>...CO<sub>2</sub> complexes, the strength of **T3** is close to that of **T1** reported by Wallen et al. [38]. Thus, the interaction energies of **T1** in this work are -14.4 kJ.mol<sup>-1</sup> at MP2/aug-cc-pVTZ//MP2/6-311++G(2d,2p) and -14.5 kJ.mol<sup>-1</sup> at CCSD(T)/6-311++G(3df,2pd)//MP2/6-311++G(2d,2p), which are in consistent with the value of -14.3 kJ.mol<sup>-1</sup> at MP2/aug-cc-pVDZ//MP2/6-31+G(d) reported in Ref. [38].

### 3.2.2. Effect of various substituted groups to strength the complexes formed by interaction of CO<sub>2</sub> with model functionalized organic compounds

We now continue to discuss in some details the effects of substitution to the overall interaction energy in obtained complexes between CO<sub>2</sub> with model functionalized organic compounds. The complexes of the interactions of CO<sub>2</sub> with CH<sub>3</sub>SZCHX<sub>2</sub> (X = H, CH<sub>3</sub>, F, Cl, Br; Z = O, S) were studied by our group and reported in Ref. [43]. In general, the CH<sub>3</sub>SOCHX<sub>2</sub>...CO<sub>2</sub> complexes are more stable than the CH<sub>3</sub>SSCHX<sub>2</sub>...CO<sub>2</sub> complexes. This firmly indicates that the >S=O, as compared to the >S=S, has a stronger interaction with CO<sub>2</sub>, which originates from a contribution of a larger attractive electrostatic interaction of the former than the latter in stabilizing the examined complexes. For the CH<sub>3</sub>SOCHX<sub>2</sub>...CO<sub>2</sub> complexes, the strength is enhanced by the X substitution in the order from H *via* F to Cl to Br and finally to CH<sub>3</sub>. Therefore, the substitution of two H atoms in a CH<sub>3</sub> group of CH<sub>3</sub>SOCH<sub>3</sub> by two alike X groups significantly influences the strength of CH<sub>3</sub>SOCHX<sub>2</sub>...CO<sub>2</sub> complexes relative to CH<sub>3</sub>SOCH<sub>3</sub>...CO<sub>2</sub> complexes. The replacement also leads to a slight enhancement of stability of the CH<sub>3</sub>SSCHX<sub>2</sub>...CO<sub>2</sub> complexes in the sequence from F, H, Cl, Br to CH<sub>3</sub>. In Ref. [41], we replaced two H atoms in a CH<sub>3</sub> group of CH<sub>3</sub>COCH<sub>3</sub> by two alike CH<sub>3</sub>, F, Cl and Br groups, and the results showed that interaction energies of complexes are in the range from -9.2 to -10.7 kJ.mol<sup>-1</sup> with both ZPE and BSSE

corrections, which are more negative than that of interactions of  $\text{CO}_2$  with hydrocarbons and fluorocarbons. Thus, the interaction energies range from  $-3.7$  to  $-4.9$   $\text{kJ}\cdot\text{mol}^{-1}$  for the complexes of  $\text{CO}_2$  with the hydrocarbons such as  $\text{CH}_4$ ,  $\text{C}_2\text{H}_6$ ,  $\text{CF}_4$ ,  $\text{C}_2\text{F}_6$ ; and from  $-2.4$  to  $-7.8$   $\text{kJ}\cdot\text{mol}^{-1}$  for the complexes of  $\text{CO}_2$  with  $\text{CH}_{4-n}\text{F}_n$  ( $n = 0 \div 4$ ) [57, 60] at the MP2/aug-cc-pVDZ level. These results are in line with the suggestion on larger stability of carbonyl relative to fluorocarbons and other functionalized compounds in interacting with  $\text{CO}_2$ . Generally, the strength of  $\text{CH}_3\text{COCHR}_2\cdots\text{CO}_2$  complexes is gently increased when  $\text{R} = \text{CH}_3$  as compared to  $\text{CH}_3\text{COCH}_3\cdots\text{CO}_2$ , while it is slightly decreased with  $\text{R} = \text{F}$ ,  $\text{Cl}$  and  $\text{Br}$ .

### 3.2.3. Interaction of $n\text{CO}_2$ ( $n = 1:3$ ) with model functionalized organic compounds

It is important to investigate the strength of interactions between  $\text{CO}_2$  and carbonyl-containing molecules, as well as the underlying their chemical nature. Due to a strong interest in  $\text{CO}_2$  as a solvent, it is imperative to consider aggregates in which a solute molecule is surrounded by a number of  $\text{CO}_2$  molecules, an unexplored area at present [69]. Expansion of the system by adding more  $\text{CO}_2$  molecules shows how the geometry and bonding in the heterodimer is affected by placement of the solute in an environment. This would make our simulation more akin to solvation phenomenon, and particularly the magnitude of cooperative effects. The complexes formed by  $\text{H}_2\text{CO}$ ,  $\text{CH}_3\text{CHO}$ , and  $(\text{CH}_3)_2\text{CO}$  with two and three molecules of  $\text{CO}_2$  are studied using *ab initio* calculations by Scheniner et al. [69]. There are a host of different geometries adopted by the complexes of the carbonyl with two or three  $\text{CO}_2$  molecules, with small energy differences. The bonding features of the heterodimers are generally carried over to these larger heterotrimers and tetramers, although the linear  $\text{C}=\text{O}\cdots\text{C}$  arrangement of the binary complexes is largely absent. The  $\text{O}\cdots\text{O}$  chalcogen bonds, absent in the heterodimers, play a major role in many of the larger complexes. The degree of cooperativity in these oligomers is generally rather small, with a maximal positive cooperativity of only 1.1  $\text{kJ}/\text{mol}$ . The binding energies of heterotetramers complexes range from  $-39.0$  to  $-50.7$   $\text{kJ}\cdot\text{mol}^{-1}$ , which are more negative than heterodimers ( $-8.8$  to  $-12.5$   $\text{kJ}\cdot\text{mol}^{-1}$ ) and trimers complexes ( $-23.1$  to  $-34.2$   $\text{kJ}\cdot\text{mol}^{-1}$ ). These results suggest that the addition of more carbon dioxide molecules into systems leads to a larger increase in stability of complexes.

### 3.2.4. Concluding remarks on interaction capacity of $\text{CO}_2$ with model functionalized organic compounds

The organic compounds functionalized by hydroxyl, carbonyl, thiocarbonyl, carboxyl and amide groups have been paid much attention as  $\text{CO}_2$ -philic compounds. The carbonyl and thiocarbonyl compounds have presented a higher stability, as compared to other functionalized ones, when they interact with  $\text{CO}_2$ . This durability has been assigned to a main contribution of the  $>\text{C}=\text{Z}\cdots\text{C}$  ( $\text{Z} = \text{O}, \text{S}$ ) Lewis acid-base interaction and/or an additional cooperation of the  $\text{C}-\text{H}\cdots\text{O}$  hydrogen bonded interaction, except for the case of the  $\text{HCOOH}\cdots\text{CO}_2$  complex, where the role of the  $\text{O}-\text{H}\cdots\text{O}$  hydrogen bond was found to be more important than the  $>\text{C}=\text{O}\cdots\text{C}$  Lewis acid-base interaction. We have also found that there is a stronger interaction of  $\text{CO}_2$  with the  $>\text{S}=\text{O}$  and  $>\text{S}=\text{S}$  containing compounds

relative to the >C=O and >C=S counterparts, and therefore it should be suggested that they would be potential groups attached on the surface of materials to adsorb CO<sub>2</sub> and used to design CO<sub>2</sub>-philic materials.

#### 4. Concluding remarks

From the contents mentioned above, we can draw some key conclusions for this chapter:

- i. Interaction capacity of CO<sub>2</sub> with various organic compounds including hydrocarbons and functionalized organic compounds along with its derivatives were investigated by using *ab initio* calculations. The obtained results show that interaction capacity between functionalized organic compounds with CO<sub>2</sub> is stronger than that of model hydrocarbons with CO<sub>2</sub>. For interactions of CO<sub>2</sub> with model hydrocarbons, the larger stability of complexes is found for interaction of aromatic relative to saturated and unsaturated hydrocarbons with carbon dioxide. In the case of interactions between functionalized organic compounds with CO<sub>2</sub>, interaction capacity of the carbonyl and sulfonyl compounds with CO<sub>2</sub> is stronger than that of other functionalized compounds. Obtained results on interaction of nCO<sub>2</sub> (n = 1–3) with functionalized organic compounds indicate that the addition of more CO<sub>2</sub> into systems leads to an increase in the stability of complexes formed.
- ii. The stability of examined complexes is determined by weakly noncovalent interaction including C–H...O, O–H...O of hydrogen bonds, X...C Lewis acid-base interaction, O...O chalcogen-chalcogen,  $\pi\cdots\pi$ ,  $p\cdots\pi^*$ , and  $\pi\cdots\pi^*$  interactions. Remarkably, contribution of the  $\pi\cdots\pi^*$  interaction to the complex formed between CO<sub>2</sub>-philic compounds and CO<sub>2</sub> has been revealed in our work. The  $\pi\cdots\pi$  interactions can significantly contribute to the adsorption of CO<sub>2</sub> in MOF/ZIF materials. Obtained results show the strength of intermolecular interaction tends to decrease in going from >C=S...C via >C=O...C to >C=X...C (X = F, Cl, Br). This observation points out enormous applicability of CO<sub>2</sub>-philic materials based on thiocarbonyls.
- iii. It is found that the functional groups such as carbonyl and sulfonyl give a more stable interaction with CO<sub>2</sub> than other functionalized groups, in which a stronger interaction of CO<sub>2</sub> with the >S=O and >S=S counterparts relative to the >C=O and >C=S ones is revealed, and they should be valuable candidates for synthesizing CO<sub>2</sub>-philic materials and finding new materials to adsorb CO<sub>2</sub>.

#### Author details

Pham Ngoc Khanh and Nguyen Tien Trung\*

\*Address all correspondence to: [nguyentien trung@qnu.edu.vn](mailto:nguyentien trung@qnu.edu.vn)

Department of Chemistry, Laboratory of Computational Chemistry and Modelling, Quy Nhon University, Quy Nhon, Binh Dinh, Vietnam

## References

- [1] Trung NT, Trang NTT, Ngan VT, Quang DT, Nguyen MT. Complexes of carbon dioxide with dihalogenated ethylenes: structure, stability and interaction. *RSC Advances*. 2016;**6**: 31401-31409
- [2] Sun Y-P, Dekker M. *Supercritical Fluid Technology in Materials Science and Engineering: Syntheses: Properties and Applications*, ed. New York; 2002
- [3] Beckman EJ. Supercritical and near-critical CO<sub>2</sub> in green chemical synthesis and processing. *Journal of Supercritical Fluids*. 2004;**28**:121-191
- [4] Kajimoto O. Homogeneous catalysis in supercritical fluids. *Chemical Reviews*. 1999;**99**: 475-494
- [5] Eckert CA, Knutson BL, Debeneditii PG. Supercritical fluids as solvents for chemical and materials processing. *Nature*. 1996;**383**:313-318
- [6] Johnston KP, Shah PS. Making nanoscale materials with supercritical fluids. *Science*. 2004;**303**:482-483
- [7] Sui R, Lo JMH, Charpentier PA. Infrared and computational studies on interactions of carbon dioxide and titania nanoparticles with acetate groups. *Journal of Physical Chemistry C*. 2009;**113**:21022-21028
- [8] Sui R, Rizkalla AS, Charpentier PA. Synthesis and formation of silica aerogel particles by a novel sol-gel route in supercritical carbon dioxide. *The Journal of Physical Chemistry B*. 2004;**108**:11886-11892
- [9] Moner-Girona M, Roig A, Molins E. Sol-gel route to direct formation of silica aerogel microparticles using supercritical solvents. *Journal of Sol-Gel Science and Technology*. 2003;**26**:645-649
- [10] Wang Y, Hong L, Tapriyal D, Kim IC, Paik I-H, Crosthwaite JM, Hamilton AD, Thies MC, Beckman EJ, Enick RM, Johnson JK. Design and evaluation of nonfluorous CO<sub>2</sub>-soluble oligomers and polymers. *The Journal of Physical Chemistry B*. 2009;**113**:14971-14980
- [11] McHugh MA, Krukonijs VJ. In: Mark HF, Bikales M, Overberger CG, Menges G, Kroschwitz JI, Editors. *Supercritical Fluids in Encyclopedia of Polymer Science and Engineering*. 2nd edn. New York: John Wiley & Sons, Inc.; 1989. 16
- [12] Beckman EJ. A challenge for green chemistry: Designing molecules that readily dissolve in carbon dioxide. *Chemical Communications*. 2004;**17**:1885-1888
- [13] Potluri VK, Xu J, Enick R, Beckman E, Hamilton AD. Peracetylated sugar derivatives show high solubility in liquid and supercritical carbon dioxide. *Organic Letters*. 2002;**4**:2333-2335
- [14] Chang F, Kim H, Joo B, Park K, Kim H. Novel CO<sub>2</sub>-soluble pyridine derivatives and the extraction of heavy metals into sc-CO<sub>2</sub>. *Journal of Supercritical Fluids*. 2008;**45**:43-50

- [15] Estorach CT, Giménez-Pedros M, Masdeu-Bultó AM, Sayede AD, Monflier E. Hydroformylation of 1-octene in supercritical carbon dioxide with alkyl p-donor ligands on rhodium using a peracetylated  $\beta$ -cyclodextrin as a solubiliser. *European Journal of Inorganic Chemistry*. 2008;**17**:2659-2663
- [16] Dalvi VH, Srinivasan V, Rosky PJ. Understanding the effectiveness of fluorocarbon ligands in dispersing nanoparticles in supercritical carbon dioxide. *Journal of Physical Chemistry C*. 2010;**114**:15553-15561
- [17] Dalvi VH, Srinivasan V, Rosky PJ. Understanding the relative effectiveness of alkanethiol ligands in dispersing nanoparticles in supercritical carbon dioxide and ethane. *Journal of Physical Chemistry C*. 2010;**114**:15562-15573
- [18] Nunes AVM, Almeida APC, Marques SR, de Sousa ARS, Casimiro T, Duarte CMM. Processing triacetyl- $\beta$ -cyclodextrin in the liquid phase using supercritical CO<sub>2</sub>. *Journal of Supercritical Fluids*. 2010;**54**:357-361
- [19] Desimond J, Guan Z, Elsbernd CS. Synthesis of fluoropolymers in supercritical carbon dioxide. *Science*. 1992;**257**:945-947
- [20] Johnston KP, Harrison KL, Clarke MJ, Howdle SM, Heitz MM, Bright FV, Carlier C, Randolph TW. Water-in-carbon dioxide microemulsions: An environment for hydrophiles including proteins. *Science*. 1996;**271**:624-626
- [21] Sarbu T, Styranec TJ, Beckman EJ. Non-fluorous polymers with very high solubility in supercritical CO<sub>2</sub> down to low pressures. *Nature*. 2000;**405**:165-168
- [22] Sarbu T, Styranec TJ, Beckman EJ. Design and synthesis of low cost, sustainable CO<sub>2</sub>-philes. *Industrial and Engineering Chemistry Research*. 2000;**39**:4678-4683
- [23] Kazarian SG, Vincent MF, Bright FV, Liotta CL, Eckert CA. Specific intermolecular interaction of carbon dioxide with polymers. *Journal of the American Chemical Society*. 1996;**118**:1729-1736
- [24] Torrisi A, Mellot-Draznieks C, Bell RG. Impact of ligands on CO<sub>2</sub> adsorption in metal-organic frameworks: First principles study of the interaction of CO<sub>2</sub> with functionalized benzenes. I. Inductive effects on the aromatic ring. *The Journal of Chemical Physics*. 2009;**130**:194703-194714
- [25] Besnard M, Cabaco MI, Danten Y. Transient complex formation in CO<sub>2</sub>-hexafluorobenzene mixtures: A combined raman and ab initio investigation. *The Journal of Physical Chemistry A*. 2009;**113**:184-192
- [26] Lauzin C, Didriche K, Lievin J, Herman M, Perrin A. Investigation of C<sub>2</sub>H<sub>2</sub>-CO<sub>2</sub> the van der Waals complex in the overtone range using cw cavity ring-down spectroscopy. *The Journal of Chemical Physics*. 2009;**130**:204306-204313
- [27] Muenter JS. An intermolecular potential function model applied to acetylene dimer, carbon dioxide dimer, and carbon dioxide acetylene. *The Journal of Chemical Physics*. 1991;**94**:2781-2793

- [28] Torrisi A, Mellot-Draznieks C, Bell RG. Impact of ligands on CO<sub>2</sub> adsorption in metal-organic frameworks: First principles study of the interaction of CO<sub>2</sub> with functionalized benzenes. II. Effect of polar and acidic substituents. *The Journal of Chemical Physics*. 2010;**132**:044705
- [29] Shen JW, Domanski KB, Kitao O, Nakanishi K. Computer simulation on supercritical carbon dioxide fluid a potential model for the benzene-carbon dioxide system from ab initio calculations. *Fluid Phase Equilibria*. 1995;**104**:375-390
- [30] Stubbs JM, Siepmanna JI. Binary phase behavior and aggregation of dilute methanol in supercritical carbon dioxide: A Monte Carlo simulation study. *The Journal of Chemical Physics*. 2004;**121**:1525-1534
- [31] Dartois E, Demyk K, d'Hendecourt L, Ehrenfreund P. Carbon dioxide-methanol intermolecular complexes in interstellar grain mantles. *Astronomy and Astrophysics*. 1999;**351**:1066-1074
- [32] Lalanne P, Tassaing T, Danten Y, Cansell F, Tucker SC. CO<sub>2</sub>-ethanol interaction studied by vibrational spectroscopy in supercritical CO<sub>2</sub>. *The Journal of Physical Chemistry A*. 2004;**108**:2617-2624
- [33] Newby JJ, Peebles RA, Peebles SA. Structure of the dimethylether-CO<sub>2</sub> van der Waals complex from microwave spectroscopy. *The Journal of Physical Chemistry A*. 2004;**108**:11234-11240
- [34] Kim KH, Kim Y. Theoretical studies for Lewis acid-base interactions and C-H...O weak hydrogen bonding in various CO<sub>2</sub> complexes. *The Journal of Physical Chemistry A*. 2008;**112**:1596-1603
- [35] Ginderen PV, Herrebout WA, van der Veken BJ. Van der Waals complex of dimethyl ether with carbon dioxide. *The Journal of Physical Chemistry A*. 2003;**107**:5391-5396
- [36] Rivelino R. Lewis acid-base interactions in weakly bound formaldehyde complexes with CO<sub>2</sub>, HCN, and FCN: Considerations on the cooperative H-bonding effects. *The Journal of Physical Chemistry A*. 2008;**112**:161-165
- [37] Blatchford MA, Raveendran P, Wallen SL. Spectroscopic studies of model carbonyl compounds in CO<sub>2</sub>: Evidence for cooperative C-H...O interactions. *The Journal of Physical Chemistry A*. 2003;**107**:10311-10323
- [38] Raveendran P, Wallen SL. Cooperative C-H...O hydrogen bonding in CO<sub>2</sub>-Lewis base complexes: Implications for solvation in supercritical CO<sub>2</sub>. *Journal of the American Chemical Society*. 2002;**124**:12590-12599
- [39] Raveendran P, Wallen SL. Sugar acetates as novel, renewable CO<sub>2</sub>-philes. *Journal of the American Chemical Society*. 2002;**124**:7274-7275
- [40] Trung NT, Nguyen MT. Interactions of carbon dioxide with model organic molecules: A comparative theoretical study. *Chemical Physics Letters*. 2013;**581**:10-15

- [41] Dai HQ, Tri NN, Trang NTT, Trung NT. Remarkable effects of substitution on stability of complexes and origin of the C–H...O(N) hydrogen bonds formed between acetone's derivative and CO<sub>2</sub>, XCN (X = F, Cl, Br). *RSC Advances*. 2014;**4**:13901-13908
- [42] Trung NT, Hung NP, Hue TT, Nguyen MT. Existence of both blue-shifting hydrogen bond and Lewis acid–base interaction in the complexes of carbonyls and thiocarbonyls with carbon dioxide. *Physical Chemistry Chemical Physics*. 2011;**13**:14033-14042
- [43] Phuong VT, Trang NTT, Vo V, Trung NT. A comparative study on interaction capacity of CO<sub>2</sub> with the >S=O and >S=S groups in some doubly methylated and halogenated derivatives of CH<sub>3</sub>SOCH<sub>3</sub> and CH<sub>3</sub>SSCH<sub>3</sub>. *Chemical Physics Letters*. 2014;**598**:75-80
- [44] Joseph J, Jemmis ED. Red-, blue-, or no-shift in hydrogen bonds: A unified explanation. *Journal of the American Chemical Society*. 2007;**129**:4620-4632
- [45] Hobza P, Sponer J, Cubero E, Orozco M, Luque FJ. C–H...O contacts in the adenine...uracil Watson–Crick and uracil...uracil nucleic acid base pairs: nonempirical ab initio study with inclusion of electron correlation effects. *The Journal of Physical Chemistry B*. 2000;**104**:6286-6292
- [46] Boys SF, Bernadi F. The calculation of small molecular interactions by the differences of separate total energies. Some procedures with reduced errors. *Molecular Physics*. 1970;**19**:553-566
- [47] Popelier P. *Atoms in Molecules*. Essex, UK: Pearson Education Ltd; 2000
- [48] Glendening ED, Baderhoop JK, Read AE, Carpenter JE, Bohmann JA, Weinhold F. *GenNBO 5.G*. WI: Theoretical Chemistry Institute, University of Wisconsin Madison; 1996-2001
- [49] Laintz KE, Wai CM, Yonker CR, Smith RD. Solubility of fluorinated metal diethyldithiocarbamates in Supercritical carbon dioxide. *Journal of Supercritical Fluids*. 1991;**4**:194-198
- [50] Wells SL, DeSimone JM. CO<sub>2</sub> technology platform: An important tool for environmental problem solving a list of abbreviations can be found at the end of the article. *Angewandte Chemie, International Edition*. 2001;**40**:518-527
- [51] Ji M, Chen X, Wai CM, Fulton JL. Synthesizing and dispersing silver nanoparticles in a water-in-supercritical carbon dioxide microemulsion. *Journal of the American Chemical Society*. 1999;**121**:2631-2632
- [52] Consani KA, Smith RD. Observations on the solubility of surfactants and related molecules in carbon dioxide at 50°C. *Journal of Supercritical Fluids*. 1990;**3**:51-65
- [53] Laitinen A, Jauhiainen O, Aaltonen O. Solubility of fluorinated pharmaceuticals in dense carbon dioxide. *Organic Process Research and Development*. 2000;**4**:353-356
- [54] Dardin A, DeSimone JM, Samulski ET. Fluorocarbons dissolved in supercritical carbon dioxide. NMR evidence for specific solute–solvent interactions. *The Journal of Physical Chemistry B*. 1998;**102**:1775-1780

- [55] Cece A, Jureller SH, Kerschner JL, Moschner KF. Molecular modeling approach for contrasting the interaction of ethane and hexafluoroethane with carbon dioxide. *The Journal of Physical Chemistry*. 1996;**100**:7435-7439
- [56] Han Y-K, Jeong HY. Comment on "Molecular modeling approach for contrasting the interaction of ethane and hexafluoroethane with carbon dioxide". *The Journal of Physical Chemistry A*. 1997;**101**:5604
- [57] Diep P, Jordan KD, Johnson JK, Beckman EJ. CO<sub>2</sub>-fluorocarbon and CO<sub>2</sub>-hydrocarbon interactions from first-principles calculations. *The Journal of Physical Chemistry A*. 1998;**102**:2231-2236
- [58] Yonker CR. Solution dynamics of perfluorobenzene, benzene, and perdeuteriobenzene in carbon dioxide as a function of pressure and temperature. *The Journal of Physical Chemistry A*. 2000;**104**:685-691
- [59] Yee GG, Fulton JL, Smith RD. Fourier transform infrared spectroscopy of molecular interactions of heptafluoro-1-butanol or 1-butanol in supercritical carbon dioxide and supercritical ethane. *The Journal of Physical Chemistry*. 1996;**96**:6172-6182
- [60] Raveendran P, Wallen SL. Exploring CO<sub>2</sub>-philicity: Effects of stepwise fluorination. *The Journal of Physical Chemistry B*. 2003;**107**:1473-1477
- [61] Alkorta I, Blanco F, Elguero J, Dobado JA, Ferrer SM, Vidal I. Carbon...carbon weak interactions. *The Journal of Physical Chemistry A*. 2009;**113**:8387-8389
- [62] Bemish RJ, Block PA, Pedersen LG, Miller RE. The ethylene-carbon dioxide complex: A double internal rotor. *The Journal of Chemical Physics*. 1995;**103**:7788-7795
- [63] Cheng L, Cao F, Sun H. Ab initio study of the  $\pi$ - $\pi$  interactions between CO<sub>2</sub> and benzene, pyridine, and pyrrole. *International Journal of Quantum Chemistry*. 2013;**113**:2261-2266
- [64] Danten Y, Tassaing T, Besnard M. Vibrational spectra of CO<sub>2</sub>-electron donor-acceptor complexes from ab initio. *The Journal of Physical Chemistry A*. 2002;**106**:11831-11840
- [65] Wojtulewski S, Grabowski SJ. Blue-shifting C-H...Y intramolecular hydrogen bonds - DFT and AIM analyses. *Chemical Physics*. 2005;**309**:183-188
- [66] Trung NT, Hue TT, Nguyen MT. Remarkable blue shifts of C-H and N-H stretching frequencies in the interaction of monosubstituted formaldehyde and thioformaldehyde with nitrosyl hydride. *The Journal of Physical Chemistry A*. 2009;**113**:3245-3253
- [67] Besnard M, Cabaco MI, Longelin S, Tassaing T, Danten Y. Raman investigation of the CO<sub>2</sub> complex formation in CO<sub>2</sub>-acetone mixtures. *The Journal of Physical Chemistry A*. 2007;**111**:13371-13379
- [68] Altarsha M, Ingrosso F, Ruiz-Lopez MF. A new glimpse into the CO<sub>2</sub>-philicity of carbonyl compounds. *Chemphyschem*. 2012;**13**:3397-3403
- [69] Azofra LM, Scheiner S. Tetrel, chalcogen, and C-H...O hydrogen bonds in complexes pairing carbonyl-containing molecules with 1, 2, and 3 molecules of CO<sub>2</sub>. *The Journal of Chemical Physics*. 2015;**142**:034307



---

# [<sup>11</sup>C]Carbon Dioxide: Starting Point for Labeling PET Radiopharmaceuticals

---

Lingyun Yang, Peter J. H. Scott and Xia Shao

Additional information is available at the end of the chapter

<http://dx.doi.org/10.5772/intechopen.72313>

---

## Abstract

Positron emission tomography (PET) is a powerful *in vivo* imaging technique capable of providing dynamic information on biochemical processes in the living human subject. Applications of PET in oncology, neurology, psychiatry, cardiology and other medical specialties continue to grow. The use of PET relies on the characteristics and availability of appropriately labeled radiopharmaceuticals. Carbon-11 is one of the most useful radionuclides for PET chemistry, since its introduction into a biologically active molecule does not modify the biochemical properties of the compound. [<sup>11</sup>C]Carbon dioxide (<sup>11</sup>CO<sub>2</sub>), produced by cyclotron, is the most common and versatile primary labeling precursor in the production of <sup>11</sup>C-labeled radiopharmaceuticals.

**Keywords:** positron emission tomography, Carbon-11, radiopharmaceutical, molecular imaging, cyclotron

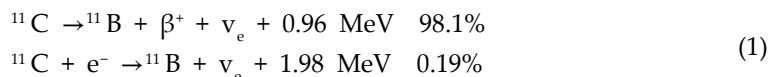
---

## 1. Introduction

Carbon-11 (<sup>11</sup>C) is an artificial radioisotope of carbon. Crane and Lauristen made the production of this short-lived radionuclide and investigated its physical properties in 1934 [1]. They demonstrated that carbon-11 decays by positron emission to the stable nuclide <sup>11</sup>B [Eq. (1)]. Due to its favorable decay characteristics ( $t_{1/2} = 20.33$  min, 98.1% by  $\beta^+$  emission, 0.19% by electron capture), carbon-11 was considered as a useful labeling tool for medical purposes. The first biological application of carbon-11 was published by Ruben in 1939 who investigated photosynthesis in plants using [<sup>11</sup>C]carbon dioxide [2]. The potential of <sup>11</sup>C-labeled compounds for non-invasive probing of physiological and biochemical processes in humans was subsequently realized [3]. The first carbon-11 experiment on humans was performed by Tobias in 1945 who studied the fixation of [<sup>11</sup>C]carbon monoxide by red blood cells [4]. However, the use of carbon-11 was

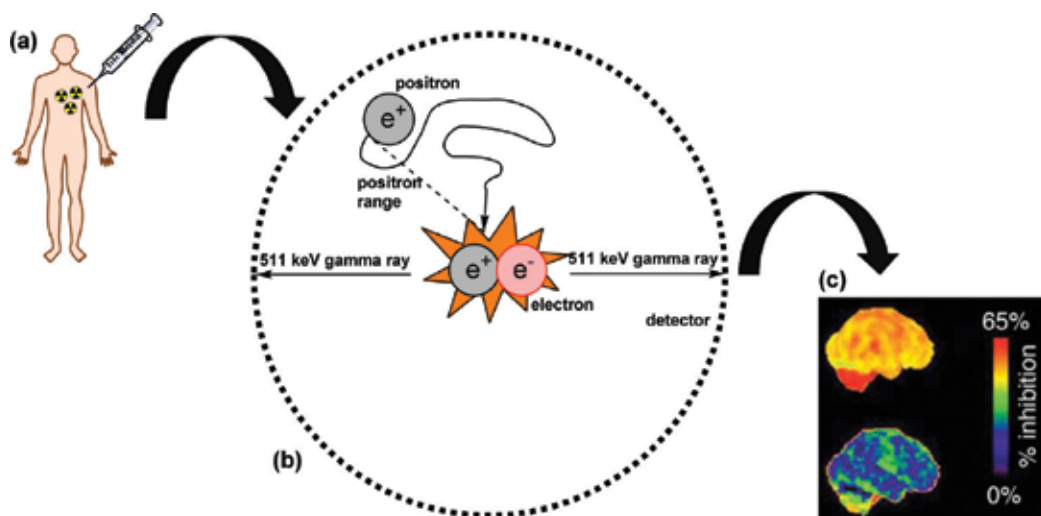
---

limited in next 20 years [5]. This delay was a consequence of easy access to reactor-produced carbon-14 from the 1950s, which superseded the use of cyclotron-produced carbon-11. Until late 1950s, the concepts of emission and transmission tomography were introduced by David Kuhl and Roy Edwards. The interest in carbon-11 was renewed and the application of carbon-11 was extended in 1960s.

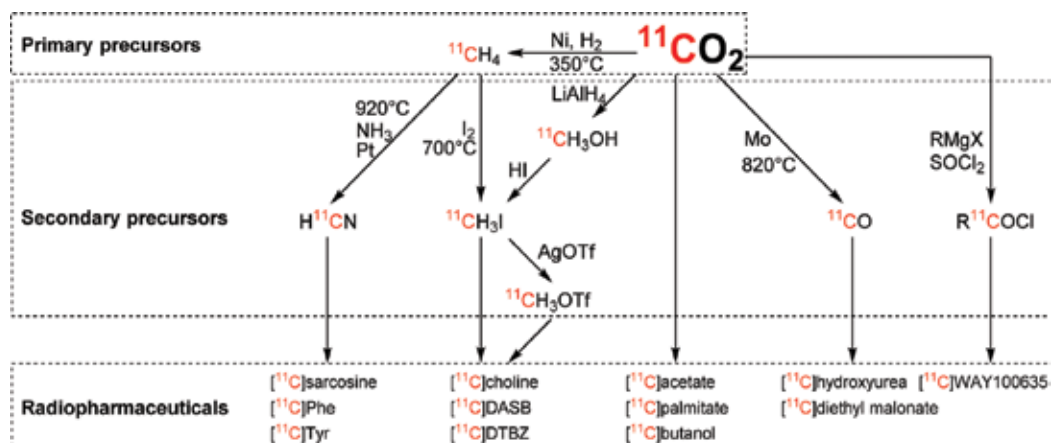


Decay of carbon-11 by positron emission or electron capture.

Positron emission tomography (PET) is a type of functional molecular imaging technique using probes, known as radiotracers, consisting of bioactive molecules tagged with positron-emitting radionuclides [6]. As carbon-11 undergoes positron emission decay, it emits a positron. The positron travels a short distance in the surrounding tissue until it collides with an electron. The annihilation produces a pair of gamma rays, which are emitted simultaneously in nearly opposite directions with energy of 511 keV each. The photons can be detected by pairs of collinearly aligned detectors in coincidence. The detectors of a PET system are installed in a ring-like pattern, which allows measurement of radioactivity through the organ of interesting at large angles and radial distances. The three-dimensional images can be generated by reconstruction (**Figure 1**). The ability to image and monitor molecular events *in vivo* and in real time is of great value for unveiling a detailed picture of fundamental biochemical and physiological processes in living organisms [7]. Information about metabolism, receptor/enzyme function, and biochemical mechanisms in living subjects can be obtained directly from PET imaging studies. The recent development of hybrid instrument combines functional PET with an anatomical modality such as computerized tomography (CT) or magnetic



**Figure 1.** The principle behind PET imaging: (a) the injection of radiopharmaceuticals; (b) positron travels a short distance and collides with an electron, then two 511 keV gamma rays emit simultaneously at approximately 180° to each other after annihilation; (c) system detects gamma rays and then generates three-dimensional images.



**Scheme 1.** Representative transformations in [<sup>11</sup>C]carbon dioxide radiochemistry.

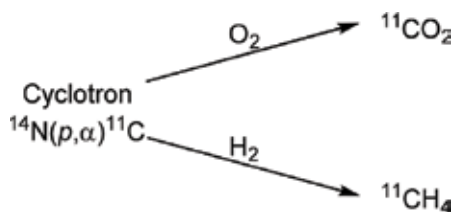
resonance imaging (MRI). The fusion offers more precise images with accurate functional assessment from PET and anatomical information from CT or MRI. Applications of PET in oncology [8–12], neurology [13–16], psychiatry [17–19], cardiology [20, 21] and other medical specialties [22–24] became one of the fastest growing areas in radiology [25].

The use of PET relies on the availability of appropriately labeled radiopharmaceuticals. Carbon-11 is one of the most useful radionuclides for PET chemistry, since the carbon is present in any organic molecule so that the introduction of carbon-11 in a molecule does not modify the properties of this molecule. In addition, the short half-life of carbon-11 allows for consecutive *in vivo* studies with injections of various radiotracers in the same subject on the same day. The pioneering work in the area of radiochemistry at the Washington University in the 1960s demonstrated the great potential of <sup>11</sup>C-labeled compounds in biological sciences [5]. The simple cyclotron production of [<sup>11</sup>C]carbon dioxide (<sup>11</sup>CO<sub>2</sub>) made it possible to be extensively used as a starting point for the synthesis of different kinds of <sup>11</sup>C-labeled compounds [26–28]. With the increasing demand of radiotracers and continuous developments of organic chemistry, a number of methodologies have been developed in recent years to enhance production of <sup>11</sup>C-radiotracers both from a technical and chemical point of view. However, [<sup>11</sup>C]carbon dioxide is still the most common and versatile primary labeling precursor in the production of <sup>11</sup>C-labeled radiopharmaceuticals. This chapter focuses on the use of [<sup>11</sup>C]carbon dioxide as the starting point for radiolabeling PET radiopharmaceuticals (**Scheme 1**).

## 2. Carbon-11 chemistry

### 2.1. Cyclotron: generation of carbon-11

Several nuclear reactions can be used to produce carbon-11 [29, 30]. Among these processes the <sup>14</sup>N(p,α)<sup>11</sup>C nuclear reaction is by far the most convenient and most commonly used method



**Scheme 2.** Generation of primary labeling precursors from cyclotron.

of producing carbon-11. The reaction is performed by high-energy proton bombardment of a cyclotron target containing nitrogen gas. Depending on the addition of gas (up to 2% of  $\text{O}_2$  or 5–10% of  $\text{H}_2$ ) to the nitrogen gas in the target, carbon-11 can be obtained as  $[^{11}\text{C}]\text{CO}_2$  or  $[^{11}\text{C}]\text{CH}_4$  (**Scheme 2**).  $[^{11}\text{C}]$ Carbon dioxide is the most important and versatile primary labeling precursor for  $^{11}\text{C}$ -labeling. Cyclotron-produced  $[^{11}\text{C}]\text{CO}_2$  can be used directly for the  $^{11}\text{C}$ -labeling of organic molecules (**Scheme 1**).

## 2.2. Radiochemistry: general considerations

Carbon-11 is a radionuclide that emits high-energy radiation. Therefore, the traditional hands-on manipulations used in synthetic chemistry are not feasible. In order to avoid unnecessary radiation exposure to the operators, the radiosynthesis of PET tracer needs to be undertaken by automated or remote-controlled synthesis equipment housed inside lead-shielded fume hoods (hot-cells) [6, 7]. This is also important from the perspective of good manufacturing practice (GMP) where a reproducible and operator-independent production is required to control the quality of the radiopharmaceuticals. **Figure 2** shows the radiochemistry laboratory at University of Michigan and a typical carbon-11 radiosynthesis module.

The half-life of carbon-11 is sufficiently long for synthesis and purification. However, the radiochemical yield is a function of chemical yield and radioactive decay. Thus the radiosynthesis time should be kept as short as possible. Ideally, a  $^{11}\text{C}$ -radiopharmaceutical is synthesized,



**Figure 2.** Automatic synthesis equipment in lead-shielded fume hoods.

Radiotracers	Labeling methods	Targets	References
[ <sup>11</sup> C]Acetate	Grignard reaction	Tricarboxylic acid cycle—Cardiac, Oncology	[35, 36]
[ <sup>11</sup> C]Butanol	Grignard reaction	Blood flow	[37]
[ <sup>11</sup> C]CFN <sup>a</sup>	Methylation	Opioid	[36, 38–40]
[ <sup>11</sup> C]Choline	Methylation	Oncology	[36, 41, 42]
[ <sup>11</sup> C]DASB <sup>b</sup>	Methylation	Serotonin transporter	[36, 43]
[ <sup>11</sup> C]DTBZ <sup>c</sup>	Methylation	Vesicular monoamine transporter 2	[36, 44]
[ <sup>11</sup> C]FMZ <sup>d</sup>	Methylation	GABA <sub>A</sub> receptor	[36]
[ <sup>11</sup> C]HED <sup>e</sup>	Methylation	Adrenergic	[36]
[ <sup>11</sup> C]Methionine	Methylation	Oncology	[36]
[ <sup>11</sup> C]OMAR <sup>f</sup>	Methylation	Cannabinoid receptor 1	[45]
[ <sup>11</sup> C]Palmitate	Grignard reaction	Cardiac	[35]
[ <sup>11</sup> C]PBR28 <sup>g</sup>	Methylation	Neuro, cardiac and oncology	[36, 46–48]
[ <sup>11</sup> C]PiB <sup>h</sup>	Methylation	Amyloid	[36]
[ <sup>11</sup> C]PMP <sup>i</sup>	Methylation	Acetylcholinesterase	[36, 49]
[ <sup>11</sup> C]Raclopride	Methylation	Dopamine	[36, 40, 43, 50]
[ <sup>11</sup> C]Sarcosine	Strecker reaction	Prostate cancer	[51]
[ <sup>11</sup> C]WAY100635 <sup>j</sup>	Grignard reaction	5HT <sub>1A</sub> receptor	[52, 53]

<sup>a</sup>[<sup>11</sup>C]Carfentanil.  
<sup>b</sup>3-Amino-4-(2-[<sup>11</sup>C]dimethylaminomethylphenylsulfanyl)-benzonitrile.  
<sup>c</sup>[<sup>11</sup>C]Dihydrotetabenazine.  
<sup>d</sup>[<sup>11</sup>C]Flumazenil.  
<sup>e</sup>[<sup>11</sup>C]Meta-hydroxyephedrine.  
<sup>f</sup>N-acetyl-N-(2-[<sup>11</sup>C]methoxybenzyl)-2-phenoxy-5-pyridinamine.  
<sup>g</sup>1-(2,4-dichlorophenyl)-4-cyano-5-(4-[<sup>11</sup>C]methoxyphenyl)-N-(piperidin-1-yl)-1H-pyrazole-3-carboxamide.  
<sup>h</sup>[<sup>11</sup>C] Pittsburgh Compound B.  
<sup>i</sup>1-[<sup>11</sup>C]Methyl-piperidin-4-yl propionate.  
<sup>j</sup>N-[2-[4-(2-[<sup>11</sup>C]methoxyphenyl)-1-piperazinyl]ethyl]-N-(2-pyridinyl)cyclohexanecarboxamide).

**Table 1.** <sup>11</sup>C-radiotracers in University of Michigan PET center for clinical application.

purified, formulated and analyzed within a timeframe of roughly 2–3 physical half-lives of the radionuclide, or 40–60 min for carbon-11. In addition, the strategies for the radiolabeling should aim to introduce carbon-11 in the synthetic sequence as late as possible [31–33].

The specific radioactivity (SA), a measure of the radioactivity per unit mass of the final radiolabeled compound, is another important aspect of <sup>11</sup>C-chemistry. Since only a trace amount of [<sup>11</sup>C]carbon dioxide is generated in the cyclotron, the theoretical maximum specific radioactivity for <sup>11</sup>C-radiolabeled compound is  $3.4 \times 10^5$  GBq/μmol. However, it is practically impossible to achieve this number, because of unavoidable isotopic dilution by naturally occurring

carbon-12 species during the processes. Typical specific activities of  $^{11}\text{C}$ -radiolabeled compounds are in the order of 50–1000 GBq/ $\mu\text{mol}$  [34]. For imaging a patient, less than 1 GBq of radioactivity is normally enough. That means very low amounts of compound need to be administered for PET imaging, typically in picomolar to nanomolar scale. This prevents undesired pharmacological or toxic effects during the *in vivo* studies. Thus, a labeling pathway should be designed to minimize contamination of carbon-12 species. Furthermore, due to tracer levels of carbon-11, the amount of the non-radioactive reagents is in large excess (about  $10^3$ – $10^4$  fold), which drives the reaction at pseudo first order kinetics. By consequence, small impurities in reagents or solvents may have a significant influence on the reaction outcomes. Therefore, the quality of reagents used in radiosynthesis needs special attention.

Radiopharmaceuticals can range from the small and simple to the large and complex. A tracer should be designed in such a way that it can be probing a specific function within the organ of interest [3]. It is important that the physical half-life of the radionuclide matches the biological half-life of the studied process. For example, carbon-11 is not suitable for radiolabeled peptides or antibodies, which need a few hours of blood circulation to accumulate the activity in a tumor.

### 2.3. Application of carbon-11: examples of radiopharmaceuticals

Since its infancy in the early 1960s, PET has attracted increasing attention as a powerful tool for investigating the biochemical transformations of drugs and molecules in the living system. With the development of PET imaging technology and novel synthetic methodology,  $^{11}\text{C}$ -labeled radiopharmaceuticals have been extensively used for the highly sensitive non-invasive measurement of biochemical physiological processes in living human subjects. As examples, **Table 1** summarizes  $^{11}\text{C}$ -radiotracers available in University of Michigan PET center for routine clinical application.

## 3. [ $^{11}\text{C}$ ]Carbon dioxide: starting point for labeling PET radiopharmaceuticals

The simple cyclotron production of [ $^{11}\text{C}$ ]carbon dioxide gave a starting point for the synthesis of important classes of compounds such as carboxylic acids [26], aldehydes [27], and alcohols [28]. However, due to low chemical reactivity of [ $^{11}\text{C}$ ]CO<sub>2</sub>, a broad spectrum of different  $^{11}\text{C}$ -labeled synthetic intermediates have been prepared as useful secondary labeling precursors (**Scheme 1**). With the increasing importance of PET in medical research and continuous developments of novel organic chemical techniques,  $^{11}\text{C}$ -labeling methodology is rapidly growing. This chapter addresses selected commonly used methods and examples. For more detailed information see comprehensive reviews [7, 54, 55]

### 3.1. [ $^{11}\text{C}$ ]CO<sub>2</sub> direct incorporation

[ $^{11}\text{C}$ ]Carbon dioxide is the most important and versatile primary labeling precursor for  $^{11}\text{C}$ -radiolabeling, since it is produced directly from cyclotron. The electrophilic carbon in [ $^{11}\text{C}$ ]

CO<sub>2</sub> can be used as a carbonyl source and trapped by an appropriate nucleophilic component. For example, [<sup>11</sup>C]acetate as a PET radiopharmaceutical for both myocardial imaging and cancer detection was synthesized via methyl magnesium chloride with [<sup>11</sup>C]CO<sub>2</sub> (**Scheme 3**) [56].

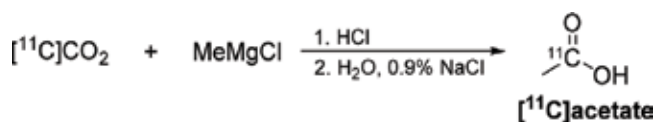
The [<sup>11</sup>C]carboxymagnesium halides also can be converted into more reactive [<sup>11</sup>C]carboxylic acid chloride to form amide with amines. The important 5HT<sub>1A</sub> receptor ligand WAY100635 was produced by this manner (**Scheme 4**) [52, 53].

More recently, [<sup>11</sup>C]CO<sub>2</sub> fixation further expanded the synthetic possibility for <sup>11</sup>C-labeling by direct incorporation of [<sup>11</sup>C]CO<sub>2</sub>. The first report on [<sup>11</sup>C]CO<sub>2</sub> fixation was the synthesis of <sup>11</sup>C-labeled carbamates [57, 58]. The scope of this method was broadened to [<sup>11</sup>C]ureas and [<sup>11</sup>C]oxazolidinones via the formation of an <sup>11</sup>C-labeled isocyanate or carbamoyl anhydride intermediate [54, 58–60]. For example, the reversible monoamine oxidase B (MAO-B) radioligand, [<sup>11</sup>C]SL25.1188, previously prepared using the technical demanding [<sup>11</sup>C]phosgene approach, was radiolabeled in high yield via [<sup>11</sup>C]CO<sub>2</sub> fixation [61, 62]. This radioligand was recently translated for human PET imaging (**Scheme 5**) [54, 63].

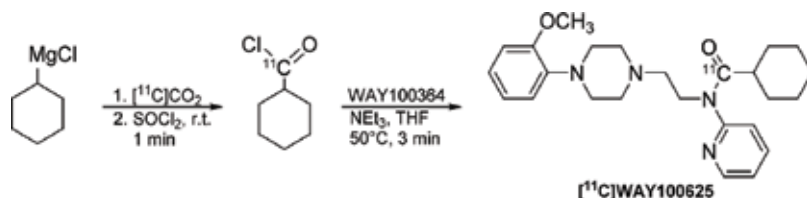
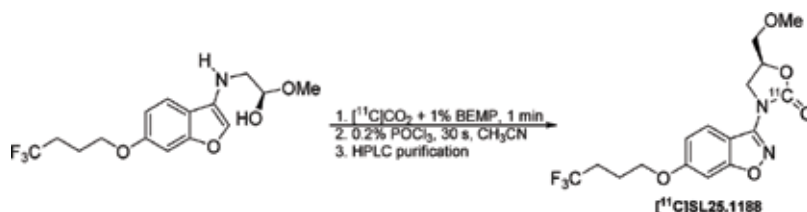
### 3.2. [<sup>11</sup>C]Methylation

The introduction of [<sup>11</sup>C]methyl iodide as a second labeling precursor 30 years ago was one of the great milestones in PET radiochemistry [64, 65]. So far, the most common method in <sup>11</sup>C-labeling is heteroatom (N, O, S) methylation. Converting [<sup>11</sup>C]MeI to more reactive [<sup>11</sup>C]methyltriflate ([<sup>11</sup>C]MeOTf) [64, 66] by passing [<sup>11</sup>C]MeI through a small column containing silver triflate around 200°C [67] significantly increases efficiencies of <sup>11</sup>C-methylation. This innovation makes it possible to <sup>11</sup>C-methylate heteroatoms in 3–5 min at room temperature. [<sup>11</sup>C]Methyl iodide can be prepared via two methods (**Scheme 1**). The so-called “wet” method developed in 1976 [64, 65] is based on reducing [<sup>11</sup>C]CO<sub>2</sub> using LiAlH<sub>4</sub> followed by reaction with hydroiodic acid. An alternative method, referred to as the “gas phase” method, was developed in the 1990s. This method exploits the reduction of [<sup>11</sup>C]CO<sub>2</sub> by H<sub>2</sub>/Ni at 350°C and then conversion of [<sup>11</sup>C]methane into [<sup>11</sup>C]MeI by iodination with iodine vapor at high temperatures (700–750°C) in the gas phase [66, 68].

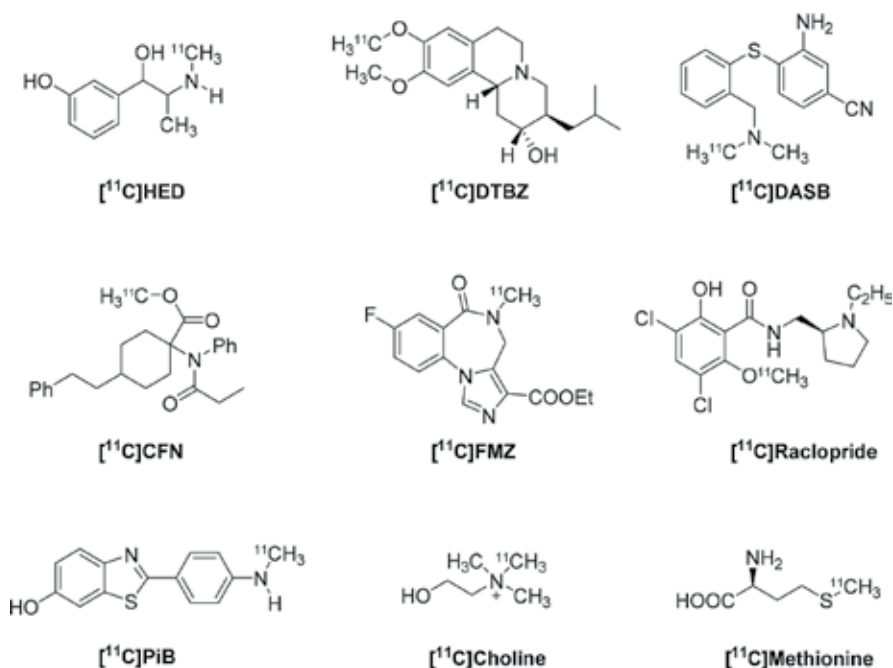
The incorporation of the [<sup>11</sup>C]methyl group into a target molecule is generally simply alkylation on N-, O-, and S-nucleophiles (e.g., HED, DTBZ, methionine). The tracer amount of [<sup>11</sup>C]MeI or [<sup>11</sup>C]MeOTf in the reaction leads to extraordinary stoichiometry. The stoichiometric relation can reach a factor of 10<sup>4</sup>:1 resulting in pseudo-first order kinetics of heteroatom methylation reactions. Therefore, the conversion rate is highly increased and the reasonable radiochemical yields can be reached within short reaction times of 3–5 min. The problems with polyalkylation in normal stoichiometric methylation of amines do not occur in the <sup>11</sup>C-methylation processes.



**Scheme 3.** Synthesis of [<sup>11</sup>C]acetate.

Scheme 4. Synthesis of [ $^{11}\text{C}$ ]WAY100635.Scheme 5. Synthesis of [ $^{11}\text{C}$ ]SL25.1188.

The reaction can be performed using a traditional vial-based approach (e.g., CFN, FMZ) or using solid support either on-cartridge (e.g., choline) or flow-based loop methods (e.g., PIB, DASB, raclopride) (Figure 3) [39, 41, 43]. All these methods are very convenient from automation prospective. The use of commercially available fully automated synthesis modules for production of clinical radiopharmaceutical doses enhances the speed, efficiency, reliability, and safety of radiosyntheses, as well as compliance with GMP regulations. For detail procedures see [38–43].

Figure 3. Representative  $^{11}\text{C}$ -radiotracers labeled by methylation.



To further expand the number of <sup>11</sup>C-labeled compounds, the development of novel <sup>11</sup>C–C bond forming reactions continues to gain attention. For example, several palladium-mediated cross-coupling reactions have been shown to be effective <sup>11</sup>C-labeling. The first application was reported in 1995 [69]. The feasibility of incorporating [<sup>11</sup>C]methyl groups into arenes, alkenes as well as alkanes was demonstrated by the reaction with the corresponding organostannanes and boranes in Stille and Suzuki cross-coupling reactions (**Scheme 6**) [70]. Due to the toxicity of the precursor and reagents used, the purification and quality control are more complicated comparing with those of simply methylation. Considering the short half-life of carbon-11, the application of this method for clinical dose production is currently underexploited. With the development of techniques and simplification of processes, this labeling strategy could be more widely adopted.

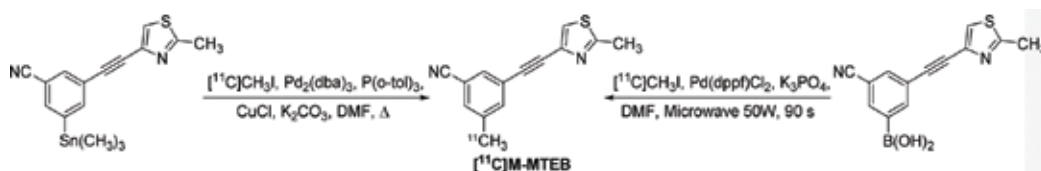
### 3.3. [<sup>11</sup>C]Cyanation

[<sup>11</sup>C]HCN is another important secondary labeling precursor (**Scheme 1**), because nitriles are not only frequently present in biologically active molecules but also represent a versatile functional group that can be readily converted into <sup>11</sup>C-labeled amides, carboxylic acids or amines (**Scheme 7**) [54, 71]. [<sup>11</sup>C]HCN is usually prepared by the reduction of [<sup>11</sup>C]CO<sub>2</sub> to [<sup>11</sup>C]CH<sub>4</sub> using H<sub>2</sub> over nickel (400°C), and then converted into [<sup>11</sup>C]HCN by reaction with NH<sub>3</sub> over platinum at elevated temperature (950°C) [72].

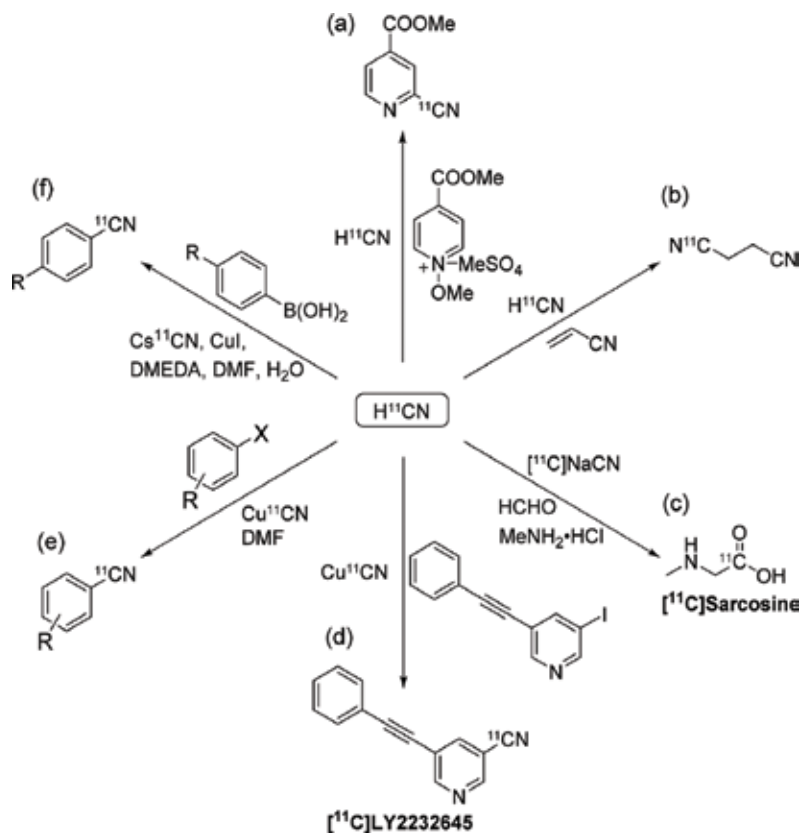
[<sup>11</sup>C]HCN can be used directly to form [<sup>11</sup>C]methyl-2-cyanoisonicotinate and [<sup>11</sup>C]1-succinonitrile by a Reissert-Kaufmann type reaction (**Scheme 7a**) and Michael addition (**Scheme 7b**), respectively [73]. It may convert to [<sup>11</sup>C]CuCN and react with aryl halides through the Rosenmund-von Braun reaction for the synthesis of [<sup>11</sup>C]LY2232645(**Scheme 7d**) [74–76]. <sup>11</sup>C-labeled amino acids, for example, [<sup>11</sup>C]Sarcosine, can be prepared using [<sup>11</sup>C]HCN in the Strecker reaction (**Scheme 7c**) [51, 77, 78]. In recent years, palladium-catalyzed and copper-mediated cyanations have gained increasing attention [79–82]. Vasdev and co-workers employed arylboronic acids and [<sup>11</sup>C]CsCN to prepare aromatic <sup>11</sup>C-nitriles (**Scheme 7f**), which was applicable to a broad range of substrates [80].

### 3.4. [<sup>11</sup>C]Carbonylation using [<sup>11</sup>C]CO

[<sup>11</sup>C]Carbon monoxide is an attractive secondary precursor for <sup>11</sup>C-chemistry since the wide variety of carbonyl containing molecules can be synthesized through carbonylation reactions. [<sup>11</sup>C]CO is readily available by the reduction of [<sup>11</sup>C]CO<sub>2</sub> over zinc or molybdenum [83, 84]. However, the application of [<sup>11</sup>C]CO was underexploited due to its poor reactivity and low solubility in organic solvents. Until recently, new methods have been developed to overcome

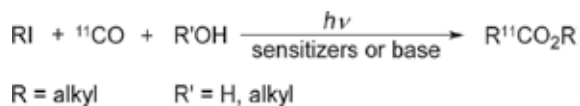


**Scheme 6.** Synthesis of [<sup>11</sup>C]M-MTEB by Suzuki or Stille reactions.



**Scheme 7.** Some transformations in  $[^{11}\text{C}]\text{HCN}$  radiochemistry: (a) radiosynthesis of  $[^{11}\text{C}]$ methyl-2-cyanoisonicotinate by a Reissert-Kaufmann type reaction; (b) direct formation of  $[^{11}\text{C}]$ 1-succinonitrile via Michael addition; (c) the Strecker reaction for the synthesis of  $[^{11}\text{C}]$ Sarcosine; (d) and (e):  $[^{11}\text{C}]\text{CuCN}$  can be reacted with aryl halides through the Rosenmund-von Braun reaction to afford  $[^{11}\text{C}]$ LY2232645 and other aromatic  $[^{11}\text{C}]$ nitriles; (f) copper-mediated synthesis of aromatic  $[^{11}\text{C}]$  nitriles from arylboronic acids.

the shortcomings, from technical and chemical points of the view [85–88]. The first report was by Kihlberg and co-workers in 1999, where  $[^{11}\text{C}]\text{CO}$  was allowed to react in a small autoclave under high pressure (>350 Bar) [89]. Low-pressure and ambient temperature techniques have been achieved lately [90–92]. The most widely applied  $^{11}\text{C}$ -carbonylation method used  $[^{11}\text{C}]\text{CO}$  is the palladium-mediated carbonylation reaction [93–96]. Rhodium-catalyzed carbonylation reactions provide an alternative route for the introduction of  $[^{11}\text{C}]\text{CO}$  into organic molecules [97–99]. Free-radical photoinitiated  $^{11}\text{C}$ -carbonylation reactions have been used to synthesize  $^{11}\text{C}$ -labeled aliphatic acid, esters and amides recently (**Scheme 8**) [100–104].



**Scheme 8.** Free-radical photoinitiated  $^{11}\text{C}$ -carbonylation reaction.

## 4. Future perspectives

This review introduces the field of carbon-11 radiochemistry through a general overview, but is not meant to be comprehensive. As the field is fast growing, more traditional chemists join the radiochemistry arena worldwide. Carbon-11, one of the most important radioisotopes in nuclear medicine, is foreseen to have endless opportunities for further innovation. Due to the short half-life, efficiency and simplicity is always the key to <sup>11</sup>C-labeling techniques. Recently developed transition-metal-mediated reactions have broadened the labeling scope and allowed <sup>11</sup>C-labeling of a range of different bioactive molecules.

<sup>11</sup>C-chemistry is a hybrid science between organic chemistry and engineering. To meet the growing demand and increasing regulation of radiopharmaceuticals, the fully automated or kit-like synthetic devices have been developed and will be required to be used in the manufacture of clinical doses to improve the reliability and safety.

Furthermore, synthetic pathways with better economical output and environmental management is another important aspect. The first example of a green radiochemistry laboratory at University of Michigan successfully prepared 11 radiopharmaceuticals for routine clinical application using ethanol as the only organic solvent [105]. The removal of all other organic solvents from the process simplifies production and quality control testing. The robust and reliable methods are increasingly applied in various PET facilities around the world.

## Author details

Lingyun Yang, Peter J. H. Scott and Xia Shao\*

\*Address all correspondence to: [xshao@umich.edu](mailto:xshao@umich.edu)

Division of Nuclear Medicine, Department of Radiology, University of Michigan Medical School, Ann Arbor, Michigan, USA

## References

- [1] Crane HR, Lauritsen CC. *Physics Review*. 1934;**45**:497-498
- [2] Ruben S, Hassid WZ, Kamen MD. *Journal of the American Chemical Society*. 1939;**61**:661-663
- [3] Antoni G, Kihlberg T, Långström B. In: Welch MJ, Redvanly CS, editors. *Handbook of Radiopharmaceuticals*. Chichester, UK: John Wiley & Sons, Ltd; 2005. pp. 141-194
- [4] Tobias CA, Lawrence JH, Roughton FJW, Root WS, Gregersen MI. *The American Journal of Physiology*. 1945;**145**:253-263
- [5] Antoni G. *Journal of Labelled Compounds and Radiopharmaceuticals*. 2015;**58**:65-72

- [6] Ametamey SM, Honer M, Schubiger PA. *Chemical Reviews*. 2008;**108**:1501-1516
- [7] Miller PW, Long NJ, Vilar R, Gee AD. *Angewandte Chemie, International Edition*. 2008;**47**:8998-9033
- [8] Mercer JR. *Journal of Pharmacy & Pharmaceutical Sciences*. 2007;**10**:180-202
- [9] Oriuchi N, Higuchi T, Ishikita T, Miyakubo M, Hanaoka H, Iida Y, Endo K. *Cancer Science*. 2006;**97**:1291-1297
- [10] Le Bars D. *Journal of Fluorine Chemistry*. 2006;**127**:1488-1493
- [11] Scott AM. In: Bailey DL, Townsend DW, Valk PE, Maisey MN, editors. *Positron Emission Tomography: Basic Sciences*. London: Springer; 2005. pp. 311-325
- [12] Fukuda H, Furumoto S, Iwata R, Kubota K. *International Congress Series*. 2004;**1264**:158-165
- [13] Nordberg A. *The Lancet Neurology*. 2004;**3**:519-527
- [14] Cai LS, Innis RB, Pike VW. *Current Medicinal Chemistry*. 2007;**14**:19-52
- [15] Cohen RM. *Molecular Imaging & Biology*. 2007;**9**:204-216
- [16] Wu C, Pike VW, Wang Y. *Current Topics in Developmental Biology*. 2005;**70**:171-213
- [17] Drevets WC. *Biological Psychiatry*. 2000;**48**:813-829
- [18] Bremner JD, Staib LH, Kaloupek D, Southwick SM, Soufer R, Charney DS. *Biological Psychiatry*. 1999;**45**:806-816
- [19] Drevets WC, Thase ME, Moses-Kolko EL, Price J, Frank E, Kupfer DJ, Mathis C. *Nuclear Medicine and Biology*. 2007;**34**:865-877
- [20] Keng FYJ. *Annals Academy of Medicine Singapore*. 2004;**33**:175-182
- [21] De Grado TR, Bergmann SR, Ng CK, Raffel DM. *Journal of Nuclear Cardiology*. 2000;**7**:686-700
- [22] Even-Sapir E, Metser U, Mishani E, Lievshitz G, Lerman H, Leibovitch I. *Journal of Nuclear Medicine*. 2006;**47**:287-297
- [23] Kulkarni B, Bentley DE, Elliott R, Julyan PJ, Boger E, Watson A, Boyle Y, El-Deredy W, Jones AKP. *Arthritis and Rheumatism*. 2007;**56**:1345-1354
- [24] Carroll VN, Truillet C, Shen B, Flavell RR, Shao X, Evans MJ, VanBrocklin HF, Scott PJH, Chin FT, Wilson DM. *Chemical Communications*. 2016;**52**:4888-4890
- [25] Schulthess GK v, Steinert HC, Hany TF. *Radiology*. 2006;**238**:405-422
- [26] Winstead MB, Winchell HS, Fawwaz R. *The International Journal of Applied Radiation and Isotopes*. 1969;**20**:859-863
- [27] Tang DY, Lipman A, Meyer GJ, Wan CN, Wolf AP. *Journal of Labelled Compounds and Radiopharmaceuticals*. 1979;**16**:435-440

- [28] Raichle ME, Eichling JO, Straatmann MG, Welch MJ, Larson KB, Terpogossian MM. *The American Journal of Physiology*. 1976;**230**:543-552
- [29] Wolf AP, Redvanly CS. *The International Journal of Applied Radiation and Isotopes*. 1977;**28**:29-48
- [30] Ferrieri RA, Wolf AP. *Radiochimica Acta*. 1983;**34**:69-83
- [31] Langstrom B, Bergson G. *Radiochemical and Radioanalytical Letters*. 1980;**43**:47-54
- [32] Langstrom B, Obenius U, Sjoberg S, Bergson G. *Journal of Radioanalytical Chemistry*. 1981;**64**:273-280
- [33] Berger G, Mazière M, Godot J-M. *Journal of Labelled Compounds and Radiopharmaceuticals*. 1981;**18**:1649-1671
- [34] Harada N, Hayashi N. *Applied Radiation and Isotopes*. 1993;**44**:629-630
- [35] Runkle AC, Shao X, Tluczek LJM, Henderson BD, Hockley BG, Scott PJH. *Applied Radiation and Isotopes*. 2011;**69**:691-698
- [36] Shao X, Hoareau R, Runkle AC, Tluczek LJM, Hockley BG, Henderson BD, Scott PJH. *Journal of Labelled Compounds and Radiopharmaceuticals*. 2011;**54**:819-838
- [37] Rodnick M, Tluczek L, Scott PJH, Shao X, Labelled J. *Journal of Labelled Compounds and Radiopharmaceuticals*. 2017;**60**:S295
- [38] Blecha JE, Henderson BD, Hockley BG, VanBrocklin HF, Zubieta J-K, DaSilva AF, Kilbourn MR, Koeppe RA, Scott PJH, Shao X. *Journal of Labelled Compounds and Radiopharmaceuticals*. 2017;**60**:375-380
- [39] Tluczek L, Shao X. *Radiochemical Syntheses*. Hoboken, NJ, USA: John Wiley & Sons, Inc.; 2012. pp. 257-264
- [40] Shao X, Kilbourn MR. *Applied Radiation and Isotopes*. 2009;**67**:602-605
- [41] Shao X, Hockley BG, Hoareau R, Schnau PL, Scott PJH. *Applied Radiation and Isotopes*. 2011;**69**:403-409
- [42] Hockley BG, Henderson B, Shao X. *Radiochemical Syntheses*. Hoboken, NJ, USA: John Wiley & Sons, Inc.; 2012. pp. 167-175
- [43] Shao X, Schnau PL, Fawaz MV, Scott PJH. *Nuclear Medicine and Biology*. 2013;**40**:109-116
- [44] Kilbourn MR. *Radiochemical Syntheses*. Hoboken, NJ, USA: John Wiley & Sons, Inc.; 2012. pp. 213-219
- [45] Shao X, Jang K, Scott PJH. *Radiochemical Syntheses*. Hoboken, NJ, USA: John Wiley & Sons, Inc; 2015. pp. 73-80
- [46] English SJ, Diaz JA, Shao X, Gordon D, Bevard M, Su G, Henke PK, Rogers VE, Upchurch GR, Piert M. *EJNMMI Research*. 2014;**4**:20

- [47] Shao X, Wang X, English SJ, Desmond T, Sherman PS, Quesada CA, Piert MR. *Nuclear Medicine and Biology*. 2013;**40**:906-911
- [48] Hoareau R, Shao X, Henderson BD, Scott PJH. *Applied Radiation and Isotopes*. 2012;**70**:1779-1783
- [49] Shao X, Scott PJH. *Radiochemical Syntheses*. Hoboken, NJ, USA: John Wiley & Sons, Inc.; 2015. pp. 63-71
- [50] Shao X. *Radiochemical Syntheses*. Hoboken, NJ, USA: John Wiley & Sons, Inc.; 2012. pp. 275-283
- [51] Xing JH, Brooks AF, Fink D, Zhang HB, Piert MR, Scott PJH, Shao X. *Synlett*. 2017;**28**:371-375
- [52] McCarron JA, Turton DR, Pike VW, Poole KG. *Journal of Labelled Compounds and Radiopharmaceuticals*. 1996;**38**:941-953
- [53] Hwang D-R, Simpson NR, Montoya J, Mann JJ, Laruelle M. *Nuclear Medicine and Biology*. 1999;**26**:815-819
- [54] Rotstein BH, Liang SH, Placzek MS, Hooker JM, Gee AD, Dolle F, Wilson AA, Vasdev N. *Chemical Society Reviews*. 2016;**45**:4708-4726
- [55] Dahl K, Halldin C, Schou M. *Clinical and Translational Imaging*. 2017;**5**:275-289
- [56] Pike VW, Eakins MN, Allan RM, Selwyn AP. *The International Journal of Applied Radiation and Isotopes*. 1982;**33**:505-512
- [57] Hooker JM, Reibel AT, Hill SM, Schueller MJ, Fowler JS. *Angewandte Chemie, International Edition*. 2009;**48**:3482-3485
- [58] Rotstein BH, Liang SH, Holland JP, Collier TL, Hooker JM, Wilson AA, Vasdev N. *Chemical Communications*. 2013;**49**:5621-5629
- [59] Mossine AV, Brooks AF, Jackson IM, Quesada CA, Sherman P, Cole EL, Donnelly DJ, Scott PJH, Shao X. *Bioconjugate Chemistry*. 2016;**27**:1382-1389
- [60] Wilson A, Garcia A, Houle S, Sadovski O, Vasdev N. *Chemistry--A European Journal*. 2011;**17**:259-264
- [61] Vasdev N, Sadovski O, Garcia A, Dollé F, Meyer JH, Houle S, Wilson AA. *Journal of Labelled Compounds and Radiopharmaceuticals*. 2011;**54**:678-680
- [62] Saba W, Valette H, Peyronneau M-A, Bramoullé Y, Coulon C, Curet O, George P, Dollé F, Bottlaender M. *Synapse*. 2010;**64**:61-69
- [63] Rusjan PM, Wilson AA, Miler L, Fan I, Mizrahi R, Houle S, Vasdev N, Meyer JH. *Journal of Cerebral Blood Flow and Metabolism*. 2014;**34**:883-889
- [64] Långström H, Lundqvist. *The International Journal of Applied Radiation and Isotopes*. 1976;**27**:357-363
- [65] Comar J-C, Cartron M, Maziere C, Marazano. *European Journal of Nuclear Medicine*. 1976;**1**:11-14

- [66] Larsen P, Ulin J, Dahlstrøm K, Jensen M. *Applied Radiation and Isotopes*. 1997;**48**:153-157
- [67] Jewett M. *Applied Radiation and Isotopes*. 1992;**43**:1383-1385
- [68] Link JM, Krohn KA, Clark JC. *Nuclear Medicine and Biology*. 1997;**24**:93-97
- [69] Andersson Y, Cheng AP, Langstrom B. *Acta Chemica Scandinavica*. 1995;**49**:683-688
- [70] Hamill TG, Krause S, Ryan C, Bonnefous C, Govek S, Seiders TJ, Cosford NDP, Roppe J, Kamenecka T, Patel S, Gibson RE, Sanabria S, Riffel K, Eng W, King C, Yang X, Green MD, O'Malley SS, Hargreaves R, Burns HD. *Synapse*. 2005;**56**:205-216
- [71] Takahashi T, Ido T, Hatano K, Iwata R, Nakanishi H. *Applied Radiation and Isotopes*. 1990;**41**:649-654
- [72] Iwata R, Ido T, Takahashi T, Nakanishi H, Iida S. *Applied Radiation and Isotopes*. 1987;**38**:97-102
- [73] Somawardhana CW, Sajjad M, Lambrecht RM. *Journal of the Chemical Society, Chemical Communications*. 1990;**5**:370-371
- [74] Ponchant M, Hinnen F, Demphel S, Crouzel C. *Applied Radiation and Isotopes*. 1997;**48**:755-762
- [75] Mathews WB, Monn JA, Ravert HT, Holt DP, Schoepp DD, Dannals RF. *Journal of Labelled Compounds and Radiopharmaceuticals*. 2006;**49**:829-834
- [76] Simeon F, Sobrio F, Gourand L, Barre J. *Journal of the Chemical Society, Perkin Transactions 1*. 2001;**7**:690-694
- [77] Gillings NM, Gee AD. *Journal of Labelled Compounds and Radiopharmaceuticals*. 2001;**44**:909-920
- [78] Studenov AR, Szalda DE, Ding Y-S. *Nuclear Medicine and Biology*. 2003;**30**:39-44
- [79] Sundermeier M, Zapf A, Beller M. *European Journal of Inorganic Chemistry*. 2003;**2003**:3513-3526
- [80] Ma L, Placzek MS, Hooker JM, Vasdev N, Liang SH. *Chemical Communications*. 2017;**53**:6597-6600
- [81] Zhao W, Lee HG, Buchwald SL, Hooker JM. *Journal of the American Chemical Society*. 2017;**139**:7152-7155
- [82] Brooks A, Makaravage K, Shao X, Burris S, Sanford M, Scott P. *Journal of Nuclear Medicine*. 2017;**58**:402
- [83] DeGrazia J. *Medical Physics*. 1981;**8**:723
- [84] Zeisler SK, Nader M, Theobald A, Oberdorfer F. *Applied Radiation and Isotopes*. 1997;**48**:1091-1095
- [85] Andersson Y, Langstrom B. *Journal of the Chemical Society, Perkin Transactions 1*. 1995;**4**:287-289

- [86] Lidstrom P, Kihlberg T, Langstrom B. *Journal of the Chemical Society, Perkin Transactions 1*. 1997;**18**:2701-2706
- [87] Kealey S, Miller PW, Long NJ, Plisson C, Martarello L, Gee AD. *Chemical Communications*. 2009;**25**:3696-3698
- [88] Dahl K, Schou M, Ulin J, Sjoberg C-O, Farde L, Halldin C. *RSC Advances*. 2015;**5**:88886-88889
- [89] Kihlberg T, Långström B. *The Journal of Organic Chemistry*. 1999;**64**:9201-9205
- [90] Eriksson J, van den Hoek J, Windhorst AD. *Journal of Labelled Compounds and Radiopharmaceuticals*. 2012;**55**:223-228
- [91] Taddei C, Bongarzone S, Gee AD. *Chemistry--A European Journal*. 2017;**23**:7682-7685
- [92] Miller PW, Long NJ, de Mello AJ, Vilar R, Audrain H, Bender D, Passchier J, Gee A. *Angewandte Chemie, International Edition*. 2007;**46**:2875-2878
- [93] Karimi B. *Langström. European Journal of Organic Chemistry*. 2003;**2003**:2132-2137
- [94] Rahman O, Kihlberg T, Långström B. *The Journal of Organic Chemistry*. 2003;**68**:3558-3562
- [95] Dahl K, Schou M, Amini N, Halldin C. *European Journal of Organic Chemistry*. 2013;**2013**:1228-1231
- [96] Dahl K, Schou M, Rahman O, Halldin C. *European Journal of Organic Chemistry*. 2014;**2014**:307-310
- [97] Barletta J, Karimi F, Långström B. *Journal of Labelled Compounds and Radiopharmaceuticals*. 2006;**49**:429-436
- [98] Barletta J, Karimi F, Doi H, Långström B. *Journal of Labelled Compounds and Radiopharmaceuticals*. 2006;**49**:801-809
- [99] Doi H, Barletta J, Suzuki M, Noyori R, Watanabe Y, Langstrom B. *Organic & Biomolecular Chemistry*. 2004;**2**:3063-3066
- [100] Itsenko O, Långström B. *The Journal of Organic Chemistry*. 2005;**70**:2244-2249
- [101] Itsenko O, Långström B. *Organic Letters*. 2005;**7**:4661-4664
- [102] Itsenko O, Kihlberg T, Långström B. *European Journal of Organic Chemistry*. 2005;**2005**:3830-3834
- [103] Itsenko O, Norberg D, Rasmussen T, Långström B, Chatgililoglu C. *Journal of the American Chemical Society*. 2007;**129**:9020-9031
- [104] Itsenko O, Kihlberg T, Långström B. *The Journal of Organic Chemistry*. 2004;**69**:4356-4360
- [105] Shao X, Fawaz MV, Jang K, Scott PJH. *Applied Radiation and Isotopes*. 2014;**89**:125-129



---

# Carbon Dioxide Capture and Oil Extraction

---



---

# Solvents for Carbon Dioxide Capture

---

Fernando Vega, Mercedes Cano, Sara Camino,  
Luz M. Gallego Fernández, Esmeralda Portillo and  
Benito Navarrete

Additional information is available at the end of the chapter

<http://dx.doi.org/10.5772/intechopen.71443>

---

## Abstract

Anthropogenic CO<sub>2</sub> emissions are considered the major contributor of greenhouse gas emissions worldwide. The mitigation of this kind of CO<sub>2</sub> emissions relies on a portfolio of alternatives where CO<sub>2</sub> absorption appears as the nearest approach to be applied at industrial scale. Researchers have been focused on developing new formulations of solvents to make more competitive CO<sub>2</sub> absorption as a carbon capture and storage (CCS) technology. In this sense, this chapter summarizes both the conventional solvents and the most recent investigations on this field. Chemical absorption is more suitable for a lot of industrial process due to the flue gas conditions: ambient pressure, low CO<sub>2</sub> concentration and large volume. Therefore numerous novel solvents came up in recent years and they are further discussed in this chapter. The most recent solvents, their mechanisms and kinetics and the advantages and disadvantages are also included. Finally, physical solvents are adequate in high CO<sub>2</sub> partial pressure applications and they are reported in the last section. Although physical absorption field is constrained to high-pressure flue gas, physical solvents provided higher performance in CO<sub>2</sub> separation process and their characteristics are also summarized.

**Keywords:** solvent, CO<sub>2</sub>, CCS, absorption, capture

---

## 1. Introduction

Carbon capture and storage (CCS) is one of the pathways for anthropogenic CO<sub>2</sub> emission mitigation. Among the wide portfolio of CCS technologies, physical and chemical absorption are considered the most close-to-market approaches to be applied at industrial scale, mainly focused on their implementation in energy production from fossil fuels [1]. Physical absorption is based on the CO<sub>2</sub> solubility into the solution without chemical reaction which is

based on Henry's law and hence high  $\text{CO}_2$  partial pressures and low-temperatures are highly recommended for its application. Chemical absorption is based on the reaction between  $\text{CO}_2$  and specific compounds—solvents—that lead to form a weak bond between  $\text{CO}_2$  and the solvent. Chemical absorption occurs indeed at low  $\text{CO}_2$  partial pressure. Low-temperature is also recommended for this mechanism. Numerous solvents have been developed since the first chemical absorption process was patented in the early 1930s. However, the implementation of  $\text{CO}_2$  absorption at industrial processes such as cement production, iron and steel manufacturing and fossil-fuel power plants requires novel solvent formulations that can address the main constraints limiting its deployment: the huge volume of treated gas, the low  $\text{CO}_2$  concentration in the flue gas and the presence of trace components such as  $\text{NO}_x$ ,  $\text{SO}_2$  and particulate matter which degrade the solvents [2, 3]. This chapter summarizes both conventional and newly developed solvents mainly focused on  $\text{CO}_2$  capture processes based on physical and chemical absorption. A deep revision of the solvents reported from the literature was made including primary, secondary, tertiary amines and non-amine-based solvents. Novel solvents such as sterically hindered amines and blends were discussed further. In respect to physical solvents, authors report the conventional solvents used by licensed processes such as Rectisol™, Selexol™, Sulfinol™ and Purisol™. Special attention will be paid in ionic liquids and novel biphasic configurations and their use as  $\text{CO}_2$  capture solvents.

## 2. Chemical absorption solvents

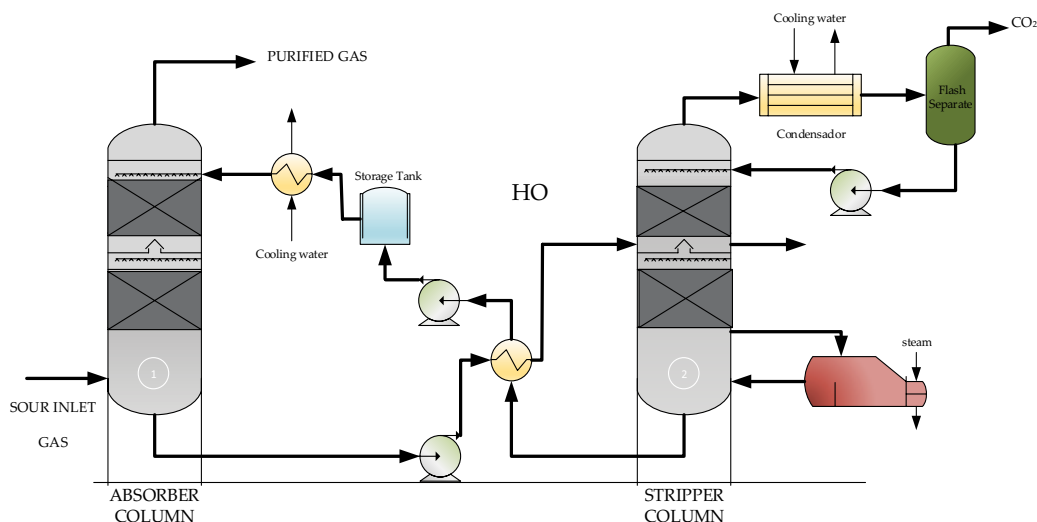
### 2.1. Conventional amine-based solvents

The amine-based chemical absorption process has been used for  $\text{CO}_2$  and  $\text{H}_2\text{S}$  removal—acid gas removal—from gas-treating plants since 1950s [4] and are considered to be by far the most developed  $\text{CO}_2$  capture process.  $\text{CO}_2$  is absorbed typically using amines to form a soluble carbonate salt. The absorber operates below  $60^\circ\text{C}$  and ambient pressure (step 1 in **Figure 1**) [4].

This reaction is reversible and the  $\text{CO}_2$  can be released by heating the solution with the carbonate salt in a separate stripping column. The  $\text{CO}_2$  stripping occurs at  $120^\circ\text{C}$  and pressures ranging between 1.8 and 3 bar [6], as illustrated in the step 2 in **Figure 1**.

Nowadays, amine-based chemical absorption came up as a potential technology that can be applied to reduce carbon dioxide emissions in industrial processes such as fossil fuels power plants, cement production and iron and steel manufacturing. Post-combustion is the nearest close-to-market and industrially developed carbon capture and storage (CCS) technology.

Specifically, the alkanolamines are volatile, cheap and safe to handle compounds and are commonly classified by the degree of substitution on the central nitrogen; a single substitution denoting a primary amine; a double substitution, a secondary amine; and a triple substitution, a tertiary amine. Each of the above-mentioned alkanolamines has at least one hydroxyl group and one amino group. In general, the hydroxyl group serves to reduce vapor pressure and increases the solubility in water, while the amine group provides the necessary alkalinity in aqueous solutions to promote the reaction with acid gases. Therefore, the molecular structures of primary


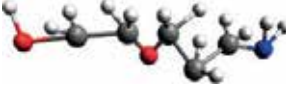
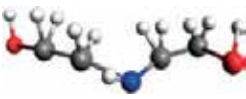
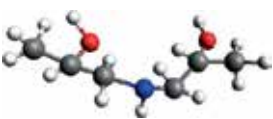



**Figure 1.** Simplified diagram of a conventional acid gas removal process using chemical absorption adapted from Ref. [5].

and secondary amines are the non-fully substituted alkanolamines and they have hydrogen atoms at the non-substituted valent sites on the central nitrogen, whereas the tertiary amines are fully substituted on the central nitrogen. This structural characteristic plays an important role in the acid gas removal capabilities of the various treating solvents [7]. **Table 1** shows the most widely used amines for the treatment of acid gases, which will be described in detail.

The performance of solvents for CO<sub>2</sub> absorption can be evaluated from several specific properties. In particular, the CO<sub>2</sub> absorption capacity, namely CO<sub>2</sub> loading, is defined as the amount of CO<sub>2</sub> that can be absorbed per mole of solvent (mole CO<sub>2</sub>/mole solvent). The maximum CO<sub>2</sub> absorption capacity can be deduced from the CO<sub>2</sub> solubility represented by vapour-liquid equilibrium (VLE) curves of each solvent, depending on the CO<sub>2</sub> partial pressure in the bulk gas and the absorption temperature [4]. The cyclic capacity, defined as the difference of the CO<sub>2</sub> loading between the rich solvent and the lean solvent, is also used for easily comparison. In terms of CO<sub>2</sub> chemical reactivity, the absorption kinetics is expressed as the rate of the CO<sub>2</sub> absorbed from the bulk gas to the bulk liquid that means mole CO<sub>2</sub> per second. Finally, the solvent resistance to be degrade in presence of O<sub>2</sub>, NO<sub>x</sub> and SO<sub>2</sub> and also under elevated temperature is compared by the solvent losses under specific operating conditions.

Primary alkanolamines such as monoethanolamine (MEA) and diglycolamine (DGA), provide high chemical reactivity, favored kinetics, medium-to-low absorption capacity and acceptable stability. Monoethanolamine (MEA), the first-generation and the most well-known amine-based absorbent, is highlighted by its high chemical reactivity with CO<sub>2</sub> and low cost. These properties can reduce the absorber height and ensure a feasible operation. Although MEA-based scrubbing technology is suitable for acid gas removal and, in particular, post-combustion capture from fossil-fired plants flue gas, it suffers from several issues during operation, including high energy requirements for stripping: high enthalpy of reaction, low absorption capacity, oxidative and thermal degradation and piping corrosion [8]. Hence, efforts have

Abbr.	Name	Industrial process	Structural formulae	Chemical structure	CO <sub>2</sub> loading
MEA	Mono ethanol amine	Natural and syngas purification	NH <sub>2</sub> -CH <sub>2</sub> -CH <sub>2</sub> OH		0.5
DGA	Diglycol amine	Syngas treatment	(HO-C <sub>2</sub> H <sub>4</sub> )-O-(C <sub>2</sub> H <sub>4</sub> -NH <sub>2</sub> )		0.25–0.35
DEA	Diethanol amine	Natural gas containing high concentrations of COS and CS <sub>2</sub>	(CH <sub>2</sub> CH <sub>2</sub> OH) <sub>2</sub> NH		0.7–1
DIPA	Diiso propanol amine	ADIP, Sulfinol: refinery gas treatment	(CH <sub>3</sub> CHOHCH <sub>2</sub> ) <sub>2</sub> NH		0.43–0.22
MDEA	Methyl diethanol amine	Solvents URCASOL, gas washing in Clauss plants	CH <sub>3</sub> N(C <sub>2</sub> H <sub>4</sub> OH) <sub>2</sub>		0.1–0.3

Gray, C atom; white, H atom; red, O atom; dark blue, N atom.

**Table 1.** Most commonly amines used in acid gas treatment [4].

focused on the development of attractive solvents to achieve high absorption/desorption capacities, energy-efficient performance and oxidative and thermal stability. Furthermore, DGA presents similar properties to MEA in many aspects, except that its low vapor pressure allows its use at higher concentrations, typically between 40 and 60%wt. in aqueous solution.

Secondary alkanolamines such as diethanolamine (DEA) and diisopropanolamine (DIPA), which have a hydrogen atom directly bonded to the nitrogen, shows intermediate properties compared to primary amines and they are considered as an alternative to MEA. DEA is more resistant to degrade and shows lower corrosion strength than MEA, whereas DIPA has lower energy requirement for solvent regeneration than MEA.

Finally, tertiary amines such as triethanolamine (TEA) or methyl diethanolamine (MDEA), that are characterized by having a high equivalent weight, which causes a low absorption capacity, low reactivity and high stability.

There are three main differences in the performance of primary and secondary amines as they are compared to tertiary amines for the CO<sub>2</sub> separation process. Primary and secondary amines are very reactive; they form carbamate by direct reaction with CO<sub>2</sub> by Zwitterion mechanism. Therefore, these amines showed limited thermodynamic capacity to absorb CO<sub>2</sub> due to the stable carbamates formation along the absorption process. On the other hand, tertiary amines can only form a bicarbonate ion and protonated amine by the base-catalyzed hydration of CO<sub>2</sub> due to their lack of the necessary N–H bond [9, 10]. Hydration is slower than the direct reaction by carbamate formation and, hence, tertiary amines show low CO<sub>2</sub> absorption rates [9].

In general, the main issues that amine-based chemical absorption has to address to be applied as industrial scale for carbon dioxide emission mitigation are listed below:

- High energy consumption during the solvent regeneration.
- Corrosion requires the use of both inhibitors and resistant materials in their application.
- Scale up from actual (800 t/day) to required (8000 t/day) CO<sub>2</sub> capacity.
- Degradation in the presence of O<sub>2</sub>, SO<sub>x</sub> and other impurities such as particles, HCl, HF and Hg.

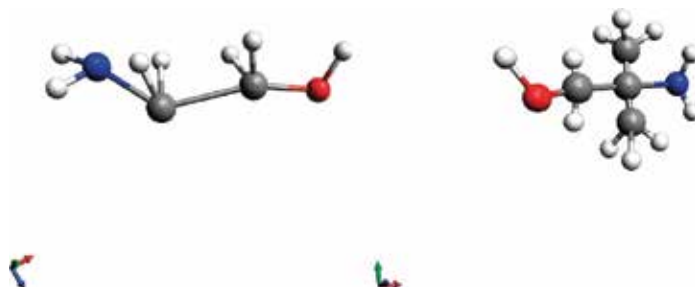
## 2.2. Sterically hindered amine solvents

Sterically hindered amines are considered a type of amines which can improve CO<sub>2</sub> absorption rates in comparison with the common primary and second amines, usually amino alcohols. A sterically hindered amine is formed by a primary or secondary amine in which the amino group is attached to a tertiary carbon atom in the first case or a secondary or tertiary carbon atom in the second (**Figure 2**).

These amines are characterized by forming carbamates of intermediate-to-low stability, introducing a bulky substituent adjacent to the amino group to lower the stability of the carbamate formed by CO<sub>2</sub>-amine reaction. This weaker bond leads to high free-amine concentration in solution, so the energy consumption to release CO<sub>2</sub> is lower than the common primary and second amines. According to Nicole Hüser et al. [11], a decrease up to 15% can be achieved using hindered amines.

The general reaction scheme of the CO<sub>2</sub>-primary or secondary amine (AmH) and the CO<sub>2</sub>-sterically hindered amine (AmCOO<sup>-</sup>) is shown in **Figure 3**. Regarding the primary or secondary reaction scheme, the symbol B represents a base that should be another amine molecule that requires to form the carbamate anion. In this case, two amine molecules are needed to absorb one CO<sub>2</sub> molecule, as it is extracted from the overall reaction.

The system CO<sub>2</sub>-sterically hindered amine requires only one amine molecule to capture one molecule of CO<sub>2</sub>. Based on this assumption, the maximum CO<sub>2</sub> loading using sterically hindered amines is higher than for unhindered, primary or secondary amines.



**Figure 2.** Molecular structure of primary amines on the left (MEA) and a sterically hindered amine on the right (AMP). Note that gray balls represent C atoms; white balls represent H atoms; red/dark gray balls represent O atoms; dark blue/black balls represent N atoms [11].

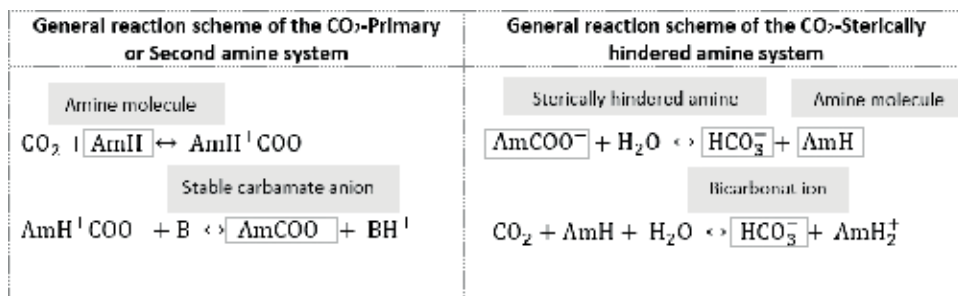




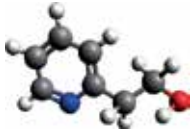
Figure 3. General reaction scheme of the CO<sub>2</sub>-amines system [11].

The use of this type of amines leads to reduce the energy requirement for the amine-based solvent regeneration up to 20% compared to conventional MEA-based scrubbing, due to the formation weak bonds [11]. Several sterically hindered amines are shown in **Table 2**.

### 2.3. Non-amine-based solvents

Non-amine-based solvents are called to those chemical solvents which do not integrate an amine group in their structure molecular. The most relevant solvent proposed as an alternative to the conventional amine-based solvents is the sodium carbonate (Na<sub>2</sub>CO<sub>3</sub>). About 30% p/p sodium carbonate slurry is used to provide a basic environment in which CO<sub>2</sub> is absorbed as bicarbonate followed by sodium bicarbonate formation [13]. The NaHCO<sub>3</sub> precipitation enhances the bicarbonate formation and, hence, the CO<sub>2</sub> capture capacity of the solvent is improved.

Sodium carbonate has shown a high performance in CO<sub>2</sub> separation from flue gas in comparison with the MEA benchmark. It produces a high CO<sub>2</sub> loading capacity (0.73 mole CO<sub>2</sub>/mole CO<sub>3</sub><sup>2-</sup>) and a reboiler duty of 3.2 MJ/kg CO<sub>2</sub> rather than 0.5 mole CO<sub>2</sub>/mole MEA and 3.5–4.2 MJ/kg CO<sub>2</sub> in case MEA is used as a solvent. Furthermore, this chemical solvent can absorb CO<sub>2</sub> in presence of pollutants such as SO<sub>2</sub> which can enable the cyclic capacity of amine-based solvents for CO<sub>2</sub> absorption [13, 14]. Despite those advantages, sodium carbonate can absorb CO<sub>2</sub> at low absorption rates, which lead to higher absorption column height. It assumes that

Abbreviation	AMP	MDA	PE
Name	2-amino-2-methyl-1-propanol	1,8-p-menthane diamine	2-piperidineethanol
Structural formulae	HO-CH <sub>2</sub> -C-(CH <sub>3</sub> )(CH <sub>3</sub> )(NH <sub>2</sub> )	(CH <sub>3</sub> NH <sub>2</sub> -C <sub>6</sub> H <sub>9</sub> -C <sub>3</sub> H <sub>6</sub> NH <sub>2</sub> )	C <sub>2</sub> H <sub>4</sub> -NH-CH-(C <sub>2</sub> H <sub>4</sub> OH)-C <sub>2</sub> H <sub>4</sub>
Chemical structure			

Gray, C atom; white, H atom; red, O atom; dark blue, N atom.

Table 2. Examples of sterically hindered amines [12].



sodium carbonate requires the use of promoters such as primary amines to enhance its CO<sub>2</sub> absorption rates [15–18]. The advantages and disadvantages to use sodium carbonate as an absorption solvent in a CO<sub>2</sub> separation process are shown in **Table 3**.

The potassium carbonate (K<sub>2</sub>CO<sub>3</sub>) is other non-amine-based solvents that can be used as a promoter the CO<sub>2</sub> capture with amine-based solvent or other class of amine, like a sterically hindered amine [12].

## 2.4. Solvent blends

As it was indicated in previous section, the high energy penalty related to amines regeneration and solvent degradation are the most significant issues hindering a large deployment of this technology. Solvent regeneration is a high-intensive energy process. Moreover, the stripper operating conditions and the solvent used to absorb CO<sub>2</sub> consume a high amount of energy. In this sense, amine blends could offer potential improvements in CO<sub>2</sub> chemical absorption to reduce the regular reboiler duty and the common solvent circulation rates [14, 19].

However, in view of taking advantage these main benefits, except its low reactivity, the addition of a small amount tertiary amines (MDEA, TEA) in primary or secondary amines aqueous solutions (MEA, DEA) to form a solvent blend enhances the overall behavior of the solvent in terms of lower energy requirements for solvent regeneration and higher resistance to solvent degradation [20, 21]. For this reason, different researchers are studying novel solvent formulations and blends, involving fast kinetic solvents such as MEA with other slow kinetic solvents like TEA, 2-amino-2-methyl-1-propanol (AMP), benzylamine (BZA) and MDEA [22, 23].

A huge number of solvent have been proposed for CO<sub>2</sub> chemical absorption applied to carbon capture. The first amine was combined with faster kinetic amines was N-methyldiethanolamine (MDEA). Amines such a methanolamine (MEA), diethanolamine (DEA) and piperazine (PZ) have used as promoters for MDEA blends. It is also possible to increase the reaction rate of fast solvents by combining them with an even faster solvent. For example, MEA is a fast solvent but it is almost 50 times slower than PZ. The CO<sub>2</sub> absorption rate of MEA can be significantly improved by adding small amounts of PZ as a promoter [24]. This blend improved the individual CO<sub>2</sub> absorption rate. Potassium carbonate promoted with PZ is also considered a promising solvent [25], along with the PZ and 2-amino-2-methyl-1-propanol (AMP) blends [26]. A summary of the most promising amines blends are given below (**Table 4**).

Advantages	Disadvantage
<ul style="list-style-type: none"> <li>Multi-pollutant capture system</li> </ul>	<ul style="list-style-type: none"> <li>Slow absorption rate. The solvent should be promoted with increasing rate additiveti</li> </ul>
<ul style="list-style-type: none"> <li>Use of a non-hazardous and non-volatile solvent</li> </ul>	<ul style="list-style-type: none"> <li>Solid and slurry management</li> </ul>
<ul style="list-style-type: none"> <li>Lower fouling and corrosion issues than amine compounds</li> </ul>	<ul style="list-style-type: none"> <li>High pollutant removal</li> </ul>

**Table 3.** Advantages and disadvantages of CCS based on chemical absorption using Na<sub>2</sub>CO<sub>3</sub> [14].

Solvent	Abbreviation	Reference
Piperazine and potassium carbonate	PZ+ K <sub>2</sub> CO <sub>3</sub>	[25]
2-amino-2-methyl-1-propanol and piperazine	AMP+ PZ	[26]
2-amino-2-methyl-1-propanol and 1,2-ethanediamine	AMP+ EDA	[27]
3-methylamino propylamine and dimethyl-monoethanolamine	MAPA + DMMEA	[28]

**Table 4.** A summary of most relevant solvent blends reported from the literature [14].

Some advantages of blending these amines are listed below [29]:

- Improved thermodynamic efficiency.
- Reduction in issues relating to degradation and operation of the solvent caused by corrosion.
- Flexibility in the range of amines available to tailor and optimize the composition of the solvent to achieve the highest absorption efficiency.
- High absorption rates observed in single amine solvents can often be maintained in blends of the individual components.
- Energy requirement for solvent regeneration can be reduced.

## 2.5. Ionic liquid

A novel generation of solvents comes recently up as an alternative for traditional amine-based solvents, namely ionic liquids (ILs). These compounds are organic salts with elevated boiling points and thus low vapor pressure, which can selectively absorb acid gases such as CO<sub>2</sub> and SO<sub>2</sub>, involving relatively low regeneration energy requirements [3]. Recently this topic was reviewed extensively by Zhang et al. [30]

ILs are typically formed with the combination of a large organic cation, that is, imidazolium, pyridinium or phosphonium cation with either an inorganic anion such as Cl<sup>-</sup>, BF<sub>4</sub><sup>-</sup> and PF<sub>6</sub><sup>-</sup>, or an organic anion, that is, RCO<sub>2</sub><sup>-</sup> and CF<sub>3</sub>SO<sub>3</sub><sup>-</sup> [31]. Special functional groups are also being under consideration for ILs formulations [30]. In general for conventional ILs, anions have more impact on the solvent performance during the absorption process, being the influence of cations considerably lower. Although ILs provide higher CO<sub>2</sub> solubility and selectivity for CCS applications, some authors stated the use of functionalized IL are required in order to make ILs competitive in comparison with amine-based chemical absorption option [30].

Conventional ILs interact with CO<sub>2</sub> as a physical solvent. They enhance the CO<sub>2</sub> solubility following a Henry's law behavior. Functionalized ILs contain an amino group to improve the CO<sub>2</sub> absorption capacity and the kinetics by means of Zwitterion mechanisms as it occurs with primary and secondary amines. Nowadays, researchers are focusing on the development of ILs as a promising CCS approach based on their exceptional properties as a solvent for CO<sub>2</sub> capture. In this respect, the key property provided by ILs derived from their extremely high capacity to be synthesized in a large number of configurations. The tuneable solvent characteristic of ILs

allows them to offer unique molecular structures specifically designed for each application, in particular for low CO<sub>2</sub> concentrated flue gas treatment [30, 32, 33]. Other properties such as their low vapor pressure must be also taking into account due to its impact on the environment. ILs are non-volatile compounds and therefore the presence of ILs in the cleaned exhaust gas after CO<sub>2</sub> separation step is negligible. In this sense, solvent losses associated to ILs are assumed to be completely avoided in a CO<sub>2</sub> capture process based on these emerging solvents. This property is also related to low energy requirements during the solvent regeneration. Several studies reported up to 15% of reduction of the specific energy consumption of MEA functionalized ILs compared to conventional MEA-based scrubbing [33, 34].

Despite their potential for carbon capture, there are some disadvantages that constrain their competitiveness of ILs compared to conventional solvents. ILs show relatively high viscosity, limiting their mass transfer capacities. Indeed, they become excessively viscous once CO<sub>2</sub> is absorbed, producing solvent pumping issues as well as mass transfer and operational difficulties during the overall CO<sub>2</sub> capture process. According to Luo and Wang [32], the increase of the viscosity after the CO<sub>2</sub> absorption is due to the formation of strong and dense hydrogen-bonded networks between the compounds formed by the Zwitterion and dication mechanisms. Authors proposed to promote ILs by the use of non-amine functionalized ILS to avoid the formation of hydrogen bonds [35, 36]. Other proposals such as introducing ether oxygen atoms into the ILs structure and adding particular molecular solvents to provide IL-based solvents were found in the literature. For instance, the use of organic amines instead of water decrease also the viscosity without reducing the CO<sub>2</sub> absorption capacity [30]. Finally, it is necessary to point out that they are also relatively expensive in comparison with common amine-based solvents [37]. Other aspect that should be further investigated in order to address the main knowledge gaps are indicated below:

- Determination of transport properties, physical properties, absorption kinetics of the best performance ILs.
- Efforts on developing new combinations of IL using membranes.
- Development of simulation tools that can predict the chemistry of the interactions in multi-components systems.
- The evaluation of the toxicity and environmental impact derived from the use of IL and its derivatives.
- Investigations on the task-specific IL and the mechanisms involved in CO<sub>2</sub>-IL interactions in order to improve the feasibility of its use as a potential CO<sub>2</sub> separation approach.

As it was mentioned previously, numerous ILs formulae have been developed for last 20 years. Pure ILs configurations, typically referred as room-temperature ionic liquid (RTILs), retain CO<sub>2</sub> by physisorption mechanism showing an unfeasible CO<sub>2</sub> absorption performance in comparison with conventional amine-based solvents. The next generation of ILs was defined from the combination of conventional ILs with a functionalized amine group, preferable. Based on this configuration, amine-functionalized IL, also called task-specific IL, reacts with CO<sub>2</sub> by chemisorption showing further improvements on the CO<sub>2</sub> capture process derived from physisorption-based ILs. The development of this type of ILs enhanced the performance of IL in both biogas/natural gas treatment and CCS. **Table 5** summarizes the best performance IL reported from the literature.

IL	Abbreviation	Field	Ref.	$\mu^*$ (cP)	CO <sub>2</sub> <sup>***</sup> load.
1-butylpyridinium tetrafluoroborate	[Bpy] [BF <sub>4</sub> ]	Post-combustion	[34]	150	<0.05 <sup>***</sup>
Tryhexyl(tetradecyl)-phosphonium imidazole	[P <sub>66614</sub> ]	Post-combustion	[35]	223–1077	0.3–0.91
1-butyl-3-methyl-imidazolium hexafluorophosphate	[bmim][PF <sub>6</sub> ]	Post-combustion	[38]	—	0.75
(Trifluoromethyl sulfonyl)imide-based IL	[Tf <sub>2</sub> N]	Biogas/natural gas upgrading	[39]	—	0.66–0.84
1-butyl-3-methyl-imidazolium acetate	[bmim][Ac]	Biogas/natural gas upgrading	[39]	—	—
Allyl-pyridinium bis(trifluoromethylsulfonyl)imide	[Apy] [Tf <sub>2</sub> N]	Pre-combustion	[40]	17.7–28	—

<sup>\*</sup>Viscosity measurements below 300 K.  
<sup>\*\*</sup>Pressure over 1 MPa.  
<sup>\*\*\*</sup>Ambient pressure.

**Table 5.** Summary of the best performance IL applied as solvents for CO<sub>2</sub> separation.

The basic of the minimum energy requirement for CO<sub>2</sub> release from ILs consist of the weak interaction between both species. In general, some studies indicated that CO<sub>2</sub>-IL interaction strongly depend on van der Waals forces in case small and symmetric molecular structures are provided, whereas electrostatic interactions dominates as large and asymmetric molecular structures are used. Besides the acid-base interaction also plays a key role as a mechanism for CO<sub>2</sub>-IL interaction. It should be noted that some authors state the relevant impact that the structure of IL has on the CO<sub>2</sub> solubility. The amount of free space provided by means, that is, the length chain, the presence of species such as F<sup>-</sup> increase the CO<sub>2</sub> capacity of IL. The higher free volume available, the higher CO<sub>2</sub> solubility of the IL [30].

Most recent applications of IL involve the use of membranes for CO<sub>2</sub> separation. Research on this field demonstrate the combination of IL with membrane significantly reduces the viscosity during the CO<sub>2</sub> absorption process and also ensures further improvements of the gas separation performance in terms of CO<sub>2</sub> permeability and selectivity [30]. The supported IL membranes (SILM), the poly(ionic liquid)-ionic liquid composite membranes, the combination of facilitated transport membranes with IL and the incorporation of task-specific IL into mixed matrix membranes have shown a high potential as a CO<sub>2</sub> separation approach. Based on the literature, two main mechanisms are identified for IL-based membranes, namely solution-diffusion and facilitated transport mechanism [30]. The new pathway discovered regarding IL and its use as a CO<sub>2</sub> separation approach requires further investigation.

## 2.6. New generation solvents for carbon dioxide capture

New generation solvents proposed are focused on energetic consumption reduction in order to make CO<sub>2</sub> chemical absorption a cost-competitive technology to be deployment at CCS industrial scale. It is well-known that most of the energy consumption takes place in the regeneration step

of the CO<sub>2</sub> capture process. Two main research lines about new generation solvents will be discussed in this section, namely water-free solvents and biphasic solvents.

### 2.6.1. Water-free solvents

Despite the benefits of using water as a diluent in order to reduce the corrosion and viscosity issues along the CO<sub>2</sub> chemical absorption plant, its presence in solvent formulation increases the energy requirements in the regeneration stage. In this sense, several novel water-free solvents are being formulated such as non-aqueous organic amine blends, aminosilicones or amines with superbase [41].

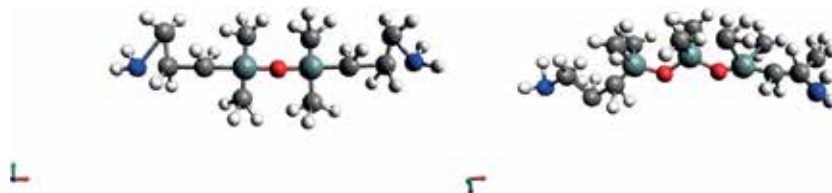
#### 2.6.1.1. Aminosilicones

Aminosilicones are one of the most relevant solvents currently under investigation. Besides the absence of water in its formulation, the hybrid nature of this type of solvents (physisorbing and chemisorbing) provides a potential improvement in CO<sub>2</sub> capture due to the possibilities that its chemical nature offers.

Perry et al. developed GAP-0 and GAP-1 aminosilicones formulated as a CO<sub>2</sub>-philic siloxane backbone and a CO<sub>2</sub> reactive amino group (**Figure 4**) [42, 43]. The absorption capacity of these compounds is higher than the theoretical of the selected amino group due to the physisorption phenomenon that occurs in this type of blends. However, the possibility of solid formation and the increase of viscosity during the absorption process make necessary to use cosolvents in order to avoid the above-mentioned issues.

#### 2.6.1.2. Non-aqueous organic blends

This type of solvents has been studied by some research groups including, for example, Kim et al. In this work, sterically hindered amines 2-[(1,1-dimethylethyl)amino]ethanol (TBAE) and 1-[(1,1-dimethylethyl)amino]-2-propanol (TBAP) were tested using organic compounds as solvents such as methanol and ethylene glycol [44–47]. The efficiency of this type of solvents is also revealed by Mani et al. In this work, AMP mixed with different alkanolamines (DEA, MDEA, MMEA and DIPA) and using organic solvents were analyzed [48, 49]. The tests concluded that, among other considerations, the absorption efficiency at equilibrium ranged 73–96% (**Table 6**).



**Figure 4.** GAP-0 (on the left) and GAP-1 aminosilicones (on the right). Note that gray balls represent C atoms; white balls represent H atoms; red/dark gray balls represent O atoms; dark blue/black balls represent N atoms; black small balls represent Si atoms.

Entry	Amine	Solvent	Amine conc. (wt%)	Loading capacity (wt%)	Average absorpt. efficiency and desorpt. temp (°C)	
					65	80
1	AMP/DEA	DEGMME	18.3	31.7	73.1	91.6
2	AMP/MDEA	EG/methanol	20.7	28.7	—	93.5
3	AMP/MMEA	EG/methanol	16.9	43.4	76.7	95.9
4	AMP/MMEA	EG/ethanol	16.8	40.7	—	92.6
5	AMP/DIPA	EG/ethanol	22.6	27.3	—	93.1

Adapted from Ref. [49].

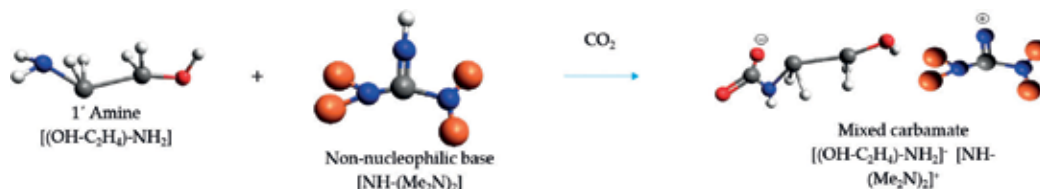
**Table 6.** CO<sub>2</sub> loading capacity at 20°C and absorption efficiency by different amines at increasing desorption temperatures. The overall amine concentration is 2.0 mol dm<sup>-3</sup>.

### 2.6.1.3. Amines with superbase promoters

Amines with superbase promoters might allow an increase in the CO<sub>2</sub> capture efficiency. This type of solvents combines a primary amine and a strong non-nucleophilic base which enhances the proton transfer from the primary amino group, facilitating the carbamate formation (**Figure 5**). CO<sub>2</sub> capture efficiency and the kinetic behavior of a primary amine using a superbase promoter could be increased over 30%. In addition, several solvents are able to work even at high temperatures (over 50°C), which make them useful in high temperature process. Nevertheless, these blends present similar issues than aminosilicones. The possibility of solid formation and the increase of viscosity during the absorption process make necessary to use organic cosolvents such as dimethylsulfoxide (DMSO), especially with nucleophilic polyamines [50, 51].

### 2.6.2. Biphasic solvents

In the last decades, it has been assumed that biphasic mixtures generation during CO<sub>2</sub> amine-based capture processes becomes an operation issue in terms of liquid circulation and homogeneity of the solvents, especially in the regeneration step. However, recent studies support the new idea that a decrease in the energy requirements using biphasic solvents would be possible.



**Figure 5.** Reaction of CO<sub>2</sub>-primary amines in the presence of a strong non-nucleophilic base. Note that gray balls represent C atoms; black big balls represent dimethyl groups; white balls represent H atoms; red/dark gray balls represent O atoms; dark blue/black balls represent N atoms.

Type	Absorbent	Absorption		Desorption	Stripping	Temp. (°C)
		Absorption rate (g/(Lh))	Rich loading (g/L)	Cyclic loading I (g/L)	Cyclic loading II (g/L)	
Primary solvent	DMCA	72	101	71	88	40–70
	MDEA	30	59	30	43	40–70
Activator	A1	130	124	86	101	40–80
	DPA	127	88	65	78	40–80
	MEA (30 wt%)	127	122	28	47	40–80
Blend 3:1	DMCA + DPA	89	90	80	86	40–75
	DMCA + A1	94	117	105	112	40–75
	MDEA + MEA	47	62	26	48	40–75

**Table 7.** Main properties of selected amines in 3 M aqueous solutions. Adapted from ref. [52].

This argument is based on the optimization of the solvent volume treated in regeneration step, stripping only the CO<sub>2</sub>-rich phase [52].

#### 2.6.2.1. TETA/ethanol blends

In recent years, polyamine compounds and blends have been studied in order to improve the CO<sub>2</sub> absorption capacity in CCS technologies. A higher amount of amine functional groups, using water as a dissolvent, provides the polyamines higher absorption rates, but in spite of that fact, regeneration penalties and solvent circulation costs due to the high viscosity of this kind of compounds made unfeasible its application in pilot plants. Triethylenetetramine (TETA) using ethanol as dissolvent was tested by Zheng et al. [53]. In this work, solid generation occurs after the CO<sub>2</sub> reaction with TETA. Solid phase generated and separated, containing a total of 81.8% of the captured CO<sub>2</sub>, allows a lower cost regeneration process due to the fact that liquid phase can be recycled back to the absorption process without energy consumption. The precipitate formed after CO<sub>2</sub> absorption can be regenerated heating to 90°C and returning to liquid phase TETA. This new solvent represents an alternative to the usual polyamine-water solvents although the high vapor pressure of ethanol must be considered in order minimize evaporation losses.

#### 2.6.2.2. Phase change amine blends

Recent studies showed that some types of blended amines have the property of forming two different liquid phases after reaction with CO<sub>2</sub> in capture process. This capacity of the solvent, provides the possibility of perform selective regeneration process, being only the rich amine treated inside the regeneration reboiler. 3-(methylamino)propylamine (MAPA) and 2-(diethylamino)ethanol (DEEA) blend was studied by Bruder and Svendsen showing a promising behavior in the CO<sub>2</sub> capture process compared with habitual solvents currently used for this proposal as, for example, 30 wt.% MEA [54].

### 2.6.2.3. Lipophilic-amine-based thermomorphic biphasic solvents

Lipophilic-amine-based thermomorphic biphasic solvents have shown potential advantages in CO<sub>2</sub> capture compared to conventional alkanolamines in terms of solvent regeneration and cyclic capacity. The improvements obtained using these types of solvent are based on its thermomorphic behavior. This phenomenon consists of the generation of two liquid phases after heating inside the reboiler. According to Zhang et al. [52], these systems can be regenerated at lower temperatures than the conventional alkanolamine blends. This temperature reduction in regeneration step allows a decrease of the energetic consumption in CO<sub>2</sub> capture processes. Amine blends used by Zhang were mostly composed of an absorption activator: A1, dipropylamine (DPA) and a regeneration promoter: N, N-dimethylcyclohexylamine (DMCA) and N-ethylpiperidine (EDP) (Table 7).

## 3. Physical absorption solvents

Physical absorption processes are highly recommended to separate CO<sub>2</sub> in pre-combustion processes that commonly operate at elevated CO<sub>2</sub> partial pressure. Physical solvents are able to selectively capture CO<sub>2</sub> in contact with a gas stream without a chemical reaction occurring. As it was indicated in the introduction section, the high partial pressures of CO<sub>2</sub> and low-temperatures are desirable to obtain an optimized performance of the physical absorption process in terms of absorption rates and solubility equilibrium of CO<sub>2</sub>. Then, the rich (CO<sub>2</sub> loaded) solvent is regenerated [55].

Focusing on the pre-combustion CO<sub>2</sub> capture process itself, seven processes using physical solvents are currently commercially available, which are discussed in the following section.

A summary of the most relevant physical properties of each solvent and the list of advantages and disadvantages can be found at the end of this chapter in Table 8.

### 3.1. Selexol™

The Selexol™ process has been widely used and effectively proven in the refinery industry, natural gas sweetening, syngas processing and fertilizer production since the 1960s. Recently, Selexol™ has also been used in IGCC for H<sub>2</sub>S, COS and CO<sub>2</sub> removal.

The Selexol™ process, licensed by Universal Oil Products (UOP), employs a mixture of different dimethyl ethers and polyethylene glycol, represented by the formulae (CH<sub>3</sub>O(C<sub>2</sub>H<sub>4</sub>O)<sub>n</sub>CH<sub>3</sub>), with n factor ranging from 3 to 9 [2]. This physical solvent was patented by DOW chemical [56]. Selexol™ provides a selective absorption of H<sub>2</sub>S, COS, mercaptans and CO<sub>2</sub> from a variety of natural and synthesis gas streams. It has shown a high performance under high-pressure, low-temperature and high acid gas process conditions.

In the Selexol™ process, the flue gas must be first dehydrated before being introduced in the absorption column. After that, the dehydrated flue gas enters the absorber at 30 atm and 0–5°C and the acid gas components are selectively absorbed into the solvent along the



Process	Advantages	Disadvantages
Selexol™	<ul style="list-style-type: none"> <li>• Non-thermal solvent regeneration</li> <li>• Non-corrosive solvent</li> <li>• Dry gas leaves from the absorber</li> </ul>	<ul style="list-style-type: none"> <li>• Most efficient at elevated pressures</li> </ul>
Rectisol™	<ul style="list-style-type: none"> <li>• Non-foaming solvent</li> </ul>	<ul style="list-style-type: none"> <li>• High refrigeration costs</li> </ul>
Ipexol-2™	<ul style="list-style-type: none"> <li>• High chemical and thermal stability</li> <li>• Non-corrosive solvent</li> </ul>	<ul style="list-style-type: none"> <li>• High capital costs</li> <li>• Amalgams formation at low T</li> </ul>
Fluor™	<ul style="list-style-type: none"> <li>• High CO<sub>2</sub> solubility</li> <li>• Non-thermal regeneration</li> <li>• Simple operation</li> <li>• Non-corrosive solvent</li> </ul>	<ul style="list-style-type: none"> <li>• High solvent circulation rates</li> <li>• Expensive solvent</li> </ul>
Purisol™	<ul style="list-style-type: none"> <li>• Non-foaming solvent</li> <li>• High chemical and thermal stability</li> <li>• Non-corrosive solvent</li> <li>• Low volatility</li> </ul>	<ul style="list-style-type: none"> <li>• High compression cost</li> <li>• Most efficient at high-pressure</li> </ul>
Sulfinol™	<ul style="list-style-type: none"> <li>• High capacity</li> <li>• Low solvent circulation rate</li> </ul>	<ul style="list-style-type: none"> <li>• Foaming issues</li> <li>• Corrosive solvent</li> <li>• Thermal regeneration</li> </ul>
Morphysorb™	<ul style="list-style-type: none"> <li>• High solvent loading capacity</li> <li>• Low energy requirement</li> <li>• Non-corrosive solvent</li> <li>• Low capital and operating costs</li> </ul>	<ul style="list-style-type: none"> <li>• New process</li> </ul>

**Table 8.** Main advantages and disadvantages of physical absorption technologies available for CO<sub>2</sub> capture [58, 59].

column. A pre-treatment absorption column can be used to accomplish the sulfur compound removal prior to CO<sub>2</sub> separation. The CO<sub>2</sub> loaded solvent is then sent to the regeneration process from which the solvent recovers its original capacity by either reducing the pressure or inert gas stripping. The recovered (lean) solvent is recycled back into the absorber, whereas the high purity CO<sub>2</sub> exits the regeneration stages to be compressed and stored.

### 3.2. Rectisol™

The Rectisol™ process is applied in H<sub>2</sub>S and CO<sub>2</sub> removal from syngas streams, mainly from heavy oil and coal gasification. The CO<sub>2</sub> stream obtained can be used in urea, methanol and ammonia production, but it is not applied for the food and beverage industry. It has a high selectivity for H<sub>2</sub>S, CO<sub>2</sub> and COS and can be configured to accomplish the separation of synthesis gas into various components depending on the final product specifications and process objectives.

Rectisol™ is licensed by Lurgi AG, which is an affiliated company of Air Liquide. This technology employs chilled methanol as solvent and can be applied for low and moderate CO<sub>2</sub> concentrated gas streams. Due to the high vapor pressure of the solvent, the absorption stage must be carried out at very low-temperatures to reduce solvent losses [57].

In the Rectisol™ process, the raw syngas is cooled before being introduced into the absorption process. The sulfur compounds must be firstly removed using a CO<sub>2</sub> loaded solvent. After that, the sulfur exempt syngas contacts with the chilled methanol in the absorber, operating at 50 atm and temperatures in the range of [-100°C, -30°C]. The rich solvent is then sent to the regeneration stage where CO<sub>2</sub> is released by flash desorption, reducing the pressure up to 1 bar. The lean solvent is recycled back to the absorber [2, 57].

### 3.3. Ifpexol™

The Ifpexol™ process introduced in 1991 can be used for natural gas applications. This process is based on two steps as follows: Ifpex-1™ removes condensable hydrocarbons and water and Ifpex-2™ removes acid gas [58]. Ifpexol™ is licensed by Prosernat and uses refrigerated methanol as physical solvent.

The Ifpexol-2™ process for acid gas removal is similar to an amine-based chemical absorption process except for the operating temperatures. The absorber operates below -29°C to minimize methanol losses, and the regenerator operates at about 6 bar. Cooling is required on the regenerator condenser to recover the methanol releasing during the regeneration step. This process usually follows the Ifpexol-1™ process so excessive hydrocarbon absorption is not as great a problem [59].

### 3.4. Fluor™

Fluor™ process is the most suitable physical absorption process to be applied for high CO<sub>2</sub> partial pressure syngas streams and has been in use since the late 1950s. Fluor™ is licensed by Fluor Daniel, Inc. and employs propylene carbonate (C<sub>4</sub>H<sub>6</sub>O<sub>3</sub>) as solvent (available as JEFFSOL™ PC solvent), which has a lower vapor pressure than those used by Rectisol™ and Selexol™. The solvent requires neither a low nor no presence of H<sub>2</sub>S and can be applied in large CO<sub>2</sub> removal applications [60, 61].

In the Fluor™ process, physical absorption occurs at moderate to high-pressure, ranging between 30 and 80 bar, and at ambient temperature. The flue gas must be dehydrated before the gas enters into the absorption column to prevent water build-up in the solvent. As indicated before, H<sub>2</sub>S must also be removed before the CO<sub>2</sub> absorption occurs. After CO<sub>2</sub> is absorbed, the CO<sub>2</sub> loaded solvent is flashed to release CO<sub>2</sub> and recovers its original capacity. The lean solvent is recycled back to the absorber, whereas the high purity CO<sub>2</sub> exits the regeneration stages to be compressed and stored [62].

### 3.5. Purisol™

The Purisol™ process is particularly suited to treat high-pressure, high CO<sub>2</sub> synthesis gas from IGCC systems because of the high selectivity for H<sub>2</sub>S. This technology is licensed by Lurgi AG and employs N-methyl pyrrolidone.

In the Purisol™ process, H<sub>2</sub>S removal is not required prior to CO<sub>2</sub> absorption occurring. The process can be operated at 50 bar and either at ambient temperature or with refrigeration down to about -15°C. The CO<sub>2</sub> desorption is accomplished by stripping with an inert gas [63].

### 3.6. Sulfinol™

The Sulfinol™ process can remove H<sub>2</sub>S, CO<sub>2</sub>, carbonyl sulfide, mercaptans and organic sulfur components from natural and synthesis gas from coal or oil gasifiers and steam reformers. This process accomplishes H<sub>2</sub>S and CO<sub>2</sub> separation in a wide variety of compositions up to around 50%v/v H<sub>2</sub>S and above 20%v/v CO<sub>2</sub>. The principle of this process aims at combining the high absorption potential of alkanolamine (chemical absorption) and the low regeneration energy requirement of the physical solvent (physical absorption).

Sulfinol™ is licensed by Shell Oil Company and employs mixtures of diisopropylamine (DIPA) or methyldiethanolamine (MDEA) and tetrahydrothiophene dioxide (SULFOLANE) in different blends. The physical solvent used (DIPA or MDEA) has a higher absorption capacity and a low energy requirement for regeneration, thus increasing the carrying capacity due to lower solvent recycled requirements. The absorber is operated at 40°C and a pressure around 60–70 bar. The rich solvent is then sent to the stripping column where CO<sub>2</sub> is released at temperatures over 110°C and vacuum pressure. It should be noted that addition of anti-foam is needed in the absorber and solvent degrades due to the presence of oxygen and stripper temperatures [64].

### 3.7. Morphysorb™

The Morphysorb™ process is applied for selective removal of H<sub>2</sub>S, CO<sub>2</sub>, COS, CS<sub>2</sub>, mercaptans and other components from coal/oil gasification syngas at IGCC facilities. This process is particularly effective for high-pressure and high acid gas applications and offers substantial savings in investment and operating cost compared to the competitive physical solvent-based processes. The operational cost is 30–40% lower than that for Selexol™ Process [65, 66].

This technology is developed by Krupp Uhde GmbH in cooperation with the Institute of Gas Technology (GTI), and employs N-formyl morpholine (NFM) and N-acetyl morpholine (NAM) mixtures as solvent (manufactured by BASF AG). In comparison with other physical solvents, the Morphysorb solvent co-absorbs fewer heavier hydrocarbons and is also suited for simultaneous water removal from the feed gas [67]. In this process, the acid gases are removed from the absorbent by flashing and the regenerated absorbent is recycled to the absorbent. The physical absorption occurs at temperatures between -20 and +40°C and at pressure of 10–150 bar [67]. The key advantage of the Morphysorb™ technology is the high acid gas capacity together with the low solubility of C1–C3 hydrocarbons, resulting in a higher product yield and a lower recycle flash stream [68].

## 4. Conclusions

Physical and chemical CO<sub>2</sub> absorption are mature technologies that can be applied to CO<sub>2</sub> emission mitigation at large scale, mainly focused on fossil-fuel power plants, cement production and steel manufacturing. This chapter summarizes the cutting-edge of the knowledge about absorbents developed for this proposal. The most relevant aspect of conventional physical and chemical solvents applied to CO<sub>2</sub> capture was summarized and their physical properties, absorption mechanisms and kinetics were further discussed. Based on the current state-of-art in the field of CO<sub>2</sub> absorption, the novel solvents and blends were also reported and new applications such as ionic liquids have been deeply discussed along the manuscript from the specific literature available on this topic.

## Acknowledgements

This work was carried out with the financial support of the Ministry of Economy and Competitiveness of the Spanish Government (OXYSOLVENT Pro.; ref: CTM-2014-58573-R) co-financed by the European Development Research Fund (EDRF) from European Union.

## Author details

Fernando Vega\*, Mercedes Cano, Sara Camino, Luz M. Gallego Fernández,  
Esmeralda Portillo and Benito Navarrete

\*Address all correspondence to: fvega1@us.es

Chemical and Environmental Engineering Department, School of Engineering, University of Seville, Seville, Spain

## References

- [1] U.S. Energy Information Administration. International Energy Outlook 2016, 1st ed. Washington: IEA; 2016
- [2] Hammond GP, Spargo J. The prospects for coal-fired power plants with carbon capture and storage: A UK perspective. *Energy Conversion and Management*. 2014;**86**:476-489
- [3] Rubin ES, Mantripragada H, Marks A, Versteeg P, Kitchin J. The outlook for improved carbon capture technology. *Progress in Energy and Combustion Science*. 2012;**38**(5):630-671
- [4] Kohl L, Nielsen RB. Alkanolamines for Hydrogen Sulfide and Carbon Dioxide Removal. *Gas Purif*. 5th ed. Houston, Texas: Gulf Publication; 1997. 900 p

- [5] Vega F, Sanna A, Navarrete B, Maroto-Valer MM, Cortes VJ. Degradation of amine-based solvents in CO<sub>2</sub> capture process by chemical absorption. *Greenhouse Gases: Science and Technology*. 2014;4(6):707-733
- [6] Rochelle GT, Bishnoi S, Chi S, Dang H, Santos J. *Research Needs for CO<sub>2</sub> Capture from Flue Gas by Aqueous Absorption/Stripping*. United States: US Department of Energy—Federal Energy Technology Center. Austin; 2001
- [7] Mitra S. *A Technical Report on Gas Sweetening by Amines*. India; 2015
- [8] Liang Z, Rongwong W, Liu H, Fu K, Gao H, Cao F, et al. Recent progress and new developments in post-combustion carbon-capture technology with amine based solvents. *International Journal of Greenhouse Gas Control*. 2015;40:26-54
- [9] Vaidya PD, Kenig EY. CO<sub>2</sub>-alkanolamine reaction kinetics: A review of recent studies. *Chemical Engineering and Technology*. 2007;30(11):1467-1474
- [10] Olajire AA. CO<sub>2</sub> capture by aqueous ammonia process in the clean development mechanism for Nigerian oil industry. *Frontiers of Chemical Science and Engineering*. 2013;7(3): 366-380
- [11] Hüser N, Schmitz O, Kenig EY. A comparative study of different amine-based solvents for CO<sub>2</sub>-capture using the rate-based approach. *Chemical Engineering Science*. 2017;157: 221-231
- [12] Sartori G, Savage DW. Sterically hindered amines for carbon dioxide removal from gases. *Industrial and Engineering Chemistry Fundamentals*. 1983;22(2):239-249
- [13] Knuutila H, Svendsen HF, Juliussen O. Kinetics of carbonate based CO<sub>2</sub> capture systems. *Energy Procedia*. 2009;1(1):1011-1018
- [14] Spigarelli BP, Kawatra SK. Opportunities and challenges in carbon dioxide capture. *Journal of CO<sub>2</sub> Utilization*. 2013;1:69-87
- [15] Sharma MM, Danckwerts PV. Fast reactions of CO<sub>2</sub> in alkaline solutions. *Chemical Engineering Science*. 1963;18:729-735
- [16] Nuchitprasittichai A, Cremaschi S. Optimization of CO<sub>2</sub> capture process with aqueous amines using response surface methodology. *Computers and Chemical Engineering*. 2011; 35(8):1521-1531
- [17] Du Y, Li L, Namjoshi O, Voice AK, Fine NA, Rochelle GT. Aqueous piperazine/N-(2-aminoethyl) piperazine for CO<sub>2</sub> capture. *Energy Procedia*. 2013;37:1621-1638
- [18] Singh P, Versteeg GF. Structure and activity relationships for CO<sub>2</sub> regeneration from aqueous amine-based absorbents. *Process Safety and Environment Protection*. 2008;86(5):347-359
- [19] Choi WJ, Seo JB, Jang SY, Jung JH, Oh KJ. Removal characteristics of CO<sub>2</sub> using aqueous MEA/AMP solutions in the absorption and regeneration process. *Journal of Environmental Sciences*. 2009;21(7):907-913

- [20] Rangwala HA, Morrell BR, Mather AE, Otto FD. Absorption of CO<sub>2</sub> into aqueous tertiary amine/mea solutions. *Canadian Journal of Chemical Engineering*. 2009;**70**(3):482-490
- [21] Cullinane JT, Rochelle GT. Carbon dioxide absorption with aqueous potassium carbonate promoted by piperazine. *Chemical Engineering Science*. 2004;**59**(17):3619-3630
- [22] Lee SS, Mun SM, Choi WJ, Min BM, Cho SW, Oh KJ. Absorption characteristics of new solvent based on a blend of AMP and 1,8-diamino-p-menthane for CO<sub>2</sub> absorption. *Journal of Environmental Sciences*. 2012;**24**(5):897-902
- [23] Tong D, Maitland G, Trusler MFP. Solubility of carbon dioxide in aqueous blends of 2-amino-2-methyl-1-propanol and piperazine. *Chemical Engineering Science*. 2013;**101**:851-864
- [24] Li L, Voice A, Li H, Namjoshi O, Nguyen T, Du YRG. Amine blends using concentrated piperazine. *Energy Procedia*. 2013;**37**:353-369
- [25] Chen E. Carbon dioxide absorption into piperazine promoted potassium carbonate using structured packing [thesis]. Austin: University of Texas; 2007
- [26] Artanto Y, Jansen J, Pearson P, Puxty G, Cottrell A, Meuleman E, et al. Pilot-scale evaluation of AMP/PZ to capture CO<sub>2</sub> from flue gas of an Australian brown coal-fired power station. *International Journal of Greenhouse Gas Control*. 2014;**20**:189-195
- [27] Kemper J, Ewert G, Grünwald M. Absorption and regeneration performance of novel reactive amine solvents for post-combustion CO<sub>2</sub> capture. *Energy Procedia*. 2011;**4**:232-239
- [28] Brúder P, Lauritsen KG, Mejdell T, Svendsen HF. CO<sub>2</sub> capture into aqueous solutions of 3-methylaminopropylamine activated dimethyl-monoethanolamine. *Chemical Engineering Science*. 2012;**75**:28-37
- [29] Singh A, Sharma Y, Wupardrasta Y, Desai K. Selection of amine combination for CO<sub>2</sub> capture in a packed bed scrubber. *Resources and Technology*. 2016;**2**:S165-S170
- [30] Zeng S, Zhang X, Bai L, Zhang X, Wang H, Wang J, et al. Ionic-liquid-based CO<sub>2</sub> capture systems: Structure, interaction and process. *Chemical Reviews*. 2017;**117**:9625-9673
- [31] Galán Sánchez LM, Meindersma GW, De Haan AB. Kinetics of absorption of CO<sub>2</sub> in amino-functionalized ionic liquids. *Chemical Engineering Journal*. 2011;**166**(3):1104-1115
- [32] Luo X, Wang C. The development of carbon capture by functionalized ionic liquids. *Current Opinion in Green and Sustainable Chemistry*. 2017;**3**:33-38
- [33] Zhang XX, Zhang XX, Dong H, Zhao Z, Zhang S, Huang Y. Carbon capture with ionic liquids: Overview and progress. *Energy & Environmental Science*. 2012;**5**(5):6668
- [34] Huang Y, Zhang X, Zhang X, Dong H, Zhang S. Thermodynamic modeling and assessment of ionic liquid-based CO<sub>2</sub> capture processes. *Industrial & Engineering Chemistry Research*. 2014;**53**:11805-11817
- [35] Wang C, Luo H, Li H, Zhu X, Yu B, Dai S. Tuning the physicochemical properties of diverse phenolic ionic liquids for Equimolar CO<sub>2</sub> capture by the substituent on the anion. *Chemistry—A European Journal*. 2012;**18**(7):2153-2160

- [36] Wang C, Luo X, Luo H, Jiang D, Li H, Dai S. Tuning the basicity of ionic liquids for equimolar CO<sub>2</sub> capture. *Angewandte Chemie International Edition*. 2011;**50**(21):4918-4922
- [37] Kumar S, Cho JH, Moon I. Ionic liquid-amine blends and CO<sub>2</sub>BOLs: Prospective solvents for natural gas sweetening and CO<sub>2</sub> capture technology – A review. *International Journal of Greenhouse Gas Control*. 2014;**20**:87-116
- [38] Blanchard LA, Hancu D, Beckman EJ, Brennecke JF. Green processing using ionic liquids and CO<sub>2</sub>. *Nature*. 1999;**399**(6731):28-29
- [39] García-Gutiérrez P, Jacquemin J, McCrellis C, Dimitriou I, Taylor SFR, Hardacre C, et al. Techno-economic feasibility of selective CO<sub>2</sub> capture processes from biogas streams using ionic liquids as physical absorbents. *Energy & Fuels*. 2016;**30**(6):5052-5064
- [40] Siefert NS, Agarwal S, Shi F, Shi W, Roth EA, Hopkinson D, et al. Hydrophobic physical solvents for pre-combustion CO<sub>2</sub> capture: Experiments, computational simulations, and techno-economic analysis. *International Journal of Greenhouse Gas Control*. 2016;**49**:364-371
- [41] Heldebrant DJ, Koech PK, Glezakou V-A, Rousseau R, Malhotra D, Cantu DC. Water-lean solvents for post-combustion CO<sub>2</sub> capture: Fundamentals, uncertainties, opportunities, and outlook. *Chemical Reviews*. 2017;**117**:9594-9624
- [42] Perry RJ, Davis JL. CO<sub>2</sub> capture using solutions of alkanolamines and aminosilicones. *Energy and Fuels*. 2012;**26**(4):2512-2517
- [43] Perry RJ, Grocela-Rocha TA, O'Brien MJ, Genovese S, Wood BR, Lewis LN, et al. Amino-silicone solvents for CO<sub>2</sub> capture. *ChemSusChem*. 2010;**3**(8):919-930
- [44] Im J, Hong SY, Cheon Y, Lee J, Lee JS, Kim HS, et al. Steric hindrance-induced zwitterionic carbonates from alkanolamines and CO<sub>2</sub>: Highly efficient CO<sub>2</sub> absorbents. *Energy & Environmental Science*. 2011;**4**(10):4284
- [45] Choi Y, Im J, Jeong JK, Hong SY, Jang HG, Cheong M. CO<sub>2</sub> absorption and desorption in an aqueous solution of heavily hindered alkanolamine: Structural elucidation of CO<sub>2</sub>-containing species. *Environmental Science and Technology*. 2014;**1**:4163-4170
- [46] Cheon Y, Jung YM, Lee J, Kim H, Im J, Cheong M, et al. Two-dimensional infrared correlation spectroscopy and principal component analysis on the carbonation of sterically hindered alkanolamines. *Chemphyschem*. 2012;**13**(14):3365-3369
- [47] Hong SY, Lee JS, Cheong M, Kim HS. Isolation and structural characterization of bicarbonate and carbonate species formed during CO<sub>2</sub> absorption/desorption by a hindered alkanolamine. *Energy Procedia*. 2014;**63**:2190-2198
- [48] Barzagli F, Lai S, Mani F. Novel non-aqueous amine solvents for reversible CO<sub>2</sub> capture. *Energy Procedia*. 2014;**63**:1795-1804
- [49] Barzagli F, Mani F, Peruzzini M. Efficient CO<sub>2</sub> absorption and low temperature desorption with non-aqueous solvents based on 2-amino-2-methyl-1-propanol (AMP). *International Journal of Greenhouse Gas Control*. 2013;**16**:217-223

- [50] Calabro et al. Non-aqueous amine scrubbing for removal of carbon dioxide. Patent US91 86617
- [51] Kortunov P, Baugh LS, Calabro DC, Siskin M, Kamakoti P, Li Q, Peiffer DG. Mixed amine and non-nucleophilic base CO<sub>2</sub> scrubbing process for improved adsorption at increased temperatures. Patent US 20120060686A1.
- [52] Zhang J, Nwani O, Tan Y, Agar DW. Carbon dioxide absorption into biphasic amine solvent with solvent loss reduction. *Chemical Engineering Research and Design*. 2011;**89**(8): 1190-1196
- [53] Zheng S, Tao M, Liu Q, Ning L, He Y, Shi Y. Capturing CO<sub>2</sub> into the precipitate of a phase-changing solvent after absorption. *Environmental Science & Technology*. 2014;**48**(15): 8905-8910
- [54] Arshad MW, VonSolms N, Thomsen K, Svendsen HF. Heat of absorption of CO<sub>2</sub> in aqueous solutions of DEEA, MAPA and their mixture. *Energy Procedia* 2013;**37**(1876):1532-1542.
- [55] Theo WL, Lim JS, Hashim H, Mustaffa AA, Ho WS. Review of pre-combustion capture and ionic liquid in carbon capture and storage. *Applied Energy*. 2016;**183**:1633-1663
- [56] UOP. UOP Selexol Technology for Acid Gas Removal Main [Internet]. 2009. Available from: <https://www.uop.com/?document=uop-selexol-technology-for-acid-gas-removal&download=1> [Accessed 2017-06-21]
- [57] Lurgi. The Rectisol® Process [Internet]. 2011. Available from: [https://uicgroupecho.wikispaces.com/file/view/B\\_0308e\\_Rectisol.pdf](https://uicgroupecho.wikispaces.com/file/view/B_0308e_Rectisol.pdf) [Accessed 2017-06-14]
- [58] Lecomte F, Broutin P, Lebas E, Appert O, Jones T. CO<sub>2</sub> capture : Technologies to Reduce Greenhouse Gas Emissions. 1st ed. Paris: Editions Technips; 2010. 176 p
- [59] Mokhatab S, Poe WA. Handbook of Natural Gas Transmission and Processing. 3rd ed. Gulf Professional Pub: United States; 2015. 628 p
- [60] Bucklin R, Schendel R. Comparison of fluor solvent and selexol processes. *Energy Progress*. 1984;**4**(3):137-142
- [61] Reddy S, Johnson D, Gilmartin J. Fluor's Econamine FG Plus SM Technology For CO<sub>2</sub> Capture at Coal-fired Power Plants [Internet]. 2008. Available from: <http://www.fluor.com/SiteCollectionDocuments/FluorEFG-forPost-CombustionCO2CaptureGPAConf-Feb2008.pdf> [Accessed: 2017-06-06]
- [62] Fluor Corporation. Carbon Capture Technologies for Flue gas Streams Reduce Greenhouse gas Emissions [Internet]. 2014. Available from: <http://www.fluor.com/client-markets/energy-chemicals/carbon-capture> [Accessed 2017-07-27]
- [63] Air Liquid. Natural Gas Solution [Internet]. 2013. Available from: <https://industrial.airliquide.es/> [Accessed: 2017-07-27]
- [64] Shell Global Solutions. Sour Gas Processing [Internet]. 2013. Available from: <http://www.shell.com/content/dam/shell-new/global/downloads/pdf/interactive-gas-processing-portfolio-final.pdf> [Accessed 2017-07-27]



- [65] Yu CH, Huang CH, Tan CS. A review of CO<sub>2</sub> capture by absorption and adsorption. *Aerosol and Air Quality Research*. 2012;**12**(5):745-769
- [66] Palla N (Raj), Leppin D. Technical and Operating Support for Pilot Demonstration of Morphysorb Acid Gas Removal Process. GTI Proj 61166. Contract Number DE-FC26-01NT41028. 2004;1-30
- [67] Gross M, Kolbe B, Menzel J, Pohl W. Process for the removal of CO<sub>2</sub> and sulfur compounds from industrial gases, in particular from natural gas and raw synthesis gas. Patent US006102987A
- [68] ThyssenKrupp. Physical Solvents for Acid Gas Removal [Internet]. 2011. Available from: [https://www.thyssenkrupp-industrial-solutions.com/media/products\\_services/chemical\\_plants\\_processes/uhde\\_brochures\\_pdf\\_en\\_14.pdf](https://www.thyssenkrupp-industrial-solutions.com/media/products_services/chemical_plants_processes/uhde_brochures_pdf_en_14.pdf) [Accessed: 2017-07-18]



---

# Advances in Porous Adsorbents for CO<sub>2</sub> Capture and Storage

---

Arindam Modak and Subhra Jana

Additional information is available at the end of the chapter

<http://dx.doi.org/10.5772/intechopen.70796>

---

## Abstract

The steady increase of anthropogenic CO<sub>2</sub> in ambient air, owing to the fossil fuel, power plants, chemical processing and deforestation caused by the usage of land, is a key challenge in the on-going effort to diminish the effect of greenhouse gases on global climate change by developing efficient techniques for CO<sub>2</sub> capture. Global warming as a consequence of high CO<sub>2</sub> level in the atmosphere is considered as one of the major long lasting problems in the twenty-first century. Concern over these major issues with regard to severe climate change and ocean acidification motivated us to develop the technologies that capture the evolved CO<sub>2</sub> from entering into the carbon cycle. Therefore, CO<sub>2</sub> capture and storage technology is attracting increasing interest in order to reduce carbon level in the atmosphere which in turn mitigates global climate issues. In this regard, highly efficient adsorbents e.g.; zeolites, alkali metal oxides, activated carbon, porous silica show considerable progress in post combustion CO<sub>2</sub> capture. Recently, metal-organic frameworks (MOFs), porous organic polymers (POPs), porous clays, N-doped carbon etc. are explored as versatile and quite elegant way for next-generation CO<sub>2</sub> capture. In this chapter, we will discuss the broad prospect of MOFs, POPs, nanoporous clays and porous carbon for CO<sub>2</sub> storage and sequestration through utilization of their nanospace chemistry.

**Keywords:** CO<sub>2</sub> capture and sequestration, metal-organic frameworks (MOFs), porous organic polymers (POPs), nanoporous clays, porous carbon

---

## 1. Introduction

In the late nineteenth century, Goddard Institute for Space Studies (GISS) found that global temperature is increasing on account of global warming at least 0.8°C in every year since 1951, which is continuing to increase still twenty-first century because of the release of greenhouse gases [1]. Based on such criteria “*The Intergovernmental Panel on Climate Change*” (IPCC)

---

declares that this excessive CO<sub>2</sub> emission is markedly related to global climate change and hence could adversely affect global temperature [2]. Furthermore, studies reveal that compared to the CO<sub>2</sub> level of 280 ppm during pre-industrial era, CO<sub>2</sub> concentration increases to 401 ppm in 2015, mainly because of human activity and anthropogenic industrial revolution that needs an ultimatum to check the atmospheric CO<sub>2</sub> level [3]. Thus, in order to diminish carbon level, CO<sub>2</sub> capture and storage/sequestration (CCS) as well as CO<sub>2</sub> capture and utilization (CCU) should have been implemented for considering a ultra-low carbon content environment. Regarding CCS processes, physical adsorption, absorption and membrane separation technologies are being involved to store CO<sub>2</sub> in adsorbents which later buried in deep underground. As for instances, liquid amines like monoethanolamine and diethanolamine are traditionally being utilized to store CO<sub>2</sub> through CCS processes [4], however, despite the wide use of such methods, it suffers from major drawbacks like corrosive nature and volatility of amines, decomposition of the generated salts as well as expensive regeneration cost [5]. Therefore, the requirement of new supports e.g.; porous organic polymers (POPs) [6], metal organic frameworks (MOFs) [7], zeolites [8], zeolitic imidazolate frameworks (ZIF) [9], microporous carbon [10], perovskites, hydrotalcites, clathrate hydrates [11], etc. are mandatory to overcome such drawbacks. It is worth mentioning, porous materials with suitably decorated narrow micropores/ultra narrow micropores are significant in adsorbing large quantity of CO<sub>2</sub> through utilization of hollow nanospace, hence, these materials could be promising in frontier research in order to check the adverse effect of CO<sub>2</sub> that is continuously releasing as tens of billions of tons in each year. Again, MOFs, POPs etc. having wide diversity in structure engineering, can stabilize various organometallic complexes through utilization of their surface functional sites, which in turn enhances their CO<sub>2</sub> adsorption efficacy. Although CCS has wide applications, but only storage in nanopores could partially solve the carbon emission problems because underground leaking cannot be completely ruled out. This circumstance justifies the implementation of suitable process that could simultaneously convert the captured CO<sub>2</sub> to value-added products [12]. Nevertheless, being cheap and easy availability, CO<sub>2</sub> is enriched as C1 feedstock and has broad scope of serving as C1 chemistry to produce important products e.g. fuels, commodity chemicals, agrochemicals, valuable materials and so on [13].

In this chapter, we describe the fabrication of several important solid materials for controlling environmental remediation of CO<sub>2</sub> through CCS techniques and also highlight their potential utility for CO<sub>2</sub> adsorption purposes. However, our major aim is to focus the profound application and usage of several solid-phase adsorbents like, MOFs, POPs, nanoporous carbon, porous clays for CO<sub>2</sub> capture and sequestration study.

## 2. Promising materials for CO<sub>2</sub> capture

### 2.1. Metal-organic frameworks (MOF)

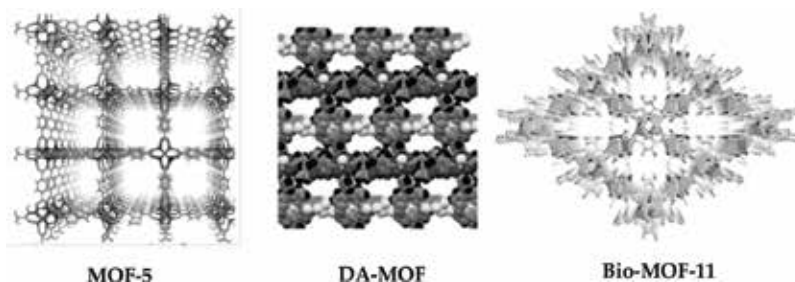
MOFs constitute of a new class of materials which could serve as an ideal platform for the development of next-generation CO<sub>2</sub> capture materials because of their large capacity for adsorption of gases and easy tailorability of their structures [14]. MOFs are also called

coordination polymers because of their propensity to build up by metal atoms (ions) linked together by multifunctional organic ligands. Therefore, MOFs synthesis is a consequence of the linkage between the inorganic and organic chemistry, and it has been considered that MOFs are pioneered by Hagrman et al. [15], Batten and Robson [16], Zhou and Kitagawa [17] and Yaghi et al. [18].

It is customary to say that the framework components of MOFs are required to precisely control for specific type of CO<sub>2</sub> capture e.g. post-combustion capture, pre-combustion capture, oxy fuel combustion and potentially even for the specific power plant in which the capture system is to be installed. In this regard, significant efforts have been made recently in improving the gas separation performances of MOFs and some studies are therefore being under consideration for evaluating the prospects of deploying these materials in real-world CO<sub>2</sub> capture [19]. This has been predominately invented by Noro et al. [20] and Yaghi et al. [18]. The wide diversity in its structure makes it possible to construct material with high surface area [21], tailor the material properties and thus its affinity towards specific gas molecules [22, 23]. Accordingly, it would be possible to develop MOF-based sorbents with large capacity and high selectivity for CO<sub>2</sub> storage purposes.

It can be stated that most of the MOFs are synthesized using non-renewable organic solvents like N,N-dimethylformamide, dioxane, etc., although few MOFs (CD-MOF) can also be made from green solvents like ethanol, water etc. [27]. During synthesis, high surface area MOFs are filled with solvent molecules. Since MOFs are being used for CO<sub>2</sub> storage, therefore, the solvent inside the pores are required to remove without any disturbance in its porous structure. However, special care must be taken to assure that the structure does not collapse. It is worthy to mention that the thermal stability of the MOF is expected to be lower than that of zeolites/zeolite analogues because MOFs have lower metal-linker binding energy than that of zeolites having stronger Si-O, Al-O linkages. In **Figure 1**, some representative MOF structures are shown.

The CO<sub>2</sub> storage capacity of MOFs is being measured at different temperature and pressure. There has also been established a positive connection between storage capacity and surface area at high pressure. Yaghi et al. [18] were first to explain the relationship between surface area and CO<sub>2</sub> uptake capacity. Among several MOFs, MOFs with square



**Figure 1.** Crystal structure of several MOFs, e.g.; MOF-5 [24], DA-MOF [25], CO<sub>2</sub>(adenine)<sub>2</sub>-(CH<sub>3</sub>CO)<sub>2</sub> (bio-MOF-11) [26], with permission from respective references.

channels (MOF-2) [28], pores with open metal sites (MOF-505,  $\text{Cu}_3(\text{BTC})_2$ ) [29], interpenetrated (IRMOF-11) [29],  $\text{CO}_2$  (adenine) $_2$ -( $\text{CH}_3\text{CO}_2$ ) $_2$  functionalized bio-MOF-11 are interesting [30]. It is important to mention that MOF-177 has the high surface area ( $4500 \text{ m}^2 \text{ g}^{-1}$ ) and possesses high uptake of  $\text{CO}_2$  (60 wt% at 35 bar) at high pressure. Very recently, ultrahigh porous MOFs are prepared by Furukawa et al. from  $\text{Zn}_4\text{O}(\text{CO}_2)_6$  unit, containing one or two organic linkers and among them MOF-210 showed highest BET surface area ( $6240 \text{ m}^2 \text{ g}^{-1}$ ) and high pore volume ( $3.6 \text{ cm}^3 \text{ g}^{-1}$ ) reported till date [31]. The ultrahigh porosity of MOF-210 has been achieved mainly because of the expanding organic linkers. As for instance, by extending the size of the 1,3,5-benzenetribenzoate (BTC) in MOF-177 by replacing with larger 4,4',4''-(benzene-1,3,5- triyl-tris(benzene-4,1-iy)) tribenzoate (BBC), MOF-200 was obtained with even higher BET than that of MOF-177 [32]. Strikingly, MOF-210 and MOF-200 show  $\sim 71$  wt%  $\text{CO}_2$  uptake capacity at 298 K and 50 bar pressure, which are highest and considered as new record among all solid porous materials. For  $\text{CO}_2$  capture at ambient condition as well as flue gas condition,  $\text{CO}_2$  capture is not only influenced by surface area but is also dependent on adsorbent- $\text{CO}_2$  interaction. In this context, Mg-MOF-74 [ $\text{Mg}_2(\text{DOT})$ ; DOT: 2,5-dioxidoterephthalate] consisting of an open framework with  $\text{Mg}^{2+}$  sites shows high  $\text{CO}_2$  storage capacity of 35.2 wt% at 298 K and 1 bar [32]. It is pertinent to mention that open metal sites are mandatory in achieving high  $\text{CO}_2$  storage capacity. In **Table 1**, we present some MOFs having significance in  $\text{CO}_2$  capture at low and high pressure.

Chemical formulae	BET ( $\text{m}^2 \text{ g}^{-1}$ )	$\text{CO}_2$ storage (wt%)	Temp. (K)	Pressure (bar)	References
MOF-177	4500	60	298	50	[31]
MOF-210	6240	71	298	50	[31]
Mg-MOF-74	1640	35.2	298	1	[32]
$\text{Cu}_2(\text{abtc})_3$	—	38.5	273	1	[36]
Dy(BTC)	655	27.2	273	1	[37]
$\text{Al}_4(\text{OH})_2(\text{OCH}_3)_4(\text{BDC-NH}_2)_3$	1268	24.1	273	1	[38]
$\text{Zn}_2(\text{BTetB})$	1370	19.7	273	1	[39]
$[\text{In}_3\text{O}(\text{diazDBC})1.5(\text{H}_2\text{O})_3](\text{NO}_3)$	892	17.9	273	1	[40]
$\text{Co}_4(\text{OH})_2(\text{p-CDC})_3$	1080	16.4	273	1	[41]
$\text{Cu}(\text{bpy})_2(\text{BF}_4)_2$	—	13.8	273	1	[42]
$\text{Cu}_2(\text{bptb})$	1217	12.6	273	1	[43]
$\text{Zn}_2(\text{BTetB})(\text{DMF})_2$	800	12.1	273	1	[30]
$\text{Zn}_2(\text{BDoBoRDC})_4$	800	12.1	273	1	[44]
$\text{Ni}(\text{bpy})_2(\text{BF}_4)_2$	—	11.9	273	1	[34]
$\text{Ni}_2(\text{bpy})_3(\text{NO}_3)_4$	—	10.6	273	1	[45]
$\text{Cd}(\text{mim})_2$	2420	5.6	273	1	[46]

**Table 1.**  $\text{CO}_2$  adsorption capacity of metal-organic frameworks at low and high pressure.

On the other hand, thermal degradation of MOFs generally happens on account of metal-ligand bond breaking. As a consequence, thermal stability of MOFs is predominately dependent on both the metal-linker bond strength and the number of linkers connected to metal sites. Indeed, MOFs can be stable up to 300°C without degradation of the framework structure [17, 18], which is crucial for post-combustion CO<sub>2</sub> capture from flue gas under moist conditions.

Since open metal sites in MOFs show considerably good CO<sub>2</sub> uptake property, one common question that may rise among readers is the effect of water on CO<sub>2</sub> uptake because water can easily coordinate to open metal sites. It has been found that in some cases small amount of water can accelerate CO<sub>2</sub> adsorption in some MOFs. Yazaydin et al. have observed that water molecules coordinated to open metal sites of Cu-BTC (HKUST-1) and thus significantly increase CO<sub>2</sub> adsorption of this framework [33]. However, in other cases; water could only destroy the MOF structure and shows a detrimental effect on CO<sub>2</sub> adsorption. Kizzie et al. showed the effect of humidity on the CO<sub>2</sub> capture performance of M/DOBC series of MOFs (M = Zn, Ni, Co and Mg; DOBC = 2,5-dioxidobenzene-1,4-dicarboxylate), demonstrating a significant decrease in the CO<sub>2</sub> uptake capacities for Mg/DOBC and Zn/DOBC [34]. Recently, Liu et al. also described water stability of various MOFs after their pretreatment, further suggesting their stability in aqueous condition [35].

## 2.2. Porous organic polymers (POP)

POPs are recently developed as an important class of porous materials, constructed from light-weight elements (C, H, O, N) and linked by strong covalent bonds, which show huge potential in a variety of applications, e.g.; gas storage and separation, catalysis, sensing, energy storage, optoelectronics and to mention a few [8, 47–49]. A series of vibrant characteristics of POPs, such as high-specific surface area, good physicochemical stability, tunable pore dimensions, topologies and chemical functionalities, make them suitable adsorbents for CO<sub>2</sub> capture.

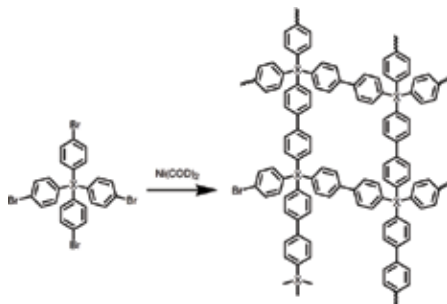
POPs are widely used and have been classified according to their synthesis conditions, which includes polymers of intrinsic microporosity (PIMs), conjugated microporous polymers (CMPs), covalent organic polymers, hypercrosslinked polymers (HCPs), crystalline triazine-based frameworks (CTFs), porous organic frameworks (POFs), porous aromatic frameworks (PAFs), polymeric organic networks (PONs) and so on. In each networks, the state-of-the art development in the design, synthesis, characterization and the CO<sub>2</sub> adsorption performances has been reviewed [50, 51]. Additionally, CO<sub>2</sub> uptake capacity and adsorption enthalpy can also be controlled through manipulation of POP surface area, pore size and/or its functionality at the surfaces. Understanding all these aspects could lead to the development of new possibilities of novel POP frameworks to target CO<sub>2</sub> capture, where the amorphous characteristics, high cross-linked ultra-microporous structures could be crucial in determining CO<sub>2</sub> adsorption performances. Herein, we describe the critical factors that directly influence the CO<sub>2</sub> uptake property for POPs.

There is a direct correlation between POP surface area and its porous structures. It is said that CO<sub>2</sub> uptake capacity is dependent on the high specific surface area. It has also been suggested that CO<sub>2</sub> uptake of an adsorbent increases with increasing CO<sub>2</sub> pressure, which demonstrates that controlling of surface property might be advantageous in tailoring CO<sub>2</sub> uptake

phenomenon. Significant development in the synthesis of high surface area POP materials has been done by several researchers, among which the synthesis of porous aromatic framework (PAF-1) developed by Qiu et al. via Yamamoto homocoupling of tetrahedral monomers (tetrakis(4-bromophenyl)methane) is significant [52]. Owing to the in-built generation of diamondoid framework topology by the cross-linking of tetrahedral monomers, it creates open and interconnected pores which give rise to high surface area (BET:  $5600 \text{ m}^2 \text{ g}^{-1}$ ) and good  $\text{CO}_2$  storage capacity ( $29.5 \text{ mmol g}^{-1}$ , 298 K, 40 bar). Later significant contribution has been developed by modifying with other quadricovalent building centers [53], which forms PPN-3 (with adamantane-system), PPN-4 (replaced tetrahedral carbon by silicon) and PPN-5 (replaced tetrahedral carbon by Germanium), as shown in **Figure 2**. Importantly, all these POPs possess exceptionally high surface area. It should be noted that PPN-4 having BET surface area of  $6461 \text{ m}^2 \text{ g}^{-1}$  considers as highest surface area among all reported POPs till date. The exceptionally high surface area enables PPN-4 to have excellent  $\text{CO}_2$  storage capacity ( $48.2 \text{ mmol g}^{-1}$ ) at 50 bar and 295 K.

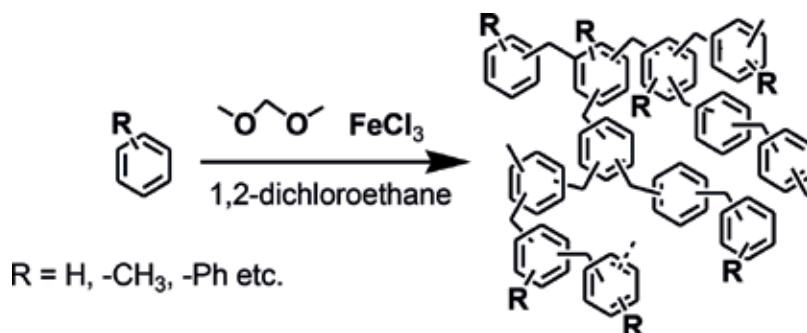
Therefore, it can be arguably said that the design followed by the synthesis of high surface area POPs from tetrahedral building block is a promising approach for  $\text{CO}_2$  storage at high pressure. Apart from BET surface area, porous structure also triggers  $\text{CO}_2$  uptake phenomenon, as controlling the pore size similar to the kinetic diameter of  $\text{CO}_2$  molecule (Size:  $3.3 \text{ \AA}$ ) can significantly enhance the storage capacity. So far many researches have been made significant effort to make POPs from tetrahedral building units as  $\text{CO}_2$  adsorbents and among them hypercrosslinked (HCPs) amorphous polymers are important. HCPs exhibit unique property in gas storage capacity due to its highly cross-linked network which prevents the interconnected porous frameworks from being collapsed [54]. In **Figure 3**, the formation of cross-linked HCP is presented.

The unique advantage for the synthesis of HCPs, possesses huge prospect in materials chemistry research because it requires cheap, readily available precursors and  $\text{FeCl}_3$  as non-toxic catalyst. Therefore, utilizing this procedure, several aromatic polymers can be easily prepared as described by Cooper et al. [55] In presence of 1,1'-binaphthol the resulting HCP shows  $1015 \text{ m}^2 \text{ g}^{-1}$  BET surface area with high  $\text{CO}_2$  uptake capacity ( $3.96 \text{ mmol g}^{-1}$ , 1 bar). The high  $\text{CO}_2$  capture capacity is hardly affected by aqueous environment owing to strong hydrophobicity of HCPs. Another interesting research has been done by Puthiaraj



**Figure 2.** Synthetic routes for high surface area PPN-4 (X: Si), PPN-5 (X: Ge), PAF-1 (X: C) from tetrahedral building blocks.

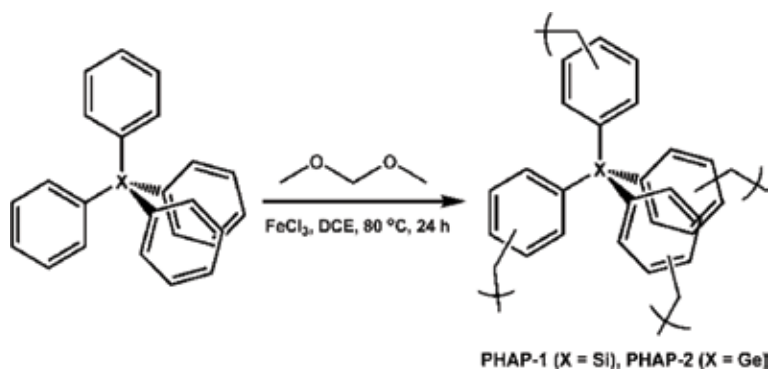




**Figure 3.** Schematic representation of the formation of hypercrosslinked porous polymers.

et al., where the knitting polymerization has been utilized for binding tetraphenyl aromatic moieties (**Figure 4**) [56]. Unlike the conventional Suzuki/Sonogashira coupling reactions, HCP polymerization promotes the cross-linking between tetrahedral aromatic moieties in a facile way. In continuation with this research, silicon (Si) and germanium (Ge) containing nanoscale hyper-cross-linked aromatic polymers (PHAPs) were reported by FeCl<sub>3</sub> mediated Friedel – Crafts alkylation between tetraphenylsilane or tetraphenylgermanium as a building block and formaldehyde dimethyl acetal as a cross-linker, which yields high surface area (1137–1059 m<sup>2</sup> g<sup>-1</sup>) stable polymers having high CO<sub>2</sub> adsorption capacity (104.3–114.4 mg g<sup>-1</sup>) with an isosteric heat of adsorption in the range of 26.5–27.3 kJ mol<sup>-1</sup> (**Figure 4**). It is worthy to mention that controlled synthesis of silicon and germanium-based nanoscale POPs is very difficult and shows intense research activities because Si and Ge are crucial in influencing physical properties of these POPs.

Although high BET surface area is necessary for influencing CO<sub>2</sub> adsorption behavior, however, it is not the prime reason, indeed adsorbate-adsorbent interaction might be quite effective for adsorption at low CO<sub>2</sub> pressure and for selective adsorption of CO<sub>2</sub> in presence of other gases. In this regard, N, P, O, S etc. atoms when incorporated into POPs, show dramatic change in adsorption capacity as well as in the selectivity; because heteroatoms can improve



**Figure 4.** Synthesis of porous hypercrosslinked aromatic polymers (PHAP) containing central hetero atoms Si, Ge other than carbon. CO<sub>2</sub> uptake capacity is given at the right; reproduced with permission from Ref. [56].

isosteric heat of adsorption between sorbent and sorbate. To address this issues POPs with different functional sites e.g. pyridine (PON-2) or thiophene (PON-3) have been prepared, which exhibit favorable interaction with CO<sub>2</sub> despite of having low surface areas [PON-2 (189 m<sup>2</sup> g<sup>-1</sup>) and PON-3 (44 m<sup>2</sup> g<sup>-1</sup>)] than only phenyl-based PON (BET 1447 m<sup>2</sup> g<sup>-1</sup>), clearly explaining the effect of hetero-atom in POP structure [57]. Based on this proposal, a variety of N-containing POPs with several functional sites e.g. carbazole, triazine, porphyrin, benzimidazole, azo, etc. have been reported by several researchers as discussed in the subsequent section.

Microporous polycarbazole (CPOP-1) through polymerization of carbazole has been prepared by Chen et al. by oxidative polymerization of carbazole with FeCl<sub>3</sub> as cheap and non-toxic catalyst [58]. CPOP-1 shows high BET surface area (2220 m<sup>2</sup> g<sup>-1</sup>), narrow pore size (0.62 nm) together with the presence of electron-rich carbazole units and high charge density at N-sites, which facilitate uptake of polarizable CO<sub>2</sub> molecule through local dipole-quadrupole interactions. The CO<sub>2</sub> uptake of CPOP-1 is as high as 4.8 mmol g<sup>-1</sup> at 273 K and 1 bar, along with its high selectivity for CO<sub>2</sub>/CH<sub>4</sub> (33) and CO<sub>2</sub>/N<sub>2</sub> (25) separation is also noticeable on account of the framework composition. Consequently, they have also prepared CPOP-(2-7) through this reaction and among them CPOP-7 exhibits the best uptake capacity for CO<sub>2</sub> (3 mmol g<sup>-1</sup> at 273 K and 1 bar) [59]. Among other N-containing polymeric adsorbents, covalent triazine frameworks (CTFs) are interesting. CTFs are efficiently applied to CO<sub>2</sub> capture purposes and are generally synthesized at high temperature (>400°C) by molten ZnCl<sub>2</sub> which usually acts as Lewis acid catalyst as well as solvents. CTFs possess moderate BET surface area (1235 m<sup>2</sup> g<sup>-1</sup>), while showing excellent CO<sub>2</sub> uptake capacity (4.2 mmol g<sup>-1</sup>, 1 atm, 273 K) [60]. Again, several PCTFs were synthesized through the modifications of CTFs using branched arms precursors. Importantly, PCTF-1 with biphenyl, PCTF-2 with terphenyl and PCTF-3 with quaterphenyl rings have been developed, which show BET surface area as 853, 811 and 395 m<sup>2</sup> g<sup>-1</sup> respectively [61]. When the middle benzene ring of CTF has been replaced by the strong polar group, such as benzothiadiazole, forming PCTF-4 which shows highest CO<sub>2</sub> uptake of 4.7 mmol g<sup>-1</sup> at 273 K and 1 bar. Later, Zou and others prepared a nitrogen-rich polysulfone/polymer (PSF/SNW-1) membrane by introducing nano-sized SNW-1 particles through intrinsically small micropores into PSF matrix via spin-coating [62]. Gas sorption measurements demonstrated that SNW-1 exhibits high adsorption capacity and good affinity towards CO<sub>2</sub> because of its high microporosity and the presence of functional amino groups. For CO<sub>2</sub> separation, it demonstrates an excellent separation performance including high separation factor (34 and 40 for CO<sub>2</sub>/CH<sub>4</sub> and CO<sub>2</sub>/N<sub>2</sub>) and high CO<sub>2</sub> permeability (22.4 barrer). Furthermore, long thermal stability is also noticeable and further satisfies that SNW-1/PSF membrane is stable and robust; exhibiting its potentiality in the practical application of CO<sub>2</sub> capture.

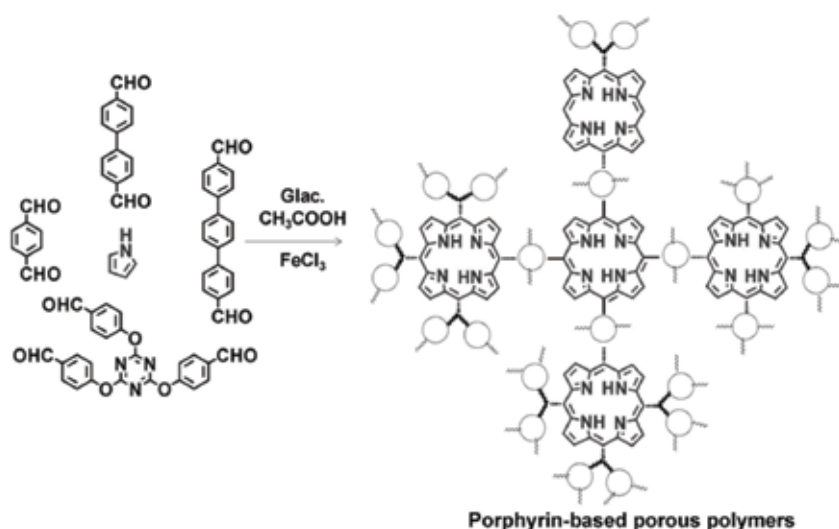
Based on the above discussion, it is evident that the effect of N-substituted POPs markedly influence CO<sub>2</sub> adsorption and separation processes. Regarding this, porphyrin containing microporous POP shows potential application in this area. Porphyrin-based POPs are generally synthesized from expensive Pd and Ni catalysts by a tedious way [63]. However, Modak and Bhaumik introduced a new method with FeCl<sub>3</sub> for the formation of porphyrin polymers through a one pot bottom up chemistry involving the condensation between pyrrole and several aromatic dialdehydes [64, 65]. In this report, authors reported the formation of Fe-POP-1/2/3 having 750–875 m<sup>2</sup> g<sup>-1</sup> BET surface area, narrow microporosity (0.75–1.1 nm)

and excellent adsorbent for CO<sub>2</sub> (19 wt%, 273 K, 1 atm; by Fe-POP-1), shown in **Figure 5**. This research has further been extended by changing aromatic dialdehydes to aromatic trialdehyde using 4,4',4''-(1,3,5-triazine-2,4,6-triyl)tris(oxy)tribenzaldehyde as tripodal precursor. The advantage of using this organic precursor is enormous, because it introduces both triazine and porphyrin networks in a single TPOP-1 material, which stores high amount of CO<sub>2</sub> (6.2 mmol g<sup>-1</sup> or 27.3 wt% at 3 bar, 273 K).

### 2.3. Porous clay materials

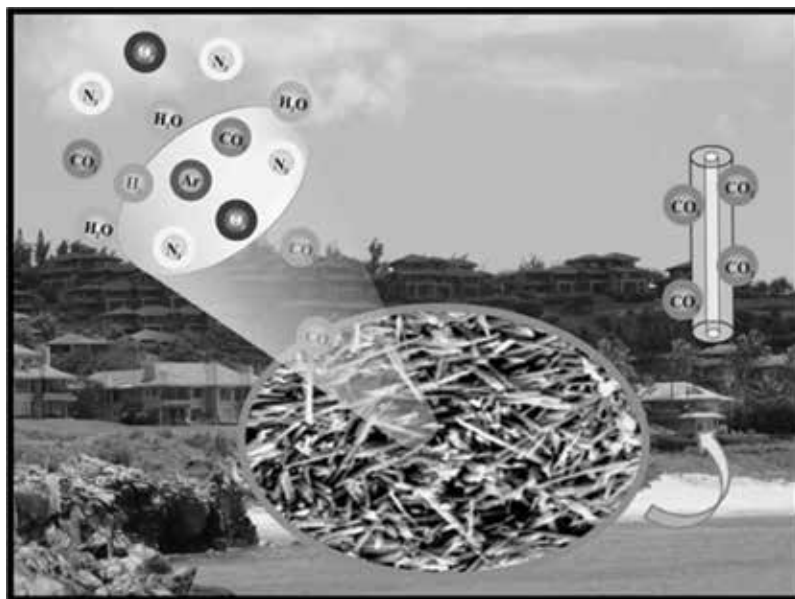
The key advantages of any porous materials involve flexible surface modification due to the availability of high surface area together with lower regeneration energy compared to the any conventional solvent methods. Among the several porous materials, clay minerals are one of the significant materials since they have unique physical properties because of their layered structure, small grain size and large surface to volume ratio. Apart from the mentioned advantages, clay possesses low cost, high mechanical and chemical stability that has been fascinated to the researchers and withdrawn specific research attention. A variety of clay minerals have been used for CO<sub>2</sub> capture, like halloysite, kaolinite, montmorillonite, nanosepiolite, bentonite, etc.

In a recent report, pristine halloysite nanotubes (HNTs) were pretreated with acid for selective removal of alumina and thus, produce mesoporous silica nanotubes (MSiNTs), which were then impregnated with polyethylenimine (PEI) to prepare an emerging nanocomposite MSiNTs/PEI (MP) for CO<sub>2</sub> adsorption [66]. Recently, Jana and coworkers demonstrate the development of several HNTs based solid adsorbents being grafted with diverse aminosilanes containing both primary and/or secondary amine sites over the surfaces of inexpensive



**Figure 5.** Schematic representation for the preparation of porphyrin-based porous polymers by electrophilic aromatic substitution of pyrrole with several aromatic dialdehydes and trialdehydes.

and easily available HNTs to capture  $\text{CO}_2$  from the ambient air under room temperature and ambient pressure [67]. They have also explored the effect of relative humidity in terms of moisture on the adsorption kinetics of the adsorbents by carrying out the experiment on the seasonal ambient air [11], exhibiting that relative humidity basically regulates the atmospheric  $\text{CO}_2$  adsorption and corresponding adsorption kinetics (**Figure 6**). Jana et al. also studied the kinetics of several stable isotopes of  $\text{CO}_2$  present in the ambient air [68]. Schaefer et al. reported the adsorption of  $\text{CO}_2$  onto kaolinite surfaces under geologic sequestration conditions and also verified through the density functional theory (DFT) [69]. Wang et al. developed montmorillonite supported PEI composite for  $\text{CO}_2$  capture [70]; the  $\text{CO}_2$  sorption efficacy was found to be  $2.54 \text{ mmol g}^{-1}$  under dry environmental condition and  $3.23 \text{ mmol g}^{-1}$  under moisture added condition. They also verified that the density of  $\text{CO}_2$  in the clay pores is comparatively stable over a wide range of  $\text{CO}_2$  pressures at a given temperature and at the excess sorption maximum.  $\text{CO}_2$  sorption increases with decreasing temperature while the high pressure sorption properties demonstrate weak temperature dependence. Elliot A. Roth and coworkers synthesized amine-containing solid sorbent for  $\text{CO}_2$  capture through the modification of the surface of montmorillonite nanoclay using aminopropyltrimethoxysilane and polyethylenimine [71]. They found that in pure  $\text{CO}_2$  and 10%  $\text{CO}_2$  in nitrogen gas streams the nanoclay loaded with only one of the amines exhibits ~6 wt% capture efficacy at  $85^\circ\text{C}$  and atmospheric pressure, whereas it is ~7.5 wt%  $\text{CO}_2$  capture efficiency when the nanoclay immobilized with both the amines. Irani et al. utilized nanosepiolite as an inorganic-organic  $\text{CO}_2$  sorbent by immobilizing tetraethylenepentamine (TEPA) onto acid-modified nanosepiolite, having capacity of  $3 \text{ mmol g}^{-1}$  for 1 vol%  $\text{CO}_2$  in  $\text{N}_2$ , along with



**Figure 6.** Schematic presentation of the trapping of  $\text{CO}_2$  from the seasonal ambient air in clay based solid nanocomposites, adapted from Ref. [11] with permission from The Royal Society of Chemistry.

~1 vol% H<sub>2</sub>O at 60°C [72]. Xiao and coworkers exploited an inexpensive and commercially available bentonite for CO<sub>2</sub> capture from flue gas after modified by sulfuric acid followed by immobilization of TEPA [73]. Hence, these low-cost clay based adsorbents introduce a new pathway in the frontier area of CO<sub>2</sub> capture and sequestration study and should make the procedure environmental friendly, robust, sustainable and thus a more attractive strategy.

## 2.4. Nanoporous carbon composite

Nanoporous carbon derived from various carbon precursors, such as polymer, biomass, coal, petroleum etc. shows enormous significance in small molecule adsorption due to high specific surface area, narrow pore size distribution, low preparation cost, easy-to-design, low energy requirements for regeneration, high stability in air and water and high flexibility in heteroatom doping/surface functionalization [74]. Porous carbons are prepared from physical/chemical activation of carbonaceous materials with CO<sub>2</sub>, steam, ZnCl<sub>2</sub>, KOH etc., which are generally employed as activating agents for the formation of microporous carbon [75]. In addition, templating method using zeolites, ZSM-5, several MOFs (MOF-5, ZIF-8, Al-PCP) acts as an effective carbon precursors in making amorphous carbon (Figure 7) [76].

Additionally, from the perspective of environmental friendliness and preparation cost, waste materials e.g. fly ash, coconut, carpet are quite popular to prepare high performance carbonaceous materials for CO<sub>2</sub> adsorption [77–79]. As for instance, porous carbons are prepared from hazelnut shells via carbonization and KOH activation. The obtained porous carbon exhibits a high specific surface area of ~1900 m<sup>2</sup> g<sup>-1</sup> and high pore volume (1–0.7) cm<sup>3</sup> g<sup>-1</sup>, which are approximately five times greater than those of carbon without activation [80]. Again, coffee residue has also been used as a sustainable source for the preparation of activated carbon with ZnCl<sub>2</sub> [81]. The textural properties of the samples thus prepared significantly depend on the ZnCl<sub>2</sub>/C ratio. On the other hand, porous carbons are also prepared through a facile one step carbonization from porous polymers. Recently, Modak et al. have prepared microporous carbon (K-COP-M) having extremely high surface area of 2186 m<sup>2</sup> g<sup>-1</sup> and contains micropore

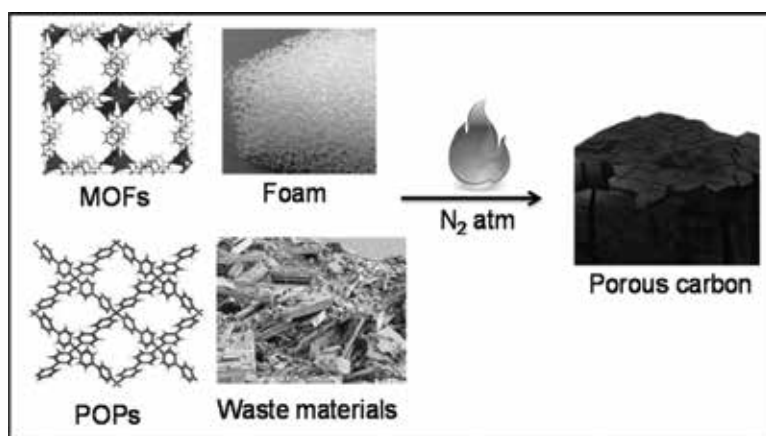


Figure 7. Schematic presentation of the formation of porous carbon from MOFs, POPs, foam and waste materials.

volume of  $0.85 \text{ cm}^3 \text{ g}^{-1}$  [82]. K-COP-M has been produced by KOH activation of COP-M polymer in an inert condition and at very high temperature ( $600\text{--}700^\circ\text{C}$ ).  $\text{CO}_2$  adsorption potential of K-COP-M-600/700 have been evaluated, indicating that these frameworks adsorb  $160\text{--}170 \text{ cm}^3 \text{ g}^{-1}$  ( $7.6\text{--}7.1 \text{ mmol g}^{-1}$ )  $\text{CO}_2$  at 1 atm and 273 K, which is higher than that of non-activated carbon derived from COP-M (i.e. COP-M-600/700 stores  $77\text{--}83 \text{ cm}^3 \text{ g}^{-1} \text{ CO}_2$ ). This signifies the utility of KOH in making effective adsorbents by creating ultra-small micropores in carbons. While heteroatom doping is significantly used in controlling the textural properties of porous carbon, carbonization of amine containing organic precursors substantially shows high N-doping and considers as an effective adsorbent of  $\text{CO}_2$  with very good selectivity. There are several reports available in this respect [49, 83], among which N-doped composite developed by Kim et al. is interesting, where polyindole-reduced graphene oxide (PIG) hybrid was synthesized and later carbonized at  $400\text{--}800^\circ\text{C}$  temperature and thus produces N-doped graphene sheets [84]. The N-doped graphene sheets are microporous having 0.6 nm pores with BET surface area of about  $936 \text{ m}^2 \text{ g}^{-1}$  and show a maximum  $\text{CO}_2$  uptake of  $3.0 \text{ mmol g}^{-1}$  at  $25^\circ\text{C}$  and 1 atm pressure. Nevertheless, high recycling stability of  $\text{CO}_2$  uptake is noticed even after 10 recycling cycles; additionally this N-doped carbon shows  $\text{CO}_2/\text{N}_2$ ,  $\text{CO}_2/\text{CH}_4$  separation ability of 23 and 4 respectively.

Alternatively, polyurethane foams (PUFs) are important thermosetting polymers and owing to its high nitrogen contents, it can be used as good precursor for N-doped carbon [85]. The global demand for polyurethanes was estimated to be 13.6 million tons in 2010, which leads to the generation of huge wastes. However, regeneration of spent polyurethane is not only high energy-consuming process, but also it produces toxic nitrogen oxides, carbon oxides etc. and causing severe environmental pollution. These wastes when carbonized at high temperature can produce nitrogen-doped carbon that can further reduce environmental pollution since these N-doped carbon shows  $\text{CO}_2$  uptake capacities of 6.67 and  $4.33 \text{ mmol g}^{-1}$  at  $0^\circ\text{C}$  and  $25^\circ\text{C}$  under 1 bar, respectively. Finally, it can be said that like MOFs, POPs and porous clays, microporous carbon is also an alternative for  $\text{CO}_2$  storage purposes.

### 3. Conclusion

In this chapter, we highlight important aspect of some promising materials, like MOFs, POPs, nanoporous carbon and porous clays as  $\text{CO}_2$  adsorbents, which possess high BET surface area, tunable microporosity and facile surface engineering for enhancing interaction with  $\text{CO}_2$ . All such features are however exempted from conventional zeolites, alkali metal oxides, activated carbon, porous silica, therefore, demonstrating the significance of new porous materials in developing carbon capture techniques. Considering the growth of rapid industrialization and abrupt emission of  $\text{CO}_2$  in the atmosphere, an increasing concern to the social as well as marine lives, would be diminished through utilization of aforesaid functional materials to adsorb  $\text{CO}_2$ . In the abovementioned sections, we have thus tried to summarize the recent advancement made in the synthesis and broad prospect of MOFs, POPs, nanoporous clays and porous carbon as potential adsorbents for  $\text{CO}_2$  capture and storage. Nevertheless, in the near future, such promising materials would motivate to the

researchers to extend this work towards low pressure CO<sub>2</sub> adsorption, which may open a new route in the frontier area of carbon capture and sequestering study through the real world CO<sub>2</sub> capture under ultra-dilute condition.

## Acknowledgements

Authors would like to acknowledge Department of Science and Technology (DST), Government of India for funding (SR/NM/NS-18/2014 and SB/WEA-008/2016) and S. N. Bose National Centre for Basic Sciences, Kolkata, India.

## Author details

Arindam Modak<sup>1</sup> and Subhra Jana<sup>1,2\*</sup>

\*Address all correspondence to: [subhra.jana@bose.res.in](mailto:subhra.jana@bose.res.in)

1 Technical Research Centre, S. N. Bose National Centre for Basic Sciences, Salt Lake, Kolkata, India

2 Department of Chemical, Biological & Macro-Molecular Sciences, S. N. Bose National Centre for Basic Sciences, Salt Lake, Kolkata, India

## References

- [1] Hansen J, Ruedy R, Sato M, Lo K. Global surface temperature change. *Reviews of Geophysics*. 2010;**48**:RG4004
- [2] GISS Surface Temperature Analysis. Available from: [http://data.giss.nasa.gov/gistemp/graphs\\_v3/](http://data.giss.nasa.gov/gistemp/graphs_v3/) [Accessed: January 2016]
- [3] Pachauri RK, Meyer, L. A IPCC. Climate change 2014: Synthesis report. Contribution of Working Groups I, II and III to the Fifth Assessment Report of the Intergovernmental Panel on Climate Change; Core Writing Team, editors. IPCC: Geneva, Switzerland, 2014.
- [4] Reichle D, Houghton J, Kane B, Ekmann J. Carbon Sequestration. Washington, DC: State of the Science; U.S. Department of Energy, Office of Science, Office of Fossil Energy; 1999
- [5] Oyenekan BA, Rochelle GT. Alternative stripper configurations for CO<sub>2</sub> capture by aqueous amines. *AIChE Journal*. 2007;**53**:3144-3154
- [6] Wang W, Zhou M, Yuan D. Carbon dioxide capture in amorphous porous organic polymers. *Journal of Materials Chemistry A*. 2017;**5**:1334-1347
- [7] Sumida K, Rogow DL, Mason JA, McDonald TM, Bloch ED, Herm ZR, Tae-Hyun Bae TH, Long JR. Carbon dioxide capture in metal-organic frameworks. *Chemical Reviews*. 2012;**112**:724-781

- [8] Stuckert NR, Yang RT. CO<sub>2</sub> capture from the atmosphere and simultaneous concentration using zeolites and amine-grafted SBA-15. *Environmental Science & Technology*. 2011;**45**:10257-10264
- [9] Sajani A, Basnayake JS, Xiadong Z, Kenneth JB. Carbonate-based zeolitic imidazolate framework for highly selective CO<sub>2</sub> capture. *Inorganic Chemistry*. 2015;**54**:1816-1821
- [10] Seema H, Kemp KC, Le NH, Park SW, Chandra V, Lee JW, Kim KS. Highly selective CO<sub>2</sub> capture by S-doped microporous carbon materials. *Carbon*. 2014;**66**:320-326
- [11] Das S, Ghosh C, Jana S. Moisture induced isotopic carbon dioxide trapping from ambient air. *Journal of Materials Chemistry A*. 2016;**4**:7632-7640
- [12] Duyara MS, ArellanoTreviño MA, Farrautoa RJ. Dual function materials for CO<sub>2</sub> capture and conversion using renewable H<sub>2</sub>. *Applied Catalysis B: Environmental*. 2015;**168-169**:370-376
- [13] Gao X, Yu B, Yang Z, Zhao Y, Zhang H, Hao L, Han B, Liu Z. Ionic liquid-catalyzed C-S bond construction using CO<sub>2</sub> as a C1 building block under mild conditions: A metal-free route to synthesis of benzothiazoles. *ACS Catalysis*. 2015;**5**:6648-6652
- [14] Kang Z, Fan L, Sun D. Recent advances and challenges of metal-organic framework membranes for gas separation. *Journal of Materials Chemistry A*. 2017;**5**:10073-10091
- [15] Hagrman PJ, Hagrman D, Zubietta J. Organic-inorganic hybrid materials: From “simple” coordination polymers to organodiamine-templated molybdenum oxides. *Angewandte Chemie, International Edition*. 1999;**38**:2638-2684
- [16] Batten SR, Robson R. Interpenetrating nets: Ordered, periodic entanglement. *Angewandte Chemie, International Edition*. 1998;**37**:1460-1494
- [17] Zhou HC, Kitagawa S. Metal-organic frameworks (MOFs). *Chemical Society Reviews*. 2014;**43**:5415-5418
- [18] Trickett CA, Helal A, Al-Maythaly BA, Yamani ZH, Cordova KE, Yaghi OM. The chemistry of metal-organic frameworks for CO<sub>2</sub> capture, regeneration and conversion. *Nature Reviews Materials*. 2017;**2**:17045
- [19] Li JR, Ma Y, McCarthy MC, Sculley J, Yu J, Jeong HK, Balbuena PB, Zhou HC. Carbon dioxide capture-related gas adsorption and separation in metal-organic frameworks. *Coordination Chemistry Reviews*. 2011;**255**:1791-1823
- [20] Noro SI, Kitaura R, Kondo M, Kitagawa S, Ishii T, Matsuzaka H, Yamashita M. Framework engineering by anions and porous functionalities of Cu(II)/4,4'-bpy coordination polymers. *Journal of the American Chemical Society*. 2002;**124**:2568-2583
- [21] Jung OS, Kim YJ, Lee YA, Park JK, Chae HK. Smart molecular helical springs as tunable receptors. *Journal of the American Chemical Society*. 2000;**122**:9921-9925
- [22] Uemura K, Kitagawa S, Fukui K, Saito K. A contrivance for a dynamic porous framework: Cooperative guest adsorption based on square grids connected by amide-amide hydrogen bonds. *Journal of the American Chemical Society*. 2004;**126**:3817-3828



- [23] Ramsahye NA, Maurin G, Bourrelly S, Llewellyn PL, Devic T, Serre C, Loiseau T, Ferey G. Adsorption of CO<sub>2</sub> in metal organic frameworks of different metal centres: Grand canonical Monte Carlo simulations compared to experiments. *Adsorption*. 2007;**13**:461-467
- [24] Sillar K, Hofmann A, Sauer J. Ab initio study of hydrogen adsorption in MOF-5. *J. Am. Chem. Soc.* 2009;**131**:4143-4150
- [25] Son HJ, Jin S, Patwardhan S, Wezenberg SJ, Jeong NC, So M, Wilmer CE, Sarjeant AA, Schatz GC, Snurr RQ, Farha OK, Wiederrecht GP, Hupp JT. Light-harvesting and ultrafast energy migration in porphyrin-based metal-organic frameworks. *J. Am. Chem. Soc.* 2013;**135**:862-869
- [26] An J, Geib SJ, Rosi NL. High and selective CO<sub>2</sub> uptake in a cobalt adeninate metal-organic framework exhibiting pyrimidine- and amino-decorated pores. *J. Am. Chem. Soc.* 2010;**132**:38-39
- [27] Gassensmith JJ, Furukawa H, Smaldone RA, Forgan RS, Botros YY, Yaghi OM, Stoddart JF. Strong and reversible binding of carbon dioxide in a green metal-organic framework. *Journal of the American Chemical Society*. 2011;**133**:15312-15315
- [28] Millward AR, Yaghi OM. Metal-organic frameworks with exceptionally high capacity for storage of carbon dioxide at room temperature. *Journal of the American Chemical Society*. 2005;**127**:17998-17999
- [29] Li H, Eddaoudi M, O'Keeffe M, Yaghi OM. Design and synthesis of an exceptionally stable and highly porous metal-organic framework. *Nature*. 1999;**402**:276-279
- [30] Eddaoudi M, Kim J, Rosi N, Vodak D, Wachter J, O'Keeffe M, Yaghi OM. Systematic design of pore size and functionality in isoreticular MOFs and their application in methane storage. *Science*. 2002;**295**:469-472
- [31] Furukawa H, Ko N, Go YB, Aratani N, Choi SB, Choi E. Ultrahigh porosity in metal-organic frameworks. *Science*. 2010;**329**:424-428
- [32] Britt D, Furukawa H, Wang B, Glover TG, Yaghi OM. Highly efficient separation of carbon dioxide by a metal-organic framework replete with open metal sites. *Proceedings of the National Academy of Sciences of the United States of America*. 2009;**106**:20637-20640
- [33] Yazaydin AO, Benin AI, Faheem SA, Jakubczak P, Low JJ, Willis RR, Snurr RQ. Enhanced CO<sub>2</sub> adsorption in metal-organic frameworks via occupation of open-metal sites by coordinated water molecules. *Chemistry of Materials*. 2009;**21**:1425-1430
- [34] Kizzie AC, Wong-Foy AG, Matzger AJ. Effect of humidity on the performance of microporous coordination polymers as adsorbents for CO<sub>2</sub> capture. *Langmuir*. 2011;**27**:6368-6373
- [35] Liu J, Thallapally PK, McGrail BP, Brown DR. Progress in adsorption-based CO<sub>2</sub> capture by metal-organic frameworks. *Chemical Society Reviews*. 2012;**41**:2308-2322
- [36] Lee YG, Moon HR, Cheon YE, Suh MP. A comparison of the H<sub>2</sub> sorption capacities of isostructural metal-organic frameworks with and without accessible metal sites: [Zn<sub>2</sub>(abtc)(dmf)<sub>2</sub>]<sub>3</sub> and [Cu<sub>2</sub>(abtc)(dmf)<sub>2</sub>]<sub>3</sub> versus [Cu<sub>2</sub>(abtc)]<sub>3</sub>. *Angewandte Chemie, International Edition*. 2008;**47**:7741-7745

- [37] Guo X, Zhu G, Li Z, Sun F, Yang Z, Qiu SA. Lanthanide metal-organic framework with high thermal stability and available Lewis-acid metal sites. *Chemical Communications*. 2006;3172-3174
- [38] Si X, Jiao C, Li F, Zhang J, Wang S, Liu S, Li Z, Sun L, Xu F, Gabelica Z, Schick C. High and selective CO<sub>2</sub> uptake, H<sub>2</sub> storage and methanol sensing on the amine-decorated 12-connected MOF CAU-1. *Energy & Environmental Science*. 2011;4:4522-4527
- [39] Bae Y-S, Farha OK, Hupp JT, Snurr RQ. Enhancement of CO<sub>2</sub>/N<sub>2</sub> selectivity in a metal-organic framework by cavity modification. *Journal of Materials Chemistry*. 2009;19:2131-2134
- [40] Moellmer J, Celer EB, Luebke R, Cairns AJ, Staudt R, Eddaoudi M, Thommes M. Insights on adsorption characterization of metal-organic frameworks: A benchmark study on the novel *soc*-MOF. *Microporous and Mesoporous Materials*. 2010;129:345-353
- [41] Farha OK, Spokoyny AM, Mulfort KL, Galli S, Hupp JT, Mirkin CA. Gas-sorption properties of cobalt(II)-carborane-based coordination polymers as a function of morphology. *Small*. 2009;15:1727-1731
- [42] Kondo A, Chinen A, Kajiro H, Nakagawa T, Kato K, Takata M, Hattori Y, Okino F, Ohba T, Kaneko K, Kanoh H. Metal-ion-dependent gas sorptivity of elastic layer-structured MOFs. *Chemistry – A European Journal*. 2009;15:7549
- [43] Wu S, Ma L, Long LS, Zheng LS, Lin W. Three-dimensional metal-organic frameworks based on functionalized tetracarboxylate linkers: Synthesis, structures, and gas sorption studies. *Inorganic Chemistry*. 2009;48:2436-2442
- [44] Spokoyny AM, Farha OK, Mulfort KL, Hupp JT, Mirkin CA. Porosity tuning of carborane-based metal-organic frameworks (MOFs) via coordination chemistry and ligand design. *Inorganica Chimica Acta*. 2010;364:266-271
- [45] Fletcher AJ, Cussen EJ, Bradshaw D, Rosseinsky MJ, Thomas KM. Adsorption of gases and vapors on nanoporous Ni<sub>2</sub>(4,4'-bipyridine)<sub>3</sub>(NO<sub>3</sub>)<sub>4</sub> metal-organic framework materials templated with methanol and ethanol: Structural effects in adsorption kinetics. *Journal of the American Chemical Society*. 2004;126:9750-9759
- [46] Tian YQ, Yao SY, Gu D, Cui KH, Guo DW, Zhang G, Chen ZX, Zhao DY. Cadmium imidazolate frameworks with polymorphism, high thermal stability, and a large surface area. *Chemistry – A European Journal*. 2010;16:1137-1141
- [47] Modak A, Mondal J, Sasidharan M, Bhaumik A. Triazine functionalized ordered mesoporous polymer: A novel solid support for Pd-mediated C–C cross-coupling reactions in water. *Green Chemistry*. 2011;13:1317-1331
- [48] Modak A, Mondal J, Bhaumik A. Highly porous organic polymer containing free –CO<sub>2</sub>H groups: A convenient carbocatalyst for indole C–H activation at room temperature. *ChemCatChem*. 2013;5:1749-1753

- [49] Modak A, Bhaumik A. High-throughput acid-base tandem organocatalysis over hollow tube-shaped porous polymers and carbons. *Chemistry Select*. 2016;**(6)**:1192-1200
- [50] Xu Y, Jin S, Xu H, Nagai A, Jiang D. Conjugated microporous polymers: Design, synthesis and application. *Chemical Society Reviews*. 2013;**42**:8012-8031
- [51] Das S, Heasman P, Ben T, Qiu S. Porous organic materials: Strategic design and structure-function correlation. *Chemical Reviews*. 2017;**117**:1515-1563
- [52] Ben T, Ren TH, Ma S, Cao D, Lan J, Jing X, Wang W, Xu J, Deng F, Simmons JM, Qiu S, Zhu G. Targeted synthesis of a porous aromatic framework with high stability and exceptionally high surface area. *Angewandte Chemie, International Edition*. 2009;**48**:9457-9460
- [53] Yuan D, Lu W, Zhao D, Zhou HC. Highly stable porous polymer networks with exceptionally high gas-uptake capacities. *Advanced Materials*. 2011;**23**:3723-3725
- [54] Tan L, Tan B. Hypercrosslinked porous polymer materials: Design, synthesis, and applications. *Chemical Society Reviews*. 2017;**46**:3322-3356
- [55] Dawson R, Stevens LA, Drage TC, Snape CE, Smith MW, Adams DJ, Cooper AI. Impact of water coadsorption for carbon dioxide capture in microporous polymer sorbents. *Journal of the American Chemical Society*. 2012;**134**:10741-10744
- [56] Puthiaraj P, Ahn WS. CO<sub>2</sub> capture by porous hyper-cross-linked aromatic polymers synthesized using tetrahedral precursors. *Industrial and Engineering Chemistry Research*. 2016;**55**:7917-7923
- [57] Jeon HJ, Choi JH, Lee Y, Choi KM, Park JH, Kang JK. Highly selective CO<sub>2</sub>-capturing polymeric organic network structures. *Advanced Energy Materials*. 2012;**2**:225-228
- [58] Chen Q, Luo M, Hammershoj P, Zhou D, Han Y, Laursen BW, Yan CG, Han BH. Microporous polycarbazole with high specific surface area for gas storage and separation. *Journal of the American Chemical Society*. 2012;**134**:6084-6087
- [59] Chen Q, Liu DP, Luo M, Feng LJ, Zhao YC, Han BH. Nitrogen-containing microporous conjugated polymers via carbazole-based oxidative coupling polymerization: Preparation, porosity, and gas uptake. *Small*. 2014;**10**:308-315
- [60] Katekomol P, Roeser J, Bojdys M, Weber J, Thomas A. Covalent triazine frameworks prepared from 1,3,5-tricyanobenzene. *Chemistry of Materials*. 2013;**25**:1542-1548
- [61] Gu C, Liu D, Huang W, Liu J, Yang R. Synthesis of covalent triazine-based frameworks with high CO<sub>2</sub> adsorption and selectivity. *Polymer Chemistry*. 2015;**6**:7410-7417
- [62] Gao X, Zou X, Ma H, Meng S, Zhu G. Highly selective and permeable porous organic framework membrane for CO<sub>2</sub> capture. *Advanced Materials*. 2014;**26**:3644-3648
- [63] Wang Z, Yuan S, Mason A, Reprogle B, Liu DJ, Yu L. Nanoporous porphyrin polymers for gas storage and separation. *Macromolecules*. 2012;**45**:7413-7419

- [64] Modak A, Nandi M, Mondal J, Bhaumik A. Porphyrin based porous organic polymers: Novel synthetic strategy and exceptionally high CO<sub>2</sub> adsorption capacity. *Chemical Communications*. 2012;**48**:248-250
- [65] Modak A, Pramanik M, Inagaki S, Bhaumik A. A triazine functionalized porous organic polymer: Excellent CO<sub>2</sub> storage material and support for designing Pd nanocatalyst for C–C cross-coupling reactions. *Journal of Materials Chemistry A*. 2014;**2**:11642-11650
- [66] Mengya N, Huaming Y, Xiangchao Z, Yutang W, Aidong T. Amine-impregnated mesoporous silica nanotube as an emerging nanocomposite for CO<sub>2</sub> capture. *ACS Applied Materials & Interfaces*. 2016;**8**:17312-17320
- [67] Das S, Maity A, Pradhan M, Jana S. Assessing atmospheric CO<sub>2</sub> entrapped in clay nanotubes using residual gas analyzer. *Analytical Chemistry*. 2016;**88**:2205-2211
- [68] Jana S, Das S, Ghosh C, Maity A, Pradhan M. Halloysite nanotubes capturing isotope selective atmospheric CO<sub>2</sub>. *Scientific Reports*. 2015;**5**:8711
- [69] Schaef HT, Glezakou VA, Owen AT, Ramprasad S, Martin PF, McGrail BP. Surface condensation of CO<sub>2</sub> onto kaolinite. *Environmental Science & Technology Letters*. 2014;**1**:142-145
- [70] Wang W, Xiao J, Wei X, Ding J, Wang X, Song C. Development of a new clay supported polyethylenimine composite for CO<sub>2</sub> capture. *Applied Energy*. 2014;**113**:334-341
- [71] Roth EA, Agarwal S, Gupta RK. Nanoclay-based solid sorbents for CO<sub>2</sub> capture. *Energy & Fuels*. 2013;**27**:4129-4136
- [72] Irani M, Fan M, Ismail H, Tuwati A, Dutcher B, Russell AG. Modified nanosepiolite as an inexpensive support of tetraethylenepentamine for CO<sub>2</sub> sorption. *Nano Energy*. 2015;**11**:235-246
- [73] Wang W, Wang X, Song C, Wei X, Ding J, Xiao J. Sulfuric acid modified bentonite as the support of tetraethylenepentamine for CO<sub>2</sub> capture. *Energy & Fuels*. 2013;**27**:1538-1546
- [74] Yang Z, Ren J, Zhang Z, Chen X, Guan G, Qiu L, Zhang Y, Peng H. Recent advancement of nanostructured carbon for energy applications. *Chemical Reviews*. 2015;**115**:5159-5223
- [75] Lozano-Castello D, Lillo-Rodenas MA, Cazorla-Amoros D, Linares-Solano A. Preparation of activated carbons from Spanish anthracite: I. Activation by KOH. *Carbon*. 2001;**39**:741-749
- [76] Radhakrishnan L, Reboul J, Furukuwa S, Srinivasu P, Kitagawa S, Yamauchi Y. Preparation of microporous carbon fibers through carbonization of Al-based porous coordination polymer (Al-PCP) with furfuryl alcohol. *Chemistry of Materials*. 2011;**23**:1225-1231
- [77] Olivares-Marín M, Sanz-Pérez ES, Wong MS, Maroto-Valer MM. Development of regenerable sorbents from abundant wastes for capture of CO<sub>2</sub>. *Energy Procedia*. 2011;**4**:1118-1124

- [78] Liu L, Singh R, Xiao P, Webley P, Zhai Y. Zeolite synthesis from waste fly ash and its application in CO<sub>2</sub> capture from flue gas streams. *Adsorption*. 2011;**17**:795-800
- [79] Ello AS, de Souza LKC, Trokourey A, Jaroniec M. Coconut shell-based microporous carbons for CO<sub>2</sub> capture. *Microporous and Mesoporous Materials*. 2013;**180**:280-283
- [80] Lewicka K. Activated carbons prepared from hazelnut shells, walnut shells and peanut shells for high CO<sub>2</sub> adsorption. *Polish Journal of Chemical Technology*. 2017;**19**:38-43
- [81] Khenniche L, Aissani F. Preparation and characterization of carbons from coffee residue: Adsorption of salicylic acid on the prepared carbons. *Journal of Chemical & Engineering Data*. 2010;**55**:728-734
- [82] Modak A, Bhaumik A. Porous carbon derived via KOH activation of a hypercrosslinked porous organic polymer for efficient CO<sub>2</sub>, CH<sub>4</sub>, H<sub>2</sub> adsorptions and high CO<sub>2</sub>/N<sub>2</sub> selectivity. *Journal of Solid State Chemistry*. 2015;**232**:157-162
- [83] Modak A, Bhaumik A. Surface-exposed Pd nanoparticles supported over nanoporous carbon hollow tubes as an efficient heterogeneous catalyst for the C–C bond formation and hydrogenation reactions. *Journal of Molecular Catalysis A: Chemical*. 2016;**425**:147-156
- [84] Saleh M, Chandra V, Kemp KC, Kim KS. Synthesis of N-doped microporous carbon via chemical activation of polyindole-modified graphene oxide sheets for selective carbon dioxide adsorption. *Nanotechnology*. 2013;**24**:255702
- [85] Wang J, Krishna R, Wu X, Sun Y, Deng S. Polyfuran-derived microporous carbons for enhanced adsorption of CO<sub>2</sub> and CH<sub>4</sub>. *Langmuir*. 2015;**31**:9845-9852



---

# Process Analytical Technology for CO<sub>2</sub> Capture

---

M.H. Wathsala N. Jinadasa, Klaus-J. Jens and  
Maths Halstensen

Additional information is available at the end of the chapter

<http://dx.doi.org/10.5772/intechopen.76176>

---

## Abstract

Carbon capture and storage, which is also known as CCS, is an obligatory climate change mitigation technology to reduce the carbon dioxide gas emissions to the atmosphere thus limiting the average global temperature increase to 2°C. Process analytical technology is a scientific tool to improve process qualities and performance through timely measurements. This chapter describes how process analytical technology can be imbedded to a carbon capture technology by giving a detailed example of implementation of a process analyzer to CO<sub>2</sub> capture by alkanolamine absorption process. Such an implementation requires success in five elements, which are described in this chapter. They are as follows: selecting an appropriate process analyzer, integration between the analyzer and the process, model development to enable the analyzer to predict a process-related chemical or physical attribute, use of the developed model in real-time application and use of the data obtained from the analyzer as an input to a process control unit. Partial least square regression model is a useful chemometric-based method to extract hidden chemical information in measurements from a process analyzer. In this chapter, four partial least square regression models are presented, which are developed to predict CO<sub>2</sub> concentration for four different alkanolamine solutions when these amines are used to absorb CO<sub>2</sub> from a combustion process.

**Keywords:** climate change, carbon dioxide capture, process analytical technology, process analyzers, chemometrics, partial least square regression, Raman spectroscopy

---

## 1. Introduction

### 1.1. Carbon dioxide and climate change

The Earth's atmosphere contains greenhouse gases such as water vapor, methane, ozone, carbon dioxide and nitrous oxide in trace levels, which have the ability to trap heat. By trapping

---

heat, temperature of the atmosphere increases which is referred to *greenhouse gas effect*. The greenhouse gas effect is a naturally occurring function in the atmosphere, but when the greenhouse gas level exceeds a certain amount, it couples with the climate and changes the natural equilibrium in the environment. Climate change mitigation actions are a top priority across the world today to fight the greatest environmental threat mankind has ever faced. Carbon dioxide (CO<sub>2</sub>) is not the strongest greenhouse gas but among all greenhouse gases, it is the most unwanted as it has made the highest influence to the climate change during the past 270 years [1]. While promoting green technologies such as renewable energy sources to reduce and avoid CO<sub>2</sub> emissions to the atmosphere, capturing CO<sub>2</sub> from the current emission sources is required to reach the climate change mitigation targets such as the 2°C target. Major CO<sub>2</sub> emission point sources are fossil fuel and biomass energy facilities, cement, iron & steel and petrochemical industry.

CO<sub>2</sub> capture and storage (CCS) is a three-step process consisting of CO<sub>2</sub> capture from emission sources; CO<sub>2</sub> transportation to storage sites and store in underground geological formations. In combustion processes, CO<sub>2</sub> can be captured either in pre-combustion or in post-combustion mode.

## 1.2. Carbon dioxide capture technologies

CO<sub>2</sub> can be separated from flue gas or fuel gas stream by processes such as absorption, adsorption, membrane separation, chemical looping, hydrate based separation, biochemical methods and cryogenic distillation. Among these separation technologies, the absorption process is the most mature because the basic technology is well known. Typical sorbents are alkanolamines and potassium bicarbonate. The most preferred option for retrofitting existing plants is post combustion capture technology (PCC), where CO<sub>2</sub> is scrubbed from the flue gas after combustion has taken place.

### 1.2.1. CO<sub>2</sub> capture by aqueous alkanolamine solvents

The basic reaction mechanism between CO<sub>2</sub> and pure amines/alkanolamines is the same; hence, both compound classes can be used for CO<sub>2</sub> capture. Although theoretically pure amine can enhance the performance of CO<sub>2</sub> capture than aqueous amines, pure amines and even high-concentrated aqueous amine solutions show implications in plant operations. Several experiments, pilot plant tests and theoretical simulations have been carried out to investigate the optimum amine concentration for CO<sub>2</sub> capture systems [2, 3]. Amine volatility for pure amine is, in general, higher than aqueous alkanolamine volatility. When the amine concentration is increased, amine degradation rate becomes higher [4] and the cost required for amine oxidation inhibitors is increased. CO<sub>2</sub> capture plants using higher amine concentrations require higher reboiler duty [5] and larger water washing sections. Therefore, aqueous alkanolamine solutions are preferred than pure amines. Furthermore, aqueous alkanolamines and in particular aqueous MEA are the commercial workhorse solvents for the CO<sub>2</sub> capture related gas sweetening industry [6].

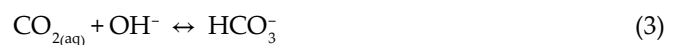
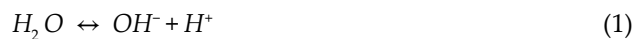


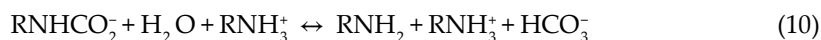
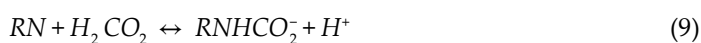
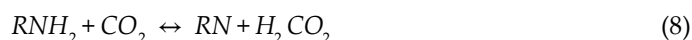
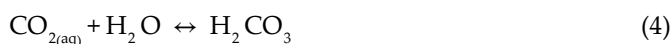
The IEA CCS road map requires to achieve 100 or more projects by 2020 to reduce the CO<sub>2</sub> capture energy penalty by 7% points by proving CO<sub>2</sub> capture technologies ready for large scale and demonstrating retrofit for 85% CO<sub>2</sub> capture [7]. The most common and cost-effective technology is absorbing CO<sub>2</sub> chemically into aqueous alkanolamine solutions such as monoethanolamine, monoethanolamine-glycol mixtures, diethanolamine, diglycolamine, diisopropanolamine, methyldiethanolamine, and mixed amines (including sterically hindered amines) [8–11]. Establishing CO<sub>2</sub> capture technology by MEA still have challenges, which have to be solved within a short period of time, such as equipment corrosion, solvent degradation, high solvent regeneration energy requirement and possible solvent emissions to the environment.

### 1.2.2. Chemical reactions of the CO<sub>2</sub>-alkanolamine-H<sub>2</sub>O system

A series of parallel equilibrium and kinetic reactions occur during CO<sub>2</sub> absorption into aqueous amine solution. This results in an electrolyte solution including ions such as OH<sup>-</sup>, HCO<sub>3</sub><sup>-</sup>, CO<sub>3</sub><sup>2-</sup>, RNHCO<sub>2</sub><sup>-</sup> and RNH<sub>3</sub><sup>+</sup> as shown in reactions from Eqs. (1)–(10). Here R represents an alkyl group such as CH<sub>3</sub> or C<sub>2</sub>H<sub>5</sub>. Reaction of CO<sub>2</sub> with this solution is a Brønsted acid-base neutralization reaction leading to a drop in solution pH as CO<sub>2</sub> is absorbed. The chemical composition of this solution varies according to overall solution pH.

Carbon dioxide gas physically dissolves in water to give a solvated form of carbon dioxide which is, CO<sub>2(aq)</sub> (Eq. (2)). Thereafter, CO<sub>2(aq)</sub> reacts chemically with water to give carbonic acid (Eq. (4)) which forms equilibria with bicarbonate (Eq. (5)) and carbonate (Eq. (6)) ions according to the respective pKa values. Amines are categorized as primary (RNH<sub>2</sub>), secondary (R<sub>2</sub>NH), tertiary (R<sub>3</sub>N) and sterically hindered amines (e.g., t-RNH<sub>2</sub>) based on their chemical structure. Amine reactivity of the CO<sub>2</sub>-alkanolamine-water system is determined by the N atom lone electron pair in a Zwitterion reaction mechanism [7]. Accepting a proton at the N lone electron pair, amines react as Brønsted bases according to a Brønsted acid–base reaction type. The N lone electron pair can also react with, for example, the carbon atom of the CO<sub>2</sub> molecule according to a Lewis acid-base reaction type. Carbonic acid reacts in aqueous solution with all amines in a 1:1 manner by a Brønsted acid-base reaction type to form protonated amine bicarbonate. Primary and secondary alkanolamines may also react rapidly with CO<sub>2</sub> through a Lewis acid-base reaction type to form amine carbamate. During carbamate formation, two amine molecules react with one CO<sub>2</sub> molecule; therefore, aqueous amine solutions forming protonated amine bicarbonate only achieve a higher CO<sub>2</sub> loading than aqueous primary or secondary amine solutions forming amine carbamates only.





These equilibrium equations (Eqs. (1)–(10)) can be manipulated for amine and absorbed  $\text{CO}_2$  considering the carbon and amine balance. The total number of moles of the  $\text{CO}_2$  is the sum of moles of carbonate, bicarbonate, carbamate ions and molecular  $\text{CO}_{2(\text{aq})}$ . The total number of amine moles is the sum of moles of protonated amine, free amine and carbamate ions. The mole ratio of  $\text{CO}_2$ :amine is known as  $\text{CO}_2$  loading. This value represents the  $\text{CO}_2$  absorption capacity by the amine and is considered as a crucial technology-related value. The reaction pathway for primary, secondary and tertiary amines is described in [12]. Primary and secondary amines react with  $\text{CO}_2$  to form carbamates which limits their theoretical  $\text{CO}_2$  absorption capacity to 0.5 mol  $\text{CO}_2$ /mol amine. Tertiary amines do not possess free proton in the nitrogen atom and hence do not directly react with  $\text{CO}_2$ . Their reaction pathway first involves increasing the hydroxyl ion concentration which contributes to react with  $\text{CO}_2$  to produce bicarbonate. Therefore, they have a higher theoretical  $\text{CO}_2$  absorption capacity which can go upto 1 mol  $\text{CO}_2$ /mol amine.

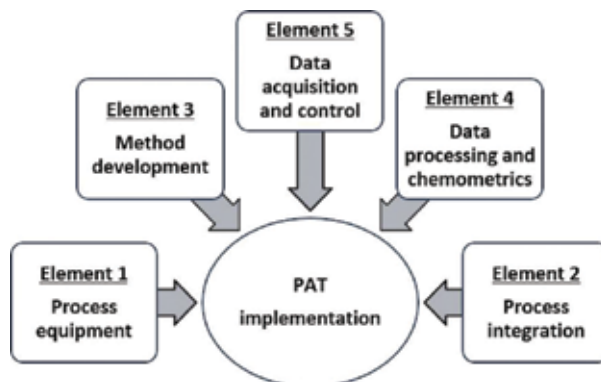
## 2. Process analytical technology and $\text{CO}_2$ capture

With reference to [13], *process analysis* is the chemical or physical analysis of materials in a process stream through in-line or on-line analyzer. *Process analyzers* can measure directly physical or chemical attributes in a system and supply data. Some key features of process analysis with respect to the laboratory analysis are: the speed of the analysis, zero manual sample handling and ability to integrate real-time data with process control. Process analytical technology (PAT) was originally defined by Food and Drug Administration (FDA) for pharmaceutical industry, as *a system for designing, analyzing, and controlling manufacturing through timely measurements (i.e., during processing) of critical quality and performance attributes*

of raw and in-process materials and processes, with the goal of ensuring final product quality [14]. However, PAT is a tool which can be applied to any process industry to increase its productivity by supplying product/process-related information real-time. Today, from laboratory to industrial scale, process analytical technology has replaced most of traditional methods to determine process-related attributes providing opportunities to understand chemical mechanisms, plant performance and optimization. CO<sub>2</sub> capturing is a continuous chemical process or a mass transfer operation where raw materials (e.g., flue gas from a power plant) are converted into a product (e.g., CO<sub>2</sub>-free-flue gas) in a process plant (e.g., absorption and desorption units). Unlike other industrial applications, CO<sub>2</sub> capturing is not an economically profitable process; instead it creates an additional burden to the economy such as increasing the cost of electricity production which creates a drawback for implementation. PAT has a considerable potential to support the strategies and methodologies to reach CCS targets. The concept of PAT within the CCS framework is not yet a well-discussed topic. However, the use of process analyzers in the CCS scientific research area has been gradually increasing during the last decade. This includes research on using different process analyzers to replace traditional laboratory methods, to understand reactions in the molecular level, and solvent selection based on spectroscopic data.

## 2.1. Implementation of a PAT tool for a CO<sub>2</sub> capture process

A successful and robust implementation of PAT is required to gain its widespread benefit to a process. It also saves money, time and resources. Since PAT applies to an entire product cycle, the implementation process should be modeled with simultaneous approach to sub-models such as business, production process, management, engineering, health-safety & environment and customer perspective. Although process analytical technologies improve the speed of the analysis, the stage of introducing such a technology requires knowledge, time and tremendous scientific work. Five elements are identified regarded to this stage and described in this section. **Figure 1** shows these five elements of a PAT implementation approach.



**Figure 1.** Elements of PAT implementation.

Element 1: Selecting a suitable process instrument for an application is challenging due to the variability of the availability. To determine a particular attribute of the process such as an analyte concentration, several simple to sophisticated measurement technologies are available. The vendors claim the general features of the instruments they sell but how deeply, accurately and precisely they response to our own application and the limitation of usage are unknown until we purchase the instrument and experience its measurements. Since PAT tools are expensive compared to traditional chemical analysis systems, the user may wish to use it for different applications. For instance, an R&D institution wants to use an analyzer to measure transparent liquid samples but later they also wish to analyze high turbid samples. An example is analysis of alkanolamine samples from an industrial CO<sub>2</sub> capture plant where samples are normally transparent when the fresh amines are used but will gradually become opaque due to thermal and oxidative degradation when the plant is operated continuously. If the user purchases an analyzer which only responses to transparent samples and is disturbed due to the fluorescence effect of turbidity in a sample, then this analyzer will stop its function when the solvent degradation starts. Therefore, if the investment requirement is to use this instrument throughout several days of plant operation, then the instrument selection becomes invalid and the whole implementation becomes unsuccessful. To avoid such disappointments in later stages of a PAT implementation, one should always thoroughly assess the selection criteria of the PAT tool. To ease this operation, the process can be started with categorizing available analyzers based on their selectivity, performance, limit of detection, complexity of usage, how it fits to the indoor and outdoor industrial environment as well as the budget. Analyzers can measure physical properties such as refractive index, thermal conductivity and viscosity. There are electrochemical analyzers measuring conductivity, pH and spectroscopic analyzers measuring concentration or any other attribute which is related to electromagnetic interaction. A detailed description about different types of process analyzers can be found in [15].

When selecting a suitable process analyzer, it becomes crucial whether the instrument can be easily integrated to the process system. Some instruments require advance mechanical modifications to the existing system or process stream in the installation process, which make them abatement only to that function. For example, if the requirement is plugging a sensor to a high-flow process stream, the engineer should assure that the plugging mechanism can withstand the maximum pressure of the system. Meanwhile, the process flow should not damage to the sensor. This kind of plugging modifications is normally fixed or permanent, and if the sensor is required to remove from the system, the process flow should be stopped and demand time. These practical problems restrict the analyzer only to this application. If we consider an insertion probe in a liquid stream, there are some critical factors affecting to the quality of the signal. They are angle of insertion, penetration depth, and turbulence of the process flow (as at some flow rates there can be bubble formation). If a probe, which has a higher penetration depth than the sample height of the measurement in an experimental set up, is selected to use, the set up should be modified to increase the sample height than the required penetration depth. If the probe is going to be inserted to a small diameter pipe, where the penetration depth is higher than the diameter, and the probe cannot be inserted to the pipeline directly. In such a case, a flow cell with higher diameter should be included to the

existing line. The volume of the new flow cell should not be larger to create stagnant places, dead zones, and inhomogeneous mixture. This can be challenging because the plant needs to be shut down before the modification. The required mechanical interface may not be easy or straightforward at some instances. Therefore, the engineer experiences the dilemma whether he should select an analyzer, which fits to the system, or he should change the system to fit to the analyzer. Normally, process analytical instruments are superior in giving fast responses. If the interest is online monitoring of concentration changes or reaction kinetics, the analyzer should give fast responses such as measurements in every minute. Frequency of calibration/maintenance of the analyzer, cleaning requirement between successive scans, required training or expertise to operate the instrument, whether the instrument can be operated continuously throughout an entire process or an experiment cycle are also limiting factors.

Element 2: Process integration implies the method of measurement taken from the application. After selecting the required process analyzer, the sample measurement is carried out inline, at line or online. Examples for inline are: an immersion probe which directly contact with the sample inside the process equipment, process line or flow cell. In such an instance, sample dilution or probe cleaning prior to each measurement is impossible. On the other hand, the user has the ability to do so if there is an autonomous sampling system, which is called on-line. There are some process analyzers, which cannot be physically integrated to the process such as liquid chromatography. Samples that are withdrawn from the process (grab samples) either manually or automatically are measured offline and called at-line measurements. Grab samples associate with the highest percentage of sampling errors.

Element 3: Process analytical instruments give both qualitative and quantitative analysis. Qualitative analysis gives the first impression to understand whether it is meaningful and worth to develop a method for quantitative analysis by a particular instrument. Process analytical instruments are calibrated and validated before they are used to demonstrate that it is suitable for intended purpose. Normally, calibration means to ensure that the instrument readings are accurate with reference to established standards. Calibration can be used before using an instrument such as a weighing balance or a pH meter. Vendor specifies when and how frequently the equipment is needed to calibrate. Normally, the validation refers that the equipment installed correctly and performing without an error comparably to the one used before. These vendors' specified calibration and validation are straightforward.

However, in the PAT terminology, *calibration and validation* imply converting the instrument signals/measurements to be suitable to perform a specific analysis. Based on measurements taken as a set of samples (*calibration set*), a multivariate regression model is developed to predict an attribute. The model prediction performance is validated based on another set of samples (*validation set*) prepared under similar environmental conditions as the *calibration set*. The model is tuned until the prediction error becomes lower than an acceptable value. For example, a model can be developed based on measurements from a spectrometer performed for a calibration set and validation set to predict pH of some chemicals. The same instrument can be used to develop models for other applications such as determining a concentration of a sample, to determine individual concentrations in a mixture of chemicals or analyzing an impurity of a sample. These kinds of model developments to analyze indirect property

are the main expectation from a PAT tool. The method of model development is described under Section 3 for an application in a CO<sub>2</sub> capture process. The calibration and validation procedure should follow the guidelines specified in *Theory of Sampling (ToS)* [16] and *Design of Experiment (DoE)*.

Element 4: Data processing and chemometrics are a subcategory of model development stage. When it comes to the implementation stage of a process analyzer to the plant, the researcher has experience from laboratory experiments or batchwise experiments on what kind of data treatment is needed. Usually raw data coming out from a process analyzer such as a spectrometer contain noise. The information in the data is hidden within this noise. Preprocessing makes data easier to read, understand and interpret. There are also some instances where univariate methods are implemented and/or data processing is not essential. After preprocessing, the data can be used as input to a chemometric model such as a principle component analysis (PCA) model or partial least square regression (PLSR) model. Different chemometric tools have different advantages. For example, PCA can be used to identify trends of variation in the data with respect to time or process conditions, and PLSR can be used to predict process features based on indirect measurements. PLSR is widely used in process applications for quantitative purposes. One such example can be found in [17] where it shows the use of PLSR to quantify all chemical ions present in a CO<sub>2</sub> capture laboratory rig operated by aqueous amine. Another example of PLSR model development and ion speciation is shown in [18] for CO<sub>2</sub> capture by ammonia process. A detailed description for PLSR theory, calibration and validation is described in the literature [19, 20].

Element 5: Data acquisition and instrument control of a process analyzer is an essential part to integrate analyzer measurements with an automative control system. In the case of univariate analysis, implementation of automation control system is easy. However, when it comes to multivariate methods, communication between the process analytical instrument and the control system is challenging. There is a gap between these two types. The reasons are that the analyzer has different file formats and sometimes the control system has been implemented in a different file format in a different flat form. For example, in the analyzer, the data may be saved in csv file format and the control system implemented in MATLAB/LabVIEW interface needs data only from a wavelength range and needs data in txt or mat format as inputs.



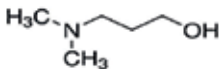
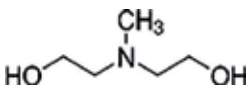
### **3. An experiment on developing a full calibration model using Raman spectroscopy**

The scope in this section is to present the methodology on how a process analytical instrument is implemented to replace traditional chemical analysis. The example described in this section is specific to CO<sub>2</sub> absorption process by amines, but a similar approach can be applied for any chemical analysis in laboratory or process plant. Analysis of CO<sub>2</sub> capture solvents is necessary almost in every R&D tasks and CO<sub>2</sub> process plants to optimize the absorption and desorption process. Some examples are investigating the effects of different types of solvents, blends, catalyzers, process parameters and equipment configuration on CO<sub>2</sub> absorption and desorption capacity.

In this example, it is shown how a Raman spectroscopy-based full spectrum calibration is performed using a laboratory experiment for four types of amines which are reacted with CO<sub>2</sub>. Sample types are described in **Table 1**. Two primary and two tertiary amines were used for preparing four regression models. The primary amines are 2-aminoethanol (MEA) and 3-amino-1-propanol (3-AP). Tertiary amines have a different chemical mechanism than primary and secondary amines when absorbing CO<sub>2</sub> and they can reach CO<sub>2</sub> loading capacity up to 1 mol CO<sub>2</sub>/mol amine. 3-dimethylamino-1-propanol (3DMA1P) and methyl diethanolamine (MDEA) are the two tertiary amines used in this experiment.

### 3.1. Sample preparation

For each model, a calibration and validation set was prepared to facilitate *test set validation* [21]. Number of samples in each calibration and validation set is given in **Table 1**. All the samples were prepared using analytical grade chemicals and Milli-Qwater (18.2 MΩ cm). Aqueous solutions and water were degassed using a rotavapor. First, two amine stock solutions having 30 w/w% (weight per total weight of solution) concentration were prepared and stirred in closed containers for 30 min using mechanical stirrers. Stirring helps to mix the two phases of water and solvent to get a homogeneous solution. CO<sub>2</sub> was bubbled into one stock solution until the whole amine sample was *maximum CO<sub>2</sub> loaded*. The meaning of *maximum CO<sub>2</sub> loaded* is that the solution is filled with equilibrium solubility of CO<sub>2</sub> at a given temperature and pressure. The time required to fully load the amine solution was calculated based on the data of volume of 30 w/w% amine sample, CO<sub>2</sub> bubbling flow rate, room temperature, pressure and equilibrium solubility. The CO<sub>2</sub> loaded amine solution was then stirred for 30 min in a closed vessel and left for 24 h at room temperature. The aim was to facilitate CO<sub>2</sub> gas dispersion homogeneously throughout the solution; to accelerate the reaction between gas and solvent and to reach equilibrated state. One gram from each stock solution was transferred to a beaker to titrate with 1 M hydrochloric acid (HCl) to determine amine

Name	Abbreviation	Chemical structure	Chemical category	Number of CO <sub>2</sub> loaded solutions	
				Calibration	Validation
2-Aminoethanol (monoethanolamine)	MEA		Primary amine	19	18
3-Amino-1-propanol	3-AP		Primary amine	22	20
3-dimethylamino-1-propanol	3DMA1P		Tertiary amine	21	20
Methyl diethanolamine	MDEA		Tertiary amine	21	20

**Table 1.** Description of samples in the calibration and validation set.

concentration. By mixing different ratios of CO<sub>2</sub> loaded amine solution with the other amine stock solution (CO<sub>2</sub> unloaded), a series of 38–42 different CO<sub>2</sub> loaded samples were prepared in 10 mL glass reactors. After the solution in each glass reactor reached equilibrium, a titration method (refer Section 3.2) was carried out to measure its true CO<sub>2</sub> concentration in units of moles CO<sub>2</sub> per mole solvent.

### 3.2. Analysis of reference samples

Determination of true CO<sub>2</sub> concentration (CO<sub>2</sub> loading) in alkanolamine samples was carried out by the *BaCl<sub>2</sub> titration-precipitation method*. 0.1 M Sodium hydroxide (NaOH), 0.1 M HCl, 1 M HCl, barium chloride (BaCl<sub>2</sub>) purchased from Merck (99%) and the titrator Mettler Toledo T50 were used for the experiment. The titration procedure is discussed in [22]. This titration is popular and a well-established method to analyze CO<sub>2</sub> loading in absorption processes both in laboratory and industrial applications. However, the method needs extensive chemical preparation; and it takes more than 2 h to analyze one sample and needs expertise and tedious manual work. The accuracy of the PLSR models is strongly affected by the accuracy and results of this analysis. All the sampling errors during sample extraction from stock solution, chemical preparation, weighing, transferring samples, dilution, filtering and titration were identified using a fish-bone analysis and addressed based on the knowledge from *Theory of Sampling* [16].

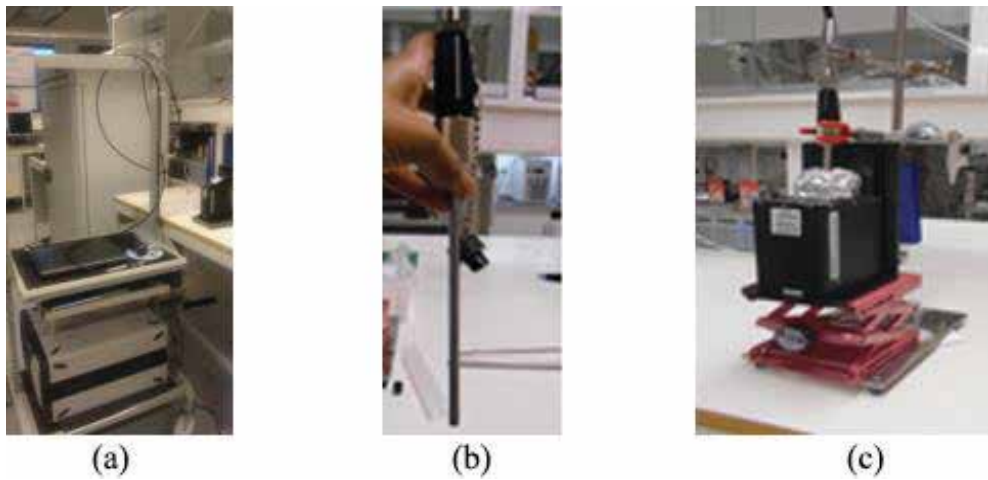
### 3.3. Raman spectroscopy

The Raman spectroscopy is a process analytical technique which can be used for batch-wise experiments where measurements are taken manually such as in laboratory tests, or for continuous operations such as in process plants where measurements can be taken continuously in each time interval. The instrument output is called a Raman spectrum which is a plot of intensity of scattered light (called Raman intensity) versus energy difference (given by wavenumber in cm<sup>-1</sup>). If the objective is to measure the concentration of a chemical sample using Raman spectroscopy, then the peaks and their intensity in a Raman spectrum indicate information about the type of chemicals and their composition respectively for the measured sample. Kaiser RXN2 Analyzer (as shown in **Figure 2a**) with 785 nm laser wavelength, 400 mW laser power and 100–3425 cm<sup>-1</sup> spectral range was the Raman spectrometer used in this experiment. An immersion optic probe was connected to the RXN2 Analyzer via a fiber optic cable (refer **Figure 2b**). During each measurement, the immersion probe was positioned vertically into the 10 mL glass reactor using a stand. The glass reactor was covered by a black box and aluminum foil to avoid interaction with fluorescence from external light sources (as shown in **Figure 2c**). Each scan was acquired as an average of six scans with 10 s over a total exposure time of 60 s to get a good signal-to-noise ratio.

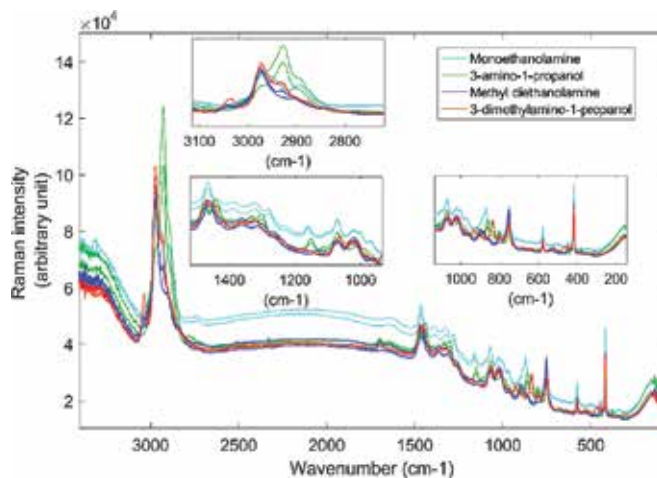
### 3.4. Data processing

The aim of the data processing is to condition the measurement signal by removing as much as possible of unwanted structure from the data. Including noisy spectra in regression model





**Figure 2.** RXN2 analyzer; (a) Raman analyzer with exciting source and detector; (b) Raman immersion probe; (c) sample is in an enclosed sample compartment (black box) and probe, which is mounted vertically, takes measurements.



**Figure 3.** Unprocessed Raman spectrum for four types of CO<sub>2</sub> loaded amine solutions.

calibration results in poor correlation between property to be predicted and measured. The RXN2 analyzer was used to generate a data matrix of  $n \times p$  where  $n$  is number of objects (e.g., different samples or measurements with time) and  $p$  is 3326 of Raman wavenumbers. This data matrix contains the chemical fingerprints of the objects and typically different types of noise. This noise comes from interference of other chemical components, laser input variations, noise from fiber optic cable or inadequate path length for the laser.

**Figure 3** shows some raw spectra for four types of CO<sub>2</sub> loaded amines where normal features of Raman spectra are visible such as baseline shifts, scattering and peak overlaps. These features avoid the raw spectra to be used directly for the calibration model. Preprocessing of

raw spectra is recommended to improve the predictability of a regression model. There are several preprocessing methods available for PAT applications [23, 24]. The optimal choice of preprocessing method is specific to the application and instrument. In this analysis, the baseline correction based on the Whittaker filter [25] and mean centering was applied which provided the lowest prediction errors as presented by root mean square error of prediction.

### 3.4.1. Variable selection

When  $\text{CO}_2$  is reacted with an amine, it is converted into different carbon ions as shown in Eqs. (1)–(10). The variables related to all these carbon species should be included as  $x$  variables for PLSR modeling. However, with reference to **Figure 3**, isolation of these variables from the rest of the spectra is not straightforward. The spectroscopy shows measurements in the wavelength range from 100 to  $3425\text{ cm}^{-1}$ . In the model development, only a selected range of wavelength was included. The spectra for all the solvents (**Figure 3**) show noise which means unwanted variation, both in higher and lower frequency ranges. The middle frequency range shows a flat behavior with some offsets between measurements. The wavelength below  $400\text{ cm}^{-1}$ , between  $1600$  and  $2600\text{ cm}^{-1}$  and after  $3100\text{ cm}^{-1}$  was excluded to remove this noise possibly arising either from the instrument, cables or measurement probe. Since these measurements are associated with a chemical reaction, there are frequencies which are assigned to vibrational mode of molecules. The reaction between alkanolamine and carbon dioxide produces carbonate, bicarbonate and carbamate ions for primary and secondary amines. Reaction between  $\text{CO}_2$  and a tertiary amine does not form carbamate. For a  $\text{CO}_2$ -loaded amine solution, the vibrational modes from carbon species and amine species appear in the Raman spectra collectively which makes it more complex to study. One can understand what kind of chemical species present in a chemical system by observing peaks which vary with different concentrations. On the other hand, knowing what kind of chemical species present in the system helps to identify the peaks which should respond differently when concentration changes. This fact is very important when selecting variables for modeling. Having a small number of variables makes the model easier to interpret.

There are disadvantages having unwanted variables in the model. The biggest challenge is overfitting, which makes the model correlate with the property to be predicted ( $y$  variable) during the model development stage, but future samples predict poorly. For instance, when developing a PLS model to predict total  $\text{CO}_2$  loading in an aqueous MEA solution, important  $x$  variables are the vibrational modes coming from carbon species (i.e., carbonate, bicarbonate and carbamate ions). According to the vapor-liquid equilibrium in the system, the protonated MEA and free MEA concentrations correlate almost linearly with  $\text{CO}_2$  loading less than  $0.5\text{ mol CO}_2/\text{mol MEA}$  [9]. Therefore, by mistake, one can include the variables assigned to protonated MEA and free MEA to show a good correlation with  $\text{CO}_2$  concentration. However, when this model is used for samples except those are in the calibration and validation sets, predictions will be unreliable.

When there is little or no knowledge on how the  $x$  variables relate to the  $y$  variable, variable selection becomes further critical. In principle, all combinations of  $x$  variables must be tried to

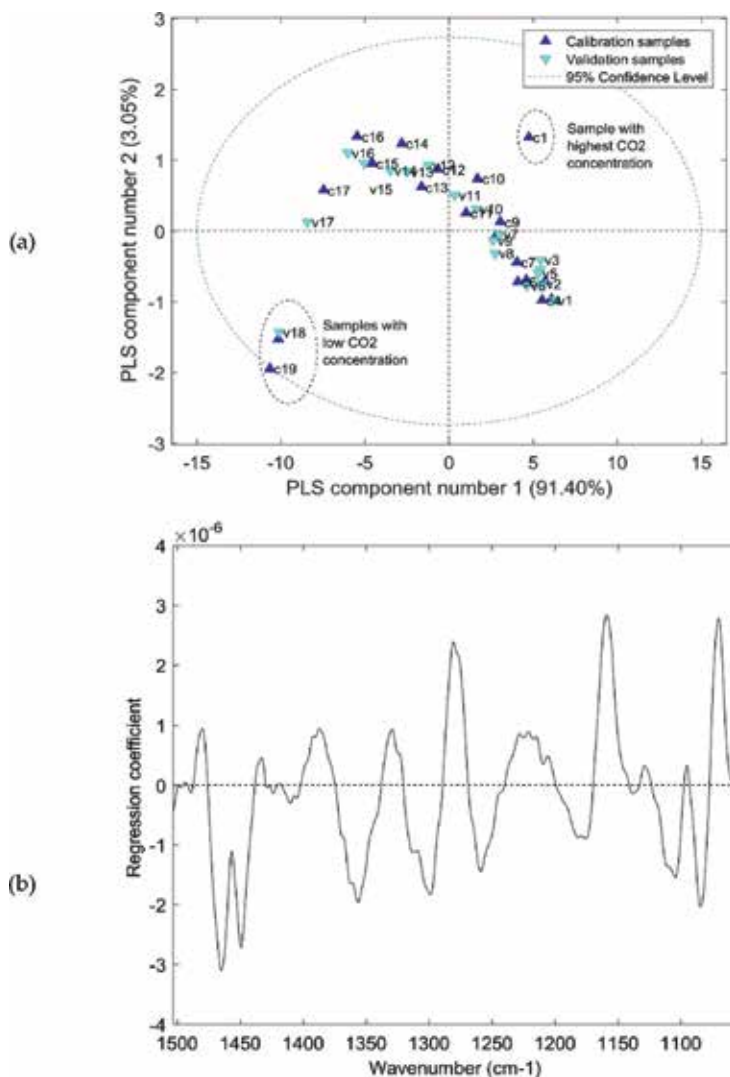
find the optimal choice which is not possible and practical. At such instances, variable selection methods such as iPLS (interval partial least squares regression), genetic algorithms (GA), selectivity ratio and jack-knife can be used [26]. Similar to finding the optimal preprocessing method, finding the optimal variable range is specific to the application and is an iterative procedure. In this example, the selection of the variable range for each model was performed which included vibrational modes of important carbon species available in literature [18]. Due to the overlapping of peaks, it was difficult to isolate the exact area for related vibrational modes and therefore 1000–1500 cm<sup>-1</sup> and 1000–1164 cm<sup>-1</sup> regions were selected for primary and tertiary amines respectively which made the models with the lowest RMSEPs.

### 3.5. Results

The calibration and validation results for each of the four respective PLSR models for CO<sub>2</sub> concentration in MEA, MDEA, 3-AP and 3-DMA1P solutions are presented in this section. Data preprocessing and model development were implemented in PLS Toolbox 8.21 in the MATLAB 2016a software (MathWorks Inc.).

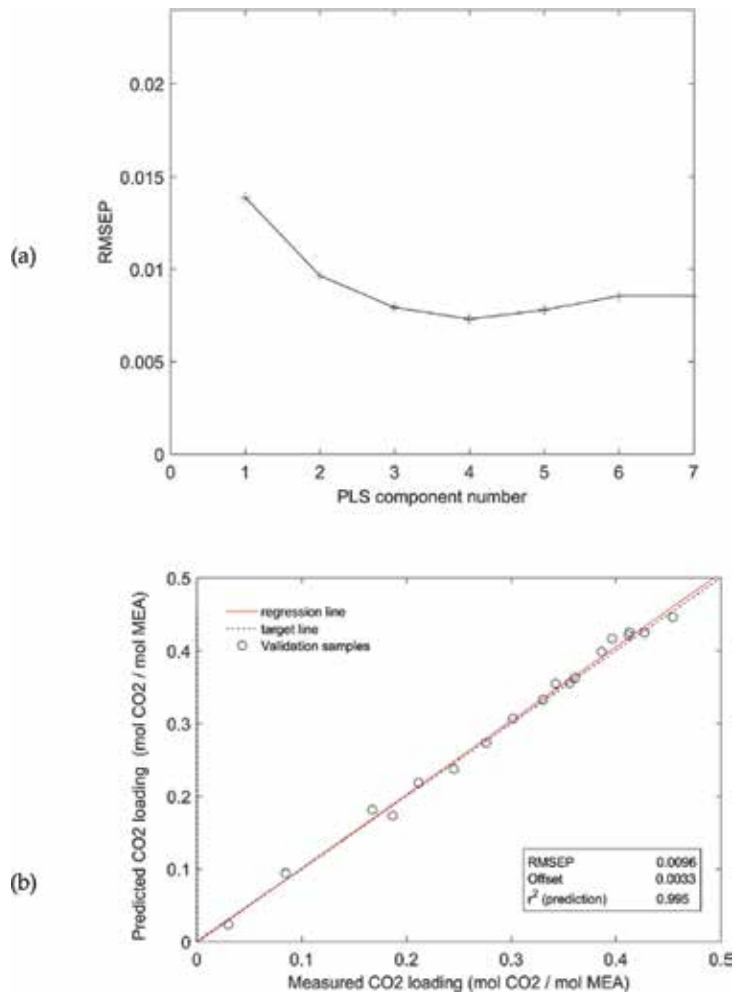
The model behavior is presented using four graphs for each amine solution (from **Figures 4–11**) which are the score plot (t1–t2), regression coefficients, RMSEP and predicted CO<sub>2</sub> loading versus the measured loading. In the plots, *c* represents calibration samples and *v* represents validation samples. Samples are numbered as 1, 2, 3, 4 onwards with decreasing CO<sub>2</sub> concentration. The regression coefficient plot is an indication on what weight of each wavenumber contributes to the prediction. The higher the regression weight, the higher the importance of the assigned wavelength to the prediction. The regression plot can be mapped with the vibrational modes of carbon species which are chemically important to the total CO<sub>2</sub> loading.

The score plot gives the overview of the span of the calibration data and validation data. Even without knowing the value of CO<sub>2</sub> loading (*y variable*), by visualizing the sample location in the score plot, one can understand whether the sample is highly or less concentrated with CO<sub>2</sub>. Score plot can also be used to identify outliers which mean samples that show nonrepresentative *x variables*. There can be various reasons for outliers such as impurities in samples, different sample type, instrument error and sampling errors. During the model development stage, if such outliers are identified, they should be carefully analyzed and removed from the model. When the model is used for process monitoring, visualization of such outliers helps in the quick identification of the abnormal behavior in the process. With the increasing number of PLS components, the prediction error of the models varies. A plot of RMSEP versus number of PLS components is used to conclude the required number of PLS components for the model. It is always preferable to select a small number of PLS components to avoid model complexities. An optimum number of PLS components avoids the risk of overfitting of the model. The aim of the model is to use the instrument for predicting CO<sub>2</sub> concentration. The predicted versus measured plots show how far the measured values deviate with respect to the predicted values for the validation set. This deviation is interpreted with statistical parameters such as *r*<sup>2</sup>, RMSEP and offset. When *test set validation* is used, this plot gives an image on how the model will align with future data.



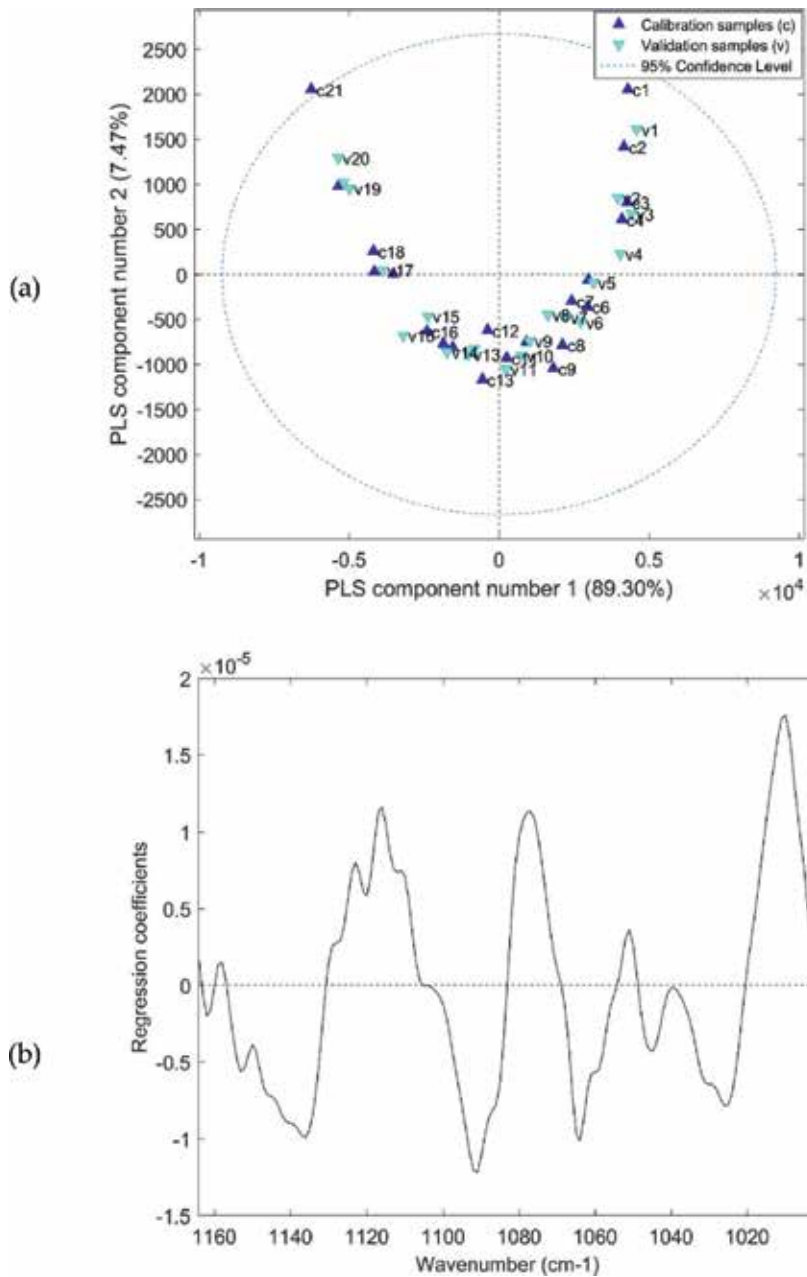
**Figure 4.** Results from PLSR model for MEA; (a) score plot of PLS components 1 vs. 2 showing calibration and validation samples; (b) regression coefficients based on a 2-component PLSR model.

**Figure 4(a)** is the score plot of PLS component 1 vs. 2 for MEA model. According to this plot, PLS component 1 describes more than 90% of variation of data while PLS component 2 describes around 3% of variation. The sample with the highest CO<sub>2</sub> concentration (*c1*) and that with the lowest CO<sub>2</sub> concentration (*c19*, *v18*) appear isolated in the score plot implying they have extreme concentration values. The samples are spread in the plot as a pattern where they move from right to left in the direction of PLS component 1 as the concentration decreases. When this model is used for new data, they will appear in the same data swarm area. Samples with high CO<sub>2</sub> concentration will appear in the positive side of PLS component 1 and when



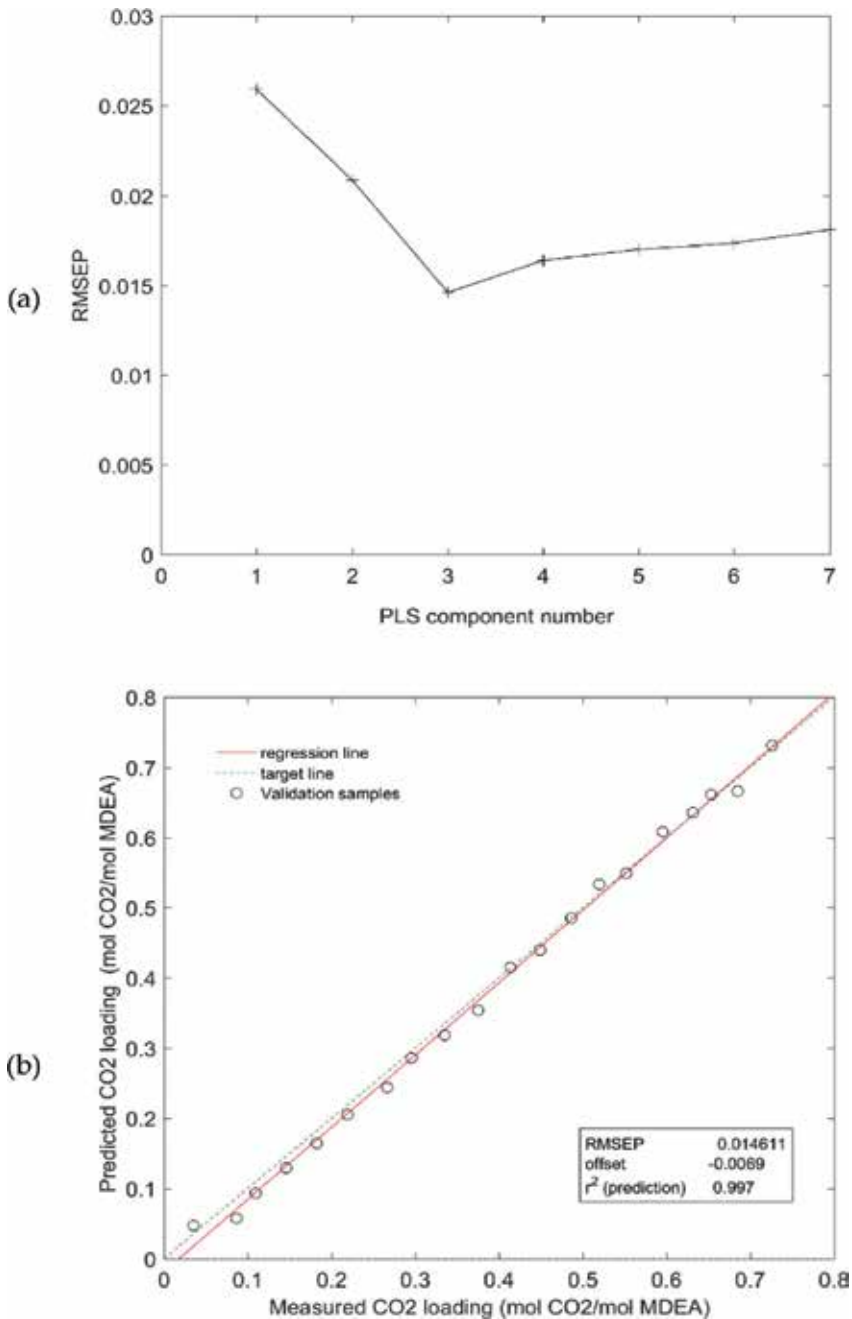
**Figure 5.** Results from PLSR model for MEA; (a) RMSEP with respect to number of PLS components and (b) predicted versus measured CO<sub>2</sub> loading.

their concentration increases, they move toward the negative side of PLS component 1. **Figure 4(b)** is the plot of regression coefficients between the wavenumber 1000–1500 cm<sup>-1</sup>. Wavenumbers having positive and negative regression coefficients contribute positively and negatively respectively for the predicted property. **Figure 5(a)** shows the variation of RMSEP with increasing number of PLS component. According to this plot, RMSEP becomes the lowest at fourth PLS component. Having a higher number of PLS components in the model increases model complexity and include more noise to the model. There is not much difference in the prediction error between PLS component 2 and PLS component 4. Therefore, two PLS components were selected for the prediction model. **Figure 5(b)** shows how well the model fits when using for the validation data set to predict CO<sub>2</sub> concentration using their Raman spectra.



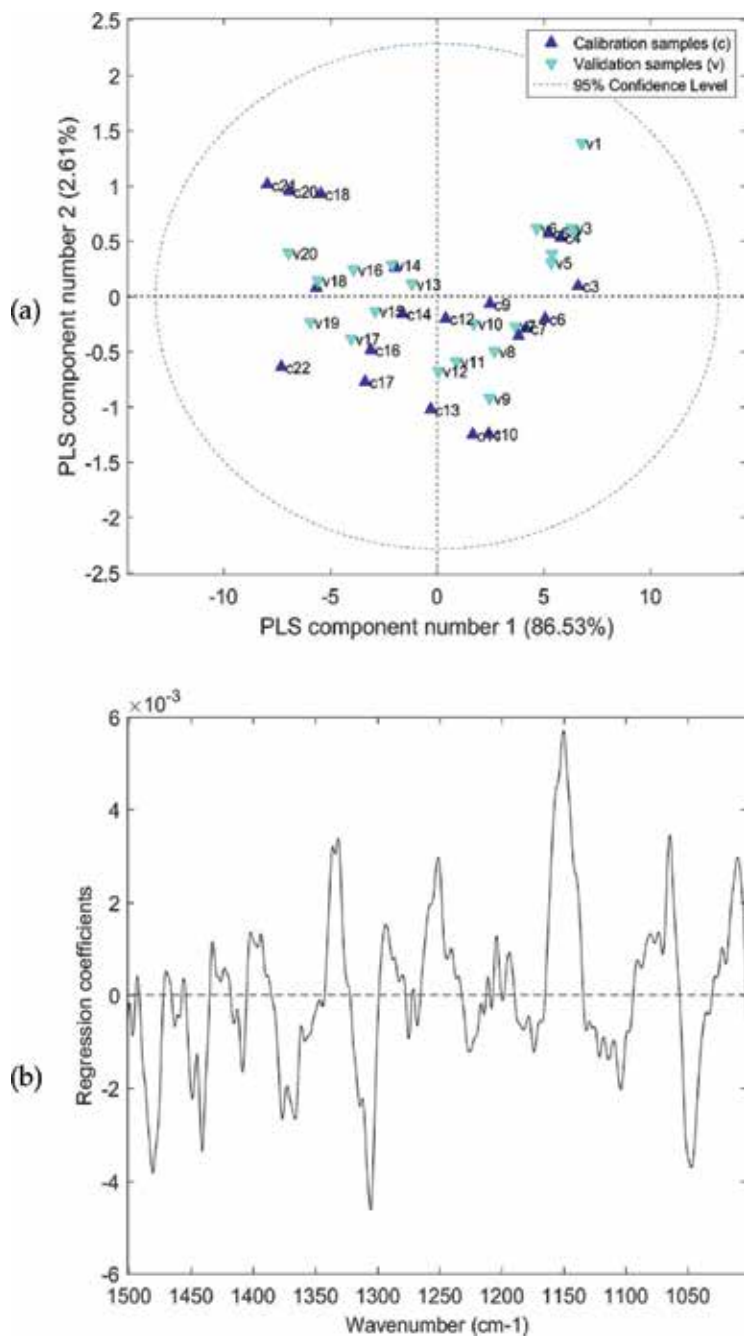
**Figure 6.** Results from PLSR model for MDEA; (a) score plot of PLS components 1 vs. 2 showing calibration and validation samples and (b) regression coefficients based on a 3-component PLSR model.

Similarly, in **Figure 6(a)**, score plot for the MDEA model shows a data swarm with a pattern moving from positive to negative side of PLS component 1 when the concentration decreases in MDEA samples. Plot of regression coefficients between wavenumber 1000 and 1164  $\text{cm}^{-1}$  as shown in **Figure 6(b)** indicates that there are both positively and negatively correlated



**Figure 7.** Results from PLSR model for MDEA; (a) RMSEP with respect to number of PLS components and (b) predicted versus measured CO<sub>2</sub> loading.

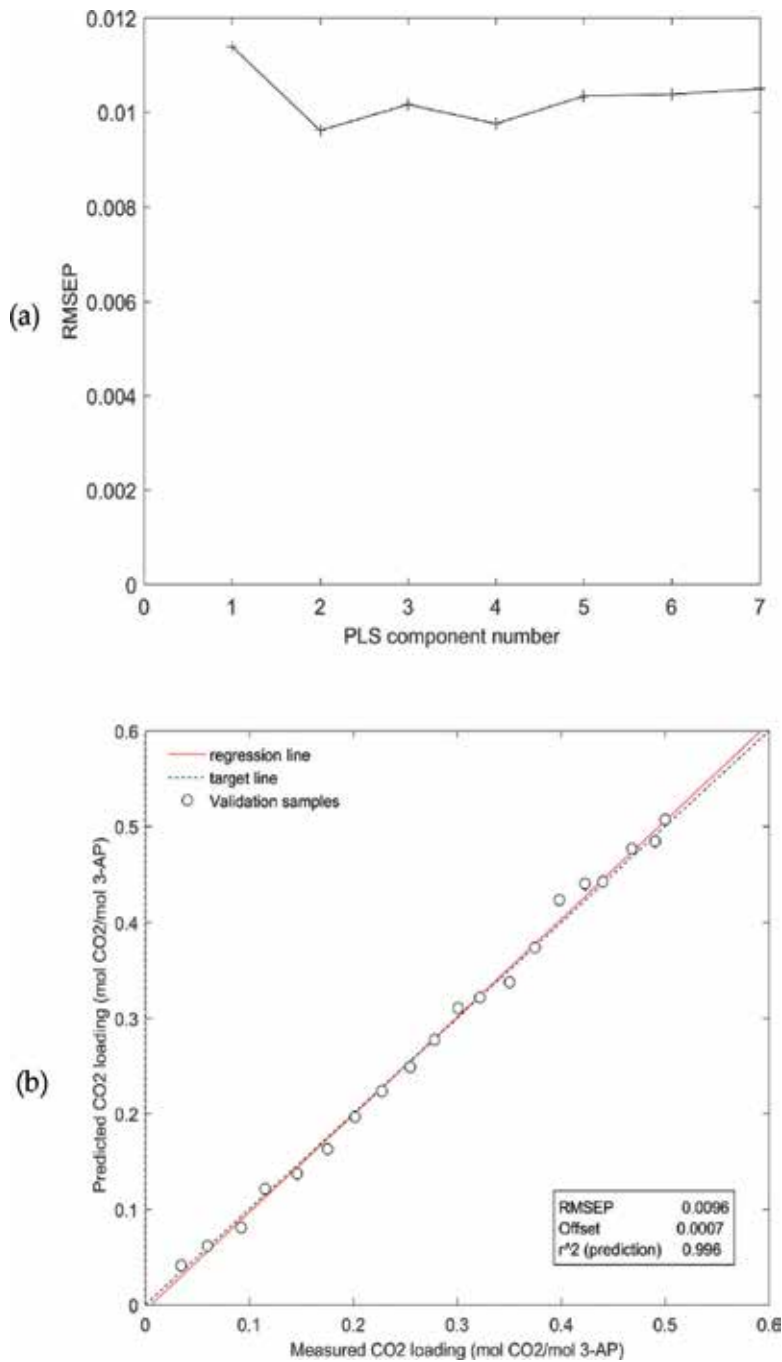
frequencies for the model in this range. Since the model shows the lowest RMSEP at PLS component 3 as given in **Figure 7(a)**, three components were selected for the model and model predictions for validation data set are shown in **Figure 7(b)** resulting an  $r^2$  of 0.995.



**Figure 8.** Results from PLSR model for 3-AP; (a) score plot of PLS components 1 vs. 2 showing calibration and validation samples and (b) regression coefficients based on a 2-component PLSR model.

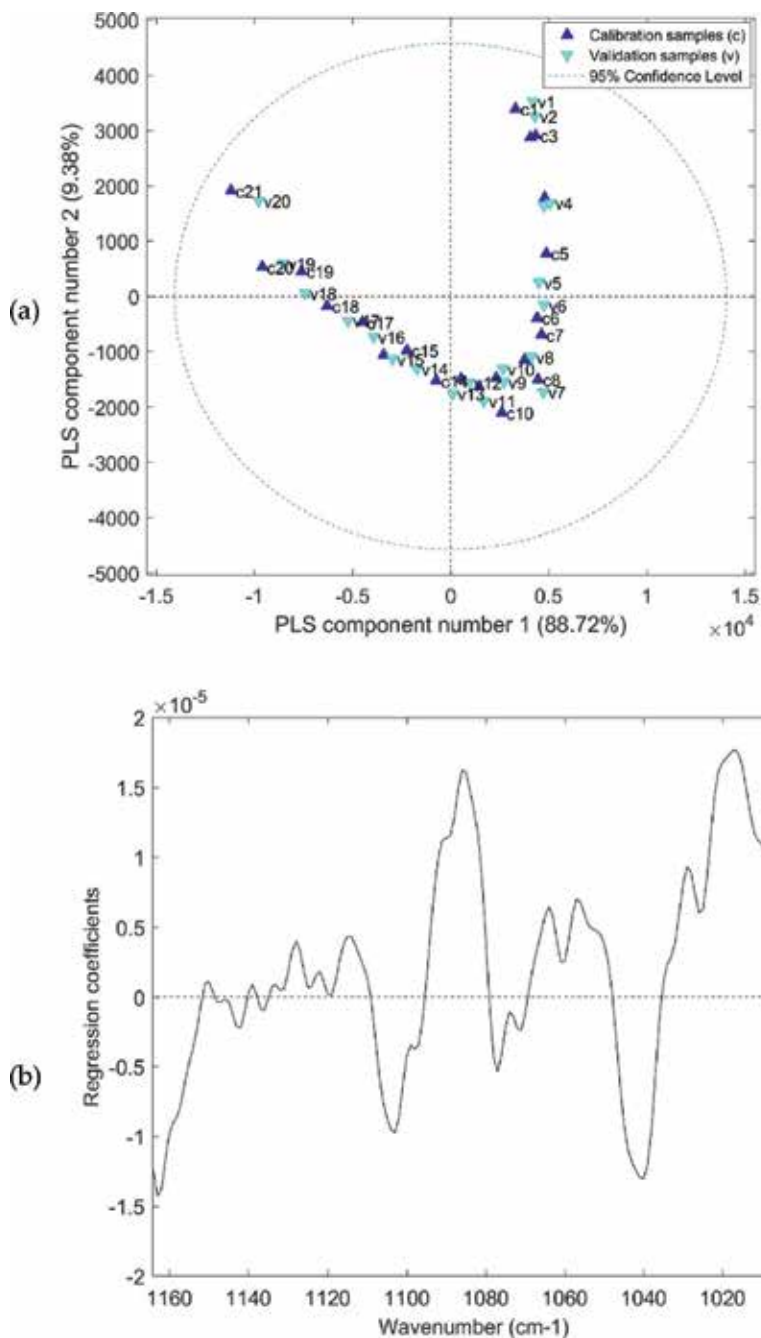
**Figure 8(a)** shows the movement of samples from positive to negative side of PLS component 1 as the  $\text{CO}_2$  concentration decreases in  $\text{CO}_2$  loaded 3-AP solvent. The plot of regression coefficients between 1000 and 1500  $\text{cm}^{-1}$  as given in **Figure 8(b)** shows negatively and positively





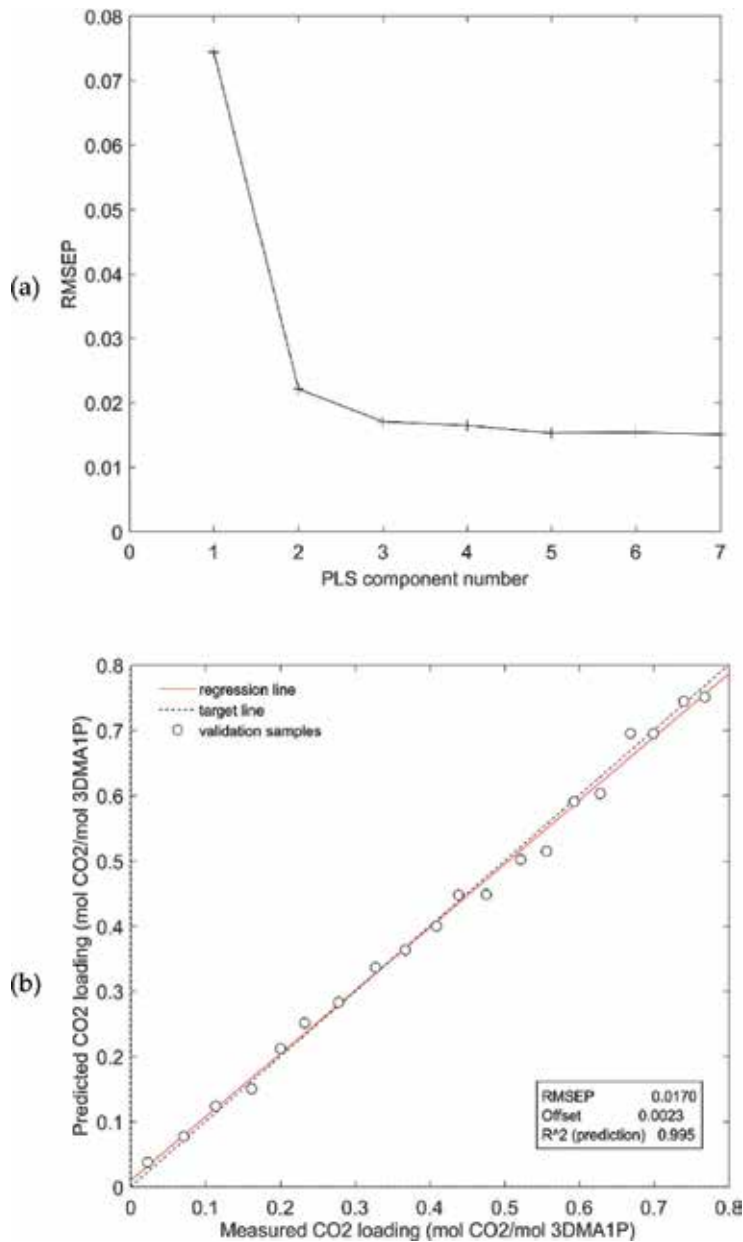
**Figure 9.** Results from PLSR model for 3-AP; (a) RMSEP with respect to number of PLS components and (b) predicted versus measured CO<sub>2</sub> loading.

correlated wavenumbers to the model predictions. According to RMSEP variation with respect to number of PLS components, two PLS components (**Figure 9(a)**) were selected for the model. **Figure 9(b)** shows how well model predicts for the test set samples. The model results



**Figure 10.** Results from PLSR model for 3DMA1P; (a) score plot of PLS components 1 vs. 2 showing calibration and validation samples and (b) regression coefficients based on a 3-component PLSR model.

for the tertiary amine 3DMA1P are shown in **Figures 10** and **11**. Similar to other solvents, the score plot shows a systematic variation of data swarm (**Figure 10(a)**) while **Figure 10(b)** shows the most and least important variables between 1000 and 1164  $\text{cm}^{-1}$  wavenumbers. Three PLS



**Figure 11.** Results from PLSR model for 3DMA1P; (a) RMSEP with respect to number of PLS components and (b) predicted versus measured CO<sub>2</sub> loading.

components were selected (**Figure 11(a)**) for solvent 3DMA1P, and the model predicts the validation samples with  $r^2$  of 0.995 (**Figure 11(b)**).

A summary of the model details for each amine solution is presented in **Table 2**. For all the predictions models, RMSEP percentages are less than 2.13% and  $r^2$  is  $\geq 0.995$ . Each PLSR model is valid only for the CO<sub>2</sub> loading range which is given in **Table 2**.

Model	CO <sub>2</sub> loading range (mol CO <sub>2</sub> /mol amine)	Variable range (cm <sup>-1</sup> )	PLS components	RMSEP (RMSEP %)	r <sup>2</sup>
MEA	0–0.4543	1000–1500	2	0.0096 (2.11)	0.995
3-AP	0–0.5149	1000–1500	2	0.0096 (1.86)	0.996
3DMA1P	0–0.7945	1000–1164	3	0.017 (2.13)	0.995
MDEA	0–0.7449	1000–1164	3	0.014 (1.88)	0.997

**Table 2.** Summary of PLSR models.

When these models are used for predictions of CO<sub>2</sub> loading in future samples, first their Raman spectra are preprocessed using Whittaker filter and mean centering. The required variable range is selected for each model and using the regression coefficient equation as shown in Eq. (11), the CO<sub>2</sub> loading is predicted.

$$Y = b_0 + b_1 X_1 + b_2 X_2 + b_3 X_3 + \dots + b_n X_n \quad (11)$$

In Eq. (11),  $Y$  is the predicted CO<sub>2</sub> concentration;  $b_0$  is regression coefficient for the intercept,  $X_n$  is the preprocessed  $n$ th variable (Raman wavenumber) and  $b_n$  is the regression coefficient relevant to variable  $X_n$ .

In PAT, chemometric modeling does not end once a model is calibrated and validated to achieve a targeted prediction accuracy and precision. The model is needed to undergo continuous improvement or remodeling. Some suggestions are assessing the current model performance using new validation data, using additional calibration data to remodel the existing model, improving data preprocessing methods, improving sampling methods, moving to more accurate reference analysis, different  $x$  variable ranges and including calibration samples with more variations.

## 4. Conclusions

Implementation of PAT tools in CO<sub>2</sub> capture process is useful in many ways to accelerate laboratory analysis, R&D tasks and full-scale plant operations. One such example is using a Raman spectroscopy to determine CO<sub>2</sub> concentration in alkanolamine solutions real-time. During the process of implementation of a process analyzer for such an application, a chemometrics-based calibration model should be prepared. Four PLSR models were developed to predict CO<sub>2</sub> concentration in two primary amines and two tertiary amines solutions during CO<sub>2</sub> absorption process. The models predictions are satisfactory where RMSEP are 2.11, 1.86, 2.13 and 1.88% for MEA, 3-AP, 3DMA1P and MDEA, respectively. The target of the present experimental work was to show the PLSR calibration model development for reaction between CO<sub>2</sub> aqueous amine solutions. Primary amine and tertiary amine type was selected for the study because they have two different types of reaction mechanisms. Hence, work on secondary alkanolamines, and so on was out of scope. However, we expect that creating

a model for secondary amines would be similar to the reported case of primary amine since both primary and secondary amines produce carbamate when reacted with CO<sub>2</sub>.

## Acknowledgements

The financial support provided by the PhD scholarship program in Process, Energy and Automation Engineering of University College of Southeast Norway is greatly acknowledged.

## Conflict of interest

The authors in this paper declare no conflicts of interest.

## Author details

M.H. Wathsala N. Jinadasa, Klaus-J. Jens and Maths Halstensen\*

\*Address all correspondence to: [maths.halstensen@usn.no](mailto:maths.halstensen@usn.no)

Applied Chemometrics Research Group (ACRG), University College of Southeast Norway, Porsgrunn, Norway

## References

- [1] IPCC. Climate change: The physical science basis. Working Group I contribution to the IPCC Fifth Assessment Report. Cambridge, United Kingdom: Intergovernmental Panel on Climate Change; 2013
- [2] Enaasen Flø N, Knuutila H, Kvamsdal HM, Hillestad M. Dynamic model validation of the post-combustion CO<sub>2</sub> absorption process. *International Journal of Greenhouse Gas Control*. 2015;**41**:127-141. DOI: <https://doi.org/10.1016/j.ijggc.2015.07.003>
- [3] Garcia M, Knuutila HK, Gu S. ASPEN PLUS simulation model for CO<sub>2</sub> removal with MEA: Validation of desorption model with experimental data. *Journal of Environmental Chemical Engineering*. 2017;**5**(5):4693-4701. DOI: <https://doi.org/10.1016/j.jece.2017.08.024>
- [4] Supap T, Idem R, Tontiwachwuthikul P, Saiwan C. Kinetics of sulfur dioxide- and oxygen-induced degradation of aqueous monoethanolamine solution during CO<sub>2</sub> absorption from power plant flue gas streams. *International Journal of Greenhouse Gas Control*. 2009;**3**(2):133-142. DOI: <https://doi.org/10.1016/j.ijggc.2008.06.009>
- [5] Brigman N, Shah MI, Falk-Pedersen O, Cents T, Smith V, De Cazenove T, et al. Results of amine plant operations from 30 wt% and 40 wt% aqueous MEA testing at the CO<sub>2</sub> technology Centre Mongstad. *Energy Procedia*. 2014;**63**:6012-6022. DOI: <https://doi.org/10.1016/j.egypro.2014.11.635>

- [6] Kohl AL, Nielsen R. Gas Purification. 5th ed. Texas: Gulf Professional Publishing; 1997
- [7] IEA. Technology Roadmap Carbon Capture and Storage. International Energy Agency; 2013
- [8] Afkhamipour M, Mofarahi M. Comparison of rate-based and equilibrium-stage models of a packed column for post-combustion CO<sub>2</sub> capture using 2-amino-2-methyl-1-propanol (AMP) solution. *International Journal of Greenhouse Gas Control*. 2013;**15**(supplement C):186-99. DOI: <https://doi.org/10.1016/j.ijggc.2013.02.022>
- [9] Austgen DM, Rochelle GT, Peng X, Chen CC. Model of vapor-liquid equilibria for aqueous acid gas-alkanolamine systems using the electrolyte-NRTL equation. *Industrial Engineering Chemistry*. 1989;**28**(7):1060-1073
- [10] Sidi-Boumedine R, Horstmann S, Fischer K, Provost E, Fürst W, Gmehling J. Experimental determination of carbon dioxide solubility data in aqueous alkanolamine solutions. *Fluid Phase Equilibria*. 2004;**218**:85-94
- [11] Tontiwachwuthikul P, Meisen A, Lim CJ. CO<sub>2</sub> absorption by NaOH, monoethanolamine and 2-amino-2-methyl-1-propanol solutions in a packed column. *Chemical Engineering Science*. 1992;**47**(2):381-390. DOI: [https://doi.org/10.1016/0009-2509\(92\)80028-B](https://doi.org/10.1016/0009-2509(92)80028-B)
- [12] Nwaoha C, Saiwan C, Supap T, Idem R, Tontiwachwuthikul P, Rongwong W, et al. Carbon dioxide (CO<sub>2</sub>) capture performance of aqueous tri-solvent blends containing 2-amino-2-methyl-1-propanol (AMP) and methyldiethanolamine (MDEA) promoted by diethylenetriamine (DETA). *International Journal of Greenhouse Gas Control*. 2016;**53**:292-304. DOI: <https://doi.org/10.1016/j.ijggc.2016.08.012>
- [13] Guenard R, Thureau G. Implementation of Process Analytical Technologies. In: Bakeev KA, editor. *Process Analytical Technology: Spectroscopic Tools and Implementation Strategies for the Chemical and Pharmaceutical Industries*. Chichester: John Wiley & Sons, Ltd.; 2010. p. 17-36
- [14] FDA. FDA Guidance for Industry: PAT—A Framework for Innovative Pharmaceutical Development, Manufacturing and Quality Assurance Food and Drug Administration; 2004 [Available from: <http://www.gmp-compliance.org/guidemgr/files/PAT-FDA-6419FNL.PDF> [Accessed: 22/12/2017]
- [15] *Process Analytical Technology: Spectroscopic Tools and Implementation Strategies for the Chemical and Pharmaceutical Industries*. 2nd ed. Bakeev KA, editor. Chichester: John Wiley & Sons, Ltd.; 2010
- [16] Esbensen KH, Paasch-Mortensen, P. Process sampling: Theory of sampling—The missing link in process analytical technologies (PAT). In: Bakeev KA, editor. *Process Analytical Technology: Spectroscopic Tools and Implementation Strategies for the Chemical and Pharmaceutical Industries*. 2nd ed. Chichester, UK: John Wiley & Sons, Ltd; 2010
- [17] Jinadasa MHW, Jens K-J, Øi LE, Halstensen M. Raman spectroscopy as an online monitoring tool for CO<sub>2</sub> capture process: Demonstration using a laboratory rig. *Energy Procedia*. 2017;**114**:1179-1194. DOI: <https://doi.org/10.1016/j.egypro.2017.03.1282>

- [18] Halstensen M, Jilvero H, Jinadasa WN, Jens K-J. Equilibrium measurements of the NH<sub>3</sub>-CO<sub>2</sub>-H<sub>2</sub>O system: Speciation based on Raman spectroscopy and multivariate modeling. *Journal of Chemistry*. 2017;**2017**:13. DOI: 10.1155/2017/7590506
- [19] Esbensen KH, Guyot D, Westad F, Houmoller LP. *Multivariate Data Analysis: In Practice*. CAMO Software; 2010
- [20] Martens H, Tormod N. *Multivariate calibration*. Canada: John Wiley & Sons; 1989
- [21] Esbensen KH, Geladi P. Principles of proper validation: Use and abuse of re-sampling for validation. *Journal of Chemometrics*. 2010;**24**(3-4):168-187. DOI: 10.1002/cem.1310
- [22] Weiland RH, Trass O. Titrimetric determination of acid gases in alkali hydroxides and amines. *Analytical Chemistry*. 1969;**41**(12):1709-1710. DOI: 10.1021/ac60281a024
- [23] Liland KH, Almøy T, Mevik B-H. Optimal choice of baseline correction for multivariate calibration of spectra. *Applied Spectroscopy*. 2010;**64**(9):1007-1016. DOI: 10.1366/000370210792434350
- [24] Rinnan Å, Berg F, Engelsen S. Review of the Most Common pre-Processing Techniques for Near-Infrared Spectra. *TRAC—Trends in Analytical Chemistry*. 2009;**28**(10):1201-1222
- [25] Eilers PHC. A perfect smoother. *Analytical Chemistry*. 2003;**75**(14):3631-3636
- [26] Andersen CM, Bro R. Variable selection in regression—A Tutorial. *Journal of Chemometrics*. 2010;**24**(11-12):728-737





---

# **Carbon Dioxide Use in High-Pressure Extraction Processes**

---

Vânia Maria Borges Cunha, Marcilene Paiva da Silva,  
Wanessa Almeida da Costa,  
Mozaniel Santana de Oliveira,  
Fernanda Wariss Figueiredo Bezerra,  
Anselmo Castro de Melo,  
Rafael Henrique Holanda Pinto,  
Nelio Teixeira Machado, Marilena Emmi Araujo and  
Raul Nunes de Carvalho Junior

Additional information is available at the end of the chapter

<http://dx.doi.org/10.5772/intechopen.71151>

---

## **Abstract**

This chapter describes the use of carbon dioxide at high pressures as an alternative for the extraction of bioactive compounds in a more sustainable way, addressing some of its physicochemical properties, such as pressure, temperature, density, solvation, selectivity, and its interaction with the solute when modified by other solvents such as ethanol and water. This extraction process is considered chemically “green,” when compared to conventional extraction processes using toxic organic solvents.

**Keywords:** supercritical CO<sub>2</sub>, high pressure, density, vegetable matrix, bioactive compounds

---

## **1. Introduction**

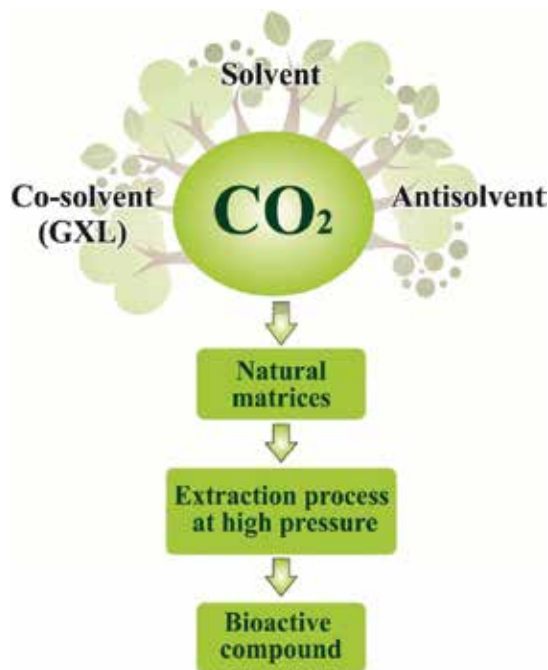
Separation technologies with fluids at high pressures are essentially vital to get new natural products of vegetable or marine origin that have biological activity, so-called bioactive extracts. Among the developed technologies, the supercritical fluid technology offers products free of residual solvent and that typically present high quality, when compared to products obtained by conventional techniques. The extracts of bioactive compounds can be obtained by extraction

---

of solid matrices (leaves, seeds, pulps, etc.) or by extraction/fractionation of liquid mixtures (aqueous solutions, fish oils, microalgae oils, vegetable oil, deodorize distillates, etc.) [1–5]. In processes at high pressures, which are near or above the critical point (pressure and temperature), the solvent density increases drastically and this is the most important parameter associated to the solvent power. As illustrated in **Figure 1**, carbon dioxide, a non-toxic substance, acting as solvent, co-solvent, or anti-solvent, is the most important fluid used in the supercritical fluid technology in extraction, separation, fractionation, micronization, and encapsulation processes applied to obtain extracts concentrated with bioactive compounds for food, pharmaceutical, and cosmetic applications [6–9].

Carbon dioxide has a critical temperature near to room temperature, contributing to the operating conditions (pressure and temperature) to extract thermolabile substances, such as bioactive compounds. In addition, this substance is non-polar and to enlarge the application spectrum to extract bioactive compounds, ethanol, water, or both are usually used as co-solvents. Moreover, carbon dioxide acts as co-solvent when in the mixture it is used more than 60% of ethanol or water, and as anti-solvent, when the solute extract is not soluble in carbon dioxide during the depressurizing step.

The information accuracy related to the physical (pressure, temperature, and density) and transport properties (diffusivity, viscosity) and the accuracy of thermodynamic and mass transfer relations used for the solvent, co-solvent, and solute reach directly the costs of investment in extraction/separation units in supercritical conditions. The thermodynamic phase equilibrium determines the limits for the mass transfer among different phases, which are



**Figure 1.** Carbon dioxide applications.

involved in various processes. The cubic equations of state are the most commonly applied models for the correlation and prediction of phase equilibrium at high pressures and are available in major commercial process simulators. In addition, they are used to calculate other thermodynamic properties, for both pure substances and mixtures, among which, the liquid and vapor phases density, enthalpy, and entropy.

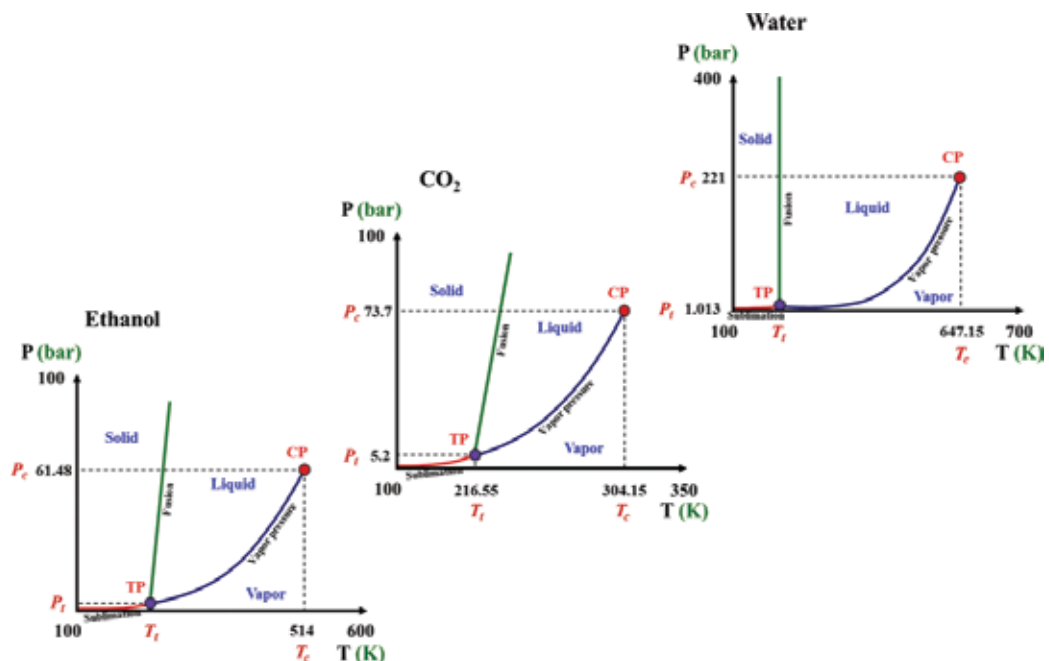
This chapter intends to show the recent application scenarios of the carbon dioxide use at high pressures as solvent, to obtain natural extracts enriched with bioactive compounds, including the use of water as co-solvent to enhance the mixture solvating power. In this chapter, the description of the experimental strategy used for the supercritical carbon dioxide extraction of bioactive compounds from açai berry pulp was emphasized. The primary properties of pure carbon dioxide were also described and calculated using equations of state.

## 2. Diagrams of pure substances

### 2.1. P-T diagram

The pressure versus temperature (P-T) diagram describes the different aggregation states of pure substances called solid, liquid, and vapor/gas.

**Figure 2** is a schematic representation of the P-T diagrams for carbon dioxide and the substances most commonly employed as co-solvent, ethanol, and water, in high-pressure extraction processes



**Figure 2.** Solid-liquid-gas-supercritical fluid phase diagram. TP = triple point.  $C_P$  = critical point.  $P_c$  = critical pressure.  $T_c$  = critical temperature.  $T_t$  = triple point temperature.  $P_t$  = triple point pressure.

of bioactive compounds. The curves represent the boundaries (phase transition or phase equilibrium) between the different states, known as saturation curves. The curve between the solid and liquid phases is called fusion; the curve between solid and vapor phases is called sublimation and that one between liquid and vapor phases is called vapor pressure (also known as boiling curve).

The behavior of the thermodynamic diagrams of pure substances culminates in the determination of the reference equilibrium points that has great importance in the development of thermodynamic models for different processes applications. In the P-T diagram, there are two points: the triple point, where the three phases are in equilibrium and the critical point, which is particularly of fundamental interest for applications in processes that use solvents at high pressures.

The critical point of a pure substance is the maximum thermodynamic state reached by the saturation curve between liquid and vapor phases. When the substance is in the state above the critical temperature ( $T_c$ ) and the critical pressure ( $P_c$ ), it is called supercritical fluid, and when the pressure is above  $P_c$  and the temperature below  $T_c$ , the thermodynamic state is called subcritical liquid. The technology with fluids at high pressures consists in the use of substances that act like solvent when they are in the thermodynamic state near or above the critical point. The triple point of carbon dioxide is at pressure of 5.18 bar and at temperature of 216.58 K ( $-56.57^\circ\text{C}$ ), and the critical point is at pressure of 73.7 bar and at temperature of 304.15 K ( $31^\circ\text{C}$ ) [10].

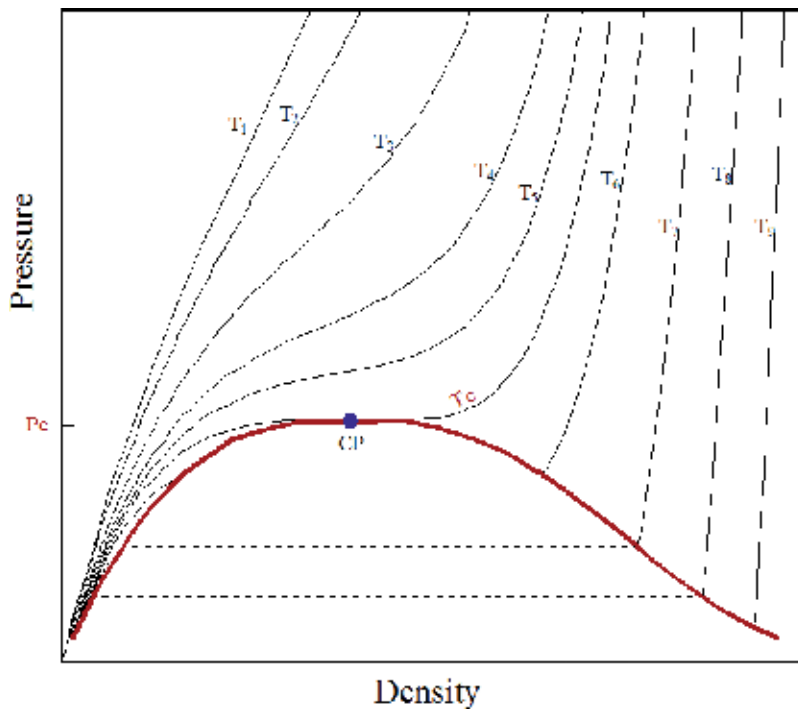
## 2.2. P- $\rho$ -T diagram

Density ( $\rho$ ) is the most important thermodynamic property to define the solvating power of a solvent at high pressures, increasing the density of the solvent increases its solvating power. To better understand the influence of density on the solvating power to increase or decrease the solubility of an extract within a solvent at high pressures, one needs information concerning the density as a function of system pressure and temperature.

**Figure 3** shows the schematic representation of the density behavior ( $\rho = 1/V$ ) of a pure substance with temperature and pressure variations, where  $V$  is the specific volume (volume per mass unit). In **Figure 3**, the density versus pressure isotherms are presented in descending order from T1 to T9. The red line represents the saturation curve between the liquid and vapor phases. The highest point of the saturation curve is the critical point. The dotted line within the saturation curve is the two-phase region. In the saturation curve, there is a sudden difference in the density between the liquid and vapor phases.

The behavior of the P- $\rho$ -T diagram shows that the density at constant temperature increases with the increasing pressure and at constant pressure increases with the decreasing temperature. In the region near the critical point, small variations of pressure and/or temperature cause great variations in density. For carbon dioxide, the critical point is at the pressure of 73.7 bar and at the temperature of 304.15 K ( $31^\circ\text{C}$ ); it makes carbon dioxide the most applied solvent to extract thermo-sensible substances.

Below the critical temperature, in the subcritical region, the isotherms present two types of behavior: for the vapor region, at constant pressure, the density increases with the decreasing temperature and for the liquid region, the density varies very little with the temperature.



**Figure 3.** Pressure-density (P-ρ) phase diagram for carbon dioxide. CP = critical point ( $P_c$ ,  $T_c$ , and  $\rho_c$ ). CP = critical point ( $P_c$ ,  $T_c$ , and  $\rho_c$ ).

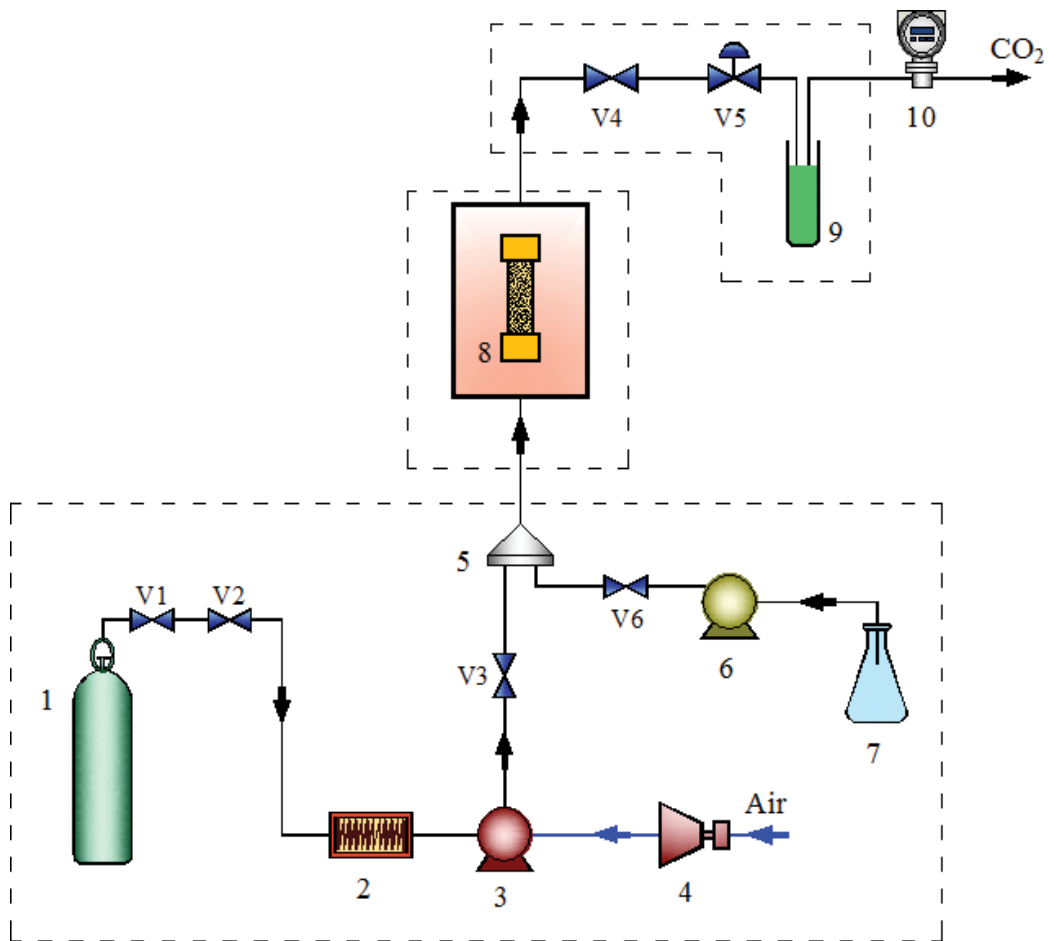
### 3. Supercritical fluid extraction

The extraction/separation processes applied to solid matrix using carbon dioxide as solvent are the most studied supercritical processes in the search for new natural products that have biological activity, according to numerous applications described in the literature [1, 4–6, 11–18].

#### 3.1. General process steps

Generally, the supercritical fluid extraction applied to a natural solid matrix consists of three steps: the system supply of solvent/co-solvent, the extraction unit, and the extract separation system from solvent/co-solvent. **Figure 4** presents a general scheme of the supercritical fluid extraction unit without solvent recycle. The system supply of solvent/co-solvent consists by a booster air-driven fluid pump, a cooling bath, a co-solvent recipient, a co-solvent pump, and a mixer. The extract separation system from solvent/co-solvent consists by a control valve for extraction pressure reduction and a separation vessel to collect the extract.

Regarding the extraction, the supercritical solvent continuously flows through a fixed bed of solid particles and dissolves the extractable components of the solid. The solvent is fed into the extractor and evenly distributed at the inlet of the fixed bed. The system solvent and soluble components leave the extractor and feed the precipitator/separator, where the solvent products



**Figure 4.** Scheme of a supercritical fluid extraction plant applying solvent/co-solvent. CO<sub>2</sub> cylinder (1); cooling bath (2); booster (CO<sub>2</sub> pump-3 and Compressor-4); mixer (5); CO-solvent pump (6); co-solvent recipient (7); extraction unit (8); control valve (V-5); separation vessel (9); flow meter (10).

are separated by expansion (depressurizing), since at low pressures the density of the solvent sharply decreases, therefore it decreases the solubilizing power of the solvent as well and the products precipitate.

The choice of the operating condition ( $P$  and  $T$ ) is a determining factor that contributes to the maximization of the extracts solubility in the supercritical solvent, and consequently the extraction yields. Thus, increasing the density of the supercritical fluid, the solubility of the solvent maximizes. The solubility increasing can also occur when a co-solvent is added, which changes the solvent power and, in this way, the new solvent is a mixture [19, 20].

To design a high-pressure fluid extraction process of valuable compounds from new natural solid matrices, it is necessary to define the size of the extraction unit and some important parameters have to be determined to obtain the optimum process conditions for each application. Brunner

[19] and Kiran et al. [21] described the most important parameters, and among the variables that determine the process, operating conditions (pressure and temperature), amount of solvent, conditions of solvent removal from extract (precipitation), pretreatment of solid matrix, and other mass transfer parameters can be highlighted.

In general, the parameters that define the behavior of the mass transfer at processes at high pressures are related to the configuration of the bed: particle size, height, and diameter, preparation of the raw material, solvent flow, among others, which contribute to define the shape of the kinetic extraction curves. The phenomenological discussions about supercritical fluid extraction mass transfer applied to solid matrices have been discussed in the literature [19, 22–24].

### 3.2. Supercritical carbon dioxide extraction of bioactive compounds: a case study

The experimental strategy used for the supercritical carbon dioxide extraction process of bioactive compounds is based on the previous results collected by our research group in obtaining açai extracts [25].

Açai is a dark purple, berry-like fruit from typical Amazon palm tree *Euterpe oleracea* Mart., integrated in the daily dietary habit of the native people.

Recently, many studies have suggested its use as a functional food or food ingredient due to its antioxidant activity, explained by the high content of phenolic compounds, such as anthocyanins, specially cyanidin-3-glucoside and cyanidin-3-rutinoside, flavones, and phenolic acids [26–28]. Phenolic constituents are generally associated with health-promoting properties and prevention of diseases [29–33]. Anthocyanins constitute a group of pigments, also important in the food industry, for the replacement of artificial colors [34–36].

The supercritical extraction experiments of the lyophilized açai pulp under development were carried out in a Spe-ed™ SFE commercial unit (Allentown, PA, USA: model 7071 from Applied Separations) which is coupled to the solvent + co-solvent delivery system of Laboratory of Supercritical Extraction (LABEX), Faculty of Food Engineering-UFGA. The schematic representation of the supercritical extraction system is shown in **Figure 5**.

The first step consisted of the extraction with supercritical CO<sub>2</sub> (pure) to obtain extracts rich in fatty acids and byproducts of the residual solid matrix (defatted pulp). Analyses of the content of bioactive compounds (anthocyanins and total phenolic compounds) were performed. The second stage that is under development consists of the extraction with supercritical CO<sub>2</sub> combined with water as co-solvent applied to the residual solid matrix to obtain extracts concentrated in anthocyanins.

In the first stage, Batista et al. [25] subjected samples of lyophilized açai pulp to the supercritical carbon dioxide extraction process. Among the results, the study of the process variables (temperature, pressure, and solvent density) that maximize the extraction yield of açai oil, the quantification of the total anthocyanins content and total phenolic compounds content, and the evaluation of the allelopathic potential of the extracts obtained can be highlighted.

**Figure 6** shows the experimental results of the 50, 60, and 70°C isotherms on dry basis and their standard deviations. In this study, the highest global yield was equal to  $45.4 \pm 0.58\%$ ,

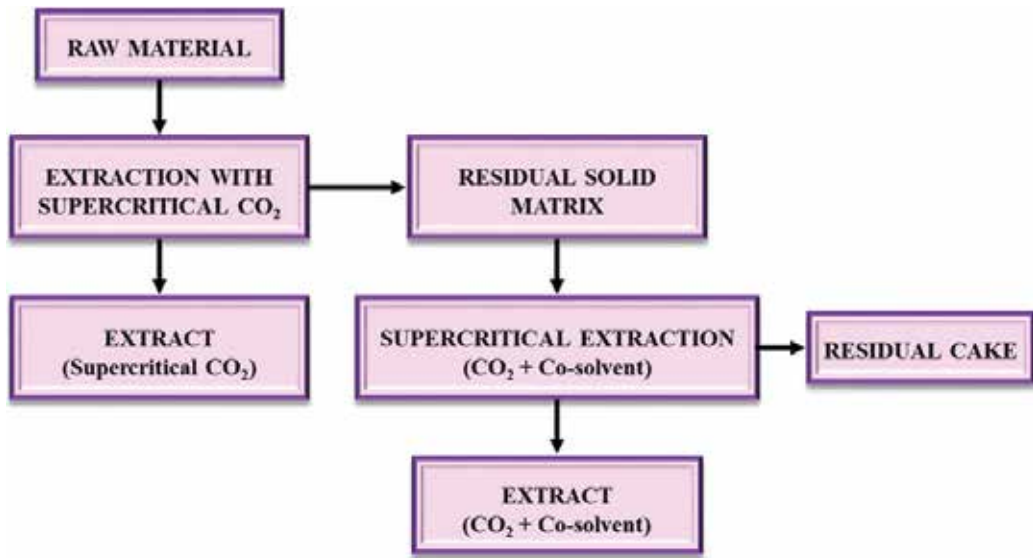


Figure 5. Experimental protocol for the bioactive compounds extraction.

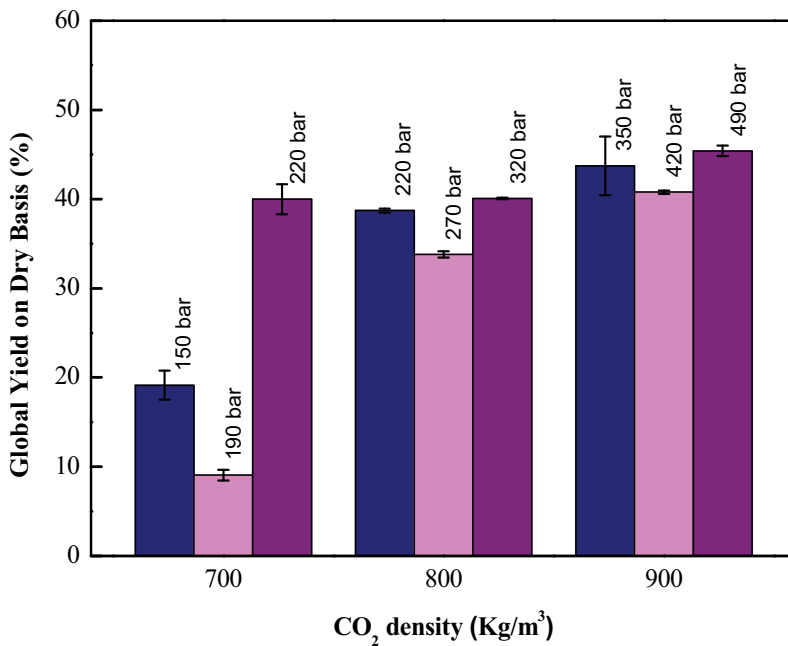


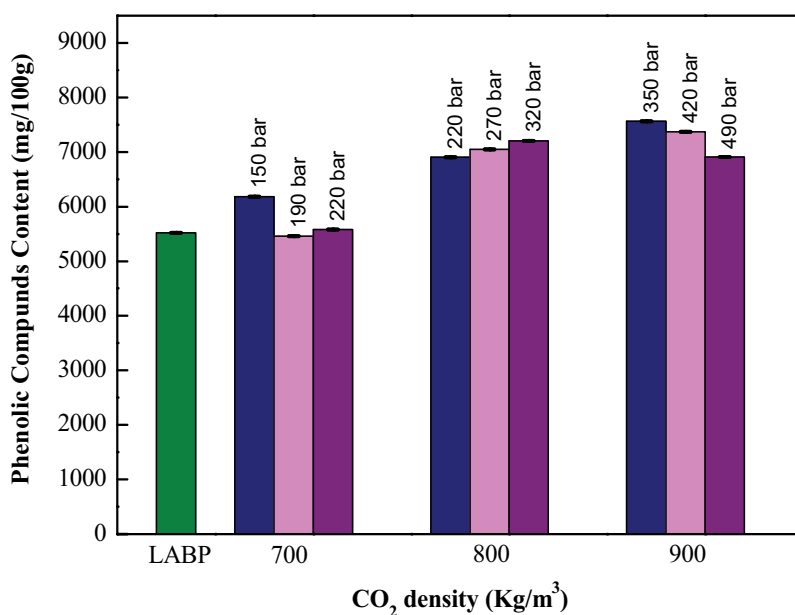
Figure 6. Global yield on dry basis versus density of supercritical CO<sub>2</sub> extraction of lyophilized açai berry oil. (■) 50°C, (■) 60°C, and (■) 70°C isotherms [17].



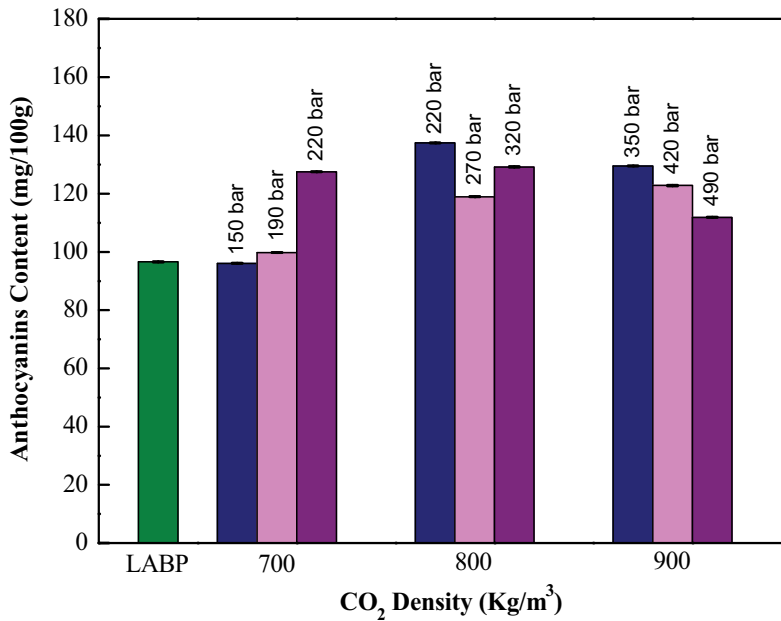
obtained at 70°C and 490 bar, while the lowest global yield was equal to  $9.07 \pm 0.6\%$ , obtained at 60°C and 190 bar. The density is related to the CO<sub>2</sub> solubility and is directly influenced by temperature and pressure. Here, the most important parameter was the density, since when it increased (in all isotherms), the oil global yield also increased.

The analysis of the phenolic compounds in the lyophilized açai berry pulp showed an increase in its content comparing the samples before and after the extraction with supercritical CO<sub>2</sub>, in different conditions. Its highest content was equal to 7565 mg/100 g and was obtained in the condition of 70°C and 350 bar. The standard deviation for each condition was lower than 0.18% (**Figure 7**). Regarding anthocyanins, there was also an increase in its content. Before the extraction with supercritical CO<sub>2</sub>, the total concentration was equal to  $96.58 \pm 0.11$  mg/100 g, and after the extraction, it reached up to 137.5 mg/100 g of sample in the condition of 50°C and 220 bar. The standard deviation was lower than 0.15%. **Figure 8** shows the values obtained and their specific deviation. It can be inferred that since the extracts of the lyophilized açai berry pulp obtained by supercritical CO<sub>2</sub> are rich in phenolic compounds and anthocyanins, it presents great potential in nutraceutical applications.

The results of the fatty acid profile analysis of açai extracts indicate a low saturated/unsaturated ratio except for the condition of 70°C and 320 bar. The SFA content reached 99.67% at the condition of 70°C and 320 bar.



**Figure 7.** Total phenolic compounds content in lyophilized açai berry pulp before and after extraction with supercritical CO<sub>2</sub>. (■) 50°C, (■) 60°C, and (■) 70°C isotherms [17].



**Figure 8.** Total anthocyanins compounds content in lyophilized açai berry pulp before and after extraction with supercritical CO<sub>2</sub>. (■) 50°C, (■) 60°C, and (■) 70°C isotherms [17].

## 4. High-pressure carbon dioxide properties

### 4.1. Thermodynamic properties

The influence of the density in the solvation power by the tunable operating conditions ( $P$ ,  $T$ ) is the most important thermodynamic effect in the high-pressure fluid processes.

Above the critical point, the supercritical extraction process can operate over a wide range of operating conditions ( $P$ ,  $T$ ) and the simplest density behavior can be obtained through an isotherm, being possible to select a wide range of operating pressures, as shown in **Figure 3** of the item 2.2 for the isotherms  $T_1 > T_2 > T_3 > T_4 > T_5$ .

The density is defined by the inverse of specific volume, and for practical purpose, could be calculated by volumetric properties ( $P$ - $V$ - $T$ ) using equation of state.

#### 4.1.1. $P$ - $V$ - $T$ diagram calculation with equations of state

To describe the  $P$ - $V$ - $T$  diagram behavior, it is necessary to use precise equations of state (EOS) with specific parameters for pure substances. In the case of carbon dioxide, the equations of Bender [19] and Span and Wagner [37] are the most used. The Bender equation is presented below, where the parameters were determined from experimental PVT data of carbon dioxide. **Table 1** shows the parameters of the Bender equation.

i	a <sub>i</sub>	i	a <sub>i</sub>
1	0.22488558	11	0.12115286
2	0.13717965 × 10 <sup>3</sup>	12	0.10783386 × 10 <sup>-3</sup>
3	0.14430214 × 10 <sup>5</sup>	13	0.43962336 × 10 <sup>-2</sup>
4	0.29630491 × 10 <sup>7</sup>	14	-0.36505545 × 10 <sup>8</sup>
5	0.20606039 × 10 <sup>9</sup>	15	0.19490511 × 10 <sup>11</sup>
6	0.45554393 × 10 <sup>-1</sup>	16	-0.29186718 × 10 <sup>13</sup>
7	0.77042840 × 10 <sup>-2</sup>	17	0.24358627 × 10 <sup>8</sup>
8	0.40602371 × 10 <sup>5</sup>	18	-0.37546530 × 10 <sup>11</sup>
9	0.40029509	19	0.11898141 × 10 <sup>14</sup>
10	-0.39436077 × 10 <sup>-3</sup>	20	0.50000000 × 10 <sup>1</sup>

**Table 1.** Bender equation constants for CO<sub>2</sub> [19].

$$P = \frac{T}{V} \left[ R + \frac{B}{V} + \frac{C}{V^2} + \frac{D}{V^3} + \frac{E}{V^4} + \frac{F}{V^5} + \left( G + \frac{H}{V^2} \right) \frac{1}{V^2} \exp(-a_{20}/V^2) \right] \quad (1)$$

where

$$B = a_1 - \frac{a_2}{T} - \frac{a_3}{T^2} - \frac{a_4}{T^3} - \frac{a_5}{T^4} \quad (2)$$

$$C = a_6 + \frac{a_7}{T} + \frac{a_8}{T^2} \quad (3)$$

$$D = a_9 + \frac{a_{10}}{T} \quad (4)$$

$$E = a_{11} + \frac{a_{12}}{T} \quad (5)$$

$$F = \frac{a_{13}}{T} \quad (6)$$

$$G = \frac{a_{14}}{T^3} + \frac{a_{15}}{T^4} + \frac{a_{16}}{T^5} \quad (7)$$

$$H = \frac{a_{17}}{T^3} + \frac{a_{18}}{T^4} + \frac{a_{19}}{T^5} \quad (8)$$

$$a_{20} \approx V_C^2 \quad (9)$$

**Figure 9** shows the calculation with Bender equation [19] of state for the P-V-T diagram isotherms and saturation curve, including an isotherm close to the critical temperature of the carbon dioxide. The calculations were performed using a Microsoft Excel spreadsheet. The equation presents accuracy in calculations when compared to data taken from IUPAC International Thermodynamic Table.

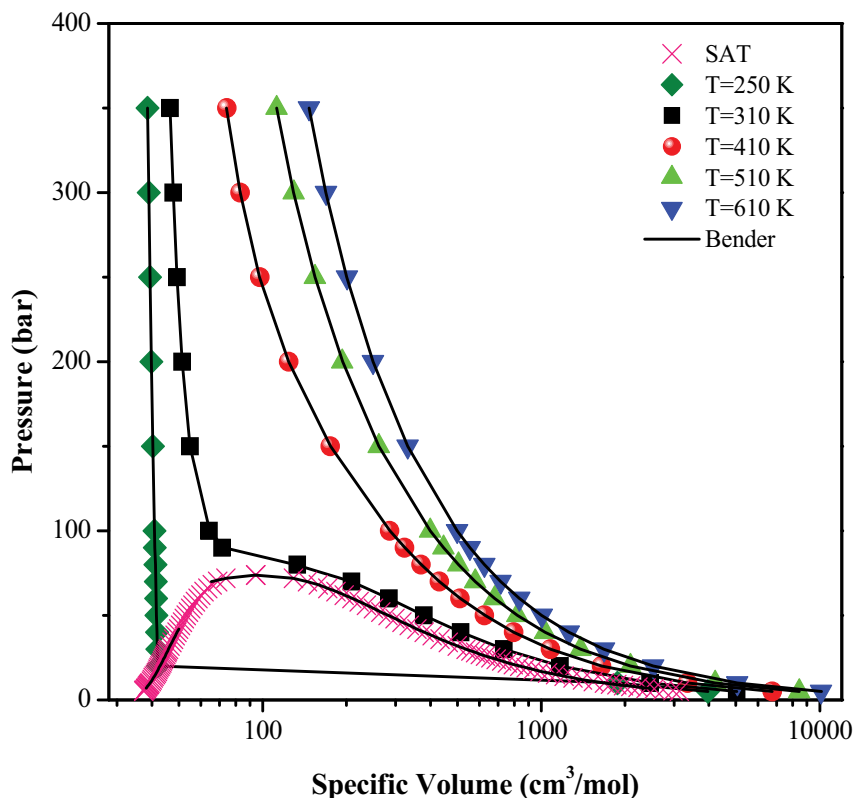


Figure 9. P-V-T diagram of carbon dioxide calculated with Bender EOS and compared to IUPAC data (symbols).

However, for applications of supercritical technology, it is necessary to calculate other thermodynamic properties. The thermodynamic properties of the pure solvent (density, enthalpy, and entropy) and the thermodynamic properties of the solute/solvent mixture, among which the equilibrium compositions, enthalpies, and mixing entropies, must be calculated in the operating conditions throughout the process. The cubic equation of state, also called Van der Waals type equation, represents an alternative, since the Bender-type equation described above is complex. In these cases, the cubic equations of state of Peng-Robinson (PR) [38] and Soave Redlich-Kwong (SRK) [39] are presented as the most commonly applied options in process simulations (Table 2). These equations of state use various thermodynamic properties and the following physical properties of the pure substance: critical pressure, critical temperature, and the acentric factor, which are tabulated, in the case of carbon dioxide.

Table 3 shows the calculated values of the carbon dioxide densities for some isotherms above the critical point using the equations of Peng-Robinson [38] and Soave-Redlich-Kwong [39]. The computational package PE 2000 developed by Pfohl et al. [40] was used for calculations. The results are compared to data taken from IUPAC International Thermodynamic Table and from NIST Chemistry Webbook (NIST Standard Reference Database). The Peng-Robinson equation of state presented the best results for the carbon dioxide density calculation in the conditions of pressure and temperature of Table 3 when compared with different databases.

Cubic equations	
PR	$P = \frac{RT}{V-b} - \frac{a(T)}{V(V+b) + b(V-b)}$ $a = 0.45724 \frac{R^2 T_c^2}{P_c} \times \alpha(T_r, \omega)$ $b = 0.07780 \frac{RT_c}{P_c}$ $\alpha(T_r, \omega) = \{1 + km[1 - (T_r)^{1/2}]\}^2$ $km = 0.37464 + 1.54226\omega - 0.26992\omega^2$
SRK	$P = \frac{RT}{V-b} - \frac{a(T)}{V(V+b)}$ $a = 0.42748 \frac{R^2 T_c^2}{P_c} \times \alpha(T_r, \omega)$ $b = 0.08664 \frac{RT_c}{P_c}$ $\alpha(T_r, \omega) = \{1 + km[1 - (T_r)^{1/2}]\}^2$ $km = 0.480 + 1.574\omega - 0.176\omega^2$

Table 2. Cubic equations of state.

Pressure (bar)	Temperature (°C/K)	CO <sub>2</sub> density (kg/m <sup>3</sup> )			
		PR	SRK	NIST	IUPAC
100	36.85/310	617.3	563.0	683.4	686.5
200		847.8	763.8	855.5	857.0
300		941.1	846.6	921.5	922.7
100	46.85/320	418.1	390.6	444.6	449.4
200		781.5	707.9	801.5	803.1
250		845.3	763.8	848.0	849.5
300		893.0	805.9	882.4	883.7
400		963.2	868.2	933.2	934.4
100	66.85/340	260.5	246.2	258.1	258.6
200		643.2	589.3	678.7	680.5
250		731.7	666.7	751.9	753.3
300		794.4	721.8	800.6	801.8
400		882.9	799.6	866.7	867.9

Table 3. Carbon dioxide density calculated with different equations of state.

Figure 10 shows the calculation with Peng-Robinson [38] equation of state for P-V-T diagram isotherms and saturation curve, including an isotherm close to the critical temperature of the carbon dioxide. The Peng-Robinson equation of state was able to describe all the phases of the carbon dioxide P-V-T diagram for the isotherms studied when compared to data taken from IUPAC International Thermodynamic Table.

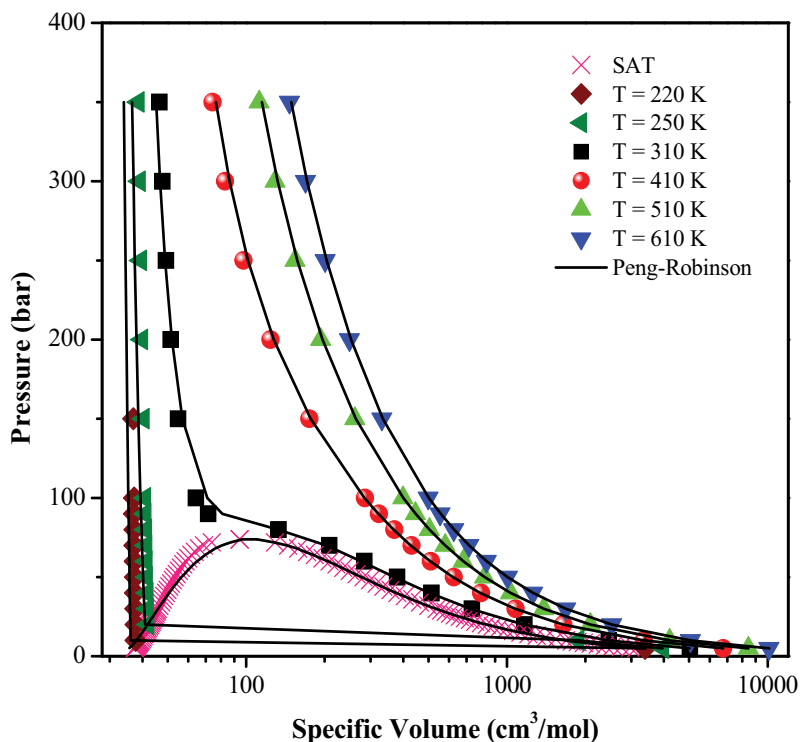


Figure 10. PVT diagram of carbon dioxide calculated with Peng-Robinson EOS and compared to IUPAC data (symbols).

From a process point of view, the accuracy of the cubic equations of state was good, considering that the operating conditions commonly applied in CO<sub>2</sub> extraction at high pressures are close to the values of temperature and pressure used in Table 3.

#### 4.2. Other high-pressure carbon dioxide properties

The application of the high-pressure fluid extraction technologies in both laboratory and industrial scales requires not only the knowledge of the physical and thermodynamic properties of the solvent, but also requires the understanding of thermal and transport properties behavior. Among them, the most commonly cited are viscosity, diffusivity, thermal conductivity, and dielectric constant.

The dielectric constant describes the ability of a solvent to be polarized. The dielectric constant value is associated with the ability to dissolve electrolytes or polar compounds. The dielectric constant increases with temperature for most substances [41]. The dielectric constant of supercritical carbon dioxide with approximate value of a hydrocarbon alone does not characterize it as an important solvent; it only identifies it as a non-polar substance. Its solvation power is mainly related to the considerable increase of its density in the supercritical region with the properties as viscosity and diffusivity complementing the characteristics that makes supercritical carbon dioxide a differentiated solvent.

Under supercritical conditions, the thermal conductivity is influenced by both temperature and pressure and at constant pressure this property increases with increasing temperature, and on the other hand, at constant temperature, the thermal conductivity increases with pressure [42].

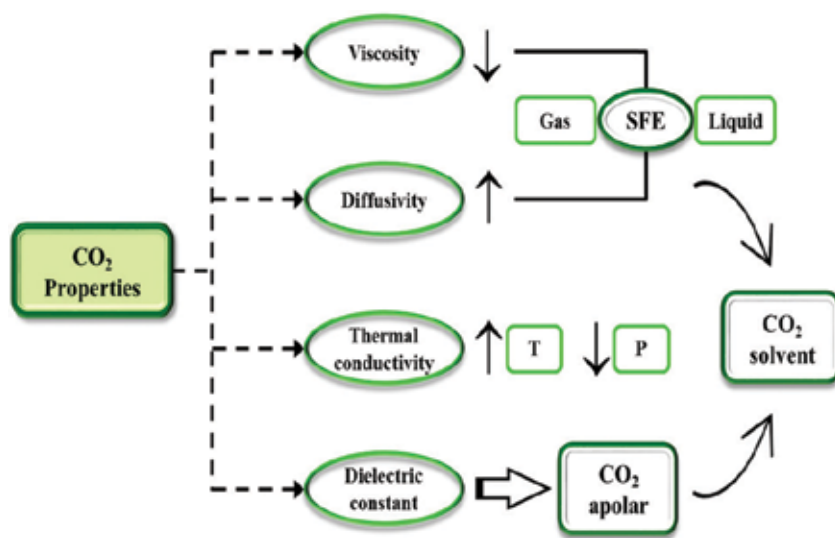
Carbon dioxide and other supercritical solvents have low viscosity and high diffusivity values. The viscosity and thermal conductivity of gases and liquids differ by one to two orders of magnitude, and the diffusivity values of gases and liquids differ by four orders of magnitude [41].

In the supercritical state, the substances have intermediate characteristics between the properties of a gas and a liquid, which contributes to more favorable hydrodynamic properties than the liquids, with diffusion coefficients close to those of a gas, which provides a fast and efficient mass transfer. Another feature of the supercritical fluid includes its low viscosity, which facilitates the penetration of the fluids into a solid matrix. Therefore, high diffusivity and low viscosity lead to a faster extraction time providing a dissolving power so that the supercritical fluid is considered a solvent.

**Table 4** shows that supercritical fluids are characterized by transport properties (viscosity and diffusivity) between gases and liquids. The viscosity of a supercritical fluid is smaller than the viscosity of a gas and the diffusivity of the liquid is greater than the diffusivity of a supercritical fluid. In summary, the scheme of **Figure 11** shows the basic properties of supercritical carbon dioxide, which become fundamental in high pressures extraction processes.

	Unit	Gas	SCF	Liquid
Viscosity	Pa s	$10^{-5}$	$10^{-4}$ to $10^{-5}$	$10^{-3}$
Diffusivity	$\text{cm}^2/\text{s}$	$10^{-1}$	$10^{-3}$ to $10^{-4}$	$10^{-6}$

**Table 4.** Order of magnitude of transport properties.



**Figure 11.** Carbon dioxide properties.

## 5. High-pressure carbon dioxide applications

The most cited drawback of using supercritical carbon dioxide as solvent is the high investment cost for equipment acquisition and operation. However, the extraction with supercritical carbon dioxide presents a lower extraction time because of its diffusivity and low surface tension, greater selectivity in the compounds of interest and little or no consumption of organic solvents [43–46].

### 5.1. Essential oil extraction

Essential oils have been used to prevent or treat human diseases for several centuries. The extraction of the volatile compounds present in edible or medicinal aromatic plants is generally carried out by hydrodistillation; however, the authors report that some compounds may undergo hydrolysis during the extraction period [47]. Although there are other techniques for isolating essential oils, the use of CO<sub>2</sub> as supercritical fluid has been considered a “chemically green” unconventional extraction technique that does not alter or degrade the substances present in oils because it uses relatively low temperatures in the extraction process.

Guan et al. [48] performed a comparison between conventional extraction methods and extraction with supercritical CO<sub>2</sub> and observed that the extraction using supercritical CO<sub>2</sub> as solvent was less effective with recovery rate of 57.36% for eugenol compared to steam distillation with 58.2%, but it was more effective when compared to hydrodistillation with recovery rate of 48.82% and Soxhlet extraction with 57.24%. However, when compared with the extraction of eugenol acetate, the extraction with supercritical CO<sub>2</sub> presented higher yields in relation to the other extraction methods.

Extraction of chemically active volatile molecules with supercritical CO<sub>2</sub> is very widespread [49–51]. This is due to the possible applications as agents that promote biological activities [52], such as antioxidant activity [53], anti-inflammatory activity [54], insecticidal activity [55], and phytotoxic activity [56]. In **Table 5**, some studies in the literature on the extraction of essential oils with supercritical CO<sub>2</sub> can be observed.

Aromatic plant	Bioactive compounds	References
<i>Juniperus communis</i> L.	Germacone D and 1-octadecene.	[57]
<i>Satureja hortensis</i>	γ-Terpinene, thymol, and carvacrol	[58]
<i>Myrtus communis</i> L.	Methyl eugenol, 1,8 cineole, and beta- caryophyllene	[59]
<i>Leptocarpha rivularis</i>	α-thujone, β-caryophyllene, and caryophyllene oxide	[60]
<i>Piper nigrum</i> L.	β-caryophyllene, limonene, sabinene, 3-carene, β-pinene, and α-pinene	[53]
<i>Camellia sinensis</i> L.	9-Thiabicyclo[3.3.1]non-7-en-2-ol, tricosane, heneicosane, tetracosane, and dibutyl phthalate	[61]

**Table 5.** Published studies on extraction of essential oils using CO<sub>2</sub> as supercritical fluid.



As given above, it is observed that the process of extraction of essential oils using supercritical CO<sub>2</sub> is ecologically a cleaner method than the conventional ones, and it has been seen as one of the most viable alternatives.

## 5.2. Phytosterols extraction

Phytosterols (plant sterols) are non-volatile triterpenes. The great majority of these compounds are formed by carbon with one or two carbon-carbon double bonds [62]. And the most common phytosterols found in plants are  $\beta$ -sitosterol, campesterol, and stigmasterol [63]. These compounds have various biological activities such as lowering the total serum or plasma cholesterol levels and the low-density lipoprotein cholesterol levels. In addition, they have antitumor activities inhibiting the development of colon cancer [64, 65].

For the extraction of these phytosterols, the supercritical CO<sub>2</sub> has been shown to be an efficient technique for extraction of fixed oils from vegetable matrices. Studies report that this solvent may be superior to obtain oils in relation to the conventional extraction, exhibiting a recovery rate of phytosterols of 836.5 mg/100 g versus 30.5/100 g using a Soxhlet-type extraction apparatus [66]. A very important parameter for the extraction of phytosterols with supercritical CO<sub>2</sub> is the increase of the pressure, because it favors the solvation power and consequently the solubilization of these compounds, with a recovery rate of up to 7262.80 mg.kg<sup>-1</sup> [67]. **Table 6** presents some articles published in the literature on the extraction of phytosterols using supercritical CO<sub>2</sub>.

## 5.3. Carotenoid extraction

Carotenoids are tetraterpenes present in plants that have several applications in food [72], cosmetic [73], and pharmaceutical [74] areas. Some of the benefits provided by these pigments are: antioxidant activity and strengthening of the immune system against degenerative diseases such as cancer, cardiovascular diseases, muscle degeneration, inflammation, hypertension, insulin resistance and obesity [75, 76].

Because of their hydrophobic characteristics, carotenoids are usually extracted using organic solvents such as hexane and petroleum ether. Carotenoids with hydrophilic characteristics can be obtained with more polar solvents such as acetone, ethanol, and ethyl acetate [77]. The

Plants	Phytosterols	References
<i>Cucurbita pepo</i> convar	Desmosterol, campesterol, stigmasterol, $\beta$ -sitosterol, spinasterol, $\Delta$ 7,22,25-stigmastatrienol, $\Delta$ 7-stigmastenol, $\Delta$ 7,25-stigmastadienol, and $\Delta$ 7-avenasterol	[68]
<i>Brassica napus</i>	$\beta$ -sitosterol, campesterol and brassicasterol	[69]
<i>Hippophae rhamnoides</i> L.	$\beta$ -sitosterol	[70]
<i>Sesamum indicum</i> L.	$\beta$ -sitosterol + sitostanol, cholesterol, campesterol + campestanol +24-methylene cholesterol, $\Delta$ -5 avenasterol and stigmasterol, while lower levels of $\Delta$ -5,24 stigmastadienol, brassicasterol, clerosterol + $\Delta$ -5-23 stigmastadienol, $\Delta$ -7 avenasterol, eritrodiol and $\Delta$ -7 stigmasterol	[71]

**Table 6.** Phytosterols extracted using supercritical CO<sub>2</sub>

techniques used to extract this compound may be maceration, Soxhlet, microwave-assisted extraction [78, 79], ultrasound-assisted extraction [80], pressurized liquid extraction [81, 82], and supercritical fluid technology using low temperature. The process is performed in a short time in relation to conventional processes and does not use toxic solvents to collect the compound of interest [83]. In **Table 7**, some published works that used supercritical CO<sub>2</sub> to obtain carotenoids are shown.

#### 5.4. Fatty acids extraction

Fatty acids (FA) belong to the lipid class and differ according to the size of the C chain (2–80), the presence or absence of double bonds (saturated or unsaturated) or their radical function as the groups hydroxyl, epoxy, and halogen atoms [89]. Ingestion of FA is essential to have an adequate energy balance in the human organism in addition to reducing the risk of some diseases such as diabetes [90], hypertension [91], coronary diseases [92], and inflammation [93].

Some of its applications are in food, nutraceutical, and cosmetic industries, and in the production of lubricants, biodiesel, and glycerol [94–96]. Some of the extraction methods that can be used to obtain FA are mechanical extraction [97], extraction by supercritical fluids and organic solvent [98], microwave-assisted extraction [99], and supercritical CO<sub>2</sub> extraction [98]. **Table 8** shows some studies that used supercritical CO<sub>2</sub> to obtain the main classes of the FA group.

#### 5.5. Extraction with supercritical CO<sub>2</sub> modified with ethanol/water

The extraction with supercritical CO<sub>2</sub> modified with water in different proportions is carried out to obtain bioactive compounds of high polarity, because as mentioned above, CO<sub>2</sub> is an

Raw material	Carotenoid	References
Tomato juice	Lycopene and $\beta$ -carotene	[84]
<i>Hemerocallis disticha</i>	Lutein and zeaxanthin	[85]
<i>Dunaliella salina</i>	9-cis and trans- $\beta$ -carotenes	[86]
<i>Undaria pinnatifida</i> , <i>Haematococcus pluvialis</i> , and <i>Chlorella vulgaris</i>	Fucoxanthin, astaxanthin, lutein, and $\beta$ -carotene	[87]
<i>Fucus serratus</i> and <i>Laminaria digitata</i>	Xanthophyll and fucoxanthin	[88]

**Table 7.** Published studies about carotenoid extraction using CO<sub>2</sub>

Raw material	Fatty acid	Reference
<i>Cucurbita ficifolia</i> , Bouché	$\omega$ 6-linoleic acid, palmitic acid, oleic acid	[100]
<i>Farfantepenaeus paulensis</i>	Palmitic acid, oleic acid, stearic acid, palmitoleic acid, and linoleic acid	[101]
<i>Cannabis sativa</i> L.	Linoleic acid and linolenic acid	[102]
<i>Chaetoceros muelleri</i>	Myristic acid, palmitic acid, and palmitoleic acid	[103]
Saw Palmetto	Lauric acid, myristic acid, and oleic acid	[104]

**Table 8.** Published studies about fatty acids extraction using CO<sub>2</sub>

Raw material	Compounds	References
<i>Myrciaria cauliflora</i>	Anthocyanin	[8]
Elderberry ( <i>Sambucus nigra</i> )	Anthocyanins	[110]
<i>Vitis vinifera</i> var. <i>Malvasia nera</i>	Anthocyanins	[111]
<i>Arrabidaea chica</i>	Anthocyanins and luteolin	[112]
<i>Scutellaria lateriflora</i> L.	Baicalin, dihydrobaicalin, lateriflorin, ikonnikoside I, scutellarin, oroxylin A 7-O-glucuronide, oroxylin A, baicalein, wogonin	[113]
<i>Vaccinium myrtillus</i> L.	Delphinidin 3-O-galactoside, delphinidin 3-O-glucoside, cyanidin 3-O-galactoside, delphinidin 3-O-arabinoside, cyanidin 3-O-glucoside, petunidin 3-O-galactoside, cyanidin 3-O-arabinoside, petunidin 3-O-glucoside, peonidin 3-O-galactoside, petunidin 3-O-arabinoside, peonidin 3-O-glucoside, malvidin 3-O-galactoside, peonidin 3-O-arabinoside, malvidin 3-O-glucoside, malvidin 3-O-arabinoside and malvidin 3-O-xyloside	[114]

**Table 9.** Phenolic compounds extracted with supercritical CO<sub>2</sub> modified with ethanol/water.

non-polar molecule and does not have “power” to solubilize polar substances as is the case of the phenolic compounds (phenolic acids and flavonoids) [105, 106]. As previously mentioned, parameters of processes, such as temperature and pressure, can influence the extraction of bioactive compounds. Besides these two parameters, anthocyanins are also important for the extraction of phenolic compounds. Solvent flow rate, percentage of co-solvent, co-solvent type (ethanol or water), and extraction time are parameters that directly implicate the yield of these substances at the end of the extraction process [107].

Further examples of extraction of phenolic compounds using supercritical CO<sub>2</sub> modified with co-solvents can be analyzed in the studies [106, 108, 109]. They extracted various flavonoids like quercetin, catechin, epicatechin from cranberry, blueberry, and raspberry. **Table 9** presents some studies in which supercritical CO<sub>2</sub> modified with ethanol/water were used to extract chemically active phenolic compounds.

## 6. Conclusion

Carbon dioxide can be safely applied in high-pressure extraction processes due to its numerous advantageous characteristics. It is neither toxic nor inflammable, being able to act as solvent, co-solvent, or anti-solvent, which allows it to be used in natural products and foodstuff processing that require treatments intending to preserve their nutritional and sensory properties. Since it is a non-polar substance, it is suitable for extraction of non-polar bioactive compounds when used in pure form. When associated with a polar co-solvent, it can be used for extraction of polar compounds such as phenolic compounds and anthocyanins. Therefore, these characteristics make carbon dioxide the most important fluid used in high-pressure processes for extraction, separation, fractionation, micronization, and encapsulation, applied to obtain concentrated extracts with bioactive compounds for food, pharmaceutical, and cosmetic applications.

## Acknowledgements

Costa W.A. (1427204/2014), Cunha V.M.B. (1566277/2015), Oliveira M.S. (1662230/2016), Silva M.P. (1636612/2016), Bezerra F.W.F. (1718822/2017), Pinto R.H.H. (1662902/2016) thank CAPES for the doctorate scholarship.

## Author details

Vânia Maria Borges Cunha<sup>1</sup>, Marcilene Paiva da Silva<sup>1</sup>, Wanessa Almeida da Costa<sup>2</sup>, Mozaniel Santana de Oliveira<sup>1</sup>, Fernanda Wariss Figueiredo Bezerra<sup>1</sup>, Anselmo Castro de Melo<sup>1</sup>, Rafael Henrique Holanda Pinto<sup>1</sup>, Nelio Teixeira Machado<sup>3</sup>, Marilena Emmi Araujo<sup>3</sup> and Raul Nunes de Carvalho Junior<sup>1,2\*</sup>

\*Address all correspondence to: raulncj@ufpa.br

1 LABEX/FEA (Faculty of Food Engineering), Program of Post-Graduation in Food Science and Technology, Federal University of Para, Belém, Pará, Brazil

2 Program of Post-Graduation in Natural Resources Engineering, Federal University of Para, Belém, Pará, Brazil

3 Laboratory of Separation Processes and Applied Thermodynamics (TERM@), Faculty of Chemical Engineering-UFGA, Belém, Pará, Brazil

## References

- [1] Sahena F, Zaidul ISM, Jinap S, Karim AA, Abbas KA, Norulaini NAN, Omar AKM. Application of supercritical CO<sub>2</sub> in lipid extraction—A review. *Journal of Food Engineering*. 2009;**95**:240-253. DOI: 10.1016/j.jfoodeng.2009.06.026
- [2] Vardanega R, Prado JM, Meireles MAA. Adding value to agri-food residues by means of supercritical technology. *Journal of Supercritical Fluids*. 2015;**96**:217-227. DOI: 10.1016/j.supflu.2014.09.029
- [3] Fornari T, Vázquez L, Torres CF, Ibáñez E, Señoráns FJ, Reglero G. Countercurrent supercritical fluid extraction of different lipid-type materials: Experimental and thermodynamic modeling. *Journal of Supercritical Fluids*. 2008;**45**:206-212. DOI: 10.1016/j.supflu.2008.03.001
- [4] Rubio-Rodríguez N, Beltrán S, Jaime I, de Diego SM, Sanz MT, Carballido JR. Production of omega-3 polyunsaturated fatty acid concentrates: A review. *Innovative Food Science & Emerging Technologies*. 2010;**11**:1-12. DOI: 10.1016/j.ifset.2009.10.006
- [5] Herrero M, Ibáñez E. Green processes and sustainability: An overview on the extraction of high added-value products from seaweeds and microalgae. *Journal of Supercritical Fluids*. 2015;**96**:211-216. DOI: 10.1016/j.supflu.2014.09.006

- [6] Herrero M, Mendiola JA, Cifuentes A, Ibáñez E. Supercritical fluid extraction: Recent advances and applications. *Journal of Chromatography. A.* 2010;**1217**:2495-2511. DOI: 10.1016/j.chroma.2009.12.019
- [7] Beh CC, Mammucari R, Foster NR. Lipids-based drug carrier systems by dense gas technology: A review. *Chemical Engineering Journal.* 2012;**188**:1-14. DOI: 10.1016/j.cej.2012.01.129
- [8] Santos DT, Albarelli JQ, Beppu MM, Meireles MAA. Stabilization of anthocyanin extract from Jabuticaba skins by encapsulation using supercritical CO<sub>2</sub> as solvent. *Food Research International.* 2013;**50**:617-624. DOI: 10.1016/j.foodres.2011.04.019
- [9] Keven Silva E, Meireles MAA. Encapsulation of food compounds using supercritical technologies: Applications of supercritical carbon dioxide as an antisolvent. *Food and Public Health.* 2014;**4**:247-258. DOI: 10.5923/j.fph.20140405.06
- [10] Smith R, Inomata H, Peters C. Introduction to supercritical fluids: A spreadsheet-based approach. *Supercritical Fluid Science and Technology.* 2013;**4**:55-119. DOI: 10.1016/B978-0-444-52215-3.00002-7
- [11] Casas L, Mantell C, Rodríguez M, Torres A, Macías FA, Martínez de la Ossa E. Effect of the addition of cosolvent on the supercritical fluid extraction of bioactive compounds from *Helianthus annuus* L. *Journal of Supercritical Fluids.* 2007;**41**:43-49. DOI: 10.1016/j.supflu.2006.09.001
- [12] Passos CP, Silva RM, Da Silva FA, Coimbra MA, Silva CM. Supercritical fluid extraction of grape seed (*Vitis vinifera* L.) oil. Effect of the operating conditions upon oil composition and antioxidant capacity. *Chemical Engineering Journal.* 2010;**160**:634-640. DOI: 10.1016/j.cej.2010.03.087
- [13] Pereira CG, Meireles MAA. Supercritical fluid extraction of bioactive compounds: Fundamentals, applications and economic perspectives. *Food and Bioprocess Technology.* 2010;**3**:340-372. DOI: 10.1007/s11947-009-0263-2
- [14] Moraes MN, Zabot GL, Prado JM, Meireles MAA. Obtaining antioxidants from botanic matrices applying novel extraction techniques. *Food and Public Health.* 2013;**3**:195-214. DOI: 10.5923/j.fph.20130304.04
- [15] Danh LT, Han LN, Triet NDA, Zhao J, Mammucari R, Foster N. Comparison of chemical composition, antioxidant and antimicrobial activity of lavender (*Lavandula angustifolia* L.) essential oils extracted by supercritical CO<sub>2</sub>, hexane and hydrodistillation. *Food and Bioprocess Technology.* 2013;**6**:3481-3489. DOI: 10.1007/s11947-012-1026-z
- [16] Rodrigues RB, Lichtenthäler R, Zimmermann BF, Papagiannopoulos M, Fabricius H, Marx F, Maia JGS, Almeida O. Total oxidant scavenging capacity of *Euterpe oleracea* Mart. (Açaí) seeds and identification of their polyphenolic compounds. *Journal of Agricultural and Food Chemistry.* 2006;**54**:4162-4167. DOI: 10.1021/jf058169p
- [17] Piras A, Rosa A, Marongiu B, Atzeri A, Dessì MA, Falconieri D, Porcedda S. Extraction and separation of volatile and fixed oils from seeds of *Myristica fragrans* by supercritical

- CO<sub>2</sub>: Chemical composition and cytotoxic activity on Caco-2 cancer cells. *Journal of Food Science*. 2012;**77**:C448-C453. DOI: 10.1111/j.1750-3841.2012.02618.x
- [18] de Oliveira MS, da Costa WA, Pereira DS, Botelho JRS, de Alencar Menezes TO, de Aguiar Andrade EH, da Silva SHM, da Silva Sousa Filho AP, de Carvalho RN. Chemical composition and phytotoxic activity of clove (*Syzygium aromaticum*) essential oil obtained with supercritical CO<sub>2</sub>. *Journal of Supercritical Fluids*. 2016;**118**:185-193. DOI: 10.1016/j.supflu.2016.08.010
- [19] Brunner G. *Gas Extraction*. Heidelberg: Steinkopff; 1994. DOI: 10.1007/978-3-662-07380-3
- [20] Kiran E, Brennecke JF. Current state of supercritical fluid science and technology. In: Comstock MJ, editor. *Supercritical Fluid Engineering Science, Fundamentals and Applications*. 514th ed. California: Los Angeles; 1992. pp. 1-8. DOI: 10.1021/bk-1992-0514.ch001
- [21] Kiran E, DeBenedetti PG, Peters CJ. *Supercritical Fluids. Fundamentals and Applications*. Dordrecht: Springer Netherlands; 2000. DOI: 10.1007/978-94-011-3929-8
- [22] Meireles MAA. *Extracting Bioactive Compounds for Food Products: Theory and Applications*. 1st ed. London, New York: CRC Press Taylor & Francis Group Boca Raton; 2008
- [23] Jesus SP, Meireles MAA. Supercritical fluid extraction: A global perspective of the fundamental concepts of this eco-friendly extraction technique. In: Chemat F, Vian MA, editors. *Green Chemistry and Sustainable Technology*. Berlin, Heidelberg: Springer Berlin Heidelberg; 2014. pp. 39-72. DOI: 10.1007/978-3-662-43628-8\_3
- [24] Sovová H, Stateva RP. Supercritical fluid extraction from vegetable materials. *Reviews in Chemical Engineering*. 2011;**27**:79-156. DOI: 10.1515/REVCE.2011.002
- [25] de Batista CCR, de Oliveira MS, Araújo ME, Rodrigues AMC, Botelho JRS, da Silva Souza Filho AP, Machado NT, Carvalho RN. Supercritical CO<sub>2</sub> extraction of açai (*Euterpe oleracea*) berry oil: Global yield, fatty acids, allelopathic activities, and determination of phenolic and anthocyanins total compounds in the residual pulp. *Journal of Supercritical Fluids*. 2016;**107**:364-369. DOI: 10.1016/j.supflu.2015.10.006
- [26] Dias ALS, Rozet E, Chataigné G, Oliveira AC, Rabelo CAS, Hubert P, Rogez H, Quetin-Leclercq J. A rapid validated UHPLC-PDA method for anthocyanins quantification from *Euterpe oleracea* fruits. *Journal of Chromatography B*. 2012;**907**:108-116. DOI: 10.1016/j.jchromb.2012.09.015
- [27] Gouvêa ACMS, De Araujo MCP, Schulz DF, Pacheco S, Godoy RLDO, Cabral LMC. Anthocyanins standards (cyanidin-3-O-glucoside and cyanidin-3-O-rutinoside) isolation from freeze-dried açai (*Euterpe oleraceae* Mart.) by HPLC. *Ciencia e Tecnologia de Alimentos*. 2012;**32**:43-46. DOI: 10.1590/S0101-20612012005000001
- [28] Lichtenthaler R, Rodrigues RB, Maia JGS, Papagiannopoulos M, Fabricius H, Marx F. Total oxidant scavenging capacities of *Euterpe oleracea* Mart. (Açai) fruits. *International Journal of Food Sciences and Nutrition*. 2005;**56**:53-64. DOI: 10.1080/09637480500082082

- [29] Kang J, Thakali KM, Xie C, Kondo M, Tong Y, Ou B, Jensen G, Medina MB, Schauss AG, Wu X. Bioactivities of açai (*Euterpe precatoria* Mart.) fruit pulp, superior antioxidant and anti-inflammatory properties to *Euterpe oleracea* Mart. Food Chemistry. 2012;**133**:671-677. DOI: 10.1016/j.foodchem.2012.01.048
- [30] Gordon A, Cruz APG, Cabral LMC, de Freitas SC, Taxi CMAD, Donangelo CM, de Andrade Mattietto R, Friedrich M, da Matta VM, Marx F. Chemical characterization and evaluation of antioxidant properties of Açai fruits (*Euterpe oleraceae* Mart.) during ripening. Food Chemistry. 2012;**133**:256-263. DOI: 10.1016/j.foodchem.2011.11.150
- [31] Vidigal MCTR, Minim VPR, Carvalho NB, Milagres MP, Gonçalves ACA. Effect of a health claim on consumer acceptance of exotic Brazilian fruit juices: Açai (*Euterpe oleracea* Mart.), Camu-camu (*Myrciaria dubia*), Cajá (*Spondias lutea* L.) and Umbu (*Spondias tuberosa* Arruda). Food Research International. 2011;**44**:1988-1996. DOI: 10.1016/j.foodres.2010.11.028
- [32] Hogan S, Chung H, Zhang L, Li J, Lee Y, Dai Y, Zhou K. Antiproliferative and antioxidant properties of anthocyanin-rich extract from açai. Food Chemistry. 2010;**118**:208-214. DOI: 10.1016/j.foodchem.2009.04.099
- [33] Kang J, Li Z, Wu T, Jensen GS, Schauss AG, Wu X. Anti-oxidant capacities of flavonoid compounds isolated from acai pulp (*Euterpe oleracea* Mart.). Food Chemistry. 2010;**122**:610-617. DOI: 10.1016/j.foodchem.2010.03.020
- [34] Xu Z, Wu J, Zhang Y, Hu X, Liao X, Wang Z. Extraction of anthocyanins from red cabbage using high pressure CO<sub>2</sub>. Bioresource Technology. 2010;**101**:7151-7157. DOI: 10.1016/j.biortech.2010.04.004
- [35] Cerón IX, Higuera JC, Cardona CA. Design and analysis of antioxidant compounds from Andes berry fruits (*Rubus glaucus* Benth) using an enhanced-fluidity liquid extraction process with CO<sub>2</sub> and ethanol. Journal of Supercritical Fluids. 2012;**62**:96-101. DOI: 10.1016/j.supflu.2011.12.007
- [36] Santos DT, Veggi PC, Meireles MAA. Optimization and economic evaluation of pressurized liquid extraction of phenolic compounds from Jaboticaba skins. Journal of Food Engineering. 2012;**108**:444-452. DOI: 10.1016/j.jfoodeng.2011.08.022
- [37] Span R, Wagner W. A new equation of state for carbon dioxide covering the fluid region from the triple-point temperature to 1100 K at pressures up to 800 MPa. Journal of Physical and Chemical Reference Data. 1996;**25**:1509-1596. DOI: 10.1063/1.555991
- [38] Peng D-Y, Robinson DB. A new two-constant equation of state. Industrial and Engineering Chemistry Fundamentals. 1976;**15**:59-64. DOI: 10.1021/i160057a011
- [39] Soave G. Equilibrium constants from a modified Redlich-Kwong equation of state. Chemical Engineering Science. 1972;**27**:1197-1203. DOI: 10.1016/0009-2509(72)80096-4
- [40] Pfohl O, Petkov S, Brunner G. "PE" quickly makes available the newest equations of state via the internet. Industrial and Engineering Chemistry Research. 2000;**39**:4439-4440. DOI: 10.1021/ie000778t

- [41] Brunner G. Hydrothermal and Supercritical Water Processes. Amsterdam: Supercritical fluid science and technology; 2014. DOI: 10.1016/B978-0-444-59413-6.00009-1
- [42] Bertucco A, Vetter G. High Pressure Process Technology: Fundamentals and Applications. United Kingdom: Elsevier Science & Technology; 2001. DOI: 10.1016/S0926-9614(01)80016-2
- [43] Bimakr M, Rahman RA, Taip FS, Ganjloo A, Salleh LM, Selamat J, Hamid A, Zaidul ISM. Comparison of different extraction methods for the extraction of major bioactive flavonoid compounds from spearmint (*Mentha spicata* L.) leaves. Food and Bioproducts Processing. 2011;**89**:67-72. DOI: 10.1016/j.fbp.2010.03.002
- [44] Eller FJ, Cermak SC, Taylor SL. Supercritical carbon dioxide extraction of cuphea seed oil. Industrial Crops and Products. 2011;**33**:554-557. DOI: 10.1016/j.indcrop.2010.12.017
- [45] Ruttarattanamongkol K, Siebenhandl-Ehn S, Schreiner M, Petrasch AM. Pilot-scale supercritical carbon dioxide extraction, physico-chemical properties and profile characterization of *Moringa oleifera* seed oil in comparison with conventional extraction methods. Industrial Crops and Products. 2014;**58**:68-77. DOI: 10.1016/j.indcrop.2014.03.020
- [46] Ledesma-Hernandez B, Herrero M. Bioactive Compounds from Marine Foods. Chichester, UK: John Wiley & Sons Ltd; 2013. DOI: 10.1002/9781118412893
- [47] Jiao J, Fu Y-J, Zu Y-G, Luo M, Wang W, Zhang L, Li J. Enzyme-assisted microwave hydro-distillation essential oil from *Fructus forsythia*, chemical constituents, and its antimicrobial and antioxidant activities. Food Chemistry. 2012;**134**:235-243. DOI: 10.1016/j.foodchem.2012.02.114
- [48] Guan W, Li S, Yan R, Tang S, Quan C. Comparison of essential oils of clove buds extracted with supercritical carbon dioxide and other three traditional extraction methods. Food Chemistry. 2007;**101**:1558-1564. DOI: 10.1016/j.foodchem.2006.04.009
- [49] Conde-Hernández LA, Espinosa-Victoria JR, Trejo A, Guerrero-Beltrán JÁ. CO<sub>2</sub>-supercritical extraction, hydrodistillation and steam distillation of essential oil of rosemary (*Rosmarinus officinalis*). Journal of Food Engineering. 2017;**200**:81-86. DOI: 10.1016/j.jfoodeng.2016.12.022
- [50] Shahsavarpour M, Lashkarbolooki M, Eftekhari MJ, Esmailzadeh F. Extraction of essential oils from *Mentha spicata* L. (Labiatae) via optimized supercritical carbon dioxide process. Journal of Supercritical Fluids. 2016:2-9. DOI: 10.1016/j.supflu.2017.02.004
- [51] Abbas A, Anwar F, Ahmad N. Variation in physico-chemical composition and biological attributes of common basil essential oils produced by hydro-distillation and supercritical fluid extraction. Journal of Essential Oil-Bearing Plants. 2017;**20**:95-109. DOI: 10.1080/0972060X.2017.1280418
- [52] Vági E, Simándi B, Suhajda Á, Héthelyi É. Essential oil composition and antimicrobial activity of *Origanum majorana* L. extracts obtained with ethyl alcohol and supercritical carbon dioxide. Food Research International. 2005;**38**:51-57. DOI: 10.1016/j.foodres.2004.07.006



- [53] Bagheri H, Bin Abdul Manap MY, Solati Z. Antioxidant activity of *Piper nigrum* L. essential oil extracted by supercritical CO<sub>2</sub> extraction and hydro-distillation. *Talanta*. 2014;**121**:220-228. DOI: 10.1016/j.talanta.2014.01.007
- [54] Ocaña-Fuentes A, Arranz-Gutiérrez E, Señorans FJ, Reglero G. Supercritical fluid extraction of oregano (*Origanum vulgare*) essentials oils: Anti-inflammatory properties based on cytokine response on THP-1 macrophages. *Food and Chemical Toxicology*. 2010;**48**:1568-1575. DOI: 10.1016/j.fct.2010.03.026
- [55] Pavela R, Sajfrtová M, Sovová H, Bárnét M, Karban J. The insecticidal activity of *Tanacetum parthenium* (L.) Schultz Bip. extracts obtained by supercritical fluid extraction and hydrodistillation. *Industrial Crops and Products*. 2010;**31**:449-454. DOI: 10.1016/j.indcrop.2010.01.003
- [56] Oliveira MS, da Costa WA, Pereira DS, Botelho JRS, de Alencar Menezes TO, de Aguiar Andrade EH, da Silva SHM, da Silva Sousa Filho AP, de Carvalho RN. Chemical composition and phytotoxic activity of clove (*Syzygium aromaticum*) essential oil obtained with supercritical CO<sub>2</sub>. *Journal of Supercritical Fluids*. 2016;**118**:185-193. DOI: 10.1016/j.supflu.2016.08.010
- [57] Larkeche O, Zermane a, Meniai a-H, Crampon C, Badens E. Supercritical extraction of essential oil from *Juniperus communis* L. needles: Application of response surface methodology. *Journal of Supercritical Fluids*. 2015;**99**:8-14. DOI: 10.1016/j.supflu.2015.01.026
- [58] Khajeh M. Optimization of process variables for essential oil components from *Satureja hortensis* by supercritical fluid extraction using Box-Behnken experimental design. *Journal of Supercritical Fluids*. 2011;**55**:944-948. DOI: 10.1016/j.supflu.2010.10.017
- [59] Zermane A, Larkeche O, Meniai A-H, Crampon C, Badens E. Optimization of essential oil supercritical extraction from Algerian *Myrtus communis* L. leaves using response surface methodology. *Journal of Supercritical Fluids*. 2014;**85**:89-94. DOI: 10.1016/j.supflu.2013.11.002
- [60] Uquiche E, Cirano N, Millao S. Supercritical fluid extraction of essential oil from *Leptocarpha rivularis* using CO<sub>2</sub>. *Industrial Crops and Products*. 2015;**77**:307-314. DOI: 10.1016/j.indcrop.2015.09.001
- [61] Chen Z, Mei X, Jin Y, Kim E-H, Yang Z, Tu Y. Optimisation of supercritical carbon dioxide extraction of essential oil of flowers of tea (*Camellia sinensis* L.) plants and its antioxidative activity. *Journal of the Science of Food and Agriculture*. 2014;**94**:316-321. DOI: 10.1002/jsfa.6260
- [62] Moreau RA, Whitaker BD, Hicks KB. Phytosterols, phytostanols, and their conjugates in foods: Structural diversity, quantitative analysis, and health-promoting uses. *Progress in Lipid Research*. 2002;**41**:457-500. DOI: 10.1016/S0163-7827(02)00006-1
- [63] Awad AB, Fink CS. Phytosterols as anticancer dietary components: Evidence and mechanism of action. *The Journal of Nutrition*. 2000;**130**:2127-2130. <http://jn.nutrition.org/content/130/9/2127.long>

- [64] Ling WH, Jones PJH. Dietary phytosterols: A review of metabolism, benefits and side effects. *Life Sciences*. 1995;**57**:195-206. DOI: 10.1016/0024-3205(95)00263-6
- [65] Ostlund RE. Phytosterols in human nutrition. *Annual Review of Nutrition*. 2002;**22**:533-549. DOI: 10.1146/annurev.nutr.22.020702.075220
- [66] Nyam KL, Tan CP, Lai OM, Long K, Man YBC. Optimization of supercritical CO<sub>2</sub> extraction of phytosterol-enriched oil from Kalahari melon seeds. *Food and Bioprocess Technology*. 2011;**4**:1432-1441. DOI: 10.1007/s11947-009-0253-4
- [67] Nyam KL, Tan CP, Lai OM, Long K, Che Man YB. Optimization of supercritical fluid extraction of phytosterol from roselle seeds with a central composite design model. *Food and Bioprocess Technology*. 2010;**88**:239-246. DOI: 10.1016/j.fbp.2009.11.002
- [68] Hrabovski N, Sinadinović-Fišer S, Nikolovski B, Sovilj M, Borota O. Phytosterols in pumpkin seed oil extracted by organic solvents and supercritical CO<sub>2</sub>. *European Journal of Lipid Science and Technology*. 2012;**114**:1204-1211. DOI: 10.1002/ejlt.201200009
- [69] Uquiche E, Romero V, Ortíz J, Del Valle JM. Extraction of oil and minor lipids from cold-press rapeseed cake with supercritical CO<sub>2</sub>. *Brazilian Journal of Chemical Engineering*. 2012;**29**:585-597. DOI: 10.1590/S0104-66322012000300016
- [70] Sajfrtová M, Ličková I, Wimmerová M, Sovová H, Wimmer Z.  $\beta$ -Sitosterol: Supercritical carbon dioxide extraction from sea buckthorn (*Hippophae rhamnoides* L.) seeds. *International Journal of Molecular Sciences*. 2010;**11**:1842-1850. DOI: 10.3390/ijms11041842
- [71] Botelho JRS, Medeiros NG, Rodrigues AMC, Araújo ME, Machado NT, Guimarães Santos A, Santos IR, Gomes-Leal W, Carvalho RN. Black sesame (*Sesamum indicum* L.) seeds extracts by CO<sub>2</sub> supercritical fluid extraction: Isotherms of global yield, kinetics data, total fatty acids, phytosterols and neuroprotective effects. *Journal of Supercritical Fluids*. 2014;**93**:49-55. DOI: 10.1016/j.supflu.2014.02.008
- [72] Wang H, Yang A, Zhang G, Ma B, Meng F, Peng M, Wang H. Enhancement of carotenoid and bacteriochlorophyll by high salinity stress in photosynthetic bacteria. *International Biodeterioration and Biodegradation*. 2017;**121**:91-96. DOI: 10.1016/j.ibiod.2017.03.028
- [73] Martins N, Ferreira ICFR. Wastes and by-products: Upcoming sources of carotenoids for biotechnological purposes and health-related applications. *Trends in Food Science and Technology*. 2017;**62**:33-48. DOI: 10.1016/j.tifs.2017.01.014
- [74] Huang JJ, Lin S, Xu W, Cheung PCK. Occurrence and biosynthesis of carotenoids in phytoplankton. *Biotechnology Advances*. 2017;**35**:597-618. DOI: 10.1016/j.biotechadv.2017.05.001
- [75] Riccioni G, D'Orazio N, Franceschelli S, Speranza L. Marine carotenoids and cardiovascular risk markers. *Marine Drugs*. 2011;**9**:1166-1175. DOI: 10.3390/md9071166
- [76] Gammone MA, Riccioni G, D'Orazio N. Carotenoids: Potential allies of cardiovascular health? *Food & Nutrition Research*. 2015;**59**:1-11. DOI: 10.3402/fnr.v59.26762

- [77] Saini RK, Keum Y-S. Carotenoid extraction methods: A review of recent developments. *Food Chemistry*. 2018;**240**:90-103. DOI: 10.1016/j.foodchem.2017.07.099
- [78] Figueira JA, Pereira JAM, Porto-Figueira P, Câmara JS. Ultrasound-assisted liquid-liquid extraction followed by ultrahigh pressure liquid chromatography for the quantification of major carotenoids in tomato. *Journal of Food Composition and Analysis*. 2017;**57**:87-93. DOI: 10.1016/j.jfca.2016.12.022
- [79] Hiranvarachat B, Devahastin S. Enhancement of microwave-assisted extraction via intermittent radiation: Extraction of carotenoids from carrot peels. *Journal of Food Engineering*. 2014;**126**:17-26. DOI: 10.1016/j.jfoodeng.2013.10.024
- [80] Goula AM, Ververi M, Adamopoulou A, Kaderides K. Green ultrasound-assisted extraction of carotenoids from pomegranate wastes using vegetable oils. *Ultrasonics Sonochemistry*. 2017;**34**:821-830. DOI: 10.1016/j.ultsonch.2016.07.022
- [81] Kwang HC, Lee HJ, Koo SY, Song DG, Lee DU, Pan CH. Optimization of pressurized liquid extraction of carotenoids and chlorophylls from *Chlorella vulgaris*. *Journal of Agricultural and Food Chemistry*. 2010;**58**:793-797. DOI: 10.1021/jf902628j
- [82] Damergi E, Schwitzguébel JP, Refardt D, Sharma S, Holliger C, Ludwig C. Extraction of carotenoids from *Chlorella vulgaris* using green solvents and syngas production from residual biomass. *Algal Research*. 2017;**25**:488-495. DOI: 10.1016/j.algal.2017.05.003
- [83] Millao S, Uquiche E. Extraction of oil and carotenoids from pelletized microalgae using supercritical carbon dioxide. *Journal of Supercritical Fluids*. 2016;**116**:223-231. DOI: 10.1016/j.supflu.2016.05.049
- [84] Egydio JA, Moraes ÂM, Rosa PTV. Supercritical fluid extraction of lycopene from tomato juice and characterization of its antioxidation activity. *Journal of Supercritical Fluids*. 2010;**54**:159-164. DOI: 10.1016/j.supflu.2010.04.009
- [85] Hsu YW, Tsai CF, Chen WK, Ho YC, Lu FJ. Determination of lutein and zeaxanthin and antioxidant capacity of supercritical carbon dioxide extract from daylily (*Hemerocallis disticha*). *Food Chemistry*. 2011;**129**:1813-1818. DOI: 10.1016/j.foodchem.2011.05.116
- [86] Chen J-R, Wu J-J, Lin J-C-T, Wang Y-C, Young C-C, Shieh C-J, Hsu S-L, Chang C-MJ. Low density supercritical fluids precipitation of 9-cis and all trans- $\beta$ -carotenes enriched particulates from *Dunaliella salina*. *Journal of Chromatography. A*. 2013;**1299**:1-9. DOI: 10.1016/j.chroma.2013.05.022
- [87] Goto M, Kanda H, Wahyudiono SM. Extraction of carotenoids and lipids from algae by supercritical CO<sub>2</sub> and subcritical dimethyl ether. *Journal of Supercritical Fluids*. 2015;**96**:245-251. DOI: 10.1016/j.supflu.2014.10.003
- [88] Heffernan N, Smyth TJ, FitzGerald RJ, Vila-Soler A, Mendiola J, Ibáñez E, Brunton NP. Comparison of extraction methods for selected carotenoids from macroalgae and the assessment of their seasonal/spatial variation. *Innovative Food Science & Emerging Technologies*. 2016;**37**:221-228. DOI: 10.1016/j.ifset.2016.06.004

- [89] Gunstone D, Norris FA. *Lipids in Foods: Chemistry, Biochemistry and Technology*. Oxford: Elsevier; 1983
- [90] Stirban A, Nandrea S, Go C, Tamler R, Pop A, Negrean M, Gawlowski T. Effects of n-3 fatty acids on macro- and microvascular function in subjects with type 2 diabetes mellitus 1–3. *The American Journal of Clinical Nutrition*. 2010;**91**:808-813. DOI: 10.3945/ajcn.2009.28374.1
- [91] Begg DP, Sinclair AJ, Stahl L, Premaratna SD, Hafandi A, Jois M, Weisinger RS. Hypertension induced by omega-3 polyunsaturated fatty acid deficiency is alleviated by alpha-linolenic acid regardless of dietary source. *Hypertension Research*. 2010;**33**:808-813. DOI: 10.1038/hr.2010.84
- [92] De CR. N-3 fatty acids in cardiovascular disease. *The New England Journal of Medicine*. 2011;**364**:2439-2450
- [93] Oh DY, Talukdar S, Bae EJ, Imamura T, Morinaga H, Fan W, Li P, Lu WJ, Watkins SM, Olefsky JM. GPR120 is an Omega-3 fatty acid receptor mediating potent anti-inflammatory and insulin-sensitizing effects. *Cell*. 2010;**142**:687-698. DOI: 10.1016/j.cell.2010.07.041
- [94] Issariyakul T, Dalai AK. Biodiesel from vegetable oils. *Renewable and Sustainable Energy Reviews*. 2014;**31**:446-471
- [95] Hafis SM, Ridzuan MJM, Rahayu A, Farahana RN, Nor Fatin B, Syahrullail S. Properties of palm pressed fibre for metal forming lubricant applications. *Procedia Engineering*. 2013;**68**:130-137
- [96] Pádua MS, Paiva LV, Labory CRG, Alves E, Stein VC. Induction and characterization of oil palm (*Elaeis guineensis* Jacq.) pro-embryogenic masses. *Anais da Academia Brasileira de Ciências*. 2013;**85**:1545-1556. DOI: 10.1590/0001-37652013107912
- [97] Ezeh O, Gordon MH, Niranjana K. Enhancing the recovery of tiger nut (*Cyperus esculentus*) oil by mechanical pressing: Moisture content, particle size, high pressure and enzymatic pre-treatment effects. *Food Chemistry*. 2016;**194**:354-361. DOI: 10.1016/j.foodchem.2015.07.151
- [98] Koubaa M, Mhemdi H, Vorobiev E. Influence of canola seed dehulling on the oil recovery by cold pressing and supercritical CO<sub>2</sub> extraction. *Journal of Food Engineering*. 2016;**182**:18-25. DOI: 10.1016/j.jfoodeng.2016.02.021
- [99] Hu B, Li C, Zhang Z, Zhao Q, Zhu Y, Su Z, Chen Y. Microwave-assisted extraction of silkworm pupal oil and evaluation of its fatty acid composition, physicochemical properties and antioxidant activities. *Food Chemistry*. 2017;**231**:348-355. DOI: 10.1016/j.foodchem.2017.03.152
- [100] Bernardo-Gil MG, Casquilho M, Esquível MM, Ribeiro MA. Supercritical fluid extraction of fig leaf gourd seeds oil: Fatty acids composition and extraction kinetics. *Journal of Supercritical Fluids*. 2009;**49**:32-36. DOI: 10.1016/j.supflu.2008.12.004

- [101] Sánchez-Camargo AP, Martínez-Correa HA, Paviani LC, Cabral FA. Supercritical CO<sub>2</sub> extraction of lipids and astaxanthin from Brazilian redspotted shrimp waste (*Farfantepenaeus paulensis*). *Journal of Supercritical Fluids*. 2011;**56**:164-173. DOI: 10.1016/j.supflu.2010.12.009
- [102] Tomita K, Machmudah S, Quitain AT, Sasaki M, Fukuzato R, Goto M. Extraction and solubility evaluation of functional seed oil in supercritical carbon dioxide. *Journal of Supercritical Fluids*. 2013;**79**:109-113. DOI: 10.1016/j.supflu.2013.02.011
- [103] Wang XW, Liang JR, Luo CS, Chen CP, Gao YH. Biomass, total lipid production, and fatty acid composition of the marine diatom *Chaetoceros muelleri* in response to different CO<sub>2</sub> levels. *Bioresource Technology*. 2014;**161**:124-130. DOI: 10.1016/j.biortech.2014.03.012
- [104] Bartolomé Ortega A, Calvo Garcia A, Szekely E, Škerget M, Knez Ž. Supercritical fluid extraction from saw palmetto berries at a pressure range between 300 bar and 450 bar. *Journal of Supercritical Fluids*. 2017;**120**:132-139. DOI: 10.1016/j.supflu.2016.11.003
- [105] De Melo MMR, Silvestre AJD, Silva CM. Supercritical fluid extraction of vegetable matrices: Applications, trends and future perspectives of a convincing green technology. *Journal of Supercritical Fluids*. 2014;**92**:115-176. DOI: 10.1016/j.supflu.2014.04.007
- [106] Vatai T, Škerget M, Knez Ž. Extraction of phenolic compounds from elder berry and different grape marc varieties using organic solvents and/or supercritical carbon dioxide. *Journal of Food Engineering*. 2009;**90**:246-254. DOI: 10.1016/j.jfoodeng.2008.06.028
- [107] Mantell C, Rodríguez M, Martínez de la Ossa E. A screening analysis of the high-pressure extraction of anthocyanins from red grape pomace with carbon dioxide and cosolvent. *Engineering in Life Sciences*. 2003;**3**:38-42. DOI: 10.1002/elsc.200390004
- [108] Ghafoor K, AL-Juhaimi FY, Choi YH. Supercritical fluid extraction of phenolic compounds and antioxidants from grape (*Vitis labrusca* B.) seeds. *Plant Foods for Human Nutrition*. 2012;**67**:407-414. DOI: 10.1007/s11130-012-0313-1
- [109] L.E. Laroze, B. Díaz-Reinoso, A. Moure, M.E. Zúñiga, H. Domínguez, Extraction of antioxidants from several berries pressing wastes using conventional and supercritical solvents, *European Food Research and Technology* 231 (2010) 669-677. doi:10.1007/s00217-010-1320-9
- [110] Seabra IJ, Braga MEM, Batista MTP, de Sousa HC. Fractioned high pressure extraction of anthocyanins from elderberry (*Sambucus nigra* L.) pomace. *Food and Bioprocess Technology*. 2010;**3**:674-683. DOI: 10.1007/s11947-008-0134-2
- [111] Blevé M, Ciurlia L, Erroi E, Lionetto G, Longo L, Rescio L, Schettino T, Vasapollo G. An innovative method for the purification of anthocyanins from grape skin extracts by using liquid and sub-critical carbon dioxide. *Separation and Purification Technology*. 2008;**64**:192-197. DOI: 10.1016/j.seppur.2008.10.012
- [112] Paula JT, Paviani LC, Foglio MA, Sousa IMO, Duarte GHB, Jorge MP, Eberlin MN, Cabral FA. Extraction of anthocyanins and luteolin from *Arrabidaea chica* by sequential extraction in fixed bed using supercritical CO<sub>2</sub>, ethanol and water as solvents. *Journal of Supercritical Fluids*. 2014;**86**:100-107. DOI: 10.1016/j.supflu.2013.12.008

- [113] Bergeron C, Gafner S, Clausen E, Carrier DJ. Comparison of the chemical composition of extracts from *Scutellaria lateriflora* using accelerated solvent extraction and supercritical fluid extraction versus standard hot water or 70% ethanol extraction. *Journal of Agricultural and Food Chemistry*. 2005;**53**:3076-3080. DOI: 10.1021/jf048408t
- [114] Paes J, Dotta R, Barbero GF, Martínez J. Extraction of phenolic compounds and anthocyanins from blueberry (*Vaccinium myrtillus* L.) residues using supercritical CO<sub>2</sub> and pressurized liquids. *Journal of Supercritical Fluids*. 2014;**95**:8-16. DOI: 10.1016/j.supflu.2014.07.025

---

# **A Review on the Application of Enhanced Oil/Gas Recovery through CO<sub>2</sub> Sequestration**

---

Abdelmalek Atia and Kamal Mohammedi

Additional information is available at the end of the chapter

<http://dx.doi.org/10.5772/intechopen.79278>

---

## **Abstract**

Global warming is considered as one of very important problems in the last few years. This phenomenon is caused primarily by increase in greenhouse gases such as carbon dioxide (CO<sub>2</sub>). Natural events and human activities are believed to be the principal sources of this problem. A promising long-term solution for mitigating global heating is to inject CO<sub>2</sub> into oil field geological formations for combination between CO<sub>2</sub> sequestration and enhanced oil recovery. This chapter aims to give an extensive literature survey and examines research papers that focus on EOR-CO<sub>2</sub> processes and projects that have been tested in the field.

**Keywords:** CO<sub>2</sub> sequestration, EOR, global warming, energy

---

## **1. Introduction**

The growing concern over the climate change caused by global warming due to a high emission of greenhouse gases (essentially carbon dioxide (CO<sub>2</sub>)) has increased the interest in finding various techniques to resolve this problem. The injection of this gas for enhanced oil recovery has been tested with full success in several fields over the world.

Traditionally, oil recovery operations have been subdivided into three stages: primary, secondary, and tertiary as shown in **Figure 1**. Historically, these stages described the production from a reservoir in a chronological sense. Primary production, the initial production stage,

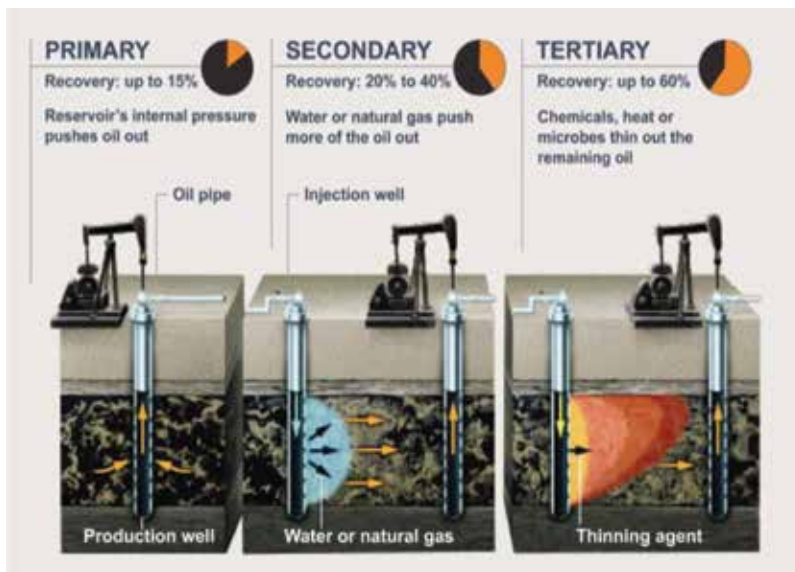


Figure 1. Oil recovery stages [1].

resulted from the displacement energy naturally existing in a reservoir; the driving energy may be derived from the expansion of the gas cap or an active aquifer, from the liberation and expansion of dissolved gas, from gravity drainage, or from a combination of all these mechanisms. Secondary recovery, the second stage of operations, usually was implemented after primary recovery declined. Traditional secondary production processes are gas injection, water flooding, or water alternative gas injection (WAG). Tertiary recovery or enhanced oil recovery (EOR) is a term used to describe a set of processes intended to increase the production of oil beyond what could normally be extracted when using conventional oil production techniques, while traditional oil production (primary and secondary stage) can recover up to 35–45% of the original oil in place (OOIP). The application of an EOR technique is typically performed toward what is normally perceived to be the end of the life of an oil field, and tertiary production used miscible gases (e.g.,  $\text{CH}_4$ ,  $\text{CO}_2$ ), chemicals, and/or thermal energy to displace additional oil (5–15%).

## 2. Carbon dioxide properties

Carbon dioxide is formed from the combination of two elements: carbon and oxygen. It is produced from the combustion of coal or hydrocarbons.  $\text{CO}_2$  is a colorless, odorless, and non-toxic stable compound found in a gaseous state at standard conditions. In petroleum engineering application, it can be in a gas or a liquid state depending on the PVT conditions. **Table 1** gives the main properties of carbon dioxide. The phase diagram (**Figure 2**) of  $\text{CO}_2$  is



Property	Value
Molecular weight	44 g/mol
Critical temperature	31°C
Critical pressure	73.77 bar
Critical density	467.6 kg/m <sup>3</sup>
Triple point temperature	-56.5°C
Triple point pressure	5.18 bar
Boiling (sublimation) point (1.013 bar)	-78.5°C
Critical Z factor	0.274
Solid phase	
Density of carbon dioxide snow at freezing point	1562 kg/m <sup>3</sup>
Latent heat of vaporization (1.013 bar at sublimation point)	571.1 kJ/kg <sup>1</sup>
Liquid phase	
Vapor pressure (at 20°C)	58.5 bar
Liquid density (at -20°C and 19.7 bar)	1032 kg/m <sup>3</sup>
Viscosity (at STP)	99 μPa s
Characteristics of CO <sub>2</sub> gas phase	
Gas density	2.814 kg/m <sup>3</sup>
Gas density (according to STP)	1.976 kg/m <sup>3</sup>
Specific volume (according to STP)	0.506 m <sup>3</sup> /kg
C <sub>p</sub> (according to STP)	0.0364 kJ/(mol K)
C <sub>v</sub> (according to STP)	0.0278 kJ/(mol K)
C <sub>p</sub> /C <sub>v</sub>	1.308
Viscosity (according to STP)	13.72 μPa s
Thermal conductivity (according to STP)	14.65 mW/(m K)
Enthalpy (according to STP)	21.34 kJ/mol
Entropy (according to STP)	117.2 J mol/K

*Note:* STP stands for standard temperature and pressure, which are 0°C and 1.013 bar.

**Table 1.** Carbon dioxide properties [3].

also a key data since we can inject it under different temperature and pressure conditions. The three phases are shown in this diagram, with the triple and critical point. Above the critical point, the CO<sub>2</sub> is considered as a supercritical fluid.

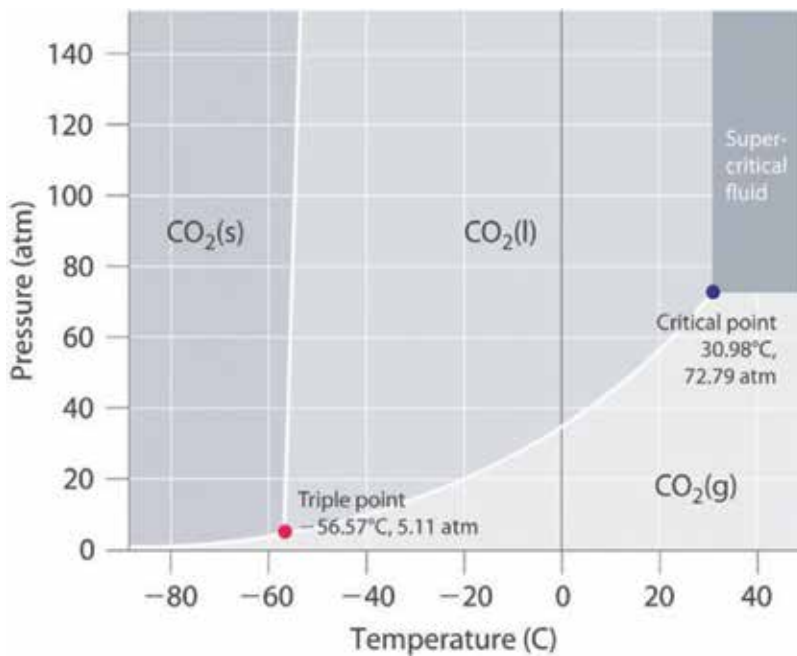


Figure 2. CO<sub>2</sub> phase diagram [2].

### 3. Carbon capture and storage

Carbon dioxide is the most important greenhouse gas, because it is emitted into the atmosphere in large quantities [4]. Carbon capture and storage (CCS) has been recognized as a new project around the world that should help mitigate CO<sub>2</sub> emissions significantly. The idea behind CCS is simple and can be divided into three steps: capture of CO<sub>2</sub> (e.g., from a fossil fuel power plant), transportation of the captured CO<sub>2</sub>, and permanent storage into different geological formations (e.g., saline aquifer and oil and reservoirs), with the aim of isolating CO<sub>2</sub> from the atmosphere [5] (Figure 3).

Several scenarios describing the emission of greenhouse gases and models for the estimation of their influence on the global climate have been examined by the members of several association interests by this subject like the Intergovernmental Panel on Climate Change (IPCC) and the International Energy Agency (IEA). Based on the assumptions of IPCC, the climate model global temperature increases between 1 and 6°C were predicted by the year 2100, while some regions might benefit from higher temperatures [6]. The IEA Agency estimates that CCS projects should contribute to about 15–20% of the total greenhouse gas emissions mitigation by 2050, and without the application of CCS, the overall costs to halve CO<sub>2</sub> emissions by 2050 would rise by 70% [5]. It has been estimated that geological formations worldwide are able to store more than 10,000 Gt of carbon dioxide; this huge quantity is large compared to the cumulated anthropic emissions of carbon dioxide [3].

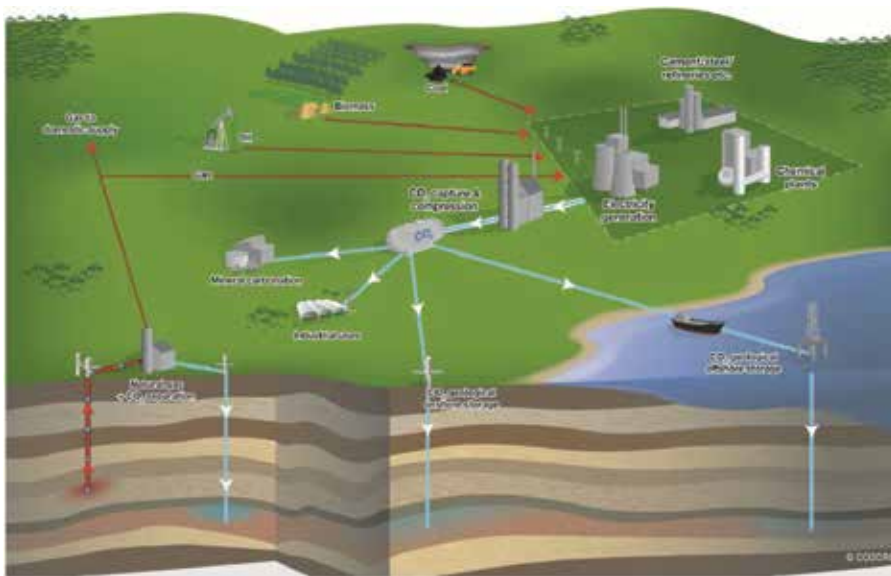


Figure 3. A schematic diagrams of possible CCS projects [5].

#### 4. EOR methods

Many EOR methods have been used in the past, with varying degrees of success, for the recovery of light and heavy oils, as well as tar sands. There are two main categories of EOR: thermal and non-thermal methods (include gas and chemical methods). Each main category includes some individual processes [7].

Thermal methods are primarily intended for heavy oils and tar sands; these methods recover the oil by introducing heat into the reservoir. Thermal method is based on a set of displacement mechanisms to enhance oil recovery. The most important mechanism is the reduction of crude oil viscosity with increasing temperature [8]. However, the viscosity reduction is less for lighter crude oil. Therefore, thermal methods have had limited success in the field of light crudes.

Non-thermal methods (gas and chemical methods) are normally used for light oils <100 cp. In a few cases, they are applicable to heavy oils <2000 cp, which are unsuitable for thermal methods.

Gas methods, particularly carbon dioxide (CO<sub>2</sub>), recover the oil mainly by injecting gas into the reservoir. Gas methods sometimes are called miscible process or solvent methods. The reservoir geology and fluid properties determine the suitability of a process for a given reservoir. Currently, gas methods account for most EOR production and are very successful especially for the reservoirs with low permeability, high pressure, and lighter oil [9].

Vapor extraction (VAPEX) is among the gas methods (Figures 4 and 5). It is a promising technique for the recovery of heavy oils and bitumen in reservoirs where thermal methods,

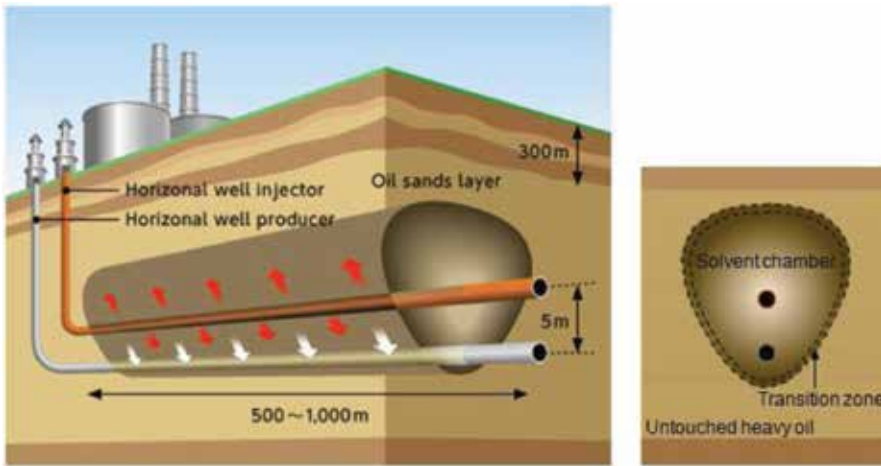


Figure 4. The VAPEX heavy oil recovery process [11].

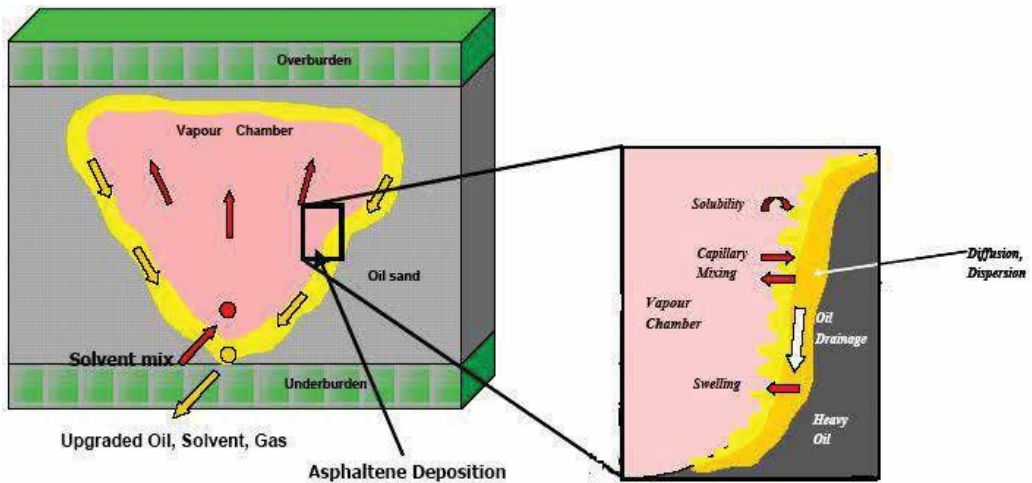


Figure 5. Mechanism involved in the VAPEX process [12].

such as steam-assisted gravity drainage (SAGD), cannot be applied. In the VAPEX process, a pair of horizontal injector-producer wells is employed. The gaseous hydrocarbon solvent (propane, butane, or a mixture of them) is injected into the deposit from the top well, and the diluted oil drains are gravitated downward to the bottom producing well. Recently, an attractive option was developed using  $\text{CO}_2$  as a solvent in the VAPEX process. The high solubility and viscosity reduction potential of  $\text{CO}_2$  could provide improvement to VAPEX performance. It also creates new opportunities for  $\text{CO}_2$  sequestration [10].

Chemical methods include polymer floods, surfactant flooding, alkaline flooding, and so on. The mechanisms of chemical methods are dependent on the chemical materials added into the reservoir. The chemical methods may provide one or several effects: interfacial tension

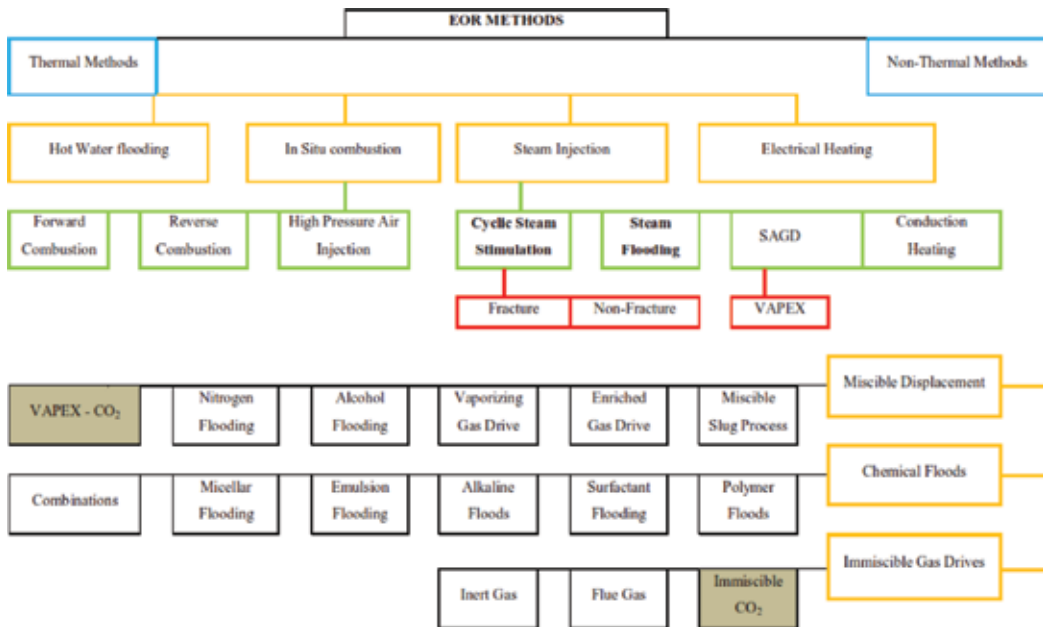


Figure 6. Classification of EOR methods.

reduction, viscosity reduction, wettability alteration, and mobility control. Meanwhile, there are many researchers on the background of EOR process; for a detailed review of enhanced oil recovery, we refer the interested reader to Thomas [7], and general classifications of these methods are shown in Figure 6.

## 5. Oil recovery by CO<sub>2</sub> injection

### 5.1. CO<sub>2</sub>-EOR: definition and advantages

The combustion and flaring of fossil fuels produce large quantities of CO<sub>2</sub>. The Intergovernmental Panel on Climate Change stresses the need to control anthropogenic greenhouse gases in order to mitigate the climate change that is adversely affecting the planet. Moreover, in some fields, the hydrocarbon gases produced along with the oil are re-injected into the reservoir to enhance oil production. Nevertheless, in some fields, the hydrocarbon gas is sold, and the gas itself is considered as a source of energy. An attractive option is the use of CO<sub>2</sub> as one of the main components of the solvent mixture for EOR process.

Enhanced oil recovery using CO<sub>2</sub> is an attractive oil recovery process that involves the injection of CO<sub>2</sub> to oil reservoirs and produce petroleum substances that would otherwise remain unrecoverable [13]. Typically, only around one-third of the oil is produced after primary and secondary oil recovery methods. Much of the remaining oil are trapped by capillary forces as disconnected drops, surrounded by water, or as a continuous phase at low saturation with gas occupying the larger fraction of the pore space. EOR operations

using carbon dioxide have been practiced for more than 50 years; the results revealed that 6–15% of original oil in place can be recovered by these kinds of processes [14].

The low saturation pressure of  $\text{CO}_2$  compared to  $\text{CH}_4$  or  $\text{N}_2$  and its low price compared with other hydrocarbon solvents are the incentives for the use of  $\text{CO}_2$  in the EOR process. Moreover, a mixture of hydrocarbon solvents with  $\text{CO}_2$  may be less likely to precipitate asphaltene, which is a great problem in enhanced oil recovery [15]. Furthermore, at high pressures,  $\text{CO}_2$  density has a density close to that of a liquid and is greater than that of either nitrogen ( $\text{N}_2$ ) or methane ( $\text{CH}_4$ ), which makes  $\text{CO}_2$  less prone to gravity segregation compared with  $\text{N}_2$  or  $\text{CH}_4$  [16].

## 5.2. Oil recovery mechanisms by $\text{CO}_2$ dissolution

When  $\text{CO}_2$  is injected into the reservoir, it interacts physically and chemically with rocks and fluids that are present in the reservoir, creating favorable mechanisms that can make enhancement in oil recovery. Among these mechanisms include a high dissolution of  $\text{CO}_2$  into crude oil via mass transfer followed by the following aspects: an increase of oil density, a reduction of the viscosity of the original crude oil, vaporization of intermediate components of the oil, a reduction of  $\text{CO}_2$ -oil interfacial tension, oil swelling, a reduction of water-oil interfacial tension, and an improvement of reservoir permeability [17].

The main scenario followed by  $\text{CO}_2$  sequestration is the mechanism of fluid density increasing caused by the dissolution and mixing of injected  $\text{CO}_2$  into fluid. In the past, there are a set of studies that have not taken the effect of density increase from mixing into account; this mechanism in the modeling of  $\text{CO}_2$  injection has been ignored [18–21]. However, as shown in other studies, this may not be true;  $\text{CO}_2$  has an effect on the density of fluid that is present in the reservoir [22, 23]. Its dissolution and mixing leads to density increase followed by density-driven natural convection phenomena. There are several published studies which reported that this phenomenon has a significant enhancement in hydrocarbon recovery and sequestration potential [24–27].

## 5.3. Literature review on EOR/EGR- $\text{CO}_2$

$\text{CO}_2$  storage studies started almost two decades ago. Despite this fact, still vast areas of research have not been covered in detail in the area of coupled enhanced oil recovery with  $\text{CO}_2$  sequestration [28].

DeRuiter et al. [22] studied the solubility and displacement of heavy crude oils with  $\text{CO}_2$  injection; they have found that the oils exhibit an increase in density due to  $\text{CO}_2$  solubility. The two samples in their study with API gravities of 18.5 and 14 exhibited an increase in density upon  $\text{CO}_2$  dissolution.

Morel et al. [29] and Le Romancer et al. [30] studied the effects of diffusion of nitrogen ( $\text{N}_2$ ) and  $\text{CO}_2$  on light oil using an outcrop core system. During 2010, Jamili et al. [31] simulated these previous experiments. These authors reported that diffusion was the main mass transfer mechanism between the matrix and fracture during nitrogen ( $\text{N}_2$ ) injection. On the other side,  $\text{CO}_2$  experiments conducted have shown that both diffusion and convection were important mechanisms.

Mehrotra and Svrcek [32–34] during the 1980s reported extensive experimental data on the dissolution of carbon dioxide on different bitumen samples in Alberta reservoirs. Their experimental data confirm a higher solubility of carbon dioxide in bitumen, and they found that this solubility increases as the injection pressure increases.

Darvish et al. [35] performed a set of experiments of CO<sub>2</sub> injection in an outcrop chalk core saturated with oil and was surrounded by an artificial fracture at reservoir conditions. These authors observed the production of gas enriched with methane at an early stage. Next, the amount of intermediate components increased in the production stream, and during the end of the experiments, the heavier components were recovered. Their results were also confirmed by simulation study performed by Moortgat et al. [36].

Malik and Islam [37] conclude that in the Weyburn field of Canada, horizontal injection wells have showed to be efficient for CO<sub>2</sub>-flooding process to improve oil recovery while increasing the CO<sub>2</sub> storage potential. Besides employing horizontal wells, Jessen et al. [38] have applied different well control techniques including completion equipment for both injection and production wells, at the same time improving the amount of injected and stored CO<sub>2</sub> as well as enhancing oil recovery.

Recently, Li-ping et al. [39] conducted an evaluation study around Ordos Basin in Yulin city of China; this Basin was divided into 17 reservoirs and is considered as the first largest low-permeability prolific onshore basin in China with proved reserves more than 10<sup>9</sup> t. These authors conclude that Ordos Basin has good geographical and geological conditions for CO<sub>2</sub> storage, and it has nine reservoirs suitable for CO<sub>2</sub> immiscible flooding and eight reservoirs suitable for CO<sub>2</sub> miscible flooding. The average incremental oil recovery ratios for immiscible and miscible flooding are 6.44 and 12%, respectively.

The booming development and production of shale gas largely depend on the extensive application of water-based hydraulic fracturing treatments. Hence, high water consumption and formation damage are two issues associated with this procedure. More recently, Pei et al. [40] investigated the feasibility of using CO<sub>2</sub> for reservoir fracturing and enhanced gas recovery (EGR) in order to reduce water usage and resource degradation, guarantee the environmental sustainability of unconventional resource developments, and create new opportunity for CO<sub>2</sub> storage. This study shows that this proposed CO<sub>2</sub>-EGR process was mostly like to be successful in the Barnett shale reservoir, but there are some scientific and engineering questions that need to be further investigated to push the proposed technology to be applicable in practice.

Song investigated the effect of operational schemes, reservoir types, and development parameters on both the amount of incremental oil produced and CO<sub>2</sub> stored in high water cut oil reservoirs during CO<sub>2</sub> water-alternating-gas (WAG) flooding by running a compositional numerical simulator. The author's study shows that the five-spot pattern is more suitable for WAG flooding. Appropriately expanding well spacing improves the economic efficiency, even though the recovery factor decreases slightly. In addition, oil price, rather than CO<sub>2</sub> injection cost, is considered as the parameter that impacts the economic efficiency of WAG flooding more significantly [41].

Er et al. [42] investigated the effect of injection flow rate of CO<sub>2</sub> on oil recovery using synthetic micro-scale fractured system saturated by normal decane (n-C<sub>10</sub>). The authors concluded that

for immiscible CO<sub>2</sub> displacement, the amount of oil trapped in the system was reduced as well as increasing injection rates of carbon dioxide. They also observed that for miscible CO<sub>2</sub> conditions, higher CO<sub>2</sub> injection rates yielded faster oil recovery.

Coal bed methane is also tested for enhanced gas recovery and CO<sub>2</sub> storage; Blue Creek and Pocahontas are two fields of coal bed methane in USA. Pashin et al. [43] employed a diverse suite of well testing and monitoring procedures designed to determine the heterogeneity, capacity, injectivity, and performance of mature Blue Creek coal bed methane reservoirs. A total of 516 m<sup>3</sup> of water and 252 t of CO<sub>2</sub> were injected into coal in a battery of slug tests. The author's results demonstrate that significant injectivity exists in this reservoir and that reservoir heterogeneity is a critical factor to consider when implementing CO<sub>2</sub>-enhanced methane recovery programs. Based on the study by Grimm et al. [44], CO<sub>2</sub>-CBM project can be conducted in the stratigraphic interval below the Hensley Shale where this confinement horizon is greater than 183 m below the surface and is above the level of hydraulic fracturing in CBM wells.

## 6. Conclusion

With the decline of oil production and apparition of global warming problem caused by excessive emission of carbon dioxide during the last decades, it is believed that EOR/EGR-CO<sub>2</sub> technologies will play a key role to meet the energy demand and better mitigation of climate change in the years to come. If we investigate at the great number of studies cited in this study, the subject of EOR-CO<sub>2</sub> is being very important. Several physical and chemical mechanisms are associated with CO<sub>2</sub> injection, and the most important mechanism is the dissolution of carbon dioxide into fluid formation. It has been accepted from previous studies that the dissolution of CO<sub>2</sub> increases fluid density, which results in a downward density-driven convection and consequently greatly enhances oil recovery and CO<sub>2</sub> potential sequestration.

## Author details

Abdelmalek Atia<sup>1\*</sup> and Kamal Mohammedi<sup>2</sup>

\*Address all correspondence to: abdelmalek-atia@univ-eloued.dz

1 University of El Oued, Levres Lab, Algeria

2 MESOnexTeam-URMPE, UMBB, Algeria

## References

- [1] Maugeri L. Squeezing more oil from the ground. *Scientific American*. 2009;**301**:56-63
- [2] Whitson CH, Brulé MR. Phase behavior. In: Henry L, editor. *Doherty Memorial Fund of AIME*. Society of Petroleum Engineers; Richardson Texas; 2000



- [3] Metz B, Davidson O, de Coninck H, Loos M, Meyer L. Carbon dioxide capture and storage. IPCC Special; 2005
- [4] Bielinski A. Numerical simulation of CO<sub>2</sub> sequestration in geological formations. Hydraulic Engineering Institute of Stuttgart University; 2007
- [5] Nikoosokhan S. Stockage géologique du dioxyde de carbone dans les veines de charbon: du matériau au réservoir. Thèse de doctorat, Université Paris Est; 2012
- [6] Griggs DJ, Noguer M. Climate change 2001: The scientific basis. Contribution of working group I to the third assessment report of the intergovernmental panel on climate change. Weather. 2002;57:267-269
- [7] Thomas S. Enhanced oil recovery— An overview. Oil & Gas Science and Technology-Revue de l'IFP. 2008;63:9-19
- [8] Liu S. Alkaline Surfactant Polymer Enhanced Oil Recovery Process. Vol. 69; Doctoral dissertation, Rice University; 2008
- [9] Lake LW. Enhanced Oil Recovery. Prentice Hall. 1989;1(43):17-39
- [10] Zadeh AB. Use of CO<sub>2</sub> in Vapex: Experimental and Modeling Study. Canada: University of Calgary; 2013
- [11] Jia X. Enhanced Solvent Vapour Extraction Processes in Thin Heavy Oil Reservoirs. Canada: Faculty of Graduate Studies and Research, University of Regina; 2014
- [12] Upreti S, Lohi A, Kapadia R, El-Haj R. Vapor extraction of heavy oil and bitumen: A review. Energy & Fuels. 2007;21:1562-1574
- [13] Abedini A. Mechanisms of Oil Recovery During Cyclic CO<sub>2</sub> Injection Process: Impact of Fluid Interactions, Operating Parameters, and Porous Medium. Canada: Faculty of Graduate Studies and Research, University of Regina; 2014
- [14] Hustad C-W, Austell JM, Roggenkamp M, Hammer U. Mechanisms and incentives to promote the use and storage of CO<sub>2</sub> in the North Sea. In: European Energy Law Report I, Intersentia. 2004. pp. 355-380
- [15] Javaheri M, Abedi J. The effect of heavy oil viscosity reduction by solvent dissolution on natural convection in the boundary layer of VAPEX. Transport in Porous Media. 2013;99: 307-326
- [16] Bui LH. Near Miscible CO<sub>2</sub> Application to Improve Oil Recovery. USA: University of Kansas; 2010
- [17] Klins MA. Carbon Dioxide Flooding: Basic Mechanisms and Project Design; U.S. Department of Energy; 1984
- [18] Bangia V, Yau F, Hendricks G. Reservoir performance of a gravity-stable, vertical CO<sub>2</sub> miscible flood: Wolfcamp reef reservoir. Wellman unit. SPE Reservoir Engineering. 1993; 8:261-269

- [19] Cardenas RL, Alston R, Nute A, Kokolis G. Laboratory design of a gravity-stable miscible CO<sub>2</sub> process. *Journal of Petroleum Technology*. 1984;**36**:111-118
- [20] Johnston J. Weeks Island gravity stable CO<sub>2</sub> pilot. In: *SPE Enhanced Oil Recovery Symposium*; 1988
- [21] Palmer F, Nute A, Peterson R. Implementation of a gravity-stable miscible CO<sub>2</sub> flood in the 8000 foot sand, Bay St. Elaine Field. *Journal of Petroleum Technology*. 1984;**36**:101-110
- [22] DeRuiter R, Nash L, Singletary M. Solubility and displacement behavior of a viscous crude with CO<sub>2</sub> and hydrocarbon gases. *SPE Reservoir Engineering*. 1994;**9**:101-106
- [23] Ashcroft SJ, Isa MB. Effect of dissolved gases on the densities of hydrocarbons. *Journal of Chemical & Engineering Data*. 1997;**42**:1244-1248
- [24] Atia A, Mohammedi K. Pore-scale study based on lattice Boltzmann method of density driven natural convection during CO<sub>2</sub> injection project. *Chinese Journal of Chemical Engineering*. 2015;**23**(10):1593-1602
- [25] Farajzadeh R, Ranganathan P, Zitha PLJ, Bruining J. The effect of heterogeneity on the character of density driven natural convection of CO<sub>2</sub> overlying a brine layer. *Advances in Water Resources*. 2011;**34**:327-339
- [26] Javaheri M, Abedi J. Modelling of mass transfer boundary layer instability in the CO-Vapex process. In: *Canadian International Petroleum Conference*; 2008
- [27] Li Z, Dong M, Shirif E. Natural convection—An underlying mechanism in CO-VAPEX process. In: *Canadian International Petroleum Conference*; 2004
- [28] Ghomian Y. Reservoir simulation studies for coupled CO<sub>2</sub> sequestration and enhanced Oil Recovery. Doctoral dissertation, Texas University; 2008
- [29] Morel D, Bourbiaux B, Latil M, Thiebot B. Diffusion effects in gasflooded light-oil fractured reservoirs. *SPE Advanced Technology Series*. 1993;**1**:100-109
- [30] Le Romancer J, Defives D, Kalaydjian F, Fernandes G. Influence of the diffusing gas on the mechanism of oil recovery by gas diffusion in fractured reservoir. In: *IEA Collaborative Project on Enhanced Oil Recovery Workshop and Symposium*; Bergen Norway; 1994. pp. 28-31
- [31] Jamili A, Willhite GP, Green D. Modeling gas-phase mass transfer between fracture and matrix in naturally fractured reservoirs. *SPE Journal*. 2011;**16**:795-811
- [32] Mehrotra AK, Svrcek WY. Correlations for properties of bitumen saturated with CO<sub>2</sub>, CH<sub>4</sub> and N<sub>2</sub>, and experiments with combustion gas mixtures. *Journal of Canadian Petroleum Technology*. 1982;**21**(6):94-104
- [33] Mehrotra AK, Svrcek WY. Measurement and correlation of viscosity, density and gas solubility for Marguerite Lake bitumen saturated with carbon dioxide. *AOSTRA Journal of Research*. 1984;**1**:51-62

- [34] Mehrotra A, Svrcek W. Viscosity, density and gas solubility data for oil sand bitumens: Part I: Athabasca bitumen saturated with CO and C<sub>2</sub>H<sub>6</sub>. *AOSTRA Journal of Research*. 1985; **1**:263-268
- [35] Darvish GR, Utne SA, Holt T, Kleppe J, Lindeberg E. Reservoir conditions laboratory experiments of CO<sub>2</sub> injection into fractured cores (SPE99650). In: 68th EAGE Conference & Exhibition; 2006
- [36] Moortgat J, Firoozabadi A, Farshi MM. A new approach to compositional modeling of CO<sub>2</sub> injection in fractured media compared to experimental data. In: SPE Annual Technical Conference and Exhibition; 2009
- [37] Malik QM, Islam M. CO<sub>2</sub> injection in the Weyburn field of Canada: Optimization of enhanced oil recovery and greenhouse gas storage with horizontal wells. In: SPE/DOE Improved Oil Recovery Symposium; 2000
- [38] Jessen K, Kavscek AR, Orr FM. Increasing CO<sub>2</sub> storage in oil recovery. *Energy Conversion and Management*. 2005;**46**:293-311
- [39] Li-ping H, Ping-ping S, Xn-wei L, Qi-Chao G, Cheng-sheng W, Fangfang L. Study on CO<sub>2</sub> EOR and its geological sequestration potential in oil field around Yulin city. *Journal of Petroleum Science and Engineering*. 2015;**134**:199-204
- [40] Pei P, Ling K, He J, Liu Z. Shale gas reservoir treatment by a CO<sub>2</sub>-based technology. *Journal of Natural Gas Science and Engineering*. 2015;**26**:1595-1606
- [41] Song Z, Li Z, Wei M, Lai F, Bai B. Sensitivity analysis of water-alternating-CO<sub>2</sub> flooding for enhanced oil recovery in high water cut oil reservoirs. *Computers & Fluids*. 2014;**99**: 93-103
- [42] Er V, Babadagli T, Xu Z. Pore-scale investigation of the matrix– fracture interaction during CO<sub>2</sub> injection in naturally fractured oil reservoirs. *Energy & Fuels*. 2009;**24**:1421-1430
- [43] Pashin JC, Clark PE, McIntyre-Redden MR, Carroll RE, Esposito RA, Oudinot AY, et al. SECARB CO<sub>2</sub> injection test in mature coalbed methane reservoirs of the Black Warrior Basin, Blue Creek Field, Alabama. *International Journal of Coal Geology*. 2015;**144**:71-87
- [44] Grimm RP, Eriksson KA, Ripepi N, Eble C, Greb SF. Seal evaluation and confinement screening criteria for beneficial carbon dioxide storage with enhanced coal bed methane recovery in the Pocahontas Basin, Virginia. *International Journal of Coal Geology*. 2012;**90**:110-125

*Edited by Iyad Karamé,  
Janah Shaya and Hassan Srour*

Fossil fuels still need to meet the growing demand of global economic development, yet they are often considered as one of the main sources of the CO<sub>2</sub> release in the atmosphere. CO<sub>2</sub>, which is the primary greenhouse gas (GHG), is periodically exchanged among the land surface, ocean, and atmosphere where various creatures absorb and produce it daily. However, the balanced processes of producing and consuming the CO<sub>2</sub> by nature are unfortunately faced by the anthropogenic release of CO<sub>2</sub>. Decreasing the emissions of these greenhouse gases is becoming more urgent. Therefore, carbon sequestration and storage (CSS) of CO<sub>2</sub>, its utilization in oil recovery, as well as its conversion into fuels and chemicals emerge as active options and potential strategies to mitigate CO<sub>2</sub> emissions and climate change, energy crises, and challenges in the storage of energy.

Published in London, UK

© 2018 IntechOpen  
© Fotocitizen / pixabay

**IntechOpen**

